

Flavor Physics in the Randall-Sundrum Model

II. Tree-Level Weak-Interaction Processes

M. BAUER^a, S. CASAGRANDE^b, U. HAISCH^a AND M. NEUBERT^a

^a *Institut für Physik (WA THEP), Johannes Gutenberg-Universität
D-55099 Mainz, Germany*

^b *Excellence Cluster Universe, Technische Universität München
D-85748 Garching, Germany*

Abstract

A comprehensive analysis of tree-level weak interaction processes at low energy is presented for the Randall-Sundrum (RS) model with $SU(2)_L \times U(1)_Y$ bulk gauge symmetry and brane-localized Higgs sector. The complete form of the effective weak Hamiltonian is obtained, which results from tree-level exchange of Kaluza-Klein (KK) gluons and photons, the W^\pm and Z^0 bosons and their KK excitations, as well as the Higgs boson. Exact expressions are used for the bulk profiles of the various fields, and for the exchange of entire towers of KK gauge-boson states. A detailed phenomenological analysis is performed for potential new-physics effects in neutral-meson mixing and in rare decays of kaons and B mesons, including both inclusive and exclusive processes. We find that while the predictions for $\Delta F = 2$ observables are rather model-independent, $\Delta F = 1$ processes depend sensitively on the exact realizations of the electroweak gauge and the fermionic sector. In this context, we emphasize that the localization of the right-handed top quark in the extra dimension plays a crucial role in the case of rare Z^0 -mediated decays, as it determines the relative size of left- to right-handed couplings. We also extend earlier studies of quark flavor-changing neutral currents by examining observables which up to now attracted little attention. These include $D-\bar{D}$ mixing, $B \rightarrow \tau\nu_\tau$, $B \rightarrow X_s(K^*)l^+l^-$, ϵ'_K/ϵ_K , $\bar{B} \rightarrow \pi\bar{K}$, $\bar{B}^0 \rightarrow \phi K_S$, $\bar{B}^0 \rightarrow \eta' K_S$, and $B^+ \rightarrow \pi^+\pi^0$.

Contents

1	Introduction	3
2	Preliminaries	5
3	Induced Four-Fermion Interactions at Low Energies	6
3.1	Exchange of KK Photons and Gluons	7
3.2	Exchange of the Z^0 Boson and its KK Excitations	8
3.3	Exchange of W^\pm bosons and their KK excitations	9
3.4	Exchange of the Higgs Boson	10
3.5	Mixing Matrices in the ZMA	11
4	Tree-Level Weak Decay Processes	12
4.1	Neutral-Meson Mixing	12
4.1.1	Effective $\Delta S = 2$ Hamiltonian	12
4.1.2	Important Formulas for Neutral-Meson Mixing	14
4.2	Rare Non-Leptonic Decays of Kaons and B Mesons	17
4.2.1	Effective $\Delta B = 1$ Hamiltonian	18
4.2.2	Important Formulas for ϵ'_K/ϵ_K	19
4.2.3	Important Formulas for Non-Leptonic B Decays	21
4.3	Rare Leptonic Decays of Kaons and B Mesons	27
4.3.1	Effective Hamiltonian for $s \rightarrow d\nu\bar{\nu}$	27
4.3.2	Effective Hamiltonian for $b \rightarrow sl^+l^-$	27
4.3.3	Effective Hamiltonian for $b \rightarrow ul\bar{\nu}$	28
4.3.4	Important Formulas for $K \rightarrow \pi\nu\bar{\nu}$, $K_L \rightarrow \mu^+\mu^-$, and $K_L \rightarrow \pi^0l^+l^-$	29
4.3.5	Important Formulas for $B \rightarrow X_q\nu\bar{\nu}$, $B_q \rightarrow \mu^+\mu^-$, and $B \rightarrow X_sl^+l^-$	32
4.3.6	Important Formulas for $B \rightarrow K^*l^+l^-$	36
4.3.7	Important Formulas for $B \rightarrow \tau\nu_\tau$	40
5	Numerical Analysis	41
5.1	Parameter Scan	41
5.2	Benchmark Scenarios	42
5.3	Quark Mixing Matrices	44
5.4	Neutral-Meson Mixing	48
5.4.1	Numerical Analysis of $K-\bar{K}$ Mixing	49
5.4.2	Numerical Analysis of $B_{d,s}-\bar{B}_{d,s}$ Mixing	55
5.4.3	Numerical Analysis of $D-\bar{D}$ Mixing	59
5.5	Rare Leptonic Decays of Kaons and B Mesons	61
5.5.1	Numerical Analysis of $K \rightarrow \pi\nu\bar{\nu}$, $K_L \rightarrow \pi^0l^+l^-$, and $K_L \rightarrow \mu^+\mu^-$	62
5.5.2	Numerical Analysis of $B_q \rightarrow \mu^+\mu^-$ and $B \rightarrow X_q\nu\bar{\nu}$	70
5.5.3	Numerical Analysis of $B \rightarrow X_sl^+l^-$ and $B \rightarrow K^*l^+l^-$	73
5.6	Rare Non-Leptonic Decays of Kaons and B Mesons	77
5.6.1	Numerical Analysis of ϵ'_K/ϵ_K	77
5.6.2	Numerical Analysis of Non-Leptonic B Decays	82

6	Conclusions and Outlook	86
A	RG Evolution of Penguin Coefficients	89
B	Input Parameters	91

1 Introduction

Models with a warped extra dimension provide a compelling geometrical explanation of a number of mysteries left unexplained by the Standard Model (SM), most notably the gauge hierarchy and the flavor problem. In these scenarios, first proposed by Randall and Sundrum (RS) [1], one studies the SM on a background consisting of Minkowski space embedded in a slice of five-dimensional (5D) anti-de-Sitter space (AdS₅). The fifth dimension is an S^1/Z_2 orbifold of size r labeled by a coordinate $\phi \in [-\pi, \pi]$. The metric is given by

$$ds^2 = e^{-2\sigma(\phi)} \eta_{\mu\nu} dx^\mu dx^\nu - r^2 d\phi^2, \quad \sigma(\phi) = kr|\phi|, \quad (1)$$

where x^μ denote the coordinates on the four-dimensional (4D) hypersurfaces of constant ϕ with metric $\eta_{\mu\nu} = \text{diag}(1, -1, -1, -1)$, and $e^{\sigma(\phi)}$ is called the warp factor. Three-branes are placed at the orbifold fixed points $\phi = 0$ as well as $\phi = \pi$. The brane at $\phi = 0$ is called Planck or ultra-violet (UV) brane, while the brane at $\phi = \pi$ is called TeV or infra-red (IR) brane. In the original formulation of the RS model all SM fields were confined to the IR brane, while gravity probed the bulk of the higher-dimensional space-time. The hierarchy problem is then resolved through the warping of space along the fifth dimension. While the RS model only has a single fundamental scale k , the AdS₅ curvature, the effective scale of the model exponentially varies along the extra dimension due to the presence of the warp factor. For fields near the IR brane the effective Planck scale is thus redshifted to be of order the weak scale.

In later work, variations on the original setup were considered, where also the SM fields except for the Higgs boson were allowed to propagate in the bulk [2, 3, 4, 5, 6]. It was soon realized that this framework provides an interesting new approach to the flavor problem, as now also the hierarchical structures observed in the masses and mixing of the SM fermions could be explained in terms of geometrical effects [4, 6, 7, 8, 9]. Since the fermion zero modes are exponentially localized near either one of the two branes, the effective Yukawa couplings resulting from their wave-function overlap with the Higgs boson naturally exhibit exponential hierarchies. In this way one obtains an extra-dimensional realization [9, 10, 11] of the Froggatt-Nielsen mechanism [12], in which the flavor structure is accounted for apart from $\mathcal{O}(1)$ factors.

Addressing the flavor hierarchies via warping in an extra dimension makes distinctive predictions for flavor-changing processes as well. Various new sources of flavor violation arise in RS models as a consequence of non-trivial overlap factors between fermions and gauge (or Higgs) bosons, which generically are non-diagonal in the mass basis. While the new flavor-changing effects generically arise already at tree level, a dynamical mechanism referred to as RS-GIM mechanism [6, 13, 14] ensures that these effects are suppressed, for most observables, to an acceptable level. During the past years, diverse studies of the flavor structure of RS models have been performed. Properties of the generalized CKM matrix, neutral-meson mixing, and CP violation were studied in [9]. Z^0 -mediated flavor-changing neutral currents (FCNCs) in the kaon system were considered in [15], and effects of Kaluza-Klein (KK) gauge bosons on CP asymmetries in rare hadronic B -meson decays induced by $b \rightarrow s$ transitions were explored in [16]. A first general survey of $\Delta F = 2$ and $\Delta F = 1$ processes in the RS framework was presented in [13, 14]. The branching ratios for the flavor-changing top-quark decays $t \rightarrow cZ^0(\gamma, g)$ were examined in [17]. The first complete study of all operators relevant

to $K-\bar{K}$ mixing was presented in [18]. Comprehensive analyses of $B_{d,s}-\bar{B}_{d,s}$ mixing [11], rare leptonic K - and B -meson decays [19, 20] as well as of the radiative $B \rightarrow X_s \gamma$ decay [21] have been performed quite recently. Higgs- [22] and radion-mediated [23, 24] FCNCs have also been investigated. It has been recognized that the only observables where some fine-tuning of parameters appears to be unavoidable are CP-violating effects in the neutral kaon system [18, 25] and the neutron electric dipole moment [13, 14], which for generic choices of parameters turn out to be too large unless the masses of the lightest KK gauge bosons lie above (10–20) TeV. In view of these problems, several modifications of the quark flavor sector of warped extra-dimension models have been proposed. Most of them try to implement the notion of minimal flavor violation (MFV) [26, 27] into the RS framework by using a bulk flavor symmetry [28, 29, 30, 31, 32, 33]. The problem of too large electric dipole moments has been addressed using the idea of spontaneous CP violation in the context of warped extra dimensions [34].

As our benchmark scenario we consider in this work the simplest implementation of the RS model, featuring an $SU(2)_L \times U(1)_Y$ bulk gauge symmetry and a minimal, brane-localized Higgs sector. Our analysis is thus in some sense orthogonal to that of [11, 19], where $\Delta F = 2$ and $\Delta F = 1$ processes were investigated in a setup with enlarged gauge symmetry, namely $SU(2)_L \times SU(2)_R \times U(1)_X \times P_{LR}$, where P_{LR} exchanges the $SU(2)$ groups. The comparison between the findings of the latter articles and the results obtained here allows us to address the important question about the model (in)dependence of the predictions for neutral-meson mixing and rare leptonic decays of K - and B -mesons. We find that while $\Delta F = 2$ observables are relatively model-independent, predictions for $\Delta F = 1$ processes depend strongly on the exact realization of both the gauge and fermionic sectors. In this context, we emphasize that the degree of compositeness of the right-handed top quark, characterized by its localization in the extra dimension, plays a crucial role in the case of rare Z^0 -mediated decays, as it determines the relative size of left- to right-handed couplings. The present paper also extends previous studies of quark FCNCs, since it examines in detail observables which partly or even fully escaped the attention of the flavor community so far. The list of new observables includes, among others, $D-\bar{D}$ mixing, $B \rightarrow \tau \nu_\tau$, $B \rightarrow X_s (K^*) l^+ l^-$, ϵ'_K/ϵ_K , and $\bar{B} \rightarrow \pi \bar{K}$. The main question that we will address in the context of the decays $B \rightarrow \tau \nu_\tau$ and $\bar{B} \rightarrow \pi \bar{K}$ is whether possible discrepancies, as suggested by experiment, can be explained in the minimal RS scenario. In the case of ϵ'_K/ϵ_K , we will point out that the strong sensitivity of this ratio to the electroweak penguin sector leads to interesting correlations with the rare $K \rightarrow \pi \nu \bar{\nu}$ and $K_L \rightarrow \pi^0 l^+ l^-$ decays in scenarios with warped extra dimensions.

This paper is a sequel to our recent work [10], where we have derived the theoretical foundations forming the basis of the present analysis and studied in detail the implications of the RS model for electroweak precision physics. In particular, we have derived the exact solutions for the bulk profiles of the various gauge and matter fields, and given closed expressions for sums over KK gauge bosons in tree-level low-energy processes. We have also presented a systematic analysis of the flavor-changing couplings of gauge bosons and of the Higgs boson to the SM fermions. The discussion in the present paper is self-contained as far as phenomenology is concerned, but it relies on many equations and results derived in our previous work, which for the sake of brevity will not be rederived here. The two papers should therefore be studied together. We will refer to equations from our paper [10] by adding a roman “I”

before the equation number. In Section 2 we briefly recall some important notations, which will be needed throughout the paper. In Section 3 we review the different interactions between fermions and the gauge and Higgs bosons in the RS model, many of which give rise to new flavor-changing effects not present in the SM. In Section 4 we present a detailed analysis of various weak-interaction processes, including neutral-meson mixing, as well as rare non-leptonic and leptonic decays of kaons and B mesons. In each case we present the relevant effective weak Hamiltonians at tree level in the minimal RS model and collect the formulas needed for a phenomenological analysis. A detailed numerical study of all these processes is performed in Section 5. We first discuss how we efficiently perform the scan over the vast parameter space of the RS model. We then define a few benchmark parameter scenarios, which we will use to illustrate the type of effects that typically arise in such models. After a numerical analysis of quark mixing matrices we then analyse the various decay modes in detail. Section 6 contains a summary of our main results and some conclusions. In Appendix A we present formulas describing the renormalization group (RG) evolution of the Wilson coefficients of the QCD and electroweak penguin operators, whereas in Appendix B we collect the input values for the SM parameters used in the course of the article.

2 Preliminaries

Before going into the details of the structure of flavor-changing interactions in the RS model, we need to review some important notations and definitions from [10], which are needed for the further discussion. The reader is referred to this reference for more details.

In order to address the hierarchy between the fundamental Planck and the electroweak scale, the logarithm of the warp factor

$$L \equiv kr\pi \equiv \ln \frac{\Lambda_{\text{UV}}}{\Lambda_{\text{IR}}} \equiv -\ln \epsilon, \quad (2)$$

has to be chosen such that $L \approx \ln(10^{16}) \approx 37$. Below we will sometimes refer to L as the “volume” of the extra dimension. The warp factor also sets the mass scale for the low-lying KK excitations of the SM fields to be of order of the “KK scale”

$$M_{\text{KK}} \equiv k\epsilon = k e^{-kr\pi} = \mathcal{O}(\text{few TeV}). \quad (3)$$

For instance, the masses of the first KK photon and gluon are approximately equal to $2.45M_{\text{KK}}$.

Introducing a coordinate $t = \epsilon e^{\sigma(\phi)}$ along the extra dimension [4], which runs from $t = \epsilon$ on the UV brane to $t = 1$ on the IR brane, we write the KK decompositions of the left-handed (right-handed) components of the 5D $SU(2)_L$ doublet (singlet) quark fields as

$$\begin{aligned} q_L(x, t) &\propto \text{diag}[F(c_{Q_i}) t^{c_{Q_i}}] \mathbf{U}_q q_L^{(0)}(x) + \mathcal{O}\left(\frac{v^2}{M_{\text{KK}}^2}\right) + \text{KK excitations}, \\ q_R^c(x, t) &\propto \text{diag}[F(c_{q_i}) t^{c_{q_i}}] \mathbf{W}_q q_R^{(0)}(x) + \mathcal{O}\left(\frac{v^2}{M_{\text{KK}}^2}\right) + \text{KK excitations}, \end{aligned} \quad (4)$$

where $v \approx 246$ GeV denotes the Higgs vacuum expectation value, and $q = u, d$ stands for up- and down-type quarks, respectively. The fields are three-component vectors in flavor space. The 5D fields on the left-hand side refer to interaction eigenstates, while the 4D fields appearing on the right are mass eigenstates. The superscript “(0)” is used to denote the light SM fermions, often called “zero modes”. In this article we will not deal with heavy KK fermions.

The zero-mode profile [4, 6]

$$F(c) = \text{sgn}[\cos(\pi c)] \sqrt{\frac{1+2c}{1-\epsilon^{1+2c}}} \quad (5)$$

is exponentially suppressed in the “volume factor” L if the bulk mass parameters $c_{Q_i} = +M_{Q_i}/k$ and $c_{q_i} = -M_{q_i}/k$ are smaller than the critical value $-1/2$, in which case $F(c) \sim e^{L(c+\frac{1}{2})}$. Here M_{Q_i} and M_{q_i} denote the masses of the 5D $SU(2)_L$ doublet and singlet fermions. This mechanism explains in a natural way the large hierarchies observed in the spectrum of the quark masses [6, 8], which follow from the eigenvalues of the effective Yukawa matrices

$$\mathbf{Y}_q^{\text{eff}} = \text{diag}[F(c_{Q_i})] \mathbf{Y}_q \text{diag}[F(c_{q_i})] = \mathbf{U}_q \boldsymbol{\lambda}_q \mathbf{W}_q^\dagger. \quad (6)$$

The 5D Yukawa matrices \mathbf{Y}_q are assumed to be anarchic, *i.e.*, non-hierarchical with $\mathcal{O}(1)$ complex elements, and $\boldsymbol{\lambda}_q$ are diagonal matrices with entries $(\lambda_q)_{ii} = \sqrt{2} m_{q_i}/v$. The unitary matrices \mathbf{U}_q and \mathbf{W}_q in (4) and (6) have a hierarchical structure given by

$$(U_q)_{ij} \sim \begin{cases} \frac{F(c_{Q_i})}{F(c_{Q_j})}, & i \leq j, \\ \frac{F(c_{Q_j})}{F(c_{Q_i})}, & i > j, \end{cases} \quad (W_q)_{ij} \sim \begin{cases} \frac{F(c_{q_i})}{F(c_{q_j})}, & i \leq j, \\ \frac{F(c_{q_j})}{F(c_{q_i})}, & i > j. \end{cases} \quad (7)$$

Terms omitted in (4) are suppressed by at least two powers of the small ratio v/M_{KK} and can be neglected to a good approximation. We refer to this as the “zero-mode approximation” (ZMA). It allows us to derive compact analytic formulas for the flavor mixing matrices that are both transparent and accurate. While such an approach in general lead to sensible results [35], in our numerical analysis in Section 5 we nevertheless employ the exact expressions for the various matrices derived in [10].

3 Induced Four-Fermion Interactions at Low Energies

Of special interest are the dimension-six operators describing the effective four-fermion interactions at low energies induced by heavy gauge-boson exchange. In particular, these will give rise to $\Delta F = 2$ and $\Delta F = 1$ FCNC processes, which are loop-suppressed in the SM. In the RS model, such processes arise already at tree level. However, as mentioned earlier, they are protected by the RS-GIM mechanism.

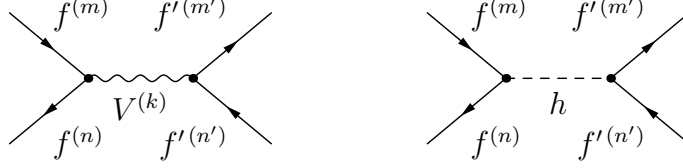


Figure 1: Contributions to the effective four-fermion interactions arising from the tree-level exchange of the gauge bosons $V = \gamma, g, Z^0, W^\pm$ and their KK excitations (left), and of the Higgs boson (right).

3.1 Exchange of KK Photons and Gluons

We begin with a discussion of the interactions induced by the exchange of KK photons and gluons. The graph on the left in Figure 1 shows an example of a diagram giving rise to such contributions. The relevant sums over KK modes can be evaluated by means of (I:34). In the case of KK photon exchange, we find that the effective Hamiltonian at low energies is given by

$$\begin{aligned} \mathcal{H}_{\text{eff}}^{(\gamma)} = & \frac{2\pi\alpha}{M_{\text{KK}}^2} \sum_{f,f'} Q_f Q_{f'} \left\{ \frac{1}{2L} (\bar{f}\gamma^\mu f) (\bar{f}'\gamma_\mu f') - 2 (\bar{f}_L\gamma^\mu \Delta'_F f_L + \bar{f}_R\gamma^\mu \Delta'_f f_R) (\bar{f}'\gamma_\mu f') \right. \\ & \left. + 2L \left(\bar{f}_L\gamma^\mu \tilde{\Delta}_F f_L + \bar{f}_R\gamma^\mu \tilde{\Delta}_f f_R \right) \otimes \left(\bar{f}'_L\gamma_\mu \tilde{\Delta}_{F'} f'_L + \bar{f}'_R\gamma_\mu \tilde{\Delta}_{f'} f'_R \right) \right\}. \end{aligned} \quad (8)$$

Here the sum over fermions implicitly includes the sum over all KK modes. The matrices Δ'_A have been defined in (I:122). These are infinite-dimensional matrices in the space of flavor and KK modes. In addition, we have defined the new mixing matrices (with $F = U, D$ and $f = u, d$, and similarly in the lepton sector) [36]

$$\begin{aligned} (\tilde{\Delta}_F)_{mn} \otimes (\tilde{\Delta}_{f'})_{m'n'} = & \frac{2\pi^2}{L^2\epsilon^2} \int_\epsilon^1 dt \int_\epsilon^1 dt' t_\epsilon^2 \\ & \times \left[a_m^{(F)\dagger} \mathbf{C}_m^{(Q)}(\phi) \mathbf{C}_n^{(Q)}(\phi) a_n^{(F)} + a_m^{(f)\dagger} \mathbf{S}_m^{(f)}(\phi) \mathbf{S}_n^{(f)}(\phi) a_n^{(f)} \right] \\ & \times \left[a_{m'}^{(f')\dagger} \mathbf{C}_{m'}^{(f')}(\phi') \mathbf{C}_{n'}^{(f')}(\phi') a_{n'}^{(f')} + a_{m'}^{(F')\dagger} \mathbf{S}_{m'}^{(Q)}(\phi') \mathbf{S}_{n'}^{(Q)}(\phi') a_{n'}^{(F')} \right], \end{aligned} \quad (9)$$

etc. Notice that the matrices $\tilde{\Delta}_A \otimes \tilde{\Delta}_B$ are not defined individually, but only as tensor products, as indicated by the \otimes symbol. The couplings to SM fermions are encoded in the upper-left 3×3 blocks of each $\tilde{\Delta}_A \otimes \tilde{\Delta}_B$ matrix. We emphasize that the result (8) is exact. In particular, no expansion in powers of v^2/M_{KK}^2 has been performed. The effective interactions arising from KK gluon exchange have a very similar structure, except that we need to restrict the sum over fermions in (8) to quarks and replace $\alpha Q_f Q_{f'}$ by $\alpha_s t^a \otimes t^a$, where the color matrices t^a must be inserted inside the quark bi-linears.

The four-fermion operators induced by KK gluon exchange give the by far dominant (leading) contribution to the effective weak Hamiltonians describing $K-\bar{K}$ ($B_{d,s}-\bar{B}_{d,s}$ and $D-\bar{D}$)

mixing. This observation is important, as it implies that mixing phenomena mainly probe the extra-dimensional aspects of the strong interactions, but are to first approximation insensitive to the precise embedding of the electroweak gauge symmetry in the higher-dimensional geometry.

3.2 Exchange of the Z^0 Boson and its KK Excitations

The induced interactions arising from the exchange of the Z^0 boson and its KK excitations have a richer structure. In this case the relevant sum over profiles is evaluated by means of relation (I:33). We obtain

$$\begin{aligned}
\mathcal{H}_{\text{eff}}^{(Z)} &= \frac{4\pi\alpha}{s_w^2 c_w^2 m_Z^2} \left[1 + \frac{m_Z^2}{2M_{\text{KK}}^2} \left(1 - \frac{1}{2L} \right) + \mathcal{O} \left(\frac{m_Z^4}{M_{\text{KK}}^4} \right) \right] \\
&\times \sum_{f,f'} \left[\bar{f}_L \gamma^\mu T_3^f (\mathbf{1} - \boldsymbol{\delta}_F) f_L + \bar{f}_R \gamma^\mu T_3^f \boldsymbol{\delta}_f f_R - s_w^2 Q_f \bar{f} \gamma^\mu f \right] \\
&\quad \times \left[\bar{f}'_L \gamma^\mu T_3^{f'} (\mathbf{1} - \boldsymbol{\delta}_{F'}) f'_L + \bar{f}'_R \gamma^\mu T_3^{f'} \boldsymbol{\delta}_{f'} f'_R - s_w^2 Q_{f'} \bar{f}' \gamma^\mu f' \right] \\
&+ \frac{4\pi\alpha L}{s_w^2 c_w^2 M_{\text{KK}}^2} \\
&\times \sum_{f,f'} \left\{ - \left[\bar{f}_L \gamma^\mu T_3^f (\boldsymbol{\Delta}_F - \boldsymbol{\varepsilon}_F) f_L + \bar{f}_R \gamma^\mu T_3^f \boldsymbol{\varepsilon}_f f_R - s_w^2 Q_f (\bar{f}_L \gamma^\mu \boldsymbol{\Delta}_F f_L + \bar{f}_R \gamma^\mu \boldsymbol{\Delta}_f f_R) \right] \right. \\
&\quad \times \left[\bar{f}'_L \gamma^\mu T_3^{f'} (\mathbf{1} - \boldsymbol{\delta}_{F'}) f'_L + \bar{f}'_R \gamma^\mu T_3^{f'} \boldsymbol{\delta}_{f'} f'_R - s_w^2 Q_{f'} \bar{f}' \gamma^\mu f' \right] \\
&\quad + \left[\bar{f}_L \gamma^\mu T_3^f (\tilde{\boldsymbol{\Delta}}_F - \tilde{\boldsymbol{\varepsilon}}_F) f_L + \bar{f}_R \gamma^\mu T_3^f \tilde{\boldsymbol{\varepsilon}}_f f_R - s_w^2 Q_f (\bar{f}_L \gamma^\mu \tilde{\boldsymbol{\Delta}}_F f_L + \bar{f}_R \gamma^\mu \tilde{\boldsymbol{\Delta}}_f f_R) \right] \\
&\quad \left. \otimes \left[\bar{f}'_L \gamma^\mu T_3^{f'} (\tilde{\boldsymbol{\Delta}}_{F'} - \tilde{\boldsymbol{\varepsilon}}_{F'}) f'_L + \bar{f}'_R \gamma^\mu T_3^{f'} \tilde{\boldsymbol{\varepsilon}}_{f'} f'_R - s_w^2 Q_{f'} (\bar{f}'_L \gamma^\mu \tilde{\boldsymbol{\Delta}}_{F'} f'_L + \bar{f}'_R \gamma^\mu \tilde{\boldsymbol{\Delta}}_{f'} f'_R) \right] \right\}. \tag{10}
\end{aligned}$$

Here we have introduced the shorthand notation $s_w \equiv \sin \theta_w$ and $c_w \equiv \cos \theta_w$ for the sine and cosine of the weak mixing angle renormalized at a scale $\mu_{\text{KK}} = \mathcal{O}(M_{\text{KK}})$. Note that this result is exact except for the expansion performed in the overall normalization of the first term, as indicated by the $\mathcal{O}(m_Z^4/M_{\text{KK}}^4)$ symbol in brackets. Apart from this, no expansion in powers of v^2/M_{KK}^2 has been performed. However, the rather complicated expression obtained above can be simplified by noting that the matrices $\boldsymbol{\delta}_A$ and $\boldsymbol{\varepsilon}_A^{(l)}$ are of $\mathcal{O}(v^2/M_{\text{KK}}^2)$. It follows that the latter ones can be discarded to very good approximation, whereas the contributions from the $\boldsymbol{\delta}_A$ matrices must only be kept to first order in v^2/M_{KK}^2 . We then obtain the simpler expression

$$\mathcal{H}_{\text{eff}}^{(Z)} = \frac{4\pi\alpha}{s_w^2 c_w^2 m_Z^2} \left[1 + \frac{m_Z^2}{2M_{\text{KK}}^2} \left(1 - \frac{1}{2L} \right) \right] J_Z^\mu J_{Z\mu}$$

$$\begin{aligned}
& - \frac{8\pi\alpha}{s_w^2 c_w^2 m_Z^2} \sum_f \left[\bar{f}_L \gamma^\mu T_3^f \boldsymbol{\delta}_F f_L - \bar{f}_R \gamma^\mu T_3^f \boldsymbol{\delta}_f f_R \right] J_{Z\mu} \\
& - \frac{4\pi\alpha L}{s_w^2 c_w^2 M_{\text{KK}}^2} \sum_f \left[\left(T_3^f - s_w^2 Q_f \right) \bar{f}_L \gamma^\mu \boldsymbol{\Delta}_F f_L - s_w^2 Q_f \bar{f}_R \gamma^\mu \boldsymbol{\Delta}_f f_R \right] J_{Z\mu} \\
& + \frac{4\pi\alpha L}{s_w^2 c_w^2 M_{\text{KK}}^2} \sum_{f,f'} \left\{ \left[\left(T_3^f - s_w^2 Q_f \right) \bar{f}_L \gamma^\mu \tilde{\boldsymbol{\Delta}}_F f_L - s_w^2 Q_f \bar{f}_R \gamma^\mu \tilde{\boldsymbol{\Delta}}_f f_R \right] \right. \\
& \quad \left. \otimes \left[\left(T_3^{f'} - s_w^2 Q_{f'} \right) \bar{f}'_L \gamma_\mu \tilde{\boldsymbol{\Delta}}_{F'} f'_L - s_w^2 Q_{f'} \bar{f}'_R \gamma_\mu \tilde{\boldsymbol{\Delta}}_{f'} f'_R \right] \right\}, \quad (11)
\end{aligned}$$

which is valid up to corrections of $\mathcal{O}(v^4/M_{\text{KK}}^4)$. Here

$$J_Z^\mu \equiv \sum_f \left[\left(T_3^f - s_w^2 Q_f \right) \bar{f}_L \gamma^\mu f_L - s_w^2 Q_f \bar{f}_R \gamma^\mu f_R \right] \quad (12)$$

is the familiar SM expression for the neutral current.

3.3 Exchange of W^\pm bosons and their KK excitations

Using (I:33) it is also straightforward to derive the effective four-fermion interactions induced by the exchange of the charged weak gauge bosons W^\pm and their KK excitations. In this case, of course, flavor-changing effects are unsuppressed already in the SM. Restricting ourselves to the phenomenologically most relevant case with leptons in the final state, and including corrections up to $\mathcal{O}(m_W^2/M_{\text{KK}}^2)$, we find

$$\mathcal{H}_{\text{eff}}^{(W)} = \frac{2\pi\alpha}{s_w^2 m_W^2} \sum_l \left\{ \left[\bar{u}_L \gamma^\mu \boldsymbol{\nu}_L d_L + \bar{u}_R \gamma^\mu \boldsymbol{\nu}_R d_R \right] \left(\bar{l}_L \gamma_\mu \nu_{lL} \right) + \text{h.c.} \right\}, \quad (13)$$

where

$$\begin{aligned}
(\mathcal{V}_L)_{mn} &= \frac{2\pi}{L\epsilon} \int_\epsilon^1 dt \left[1 - \frac{m_W^2}{2M_{\text{KK}}^2} \left(L t^2 - 1 + \frac{1}{2L} \right) \right] a_m^{(U)\dagger} \mathbf{C}_m^{(Q)}(\phi) \mathbf{C}_n^{(Q)}(\phi) a_n^{(D)}, \\
(\mathcal{V}_R)_{mn} &= \frac{2\pi}{L\epsilon} \int_\epsilon^1 dt \left[1 - \frac{m_W^2}{2M_{\text{KK}}^2} \left(L t^2 - 1 + \frac{1}{2L} \right) \right] a_m^{(U)\dagger} \mathbf{S}_m^{(Q)}(\phi) \mathbf{S}_n^{(Q)}(\phi) a_n^{(D)}.
\end{aligned} \quad (14)$$

Notice that $(\mathcal{V}_L)_{mn}$ and $(\mathcal{V}_R)_{mn}$ differ from the left- and right-handed charged-current mixing matrix $(V_L)_{mn}$ and $(V_R)_{mn}$ introduced in (I:132), as they contain besides the contribution due to the ground-state W^\pm bosons also corrections from the tower of KK excitations. Like in the case of muon decay [10], the latter contributions are suppressed by the logarithm of the warp factor with respect to the former ones, so that in leading L the elements $(\mathcal{V}_{L,R})_{mn}$ reduce to $(V_{L,R})_{mn}$. Due to the suppression proportional to two powers of light quark masses, which is evident from (I:134), the contribution from the right-handed operator is strongly suppressed

compared to the one of its left-handed counterpart. Notice finally that in order to arrive at the effective Hamiltonian (13), we have made the simplifying assumption that the left- and right-handed 5D leptonic fields all have the same bulk mass parameter and that they are localized sufficiently close to the the UV brane so as not to violate the constraints imposed by electroweak precision tests. By construction the interactions of the SM leptons with the W^\pm boson and its KK excitations are therefore flavor universal and numerically insignificant.

3.4 Exchange of the Higgs Boson

The Higgs boson is a brane-localized field in the simplest RS model, so it does not have KK excitations. Nevertheless, due to the mixing of fermion zero-modes with their KK excitations, the interactions of fermions with the Higgs boson are no longer flavor diagonal in the mass basis of the fermions [17]. Unlike in the SM, the Higgs boson of the RS model thus has FCNC couplings at tree level.

In unitary gauge, the effective four-fermion interactions resulting from Higgs-boson exchange follow directly from (I:134). The graph on the right in Figure 1 shows an example of a diagram giving rise to such a contribution. We obtain

$$\begin{aligned} \mathcal{H}_{\text{eff}}^{(h)} = \frac{1}{m_h^2} \sum_{f,f'} & \left[\bar{f}_L \frac{\mathbf{m}_f}{v} f_R - \bar{f}_L \left(\frac{\mathbf{m}_f}{v} \boldsymbol{\delta}_f + \boldsymbol{\delta}_F \frac{\mathbf{m}_f}{v} \right) f_R + \text{h.c.} \right] \\ & \times \left[\bar{f}'_L \frac{\mathbf{m}_{f'}}{v} f'_R - \bar{f}'_L \left(\frac{\mathbf{m}_{f'}}{v} \boldsymbol{\delta}_{f'} + \boldsymbol{\delta}_{F'} \frac{\mathbf{m}_{f'}}{v} \right) f'_R + \text{h.c.} \right], \end{aligned} \quad (15)$$

where $\mathbf{m}_f \equiv \text{diag}(m_{f_1}, m_{f_2}, m_{f_3})$ represents a diagonal matrix containing the masses of the zero-mode fermions. This exact expression can be simplified by noting that the matrices $\boldsymbol{\delta}_A$ are of $\mathcal{O}(v^2/M_{\text{KK}}^2)$, and terms involving two such matrices can be neglected to very good approximation. We then obtain the simpler expression

$$\mathcal{H}_{\text{eff}}^{(h)} = \frac{1}{m_h^2 v^2} \sum_{f,f'} \left[(\bar{f} \mathbf{m}_f f - 2 [\bar{f}_L (\mathbf{m}_f \boldsymbol{\delta}_f + \boldsymbol{\delta}_F \mathbf{m}_f) f_R + \text{h.c.}]) (\bar{f}' \mathbf{m}_{f'} f') \right], \quad (16)$$

which is valid up to corrections of $\mathcal{O}(v^4/M_{\text{KK}}^4)$.

At this point a couple of comments concerning the existing literature on tree-level FCNCs of the Higgs boson are in order. Analytic expressions for the relevant interactions have been first presented within the RS model with $SU(2)_L \times U(1)_Y$ bulk symmetry and minimal, brane-localized Higgs sector in [10]. Our previous work did however not include the Yukawa couplings that involve Z_2 -odd fermion profiles. This omission has been noticed in [22], where it has been argued that the latter terms embody the dominant tree-level corrections to the flavor-changing Higgs-boson couplings in the RS framework. In the course of the present work, we have revisited the issue of flavor-misalignment of fermion masses and Yukawa couplings. We find that the correct implementation of the brane-localized Yukawa couplings that involve Z_2 -odd fermion profiles affects the masses of the SM fermions and their couplings to the Higgs-boson in exactly the same way. Thus, it does *not* lead to additional Higgs FCNCs beyond those already

studied in [10].¹ We will clarify the origin of the discrepancy in a forthcoming publication [37]. Let us also mention in passing that a model-independent analysis of the flavor-misalignment of the SM fermion masses and the Yukawa couplings has been presented in [38].

3.5 Mixing Matrices in the ZMA

It is trivial to read off from (8), (11), and (16) the resulting flavor-violating transitions involving quark and lepton fields. Those will be discussed in the following section. We complete the present discussion by collecting the expressions for the various mixing matrices valid in the ZMA. We restrict ourselves to the 3×3 submatrices governing the couplings of the SM fermion fields. The elements of the $\Delta_A^{(\prime)}$ matrices that arise from the non-trivial overlap of gauge and fermion profiles are given explicitly in (I:122). In the ZMA the corresponding expressions simplify considerably (see also [15, 39]). We find

$$\begin{aligned}
\Delta_F &\rightarrow \mathbf{U}_f^\dagger \text{diag} \left[\frac{F^2(c_{F_i})}{3 + 2c_{F_i}} \right] \mathbf{U}_f, \\
\Delta_f &\rightarrow \mathbf{W}_f^\dagger \text{diag} \left[\frac{F^2(c_{f_i})}{3 + 2c_{f_i}} \right] \mathbf{W}_f, \\
\Delta'_F &\rightarrow \mathbf{U}_f^\dagger \text{diag} \left[\frac{5 + 2c_{F_i}}{2(3 + 2c_{F_i})^2} F^2(c_{F_i}) \right] \mathbf{U}_f, \\
\Delta'_f &\rightarrow \mathbf{W}_f^\dagger \text{diag} \left[\frac{5 + 2c_{f_i}}{2(3 + 2c_{f_i})^2} F^2(c_{f_i}) \right] \mathbf{W}_f,
\end{aligned} \tag{17}$$

where the diagonal matrices contain the elements shown in brackets. Note further that, to a good approximation, we have $\Delta'_A \approx \Delta_A$ for $A = F, f$, since all c_i parameters are near $-1/2$. Explicit expressions for the unitary rotations \mathbf{U}_f and \mathbf{W}_f can be found in (I:97) to (I:100). The matrices $\varepsilon_A^{(\prime)}$ vanish at leading order in the ZMA, meaning that they are suppressed by an extra factor of v^2/M_{KK}^2 . Thus we do not report them here.

The matrices δ_A arise from the fact that the fermion profiles are not orthonormal on each other. Their elements take the form (I:123). The corresponding ZMA results read

$$\begin{aligned}
\delta_F &\rightarrow \mathbf{x}_f \mathbf{W}_f^\dagger \text{diag} \left[\frac{1}{1 - 2c_{f_i}} \left(\frac{1}{F^2(c_{f_i})} - 1 + \frac{F^2(c_{f_i})}{3 + 2c_{f_i}} \right) \right] \mathbf{W}_f \mathbf{x}_f, \\
\delta_f &\rightarrow \mathbf{x}_f \mathbf{U}_f^\dagger \text{diag} \left[\frac{1}{1 - 2c_{F_i}} \left(\frac{1}{F^2(c_{F_i})} - 1 + \frac{F^2(c_{F_i})}{3 + 2c_{F_i}} \right) \right] \mathbf{U}_f \mathbf{x}_f,
\end{aligned} \tag{18}$$

where $\mathbf{x}_f \equiv \text{diag}(m_{f_1}, m_{f_2}, m_{f_3})/M_{\text{KK}}$ is a diagonal matrix containing the masses of the SM quarks in units of M_{KK} .

¹At the level of dimension six, contributions to flavor-changing Higgs-boson vertices can arise in scenarios in which the Higgs boson is a bound state of a new strongly-interacting theory, that are unlike the terms in (15) and (16), not chirally suppressed. These loop-suppressed terms are expected to be numerically dominant for all light fermion flavors, $y_{f_*}^2/(16\pi^2) \gg m_f/v$, because the couplings y_{f_*} of the composite Higgs to the other strong interacting states can be as large as 4π . While this is an interesting possibility, which has been covered in [38], we will not consider it here.

As mentioned above, the expressions for the new flavor matrices defined in (9) are tensor products, which do not factorize in the form of simple matrix products. In component notation, we obtain [36]

$$(\tilde{\Delta}_F)_{mn} \otimes (\tilde{\Delta}_{f'})_{m'n'} \rightarrow (U_f^\dagger)_{mi} (U_f)_{in} (\tilde{\Delta}_{Ff})_{ij} (W_f^\dagger)_{m'j} (W_f)_{j'n'}, \quad (19)$$

where

$$(\tilde{\Delta}_{Ff})_{ij} = \frac{2F^2(c_{F_i})}{3 + 2c_{F_i}} \frac{3 + c_{F_i} + c_{f_j}}{2(2 + c_{F_i} + c_{f_j})} \frac{2F^2(c_{f_j})}{3 + 2c_{f_j}}, \quad (20)$$

and a summation over the indices i, j is understood. Analogous expressions hold for the remaining combinations of indices F and f . Using the fact that all c_i parameters except c_{u_3} are very close to $-1/2$, it is a reasonable approximation to replace $(3 + c_{F_i} + c_{f_j})/(2 + c_{F_i} + c_{f_j})$ by 2, in which case we obtain the approximate result

$$\tilde{\Delta}_A \otimes \tilde{\Delta}_B \rightarrow \Delta_A \Delta_B. \quad (21)$$

In the same approximation, there is no need to distinguish between the Δ'_A and Δ_A matrices.

4 Tree-Level Weak Decay Processes

We now discuss a few prominent applications of the general results obtained in the previous section, focusing on FCNC processes in the quark sector. The generalization to the lepton sector is trivial (apart from the issue of Majorana mass terms). We begin with a discussion of $\Delta F = 2$ processes, giving rise to the mixing of neutral mesons with their antiparticles. We then study a plethora of inclusive and exclusive $\Delta F = 1$ transitions in the kaon and B -meson sectors. The purpose of this section is to compile in a concise way the theoretical ingredients needed for the phenomenological analysis of the various observables considered in this work. The reader primarily interested in phenomenological results can skip this section in a first reading.

4.1 Neutral-Meson Mixing

We will discuss the new contributions to neutral-meson mixing arising in the RS model on the basis of $K-\bar{K}$ mixing, where the resulting constraints have been shown to be particularly severe [11, 18, 21, 30, 36], confirming model-independent considerations presented in [40, 41]. With a simple substitution of indices, the expressions we obtain can be applied to the mixing of $B_{d,s}$ and D mesons.

4.1.1 Effective $\Delta S = 2$ Hamiltonian

We adopt the following general parametrization of new-physics effects in $K-\bar{K}$ mixing [42, 43, 44]

$$\mathcal{H}_{\text{eff}}^{\Delta S=2} = \sum_{i=1}^5 C_i Q_i^{sd} + \sum_{i=1}^3 \tilde{C}_i \tilde{Q}_i^{sd}, \quad (22)$$

where

$$\begin{aligned}
Q_1^{sd} &= (\bar{d}_L \gamma^\mu s_L) (\bar{d}_L \gamma_\mu s_L), & \tilde{Q}_1^{sd} &= (\bar{d}_R \gamma^\mu s_R) (\bar{d}_R \gamma_\mu s_R), \\
Q_2^{sd} &= (\bar{d}_R s_L) (\bar{d}_R s_L), & \tilde{Q}_2^{sd} &= (\bar{d}_L s_R) (\bar{d}_L s_R), \\
Q_3^{sd} &= (\bar{d}_R^\alpha s_L^\beta) (\bar{d}_R^\beta s_L^\alpha), & \tilde{Q}_3^{sd} &= (\bar{d}_L^\alpha s_R^\beta) (\bar{d}_L^\beta s_R^\alpha), \\
Q_4^{sd} &= (\bar{d}_R s_L) (\bar{d}_L s_R), \\
Q_5^{sd} &= (\bar{d}_R^\alpha s_L^\beta) (\bar{d}_L^\beta s_R^\alpha).
\end{aligned} \tag{23}$$

A summation over color indices α, β is understood. We write the Wilson coefficients as a sum of a SM and a new-physics contribution, $C_i \equiv C_i^{\text{SM}} + C_i^{\text{RS}}$, where in the SM only C_1^{SM} is non-zero. Using the general results from the previous section along with standard Fierz identities, we obtain for the contributions arising in the RS model

$$\begin{aligned}
C_1^{\text{RS}} &= \frac{4\pi L}{M_{\text{KK}}^2} (\tilde{\Delta}_D)_{12} \otimes (\tilde{\Delta}_D)_{12} \left[\frac{\alpha_s}{2} \left(1 - \frac{1}{N_c} \right) + Q_d^2 \alpha + \frac{(T_3^d - s_w^2 Q_d)^2 \alpha}{s_w^2 c_w^2} \right], \\
\tilde{C}_1^{\text{RS}} &= \frac{4\pi L}{M_{\text{KK}}^2} (\tilde{\Delta}_d)_{12} \otimes (\tilde{\Delta}_d)_{12} \left[\frac{\alpha_s}{2} \left(1 - \frac{1}{N_c} \right) + Q_d^2 \alpha + \frac{(s_w^2 Q_d)^2 \alpha}{s_w^2 c_w^2} \right], \\
C_4^{\text{RS}} &= \frac{4\pi L}{M_{\text{KK}}^2} (\tilde{\Delta}_D)_{12} \otimes (\tilde{\Delta}_d)_{12} [-2\alpha_s], \\
C_5^{\text{RS}} &= \frac{4\pi L}{M_{\text{KK}}^2} (\tilde{\Delta}_D)_{12} \otimes (\tilde{\Delta}_d)_{12} \left[\frac{2\alpha_s}{N_c} - 4Q_d^2 \alpha + \frac{4s_w^2 Q_d (T_3^d - s_w^2 Q_d) \alpha}{s_w^2 c_w^2} \right],
\end{aligned} \tag{24}$$

where $Q_d = -1/3$, $T_3^d = -1/2$, and $N_c = 3$. The expressions in brackets refer, in an obvious way, to the contributions from KK gluons, KK photons, and from the Z^0 boson and its KK excitations. As can be seen from (16), the contributions from flavor-changing Higgs-boson exchange are of $\mathcal{O}(v^4/M_{\text{KK}}^4)$ and, in addition, suppressed by two powers of light quark masses. They are thus entirely negligible and we refrain from giving them explicitly. The Wilson coefficients $C_{2,3}$ and $\tilde{C}_{2,3}$ do not receive tree-level contributions in the RS model, as they can only arise from scalar or tensor exchange, but not from gauge interactions. For the cases of $B_d-\bar{B}_d$ and $B_s-\bar{B}_s$ mixing the same expressions hold, but one takes the 13 and 23 entries of the mixing matrices, respectively. For the case of $D-\bar{D}$ mixing one replaces the mixing matrices $\tilde{\Delta}_{D,d}$ with $\tilde{\Delta}_{U,u}$ and takes the 12 entries. Also, in this case $Q_u = 2/3$ and $T_3^u = 1/2$ are the appropriate SM charges. Notice that the QCD contributions are in all cases larger by more than a factor of 3 than the combined QED and electroweak effects, and that the numerically dominant contribution proportional to C_4^{RS} is a pure QCD effect. KK gluon exchange thus dominates all mixing amplitudes in the original RS scenario with SM bulk gauge symmetry. We will see later that this is *not* true for $\Delta F = 1$ processes. In the present case, although QED and electroweak corrections are subleading, we will include them in our numerical analysis.

In passing, we mention that in warped extra-dimension models with extended $SU(2)_R$ symmetry and custodial protection of the $Z^0 b_L \bar{b}_L$ vertex, the corrections arising from new heavy neutral electroweak gauge bosons can compete with the KK gluon corrections to $B_{d,s}-\bar{B}_{d,s}$

mixing [11]. This implies that in this class of models the effects in the observables $\Delta m_{d,s}$, $S_{\psi K_S}$, $S_{\psi\phi}$, $\Delta\Gamma_{d,s}/\Gamma_{d,s}$, and $A_{\text{SL}}^{d,s}$ will typically be more pronounced than in RS formulations without $SU(2)_R$ symmetry. We emphasize that the same pattern of enhancement of electroweak relative to QCD effects is also present in the case of $D-\bar{D}$ mixing. Further comments on the impact of the exact realization of the electroweak sector on both $B_{d,s}-\bar{B}_{d,s}$ and $D-\bar{D}$ mixing are postponed to Sections 5.4.2 and 5.4.3.

The tree-level expressions for the Wilson coefficients given above refer to a renormalization scale $\mu_{\text{KK}} = \mathcal{O}(M_{\text{KK}})$. They must be evolved down to a scale $\mu \approx 2 \text{ GeV}$, where the hadronic matrix elements of the four-quark operators can be evaluated using lattice QCD. The evolution is accomplished with the help of formulas compiled in the literature. For the case of $K-\bar{K}$ mixing these can be found in Eq. (2.6) of [43], for $B_{d,s}-\bar{B}_{d,s}$ mixing they are given in Eq. (9) of [45], and for $D-\bar{D}$ mixing they are listed in Eq. (8) of [41]. The hadronic matrix elements of the various operators are customarily expressed in terms of parameters B_i . For the operators relevant to our analysis, one has²

$$\begin{aligned}\langle K^0 | Q_1(\mu) | \bar{K}^0 \rangle &= \langle K^0 | \tilde{Q}_1(\mu) | \bar{K}^0 \rangle = \left(1 + \frac{1}{N_c}\right) \frac{m_K f_K^2}{4} B_1(\mu), \\ \langle K^0 | Q_4(\mu) | \bar{K}^0 \rangle &= \left[\frac{m_K}{m_s(\mu) + m_d(\mu)}\right]^2 \frac{m_K f_K^2}{4} B_4(\mu), \\ \langle K^0 | Q_5(\mu) | \bar{K}^0 \rangle &= \frac{1}{N_c} \left[\frac{m_K}{m_s(\mu) + m_d(\mu)}\right]^2 \frac{m_K f_K^2}{4} B_5(\mu).\end{aligned}\tag{25}$$

These definitions are such that in the vacuum-insertion approximation (VIA)

$$\begin{aligned}[B_1(\mu)]_{\text{VIA}} &= 1, \\ [B_4(\mu)]_{\text{VIA}} &= 1 + \frac{1}{2N_c} \left[\frac{m_s(\mu) + m_d(\mu)}{m_K}\right]^2, \\ [B_5(\mu)]_{\text{VIA}} &= 1 + \frac{N_c}{2} \left[\frac{m_s(\mu) + m_d(\mu)}{m_K}\right]^2.\end{aligned}\tag{26}$$

Analogous definitions are used for the other mesons. In our numerical analysis we employ the B_i parameters from [46]. Furthermore, we use $m_K = 497.6 \text{ MeV}$ and $f_K = 156.1 \text{ MeV}$ for the kaon mass and decay constant [47]. The hadronic parameters corresponding to $K-\bar{K}$, $B_{d,s}-\bar{B}_{d,s}$, and $D-\bar{D}$ mixing can be found in Table I and Eq. (22), in Table II and Eqs. (24) and (25), and in Eq. (28) of [46], respectively. For the sake of completeness we collect the entire set of B_i parameters entering our calculations in Appendix B.

4.1.2 Important Formulas for Neutral-Meson Mixing

In the following we compile the formulas that we will employ in our numerical analysis of the mixing of neutral mesons with their antiparticles. While physical observables are phase-

²Here the meson states are normalized to $\langle K^0 | K^0 \rangle = \langle \bar{K}^0 | \bar{K}^0 \rangle = 1$.

convention independent, we stress that some of the formulas given below hold only if the standard phase convention for the CKM matrix [47] is adopted.

The K_L - K_S mass difference Δm_K and the CP-violating quantity ϵ_K are given by³

$$\Delta m_K = 2 \operatorname{Re} \langle K^0 | \mathcal{H}_{\text{eff,full}}^{\Delta S=2} | \bar{K}^0 \rangle, \quad \epsilon_K = \frac{\kappa_\epsilon e^{i\varphi_\epsilon}}{\sqrt{2} (\Delta m_K)_{\text{exp}}} \operatorname{Im} \langle K^0 | \mathcal{H}_{\text{eff,full}}^{\Delta S=2} | \bar{K}^0 \rangle, \quad (27)$$

where $\varphi_\epsilon = (43.51 \pm 0.05)^\circ$ and $\kappa_\epsilon = 0.92 \pm 0.02$ [48]. The suppression factor κ_ϵ parametrizes the effects due to the imaginary part of the isospin-zero amplitude in $K \rightarrow \pi\pi$ decays [49, 50, 51].

Taking into account all indirect constraints from the global unitarity-triangle fit [52], we obtain the SM prediction

$$|\epsilon_K|_{\text{SM}} = (2.0 \pm 0.5) \cdot 10^{-3}, \quad (28)$$

where the quoted error corresponds to a frequentist 68% confidence level (CL). The dominant theoretical uncertainty arises from the lattice QCD prediction $B_1(2 \text{ GeV}) = 0.55 \pm 0.05$ [46], which has been scanned in its uncertainty range to obtain the best fit value. Within errors the SM prediction agrees with the experimental value $|\epsilon_K|_{\text{exp}} = (2.229 \pm 0.010) \cdot 10^{-3}$. We do not attempt a prediction for Δm_K , which is plagued by very large hadronic uncertainties.

In the $B_{d,s}$ system one has

$$\Delta m_{B_q} = 2 \left| \langle B_q | \mathcal{H}_{\text{eff,full}}^{\Delta B=2} | \bar{B}_q \rangle \right|, \quad 2\varphi_q = \arg \left(\langle B_q | \mathcal{H}_{\text{eff,full}}^{\Delta B=2} | \bar{B}_q \rangle \right), \quad (29)$$

for $q = d, s$. In all cases the effective Hamiltonian contains the SM contribution plus possible contributions from new physics, as indicated by the subscript “full”. It is also common to normalize the matrix elements of the full effective Hamiltonian to those of only the SM contribution. For instance, one can define [53]

$$C_{B_q} e^{2i\phi_{B_q}} = \frac{\langle B_q | \mathcal{H}_{\text{eff,full}}^{\Delta B=2} | \bar{B}_q \rangle}{\langle B_q | \mathcal{H}_{\text{eff,SM}}^{\Delta B=2} | \bar{B}_q \rangle}. \quad (30)$$

The coefficient C_{B_q} measures the magnitude of the mass difference Δm_q relative to the one in the SM, namely

$$C_{B_q} = \frac{\Delta m_q}{(\Delta m_q)_{\text{SM}}}, \quad (31)$$

while the phases $\phi_{B_{d,s}}$ affect the coefficients of $\sin(\Delta M_{d,st})$ in the time-dependent asymmetries of $B_d \rightarrow \psi K_s$ and $B_s \rightarrow \psi\phi$. One obtains [54]

$$S_{\psi K_s} = \sin(2\beta + 2\phi_{B_d}), \quad S_{\psi\phi} = \sin(2|\beta_s| - 2\phi_{B_s}), \quad (32)$$

where

$$V_{td} = |V_{td}| e^{-i\beta}, \quad V_{ts} = -|V_{ts}| e^{-i\beta_s}, \quad (33)$$

and $\beta \approx 22^\circ$, $\beta_s \approx -1^\circ$. In the presence of non-vanishing phases $\phi_{B_{d,s}}$, the two time-dependent asymmetries thus measure $\varphi_d = \beta + \phi_{B_d}$ and $\varphi_s = |\beta_s| - \phi_{B_s}$, and not β and β_s . We recall

³Here and below, we include in the full effective Hamiltonian a universal correction to the Fermi constant G_F of order m_W^2/M_{KK}^2 [10]. Numerically, these contributions are insignificant in all the FCNC processes we consider.

that the formulas (32) are correct only if no weak phase is present in the $B_d \rightarrow \psi K_s$ and $B_s \rightarrow \psi \phi$ decay amplitudes, as it happens to be the case, to excellent approximation, in the SM. Strictly speaking this assumption does not hold in the case at hand, because in the RS model the charged-current interactions differ from the ones present in the SM. The new contributions are, however, suppressed by m_W^2/M_{KK}^2 . Numerically, it turns out that the value of $\arg(V_{cb}^*V_{cs})$ stays below the level of 0.001° , and that the elements $(V_R)_{22}$ and $(V_R)_{23}$ appearing in the right-handed charged-current interactions do not exceed the level of 10^{-5} in magnitude [10]. These tiny corrections can be safely neglected for all practical purposes.

The width differences $\Delta\Gamma_q$ and the semileptonic CP asymmetries A_{SL}^q take the form

$$\begin{aligned} \frac{\Delta\Gamma_q}{\Gamma_q} &= - \left(\frac{\Delta m_q}{\Gamma_q} \right)_{\text{exp}} \left[\text{Re} \left(\frac{\Gamma_{12}^q}{M_{12}^q} \right)_{\text{SM}} \frac{\cos 2\phi_{B_q}}{C_{B_q}} - \text{Im} \left(\frac{\Gamma_{12}^q}{M_{12}^q} \right)_{\text{SM}} \frac{\sin 2\phi_{B_q}}{C_{B_q}} \right], \\ A_{\text{SL}}^q &= \text{Im} \left(\frac{\Gamma_{12}^q}{M_{12}^q} \right)_{\text{SM}} \frac{\cos 2\phi_{B_q}}{C_{B_q}} - \text{Re} \left(\frac{\Gamma_{12}^q}{M_{12}^q} \right)_{\text{SM}} \frac{\sin 2\phi_{B_q}}{C_{B_q}}, \end{aligned} \quad (34)$$

with [55]

$$\begin{aligned} \text{Re} \left(\frac{\Gamma_{12}^d}{M_{12}^d} \right)_{\text{SM}} &= (-5.26_{-1.28}^{+1.15}) \cdot 10^{-3}, & \text{Im} \left(\frac{\Gamma_{12}^d}{M_{12}^d} \right)_{\text{SM}} &= (-4.8_{-1.2}^{+1.0}) \cdot 10^{-4}, \\ \text{Re} \left(\frac{\Gamma_{12}^s}{M_{12}^s} \right)_{\text{SM}} &= (-4.97 \pm 0.94) \cdot 10^{-3}, & \text{Im} \left(\frac{\Gamma_{12}^s}{M_{12}^s} \right)_{\text{SM}} &= (2.06 \pm 0.57) \cdot 10^{-5}. \end{aligned} \quad (35)$$

Note that the quoted central values for $\text{Re}(\Gamma_{12}^q/M_{12}^q)_{\text{SM}}$ and $\text{Im}(\Gamma_{12}^q/M_{12}^q)_{\text{SM}}$ differ in some cases notably from older determinations. This is mainly due to a different choice of the operator basis used in [55], and it is related to unknown $\mathcal{O}(\alpha_s^2)$ and $\mathcal{O}(\alpha_s\Lambda_{\text{QCD}}/m_b)$ corrections. Although the basis chosen in the latter article leads to smaller theoretical uncertainties, the shifts observed in the central values may signal that the effects of higher-order corrections are larger than previously estimated. While such a possibility cannot be fully excluded, it would not change the conclusions drawn in our work.

The theoretical parameters describing $D-\bar{D}$ mixing can be defined in complete analogy to those for $B_{d,s}-\bar{B}_{d,s}$ mixing. Our sign convention for the phase of the dispersive part of the $D-\bar{D}$ mixing amplitude is

$$M_{12}^D = \langle D^0 | \mathcal{H}_{\text{eff,full}}^{\Delta C=2} | \bar{D}^0 \rangle \equiv |M_{12}^D| e^{-2i\varphi_D}. \quad (36)$$

In contrast to M_{12}^D , the absorptive part of the $D-\bar{D}$ mixing amplitude, Γ_{12}^D , is dominated by SM tree-level interactions and therefore essentially unaffected by the presence of new physics. The small corrections to the charged-current interactions arising in the RS model do not change this conclusion. Motivated by the measurements of meson oscillations in the D system by BaBar [56], Belle [57, 58], and CDF [59], we investigate both the magnitude and phase of the new-physics contributions to (36) in the RS model. We find that the available experimental data already have a non-trivial impact on the allowed model parameters, even if the theoretical uncertainties entering the SM prediction for $D-\bar{D}$ mixing are treated conservatively.

Studies of CP asymmetries in D decays offer another powerful probe of new physics. Experimentally the most striking signature would be the observation of a time-dependent CP asymmetry for a Cabibbo-allowed final state like $D \rightarrow \phi K_S$, in analogy to the case of $B_d \rightarrow \psi K_S$. The coefficient $S_{\phi K_S}^D$ in the time-dependent CP asymmetry of $D \rightarrow \phi K_S$ can be written as

$$S_{\phi K_S}^D = y_D (|q/p|_D - |p/q|_D) \cos 2\tilde{\varphi} - x_D (|q/p|_D + |p/q|_D) \sin 2\tilde{\varphi}, \quad (37)$$

where

$$x_D = \frac{\Delta M_D}{\Gamma_D}, \quad y_D = \frac{\Delta \Gamma_D}{2\Gamma_D}, \quad (38)$$

and

$$(q/p)_D = \sqrt{\frac{M_{12}^{D*} - \frac{i}{2}\Gamma_{12}^{D*}}{M_{12}^D - \frac{i}{2}\Gamma_{12}^D}} \quad \tilde{\varphi} = \frac{1}{2} \arg (q/p)_D$$

$$\Delta M_D = 2 \operatorname{Re} \left[|M_{12}^D|^2 - \frac{1}{4} |\Gamma_{12}^D|^2 - i \operatorname{Re} (\Gamma_{12}^D M_{12}^{D*}) \right]^{1/2},$$

$$\Delta \Gamma_D = -4 \operatorname{Im} \left[|M_{12}^D|^2 - \frac{1}{4} |\Gamma_{12}^D|^2 - i \operatorname{Re} (\Gamma_{12}^D M_{12}^{D*}) \right]^{1/2}, \quad (39)$$

while $\Gamma_D = 1/\tau_D$ denotes the mean width. Under the assumption of negligible direct CP violation, one can then show that the CP asymmetry in semileptonic D decays

$$A_{\text{SL}}^D = \frac{\Gamma(D(t) \rightarrow l^- \bar{\nu} K^{+(*)}) - \Gamma(D(t) \rightarrow l^+ \bar{\nu} K^{-(*)})}{\Gamma(D(t) \rightarrow l^- \bar{\nu} K^{+(*)}) + \Gamma(D(t) \rightarrow l^+ \bar{\nu} K^{-(*)})} = \frac{|q/p|_D^4 - 1}{|q/p|_D^4 + 1}, \quad (40)$$

can be expressed in the limit $||q/p|_D - 1| \ll 1$ and $x_D \approx y_D$ through the CP-violating parameter $S_{\phi K_S}^D$ as [60, 61]

$$A_{\text{SL}}^D = \frac{y_D}{x_D^2 + y_D^2} S_{\phi K_S}^D. \quad (41)$$

Analyzing in detail the predictions for A_{SL}^D and $S_{\phi K_S}^D$ and their correlation in the RS model, we find CP-violating effects in $D-\bar{D}$ mixing that exceed by far the SM expectation. The observation of such large mixing-induced CP asymmetries would be a clear signal of new physics. We will also comment briefly on a number of other charm decays besides $D \rightarrow \phi K_S$, which could offer further insight into the dynamics of CP violation in D decays.

4.2 Rare Non-Leptonic Decays of Kaons and B Mesons

We now study $\Delta F = 1$ processes in the quark sector, focusing on the important FCNC decays mediated by four-quark operators with flavor structure $b \rightarrow sq\bar{q}$. It is straightforward to generalize the discussion to other cases. Processes with leptons will be considered in Section 4.3.

4.2.1 Effective $\Delta B = 1$ Hamiltonian

We write the new-physics contributions to these decays using the usual operator basis Q_{1-10} augmented with chirality-flipped operators \tilde{Q}_{1-10} that are obtained from the original ones by exchanging left- by right-handed fields everywhere. Explicitly, we use

$$\begin{aligned} \mathcal{H}_{\text{eff}}^{\Delta B=1} = & \frac{G_F}{\sqrt{2}} \sum_{q=u,c} \lambda_q^{(sb)} \left(C_1 Q_1^q + C_2 Q_2^q + \sum_{i=3}^{10} C_i Q_i + C_7^\gamma Q_7^\gamma + C_8^g Q_8^g \right) \\ & + \sum_{i=3}^{10} \left(C_i^{\text{RS}} Q_i + \tilde{C}_i^{\text{RS}} \tilde{Q}_i \right), \end{aligned} \quad (42)$$

where $\lambda_q^{(pr)} \equiv V_{qp}^* V_{qr}$ and $Q_{1,2}^q$ are the left-handed current-current operators arising from W^\pm -boson exchange, Q_{3-6} and Q_{7-10} are QCD and electroweak penguin operators, and Q_7^γ and Q_8^g are the electromagnetic and chromomagnetic dipole operators. The operators relevant to our discussion are defined as

$$\begin{aligned} Q_3 &= 4 (\bar{s}_L \gamma^\mu b_L) \sum_q (\bar{q}_L \gamma_\mu q_L), & Q_4 &= 4 (\bar{s}_L^\alpha \gamma^\mu b_L^\beta) \sum_q (\bar{q}_L^\beta \gamma_\mu q_L^\alpha), \\ Q_5 &= 4 (\bar{s}_L \gamma^\mu b_L) \sum_q (\bar{q}_R \gamma_\mu q_R), & Q_6 &= 4 (\bar{s}_L^\alpha \gamma^\mu b_L^\beta) \sum_q (\bar{q}_R^\beta \gamma_\mu q_R^\alpha), \\ Q_7 &= 6 (\bar{s}_L \gamma^\mu b_L) \sum_q Q_q (\bar{q}_R \gamma_\mu q_R), & Q_8 &= 6 (\bar{s}_L^\alpha \gamma^\mu b_L^\beta) \sum_q Q_q (\bar{q}_R^\beta \gamma_\mu q_R^\alpha), \\ Q_9 &= 6 (\bar{s}_L \gamma^\mu b_L) \sum_q Q_q (\bar{q}_L \gamma_\mu q_L), & Q_{10} &= 6 (\bar{s}_L^\alpha \gamma^\mu b_L^\beta) \sum_q Q_q (\bar{q}_L^\beta \gamma_\mu q_L^\alpha). \end{aligned} \quad (43)$$

A summation over color indices α, β and flavors $q = u, d, s, c, b$ is implied. To leading order in small parameters, we obtain

$$\begin{aligned} C_3^{\text{RS}} &= \frac{\pi \alpha_s}{M_{\text{KK}}^2} \frac{(\Delta'_D)_{23}}{2N_c} - \frac{\pi \alpha}{6s_w^2 c_w^2 M_{\text{KK}}^2} (\Sigma_D)_{23}, & \tilde{C}_3^{\text{RS}} &= \frac{\pi \alpha_s}{M_{\text{KK}}^2} \frac{(\Delta'_d)_{23}}{2N_c}, \\ C_4^{\text{RS}} &= C_6^{\text{RS}} = -\frac{\pi \alpha_s}{2M_{\text{KK}}^2} (\Delta'_D)_{23}, & \tilde{C}_4^{\text{RS}} &= \tilde{C}_6^{\text{RS}} = -\frac{\pi \alpha_s}{2M_{\text{KK}}^2} (\Delta'_d)_{23}, \\ C_5^{\text{RS}} &= \frac{\pi \alpha_s}{M_{\text{KK}}^2} \frac{(\Delta'_D)_{23}}{2N_c}, & \tilde{C}_5^{\text{RS}} &= \frac{\pi \alpha_s}{M_{\text{KK}}^2} \frac{(\Delta'_d)_{23}}{2N_c} + \frac{\pi \alpha}{6s_w^2 c_w^2 M_{\text{KK}}^2} (\Sigma'_d)_{23}, \\ C_7^{\text{RS}} &= \frac{2\pi \alpha}{9M_{\text{KK}}^2} (\Delta'_D)_{23} - \frac{2\pi \alpha}{3c_w^2 M_{\text{KK}}^2} (\Sigma_D)_{23}, & \tilde{C}_7^{\text{RS}} &= \frac{2\pi \alpha}{9M_{\text{KK}}^2} (\Delta'_d)_{23} - \frac{2\pi \alpha}{3s_w^2 M_{\text{KK}}^2} (\Sigma'_d)_{23}, \\ C_8^{\text{RS}} &= C_{10}^{\text{RS}} = 0, & \tilde{C}_8^{\text{RS}} &= \tilde{C}_{10}^{\text{RS}} = 0, \\ C_9^{\text{RS}} &= \frac{2\pi \alpha}{9M_{\text{KK}}^2} (\Delta'_D)_{23} + \frac{2\pi \alpha}{3s_w^2 M_{\text{KK}}^2} (\Sigma_D)_{23}, & \tilde{C}_9^{\text{RS}} &= \frac{2\pi \alpha}{9M_{\text{KK}}^2} (\Delta'_d)_{23} + \frac{2\pi \alpha}{3c_w^2 M_{\text{KK}}^2} (\Sigma'_d)_{23}, \end{aligned} \quad (44)$$

where

$$\Sigma_A \equiv L \left(\frac{1}{2} - \frac{s_w^2}{3} \right) \Delta_A + \frac{M_{\text{KK}}^2}{m_Z^2} \delta_A, \quad \Sigma'_A \equiv L \frac{s_w^2}{3} \Delta_A + \frac{M_{\text{KK}}^2}{m_Z^2} \delta_A. \quad (45)$$

It is an interesting fact that in this case the QCD contributions from KK gluon exchange no longer give the dominant contributions to the Wilson coefficients. The effects due to Z^0 -boson exchange are enhanced by an extra factor of L , which compensates for the smaller gauge couplings. Numerically one finds that relative to $C_{4,6}^{\text{RS}}$ the Wilson coefficients C_3^{RS} , C_5^{RS} , C_7^{RS} , and C_9^{RS} are typically a factor of about 2, 1/3, 3, and 9 bigger/smaller in magnitude. The chirality-flipped coefficients \tilde{C}_{3-10} are generically very small in the model at hand, since they involve right-handed fermion profiles that are naturally more UV-localized than their left-handed counterparts. We will come back to this point in Section 5.5.1.

4.2.2 Important Formulas for ϵ'_K/ϵ_K

The Wilson coefficients of the various penguin operators in (42) enter the prediction for ϵ'_K/ϵ_K which measures the ratio of the direct and indirect CP-violating contributions to $K \rightarrow \pi\pi$. Unfortunately, unlike the rare K decays with leptons in the final state, the observable ϵ'_K/ϵ_K is affected by large hadronic uncertainties. In spite of the large theory errors, a study of ϵ'_K/ϵ_K can provide useful information on the flavor structure of the underlying theory, since this ratio depends very sensitively on the relative size of QCD and electroweak penguin contributions, which cancel to a large extent in the SM. The strong sensitivity of ϵ'_K/ϵ_K to the electroweak penguin sector can furthermore lead to interesting correlations with the rare $K \rightarrow \pi\nu\bar{\nu}$ and $K_L \rightarrow \pi^0 l^+ l^-$ decays. One goal of our work is it to investigate to which extent such correlations exist in the RS scenario.

In the presence of new-physics contributions to the Wilson coefficients of the operators Q_{3-10} and their chirality-flipped partners \tilde{Q}_{3-10} , the ratio ϵ'_K/ϵ_K can be approximated by⁴

$$\frac{\epsilon'_K}{\epsilon_K} = -\text{Im} \left(\lambda_t^{(ds)} F_{\text{SM}} + F_{\text{RS}} \right) \frac{|\epsilon_K|_{\text{exp}}}{|\epsilon_K|}, \quad (46)$$

where

$$\begin{aligned} F_{\text{SM}} &= -1.4 + 13.6 R_6 - 6.4 R_8, \\ F_{\text{RS}} &= 27.1 K_3 - 56.1 K_4 + 8.7 K_5 + 36.0 K_6 - 544.4 K_7 - 1663.5 K_8 \\ &\quad + 141.0 K_9 + 56.1 K_{10} - (11.4 K_3 + 61.5 K_4 - 177.1 K_5 - 479.1 K_6 \\ &\quad + 6.0 K_7 + 27.5 K_8 - 18.7 K_9 + 16.4 K_{10}) R_6 - (17.6 K_3 - 45.0 K_4 \\ &\quad + 90.8 K_5 + 218.6 K_6 - 8976.4 K_7 - 28190.5 K_8 + 102.4 K_9 + 23.8 K_{10}) R_8, \end{aligned} \quad (47)$$

and $|\epsilon_K|_{\text{exp}} = (2.229 \pm 0.010) \cdot 10^{-3}$ [47], while $|\epsilon_K|$ denotes the value obtained in the RS model. This formula has been derived following the approach outlined in detail in [62, 63]. The function F_{SM} comprises the information on the SM contributions to the Wilson coefficients of the $\Delta S = 1$ weak effective Hamiltonian at the next-to-leading order [64, 65, 66, 67, 68, 69]. The given expression corresponds to a charm-quark renormalization scale of $\mu_c = 1.3$ GeV and the central values of the SM parameters $\alpha_s(m_Z) = 0.118 \pm 0.003$ [47] and $m_{t,\text{pole}} = (172.6 \pm 1.4)$ GeV

⁴The fact that, accidentally, $\arg(\epsilon_K) \approx \arg(\epsilon'_K)$, implies that $\text{Re}(\epsilon'_K/\epsilon_K) \approx \epsilon'_K/\epsilon_K$.

[70]. We have employed two-loop formulas to calculate $\alpha_s(\mu)$ from $\alpha_s(m_Z)$ and to convert the top-quark mass from the pole into the $\overline{\text{MS}}$ scheme.

For the coefficients K_i entering the new-physics contribution F_{RS} we obtain

$$K_i = \frac{2s_w^2 c_w^2 m_Z^2}{\pi\alpha} \left(C_i^{\text{RS}} - \tilde{C}_i^{\text{RS}} \right), \quad i = 3, \dots, 10, \quad (48)$$

where the minus sign is a consequence of $\langle \pi\pi | \tilde{Q}_i | K \rangle = -\langle \pi\pi | Q_i | K \rangle$. The electromagnetic coupling constant α as well as the Wilson coefficients C_i^{RS} and \tilde{C}_i^{RS} are taken to be renormalized at the scale m_W . In our numerical analysis we determine C_i^{RS} and \tilde{C}_i^{RS} from the initial conditions in (44) using the leading-order RG equations for the evolution from M_{KK} down to m_W . Notice that the inclusion of running effects is necessary to obtain correct results in this case, because a non-zero value of K_8 , having the largest numerical coefficient in (47), is only generated through operator mixing. Details on the latter issue can be found in Appendix A. We also stress that the coefficients K_{3-10} (48), which in the case of ϵ'_K/ϵ_K are understood to contain the 12 elements of the mixing matrices, have to be calculated in the standard phase convention for the CKM matrix [47] in order to obtain correct results. The same applies to all Wilson coefficients appearing hereafter.

The non-perturbative parameters R_6 and R_8 are given in terms of the hadronic parameters $B_6^{(1/2)} \equiv B_6^{(1/2)}(m_c)$ and $B_8^{(3/2)} \equiv B_8^{(3/2)}(m_c)$ and the strange- and down-quark masses as

$$R_i \equiv B_i^{(j)} \left[\frac{121 \text{ MeV}}{m_s(m_c) + m_d(m_c)} \right]^2. \quad (49)$$

The hadronic parameters present the dominant source of theoretical uncertainty in the prediction of the ratio ϵ'_K/ϵ_K . The current status of the calculation of the $\langle \pi\pi | Q_{6,8} | K \rangle$ matrix elements is reviewed in [71]. While $B_8^{(3/2)} = 1.0 \pm 0.2$ is obtained in various approaches, the situation with $B_6^{(1/2)}$ is far less clear. For instance, in the framework of the $1/N$ expansion, values for $B_6^{(1/2)}$ notably above unity are obtained [72, 73, 74, 75]. For example, the articles [72, 74] find $B_6^{(1/2)} = 2.5 \pm 0.4$ and $B_8^{(3/2)} = 1.1 \pm 0.3$. On the other hand, while the lattice values of $B_8^{(3/2)}$ are compatible with unity [76, 77], they are lower than 1 for $B_6^{(1/2)}$ [78, 79].

In view of the rather uncertain value of $B_6^{(1/2)}$, we adopt a conservative point of view and scan the hadronic parameters in our SM analysis of ϵ'_K/ϵ_K over the ranges

$$B_6^{(1/2)} = [0.8, 2.0], \quad B_8^{(3/2)} = [0.8, 1.2]. \quad (50)$$

requiring in addition $B_6^{(1/2)} > B_8^{(3/2)}$, as suggested by studies of the $\langle \pi\pi | Q_{6,8} | K \rangle$ matrix elements in the framework of the $1/N$ expansion [72, 73, 74, 75]. We furthermore employ the values

$$m_s(m_c) = (115 \pm 20) \text{ MeV}, \quad m_d(m_c) = (6 \pm 2) \text{ MeV} \quad (51)$$

for the running quark masses. The quoted central value of the strange-quark mass corresponds to $m_s(2 \text{ GeV}) = 100 \text{ GeV}$, which is in the ballpark of a number of recent determinations [47].

Our SM prediction reads

$$\left(\frac{\epsilon'_K}{\epsilon_K} \right)_{\text{SM}} = \left(8.8_{-4.8}^{+41.2} \right) \cdot 10^{-4}, \quad (52)$$

where the quoted central value has been obtained from (46) by setting $F_{\text{RS}} = 0$ and $R_{6,8} = 1$. In particular, it includes the normalization factor $|\epsilon_K|_{\text{exp}}/|\epsilon_K|_{\text{SM}}$ with $|\epsilon_K|_{\text{SM}}$ taken from (28). Rather than corresponding to a 68% CL, the given uncertainties represent the ranges in which we believe that the true value of $(\epsilon'_K/\epsilon_K)_{\text{SM}}$ lies within a high probability. Note that within errors the SM prediction is in agreement with the experimental value $(\epsilon'_K/\epsilon_K)_{\text{exp}} = (16.5 \pm 2.6) \cdot 10^{-4}$ [47]. In our numerical analysis of ϵ'_K/ϵ_K in the RS scenario, we scan independently over the ranges given in (50) and (51), requiring $B_6^{(1/2)} > B_8^{(3/2)}$, and check whether it is possible to achieve agreement with the measured value. We will see later on that even with such a conservative treatment of errors the constraint from ϵ'_K/ϵ_K has a non-negligible effect on the possible new-physics effects in rare K decays within the RS model.

4.2.3 Important Formulas for Non-Leptonic B Decays

In the following we will present formulas for a few of the most interesting observables in the vast array of measurements in the field of exclusive hadronic decays of B mesons. We will consider two-body decays of the type $\bar{B} \rightarrow PP$ and $\bar{B} \rightarrow PV$, where P and V stand for light pseudoscalar and longitudinally polarized vector mesons, respectively. Parity invariance of the strong interactions allows us to relate the hadronic matrix elements of the opposite-chirality operators \tilde{Q}_i to those of the corresponding SM operators Q_i . It follows that for $\bar{B} \rightarrow PP$ decay modes the new-physics contributions enter via the differences $(C_i^{\text{RS}} - \tilde{C}_i^{\text{RS}})$ of Wilson coefficients, while for $\bar{B} \rightarrow PV$ decay modes they enter via the sums $(C_i^{\text{RS}} + \tilde{C}_i^{\text{RS}})$. The structure of the effective Hamiltonian (42) then implies that the RS contributions can be included by the replacement rule

$$\begin{aligned} \frac{G_F}{\sqrt{2}} (\lambda_u^{(sb)} + \lambda_c^{(sb)}) C_i &\rightarrow \frac{G_F}{\sqrt{2}} (\lambda_u^{(sb)} + \lambda_c^{(sb)}) C_i + (C_i^{\text{RS}} \mp \tilde{C}_i^{\text{RS}}) \\ &= \frac{G_F}{\sqrt{2}} \left[(\lambda_u^{(sb)} + \lambda_c^{(sb)}) C_i + \overset{(-)}{K}_i \right], \quad i = 3, \dots, 10, \end{aligned} \quad (53)$$

where the upper (lower) sign refers to PP (PV) modes, and the coefficients K_i have been defined in (48). For PV modes, the K_i are replaced by coefficients \bar{K}_i defined analogously, but with a relative plus sign between C_i^{RS} and \tilde{C}_i^{RS} . The remaining Wilson coefficients $C_{1,2}$, C_7^γ , and C_8^g are unchanged at tree level.

Most of the complications in the analysis of exclusive hadronic decays originate from complicated strong-interaction physics encoded in the hadronic matrix elements of the local four-quark operators in the effective weak Hamiltonian evaluated between meson states. However, the basis of operators in the RS model is the same as in the SM, apart from the addition of the chirality-flipped operators, whose matrix elements are linked to the ones of the SM by parity invariance as already noted above. The strong-interaction physics is therefore the same as in the SM. For the purposes of our analysis we will adopt the QCD factorization approach [80, 81, 82], which allows for a systematic analysis of the relevant hadronic matrix elements at leading and partially at subleading order in the heavy-quark expansion. Our phenomenological analysis will closely follow corresponding analyses in [82] for $\bar{B} \rightarrow \pi \bar{K}$ decays, and [83, 84] for the analysis of other decays into PP or PV final states. We will also resort to $SU(3)$

symmetry and Fierz relations first employed in [92]. A general analysis of new-physics effects in the decays $\bar{B} \rightarrow \pi\bar{K}$ in a wide class of models giving rise to SM four-quark operators and their chirality-flipped counterparts was presented in [93]. The RS model falls into this class of models, and we will apply some of the strategies proposed in the latter reference in our context.

In the QCD factorization approach to $\bar{B} \rightarrow M_1 M_2$ decays, the decay amplitudes are decomposed into a basis of flavor operators multiplied by coefficients $\alpha_i^q(M_1 M_2)$ and $\beta_i^q(M_1 M_2)$ [84], the latter of which account for the effects of weak annihilation. The index $q = u, c$ indicates that these coefficients are associated with a CKM factor $\lambda_q^{(sb)}$. The $\alpha_i^q(M_1 M_2)$ and $\beta_i^q(M_1 M_2)$ parameters are themselves given in terms of explicit expressions involving the Wilson coefficient functions C_i of the SM.⁵ In order to include the RS contributions, all that is required now is to apply the replacement rule (53), if not stated otherwise.

We emphasize that our study will be exploratory and focus only on a small number of relevant observables, which are particularly interesting with regard to searches for new physics. We will not be concerned here with a comprehensive analysis of strong-interaction uncertainties. For the same reason, we will not consider alternative theoretical schemes such as the perturbative QCD approach [85, 86], the phenomenological $SU(3)$ approach [87, 88], or an approach based on soft-collinear effective theory [89, 90], which is similar in spirit to QCD factorization but differs in the implementation [91]. Our main conclusions will not depend on the scheme used to evaluate the hadronic matrix elements.

We will illustrate the potential impact of the RS contributions by investigating a couple of interesting observables, which probe different aspects of the decay amplitudes such as tree, QCD, and electroweak penguin contributions. The color-allowed SM tree amplitudes are so large that no viable model of new physics can give rise to effects that could compete with them, as this would require new-physics contributions to the Wilson coefficients of $\mathcal{O}(1)$. Moreover, in the SM the QCD penguin amplitudes are larger than the electroweak penguin amplitudes by about an order of magnitude. The non-vanishing RS contributions to the electroweak penguin coefficients are instead at least as big as the coefficients of the QCD penguins, so that we expect to find larger new-physics effects in the electroweak penguin sector.

In the case of $\bar{B} \rightarrow \pi\bar{K}$ decays, the electroweak penguin coefficients are denoted by $\alpha_{3,\text{EW}}^q(\pi\bar{K})$ and $\alpha_{4,\text{EW}}^q(\pi\bar{K})$ in [84]. They receive contributions from the Wilson coefficients C_{7-10} . In the RS model the largest contribution typically stems from the coefficient C_9 . The coefficients $C_{8,10}$ vanish at the matching scale and remain moderately small when the RG evolution from the KK scale down to the weak scale is included. This is shown explicitly in Appendix A. Similarly, the C_7 terms are numerically subdominant because they are suppressed by a factor of roughly $-s_w^2/c_w^2 \approx -1/3$ with respect to C_9 . The dominance of C_9 implies that, like in the SM, $SU(3)$ symmetry and Fierz relations can be used to obtain a model-independent prediction for the leading electroweak penguin effects in terms of a single parameter q , which is free of hadronic uncertainties [92]. In the RS model this parameter is accompanied by a CP-odd phase, which we shall call ϕ . Neglecting small effects arising from

⁵See Eqs. (9), (18), and (19) of [84] for the precise definitions of these coefficients, and Eqs. (31) to (55) for explicit expressions in terms of convolutions of hard-scattering kernels with light-cone distribution amplitudes.

the QCD penguins C_{3-6} , we obtain the approximate formula

$$q = |q| e^{i\phi} \approx q_{\text{SM}} \left[1 - (138 - 45i) K_7 - (8084 + 236i) K_8 - (3430 + 45i) (K_9 + K_{10}) \right], \quad (54)$$

where $q_{\text{SM}} = (0.69 \pm 0.18) e^{i(0.2 \pm 2.1)^\circ}$ is calculable in the SM in terms of the top-quark mass and electroweak parameters. The quoted number corresponds to scenario S4 of hadronic parameters introduced in [84], for which $\gamma = (70 \pm 20)^\circ$. The same set of input will be used for all other SM predictions given below. A complete list of all the relevant theoretical input parameters can be found in Appendix B. The coefficients K_{7-10} have been defined in (48) and are understood to be evaluated at the electroweak scale. While (54) allows for a quantitative understanding of the importance of the different contributions, we will use the complete expressions for $\alpha_{3,\text{EW}}^q(\pi\bar{K})$ and $\alpha_{4,\text{EW}}^q(\pi\bar{K})$ of [84] supplemented by the shift (53) to determine q in our numerical analysis. Corrections due to $SU(3)$ breaking, QCD penguins, and electromagnetic effects in the RG evolution influence the obtained results only in a minor way.

New-physics contributions to the electroweak penguin coefficients can also have a visible impact on the results for the two ratios

$$R_* = \frac{\Gamma(B^- \rightarrow \pi^- \bar{K}^0) + \Gamma(B^+ \rightarrow \pi^+ K^0)}{2[\Gamma(B^- \rightarrow \pi^0 K^-) + \Gamma(B^+ \rightarrow \pi^0 K^+)]}, \quad (55)$$

$$R_{00} = \frac{2[\Gamma(\bar{B}^0 \rightarrow \pi^0 \bar{K}^0) + \Gamma(B^0 \rightarrow \pi^0 K^0)]}{\Gamma(B^- \rightarrow \pi^- \bar{K}^0) + \Gamma(B^+ \rightarrow \pi^+ K^0)},$$

of CP-averaged rates. The current experimental values of these ratios are $(R_*)_{\text{exp}} = 0.79 \pm 0.08$ and $(R_{00})_{\text{exp}} = 0.86 \pm 0.09$ [94]. Adding individual errors in quadrature, the theoretical SM predictions obtained using QCD factorization read $(R_*)_{\text{SM}} = 0.88 \pm 0.14$ and $(R_{00})_{\text{SM}} = 0.86 \pm 0.08$.

As another interesting example, we consider the ‘‘puzzle’’ of the observed difference ΔA_{CP} in the direct CP asymmetries $A_{\text{CP}}(B^- \rightarrow \pi^0 K^-)$ and $A_{\text{CP}}(\bar{B}^0 \rightarrow \pi^+ K^-)$. Hereafter we define the asymmetries as

$$A_{\text{CP}}(\bar{B} \rightarrow f) \equiv \frac{\Gamma(\bar{B} \rightarrow \bar{f}) - \Gamma(B \rightarrow f)}{\Gamma(\bar{B} \rightarrow \bar{f}) + \Gamma(B \rightarrow f)}. \quad (56)$$

The present world average of the considered quantity is $(\Delta A_{\text{CP}})_{\text{exp}} = (14.7 \pm 2.7)\%$ [94]. In the SM, theoretical expectations for this difference are very small, typically no more than a few percent. For our reference parameter scenario, we find numerically $(\Delta A_{\text{CP}})_{\text{SM}} = (0.7 \pm 2.9)\%$ which is about 3.5σ below the experimental determination.

To quantify the impact of new physics on R_* , R_{00} , and ΔA_{CP} one has to determine the dependence of the relevant $\bar{B} \rightarrow \pi\bar{K}$ decay amplitudes on the coefficients K_{3-10} . Following the QCD factorization approach of [84], we find the expressions

$$\begin{aligned} \mathcal{A}(B^- \rightarrow \pi^- \bar{K}^0) = & \left[(123.0 - 10.1i) \lambda_u^{(sb)} + (112.9 - 18.6i) \lambda_c^{(sb)} - (270.2 - 102.5i) K_3 \right. \\ & \left. - (368.0 + 3.1i) K_4 - (1079.9 - 384.4i) K_5 - (2951.5 - 1163.3i) K_6 \right] \end{aligned}$$

$$\begin{aligned}
& + (268.1 + 343.1 i) K_7 + (963.3 + 1038.2 i) K_8 + (19.5 + 18.4 i) K_9 \\
& + (512.3 - 16.8 i) K_{10} \Big] \cdot 10^{-8} \text{ GeV} , \\
\sqrt{2} \mathcal{A}(B^- \rightarrow \pi^0 K^-) & = \Big[- (1120.9 - 45.1 i) \lambda_u^{(sb)} + (127.7 - 19.5 i) \lambda_c^{(sb)} - (275.8 - 102.8 i) K_3 \\
& - (383.2 + 2.3 i) K_4 - (1074.6 - 383.9 i) K_5 - (2926.6 - 1162.1 i) K_6 \\
& + (159.1 + 379.8 i) K_7 - (3551.7 - 1249.6 i) K_8 - (1794.7 - 128.7 i) K_9 \\
& - (1354.4 - 68.3 i) K_{10} \Big] \cdot 10^{-8} \text{ GeV} , \\
\sqrt{2} \mathcal{A}(\bar{B}^0 \rightarrow \pi^0 \bar{K}^0) & = \Big[- (527.9 - 71.9 i) \lambda_u^{(sb)} - (101.4 - 18.6 i) \lambda_c^{(sb)} + (264.5 - 103.0 i) K_3 \\
& + (364.4 + 5.6 i) K_4 + (1076.7 - 388.3 i) K_5 + (2956.0 - 1172.9 i) K_6 \\
& + (721.2 + 212.9 i) K_7 - (1799.6 - 763.0 i) K_8 - (1448.3 - 7.0 i) K_9 \\
& - (1013.7 - 119.2 i) K_{10} \Big] \cdot 10^{-8} \text{ GeV} , \\
\mathcal{A}(\bar{B}^0 \rightarrow \pi^+ K^-) & = \Big[- (716.0 + 16.7 i) \lambda_u^{(sb)} + (116.2 - 19.5 i) \lambda_c^{(sb)} - (270.0 - 103.3 i) K_3 \\
& - (379.6 + 4.8 i) K_4 - (1071.4 - 387.8 i) K_5 - (2931.1 - 1171.7 i) K_6 \\
& - (830.2 + 176.2 i) K_7 - (2715.4 + 551.6 i) K_8 - (365.9 - 103.2 i) K_9 \\
& - (853.0 + 34.1 i) K_{10} \Big] \cdot 10^{-8} \text{ GeV} . \tag{57}
\end{aligned}$$

Analogous formulas hold in the case of the CP-conjugated amplitudes with the replacements $\lambda_q^{(sb)} \rightarrow \lambda_q^{(sb)*}$ and $K_i \rightarrow K_i^*$. Notice that the coefficients multiplying the QCD penguin contributions K_{3-6} in the different amplitudes of (57) are, up to possible overall signs, of a similar magnitude. As a result, the quantities R_* , R_{00} , and ΔA_{CP} are to first approximation independent of new physics affecting the QCD penguin sector. For a similar reason also the contribution from K_7 (K_8) cancels to a large extent in the ratios R_* (R_{00}), irrespectively of the precise nature of new physics. In the RS framework, the observables R_* , R_{00} , and ΔA_{CP} receive the largest correction from K_9 , while the remaining electroweak penguin coefficients lead to subleading but non-negligible effects.

We will use the penguin-dominated decay mode $B^- \rightarrow \pi^- \bar{K}^0$ to probe both the magnitude and CP-odd phase of the leading QCD penguin amplitude in the $\bar{B} \rightarrow \pi \bar{K}$ system. In the SM the decay $B^- \rightarrow \pi^- \bar{K}^0$ is to a very good approximation dominated by the QCD penguin amplitude $\hat{\alpha}_4^c(\pi \bar{K}) \equiv \alpha_4^c(\pi \bar{K}) + \beta_3^c(\pi \bar{K})$, and as a result the direct CP asymmetry $A_{\text{CP}}(B^- \rightarrow \pi^- \bar{K}^0)$ is expected to be very small, not exceeding the level of a few percent [84]. In our reference parameter scenario, we find $A_{\text{CP}}(B^- \rightarrow \pi^- \bar{K}^0)_{\text{SM}} = (0.4 \pm 0.7)\%$. A significant new-physics contribution to both the QCD and electroweak penguin coefficients with a new CP-odd phase could change this conclusion. The present experimental value

$A_{\text{CP}}(B^- \rightarrow \pi^- \bar{K}^0)_{\text{exp}} = (0.9 \pm 2.5)\%$ [94] still allows for larger effects, so it is interesting to see whether it is possible to saturate the experimental limits in the RS framework.

As a second measure of new-physics effects in the QCD penguin amplitudes we consider

$$R_{P/T} = \left| \frac{V_{ub}}{V_{cb}} \right| \frac{f_\pi}{f_K} \left[\frac{\Gamma(B^- \rightarrow \pi^- \bar{K}^0) + \Gamma(B^+ \rightarrow \pi^+ K^0)}{2[\Gamma(B^- \rightarrow \pi^- \pi^0) + \Gamma(B^+ \rightarrow \pi^+ \pi^0)]} \right]^{1/2}, \quad (58)$$

which in the SM determines to very good accuracy the absolute value of the penguin-to-tree ratio $\hat{\alpha}_4^c(\pi\bar{K})/(\alpha_1(\pi\pi) + \alpha_2(\pi\pi))$. We find $(R_{P/T})_{\text{SM}} = 0.10 \pm 0.03$, which should be compared to the current experimental value $(R_{P/T})_{\text{exp}} = 0.15 \pm 0.01$ [94].

To calculate $R_{P/T}$ in the RS model one needs in addition to (57) the decay amplitude for $B^- \rightarrow \pi^- \pi^0$ and its CP-conjugated counterpart. In terms of the coefficients K_{3-10} , we obtain in QCD factorization

$$\begin{aligned} \sqrt{2}\mathcal{A}(B^- \rightarrow \pi^- \pi^0) = & \left[- (1004.5 - 47.4 i)\lambda_u^{(db)} + (12.4 - 0.5 i)\lambda_c^{(db)} - (4.6 - 0.2 i)K_3 \right. \\ & - (12.5 - 0.7 i)K_4 + (4.5 - 0.4 i)K_5 + (20.5 - 1.0 i)K_6 \\ & - (107.3 - 29.7 i)K_7 - (3711.2 - 170.6 i)K_8 - (1508.6 - 71.9 i)K_9 \\ & \left. - (1519.5 - 72.6 i)K_{10} \right] \cdot 10^{-8} \text{ GeV}, \end{aligned} \quad (59)$$

and $\sqrt{2}\mathcal{A}(B^+ \rightarrow \pi^+ \pi^0)$ is obtained from the above expression by replacing $\lambda_q^{(db)} \rightarrow \lambda_q^{(db)*}$ and $K_i \rightarrow K_i^*$. In the case of $A_{\text{CP}}(B^- \rightarrow \pi^- \bar{K}^0)$, the initial conditions of $C_{3,6,7,9}$ can all contribute in a similar fashion to the prediction, although the corrections arising from the electroweak penguin sector are usually the more important ones. For $R_{P/T}$, on the other hand, one can easily convince oneself that the coefficient C_9 always gives the dominant correction, irrespectively of the exact values of the new CP-odd phases appearing in the remaining coefficients.

New-physics contributions to either the QCD or the electroweak penguin amplitudes can affect the determination of $\sin 2\beta$ from the time-dependent CP asymmetries in neutral B -meson decays into CP eigenstates f . In cases where the decay amplitude $\mathcal{A}(\bar{B}^0 \rightarrow f)$ does not contain a CP-odd phase, the coefficient S_f in the general relation

$$\frac{\Gamma(\bar{B}^0(t) \rightarrow f) - \Gamma(B^0(t) \rightarrow f)}{\Gamma(\bar{B}^0(t) \rightarrow f) + \Gamma(B^0(t) \rightarrow f)} = S_f \sin(\Delta m_B t) - C_f \cos(\Delta m_B t) \quad (60)$$

measures $\sin 2\beta$. However, if the decay amplitude receives a small correction with a different weak phase, then this relation is modified. Parametrizing the admixture as $(1 + e^{-i\gamma} d_f e^{i\phi_f})$, one finds [84]

$$S_f = \frac{\sin 2\beta + 2d_f \cos \phi_f \sin(2\beta + \gamma) + d_f^2 \sin(2\beta + 2\gamma)}{1 + 2d_f \cos \phi_f \cos \gamma + d_f^2}. \quad (61)$$

Unlike the Wilson coefficients of the SM, that are real functions, the coefficients parametrizing the RS contributions contain complex, CP-violating phases. In order to still use the above formula, it is necessary to decompose these parameters into two terms proportional to $\lambda_u^{(sb)}$ and

$\lambda_c^{(sb)}$, which is always possible since $\text{Im}(\lambda_u^{(sb)} \lambda_c^{(sb)*}) \neq 0$. To this end, we define the coefficients

$$\Delta C_i^{(\bar{u})} \equiv \frac{\sqrt{2}}{G_F} \frac{\text{Im}[(C_i^{\text{RS}} \mp \tilde{C}_i^{\text{RS}}) \lambda_c^{(sb)*}]}{\text{Im}(\lambda_u^{(sb)} \lambda_c^{(sb)*})}, \quad \Delta C_i^{(\bar{c})} \equiv \frac{\sqrt{2}}{G_F} \frac{\text{Im}[(C_i^{\text{RS}} \mp \tilde{C}_i^{\text{RS}}) \lambda_u^{(sb)*}]}{\text{Im}(\lambda_c^{(sb)} \lambda_u^{(sb)*})}, \quad (62)$$

which are invariant under phase redefinitions of the quark fields. We then obtain the replacement rule

$$\frac{G_F}{\sqrt{2}} (\lambda_u^{(sb)} + \lambda_c^{(sb)}) C_i \rightarrow \frac{G_F}{\sqrt{2}} \left(\lambda_u^{(sb)} C_i^{(\bar{u})} + \lambda_c^{(sb)} C_i^{(\bar{c})} \right), \quad C_i^{(\bar{q})} \equiv C_i + \Delta C_i^{(\bar{q})}, \quad (63)$$

instead of (53). The RS contributions are now encoded in the *real* quantities $\Delta C_i^{(\bar{q})}$, while the CP-odd phases are carried by the SM parameters $\lambda_u^{(sb)}$ and $\lambda_c^{(sb)}$.

In the SM the corresponding shifts $\Delta S_f \equiv S_f - \sin 2\beta$ for some of the most interesting decay modes are found to be positive and small [84, 95]. Employing $\sin 2\beta = 0.672 \pm 0.023$ [94], we find in the parameter scenario S4 the results

$$\begin{aligned} (\Delta S_{\phi K_S})_{\text{SM}} &= 0.022 \pm 0.013 \pm 0.010, \\ (\Delta S_{\eta' K_S})_{\text{SM}} &= 0.003 \pm 0.010 \pm 0.010, \\ (\Delta S_{\pi^0 K_S})_{\text{SM}} &= 0.138 \pm 0.054 \pm 0.010, \end{aligned} \quad (64)$$

where the second error estimates the theory uncertainty in $\sin 2\beta$ obtained from $B_d \rightarrow \psi K_S$. The current world averages of the shifts read $(\Delta S_{\phi K_S})_{\text{exp}} = (-0.23 \pm 0.18)$, $(\Delta S_{\eta' K_S})_{\text{exp}} = (-0.08 \pm 0.07)$, and $(\Delta S_{\pi^0 K_S})_{\text{exp}} = (-0.10 \pm 0.17)$ [94]. Although the result for each individual mode does not differ significantly from the SM expectation, the central values tend to lie below the SM predictions. While much more data is needed to firmly establish the presence of a new CP-violating phase beyond the SM for each of these modes, we will investigate whether the RS model is able to reproduce the observed deviations.

For the necessary decay amplitudes, we find within QCD factorization

$$\begin{aligned} \mathcal{A}(\bar{B}^0 \rightarrow \phi K_S) &= \left[- (79.7 + 3.4 i) \lambda_u^{(sb)} - (83.7 - 18.2 i) \lambda_c^{(sb)} + (2006.5 - 112.4 i) \bar{K}_3 \right. \\ &\quad + (1570.7 - 108.9 i) \bar{K}_4 + (2123.0 - 325.6 i) \bar{K}_5 + (1667.4 - 634.2 i) \bar{K}_6 \\ &\quad - (1070.5 - 151.0 i) \bar{K}_7 - (1152.3 - 295.2 i) \bar{K}_8 - (953.6 - 43.1 i) \bar{K}_9 \\ &\quad \left. - (1019.0 - 58.1 i) \bar{K}_{10} \right] \cdot 10^{-8} \text{ GeV}, \end{aligned}$$

$$\begin{aligned} \mathcal{A}(\bar{B}^0 \rightarrow \eta' K_S) &= \left[(40.6 + 38.5 i) \lambda_u^{(sb)} + (220.2 - 36.0 i) \lambda_c^{(sb)} - (2046.2 - 87.5 i) K_3 \right. \\ &\quad - (985.3 - 109.3 i) K_4 - (39.7 - 644.2 i) K_5 - (4327.2 - 2052.9 i) K_6 \\ &\quad + (652.0 - 256.3 i) K_7 + (2965.7 - 843.5 i) K_8 + (311.9 - 25.1 i) K_9 \\ &\quad \left. + (841.0 - 34.6 i) K_{10} \right] \cdot 10^{-8} \text{ GeV}, \end{aligned}$$

$$\begin{aligned}
\mathcal{A}(\bar{B}^0 \rightarrow \pi^0 K_S) = & - (373.3 - 50.8 i) \lambda_u^{(sb)} - (71.7 - 13.2 i) \lambda_c^{(sb)} + (187.0 - 72.8 i) K_3 \\
& + (257.6 + 4.0 i) K_4 + (761.3 - 274.5 i) K_5 + (2090.2 - 829.4 i) K_6 \\
& + (510.0 + 150.5 i) K_7 - (1272.5 - 539.5 i) K_8 - (1024.1 - 5.0 i) K_9 \\
& - (716.8 - 84.3 i) K_{10} \Big] \cdot 10^{-8} \text{ GeV}. \tag{65}
\end{aligned}$$

Here the coefficients \bar{K}_i entering the $\bar{B}^0 \rightarrow \phi K_S$ amplitude are defined in analogy to (48), but owing to the vector-like nature of the ϕ meson with the minus replaced by a plus sign. Numerically we find that in the RS model the shifts ΔS_f can receive contributions of comparable size from the matching corrections to $C_{3,6,7,9}$. The corrections arising from the electroweak penguin sector are typically larger than those due to the QCD penguins.

4.3 Rare Leptonic Decays of Kaons and B Mesons

In the following, we consider $\Delta F = 1$ processes in the quark sector that feature leptons in the final state. Both inclusive and exclusive transitions induced by neutral- as well as charged-current interactions are discussed. Before examining the specific decay modes in the RS model, we introduce the effective Hamiltonians describing the $s \rightarrow d\nu\bar{\nu}$, $b \rightarrow sl^+l^-$, and $b \rightarrow ul\bar{\nu}$ transitions.

4.3.1 Effective Hamiltonian for $s \rightarrow d\nu\bar{\nu}$

The effective Hamiltonian describing $s \rightarrow d\nu\bar{\nu}$ transitions reads

$$\mathcal{H}_{\text{eff}}^{s \rightarrow d\nu\bar{\nu}} = C_\nu (\bar{d}_L \gamma^\mu s_L) \sum_l (\bar{\nu}_{lL} \gamma_\mu \nu_{lL}) + \tilde{C}_\nu (\bar{d}_R \gamma^\mu s_R) \sum_l (\bar{\nu}_{lL} \gamma_\mu \nu_{lL}), \tag{66}$$

where the new-physics contributions arising in the RS model are given by

$$C_\nu^{\text{RS}} = \frac{2\pi\alpha}{s_w^2 c_w^2 M_{\text{KK}}^2} (\Sigma_D)_{12}, \quad \tilde{C}_\nu^{\text{RS}} = -\frac{2\pi\alpha}{s_w^2 c_w^2 M_{\text{KK}}^2} (\Sigma'_d)_{12}. \tag{67}$$

Higgs exchange gives no contribution here due to the tininess of neutrino masses.

4.3.2 Effective Hamiltonian for $b \rightarrow sl^+l^-$

The effective Hamiltonian for $b \rightarrow sl^+l^-$ transitions contains the following operators in addition to those entering $\mathcal{H}_{\text{eff}}^{\Delta B=1}$ as given in the previous section:

$$\begin{aligned}
\mathcal{H}_{\text{eff}}^{b \rightarrow sl^+l^-} = & C_{l1} (\bar{s}_L \gamma^\mu b_L) \sum_l (\bar{l}_L \gamma_\mu l_L) + C_{l2} (\bar{s}_L \gamma^\mu b_L) \sum_l (\bar{l}_R \gamma_\mu l_R) \\
& + \tilde{C}_{l1} (\bar{s}_R \gamma^\mu b_R) \sum_l (\bar{l}_R \gamma_\mu l_R) + \tilde{C}_{l2} (\bar{s}_R \gamma^\mu b_R) \sum_l (\bar{l}_L \gamma_\mu l_L) \\
& + C_{l3} (\bar{s}_L b_R) \sum_l (\bar{l}l) + \tilde{C}_{l3} (\bar{s}_R b_L) \sum_l (\bar{l}l), \tag{68}
\end{aligned}$$

where in the RS model

$$\begin{aligned}
C_{l1}^{\text{RS}} &= -\frac{4\pi\alpha}{3M_{\text{KK}}^2} (\Delta'_D)_{23} - \frac{2\pi\alpha(1-2s_w^2)}{s_w^2 c_w^2 M_{\text{KK}}^2} (\Sigma_D)_{23}, \\
C_{l2}^{\text{RS}} &= -\frac{4\pi\alpha}{3M_{\text{KK}}^2} (\Delta'_D)_{23} + \frac{4\pi\alpha}{c_w^2 M_{\text{KK}}^2} (\Sigma_D)_{23}, \\
\tilde{C}_{l1}^{\text{RS}} &= -\frac{4\pi\alpha}{3M_{\text{KK}}^2} (\Delta'_d)_{23} - \frac{4\pi\alpha}{c_w^2 M_{\text{KK}}^2} (\Sigma'_d)_{23}, \\
\tilde{C}_{l2}^{\text{RS}} &= -\frac{4\pi\alpha}{3M_{\text{KK}}^2} (\Delta'_d)_{23} + \frac{2\pi\alpha(1-2s_w^2)}{s_w^2 c_w^2 M_{\text{KK}}^2} (\Sigma'_d)_{23}, \\
C_{l3}^{\text{RS}} &= -\frac{2m_l}{m_h^2 v} \left[\frac{m_s}{v} (\delta_d)_{23} + \frac{m_b}{v} (\delta_D)_{23} \right], \\
\tilde{C}_{l3}^{\text{RS}} &= -\frac{2m_l}{m_h^2 v} \left[\frac{m_b}{v} (\delta_d)_{23} + \frac{m_s}{v} (\delta_D)_{23} \right],
\end{aligned} \tag{69}$$

and m_h denotes the mass of the Higgs boson. In our numerical analysis we will employ $m_h = 150 \text{ GeV}$. Even for such a low Higgs-boson mass the corrections to $b \rightarrow sl^+l^-$ arising from C_{l3}^{RS} and $\tilde{C}_{l3}^{\text{RS}}$ turn out to be tiny due to the strong chiral suppression.

Notice that electromagnetic dipole operators enter the effective Hamiltonian for $b \rightarrow sl^+l^-$ first at the one-loop level and thus are formally subleading with respect to the contributions from semileptonic operators. Whether this formal suppression translates into a numerical one can only be seen by calculating the complete one-loop matching corrections to the Wilson coefficients of the electromagnetic dipole operators in the RS model. Such a computation seems worthwhile but is beyond the scope of this work. The possibility that the inclusion of such one-loop effects could have a non-negligible impact on our results for the various $b \rightarrow sl^+l^-$ observables should however be kept in mind.

4.3.3 Effective Hamiltonian for $b \rightarrow ul\bar{\nu}$

The effective Hamiltonian inducing $b \rightarrow ul\bar{\nu}$ transitions reads

$$\mathcal{H}_{\text{eff}}^{b \rightarrow ul\bar{\nu}} = C_l (\bar{u}_L \gamma^\mu b_L) \sum_l (\bar{\nu}_{lL} \gamma_\mu l_L) + \tilde{C}_l (\bar{u}_R \gamma^\mu b_R) \sum_l (\bar{\nu}_{lL} \gamma_\mu l_L) + \text{h.c.}, \tag{70}$$

where the contributions arising in the RS model are given by

$$C_l^{\text{RS}} = \frac{2\pi\alpha}{s_w^2 c_w^2 m_Z^2} (\mathcal{V}_L)_{13}, \quad \tilde{C}_l^{\text{RS}} = \frac{2\pi\alpha}{s_w^2 c_w^2 m_Z^2} (\mathcal{V}_R)_{13}. \tag{71}$$

For simplicity, we have dropped contributions stemming from Higgs-boson exchange, which are strongly chirally suppressed by the masses of the leptons.

4.3.4 Important Formulas for $K \rightarrow \pi\nu\bar{\nu}$, $K_L \rightarrow \mu^+\mu^-$, and $K_L \rightarrow \pi^0 l^+ l^-$

Below we gather the formulas that we will use in our numerical analysis of rare decays involving kaons. We begin with the ‘‘golden modes’’ $K \rightarrow \pi\nu\bar{\nu}$ and then discuss the theoretically less clean $K_L \rightarrow \mu^+\mu^-$ and $K_L \rightarrow \pi^0 l^+ l^-$ channels, emphasizing that the latter modes can add useful information on the chiral nature of the flavor structure of possible non-standard interactions.

After summation over the three neutrino flavors, the branching ratios for the $K \rightarrow \pi\nu\bar{\nu}$ modes can be written as

$$\mathcal{B}(K_L \rightarrow \pi^0 \nu\bar{\nu}) = \kappa_L (\text{Im } X)^2, \quad (72)$$

$$\mathcal{B}(K^+ \rightarrow \pi^+ \nu\bar{\nu}(\gamma)) = \kappa_+ (1 + \Delta_{\text{EM}}) |X|^2,$$

where $\kappa_L = (2.231 \pm 0.013) \cdot 10^{-10} (\lambda/0.225)^8$ and $\kappa_+ = (0.5173 \pm 0.0025) \cdot 10^{-10} (\lambda/0.225)^8$ capture isospin-breaking corrections in relating $K \rightarrow \pi\nu\bar{\nu}$ to $K \rightarrow \pi e\nu$, while the factor $\Delta_{\text{EM}} = -0.003$ encodes long-distance QED corrections affecting the charged mode [96].

The SM and RS contributions entering the coefficient $X \equiv X_{\text{SM}} + X_{\text{RS}}$ take the form

$$X_{\text{SM}} = \frac{\lambda_t^{(ds)}}{\lambda^5} X_t + \frac{\text{Re } \lambda_c^{(ds)}}{\lambda} P_{c,u}, \quad X_{\text{RS}} = \frac{s_w^4 c_w^2 m_Z^2}{\alpha^2 \lambda^5} \left(C_\nu^{\text{RS}} + \tilde{C}_\nu^{\text{RS}} \right), \quad (73)$$

with $\lambda \equiv |V_{us}|$. The top-quark contribution [97, 98] is $X_t = 1.464 \pm 0.041$, and the parameter $P_{c,u} = (0.41 \pm 0.04) (0.225/\lambda)^4$ includes dimension-six and -eight charm-quark effects and genuine long-distance contributions due to up-quark loops [99, 100, 101, 102].⁶

Adding individual errors in quadrature, we find the following SM predictions for the two $K \rightarrow \pi\nu\bar{\nu}$ branching fractions:

$$\mathcal{B}(K_L \rightarrow \pi^0 \nu\bar{\nu})_{\text{SM}} = (2.7 \pm 0.4) \cdot 10^{-11}, \quad (74)$$

$$\mathcal{B}(K^+ \rightarrow \pi^+ \nu\bar{\nu}(\gamma))_{\text{SM}} = (8.3 \pm 0.9) \cdot 10^{-11}.$$

The quoted errors are dominated by the uncertainties due to the CKM input. In view of the expected improvement in the extraction of the mixing angles, precise measurements of the $K \rightarrow \pi\nu\bar{\nu}$ branching ratios will provide a unique test of the flavor sector of a variety of models of new physics, in particular of those where the strong Cabibbo suppression of the SM amplitude is not present.

The branching ratio of the $K_L \rightarrow \mu^+\mu^-$ decay can be expressed as [103]

$$\mathcal{B}(K_L \rightarrow \mu^+\mu^-) = \left(6.7 + [1.1 \text{Re } Y'_A + y_c \pm y_{\gamma\gamma}]^2 + [0.08 \text{Im } Y'_S]^2 \right) \cdot 10^{-9}, \quad (75)$$

where $y_c = (-0.20 \pm 0.03)$ and $y_{\gamma\gamma} = 0.4 \pm 0.5$ encode the charm-quark contribution [104] and two-photon correction [105], respectively. The sign of the latter contribution depends on the

⁶The parameter $P_{c,u}$ is affected by new-physics contributions of order $m_{Z,W}^2/M_{\text{KK}}^2$ to the neutral- and charged-current interactions present in the RS scenario. Compared to the SM contribution these corrections are negligible. The same applies to the charm-quark effects appearing in $K_L \rightarrow \mu^+\mu^-$.

sign of the $K_L \rightarrow \gamma\gamma$ amplitude, which itself depends on the sign of an unknown low-energy constant. Theoretical arguments suggest that the sign of the $K_L \rightarrow \gamma\gamma$ amplitude is positive [106]. Better measurements of $K_S \rightarrow \pi^0\gamma\gamma$ and $K^+ \rightarrow \pi^+\gamma\gamma$ could settle this issue. The error on $y_{\gamma\gamma}$ reflects only the uncertainty on the dispersive part of the two-photon amplitude, which at present is the dominant individual source of error.

The coefficients $Y'_{A,S}$ are given by

$$Y'_A = y_A + \frac{s_w^2 c_w^2 m_Z^2}{2\pi\alpha^2 \lambda_t^{(ds)}} \left(C_{l1}^{\text{RS}} - C_{l2}^{\text{RS}} + \tilde{C}_{l1}^{\text{RS}} - \tilde{C}_{l2}^{\text{RS}} \right), \quad Y'_S = \frac{s_w^4 c_w^4 m_Z^4}{\alpha^2 m_l m_s} \left(C_{l3}^{\text{RS}} - \tilde{C}_{l3}^{\text{RS}} \right), \quad (76)$$

where $y_A = (-0.68 \pm 0.03)$ is the SM contribution to the Wilson coefficient of the semileptonic axial-vector operator [107], and the coefficients C_{l1-3}^{RS} and $\tilde{C}_{l1-3}^{\text{RS}}$ are understood to contain the 12 entries of the relevant mixing matrices. The coefficient Y'_S describes the correction due to tree-level Higgs-boson exchange. This correction is scale dependent but numerically insignificant, so that in practice one can neglect its RG evolution.

In the SM one finds for the $K_L \rightarrow \mu^+\mu^-$ branching ratio

$$\mathcal{B}(K_L \rightarrow \mu^+\mu^-)_{\text{SM}} = \{7.0 \pm 0.6, 8.5 \pm 1.4\} \cdot 10^{-9}, \quad (77)$$

in the case of positive (negative) sign of the two-photon amplitude. The shown uncertainties have been obtained by adding the individual errors in quadrature. We will see later that, being measured precisely, the $K_L \rightarrow \mu^+\mu^-$ decay can lead to interesting constraints in specific scenarios of new physics.

The branching ratios of the decays $K_L \rightarrow \pi^0 l^+ l^-$ are obtained from

$$\mathcal{B}(K_L \rightarrow \pi^0 l^+ l^-) = (C_{\text{dir}}^l \pm C_{\text{int}}^l |a_S| + C_{\text{mix}}^l |a_S|^2 + C_{\gamma\gamma}^l + C_S^l) \cdot 10^{-12}, \quad (78)$$

where the chiral-perturbation-theory counterterm $|a_S| = 1.20 \pm 0.20$ has been extracted from the measurements of the $K_S \rightarrow \pi^0 l^+ l^-$ branching fraction [108, 109]. The coefficients $C_{\text{dir,int,mix},\gamma\gamma,S}^l$ read [103]

$$\begin{aligned} C_{\text{dir}}^e &= (4.62 \pm 0.24) [(\text{Im } Y_A)^2 + (\text{Im } Y_V)^2], \\ C_{\text{int}}^e &= (11.3 \pm 0.3) \text{Im } Y_V, \\ C_{\text{mix}}^e &= 14.5 \pm 0.5, \\ C_{\gamma\gamma}^e &\approx C_S^e \approx 0, \\ C_{\text{dir}}^\mu &= (1.09 \pm 0.05) [2.32 (\text{Im } Y_A)^2 + (\text{Im } Y_V)^2], \\ C_{\text{int}}^\mu &= (2.63 \pm 0.06) \text{Im } Y_V, \\ C_{\text{mix}}^\mu &= 3.36 \pm 0.20, \\ C_{\gamma\gamma}^\mu &= 5.2 \pm 1.6, \\ C_S^\mu &= (0.04 \pm 0.01) \text{Re } Y_S + 0.0041 (\text{Re } Y_S)^2. \end{aligned} \quad (79)$$

They describe the short-distance direct CP-violating contribution C_{dir}^l , the long-distance indirect CP-violating term C_{mix}^l that can be determined from the experimental data on $K_S \rightarrow \pi^0 l^+ l^-$, and a long-distance CP-conserving correction $C_{\gamma\gamma}^l$ that can be extracted from a measurement of $K_L \rightarrow \pi^0 \gamma\gamma$. The direct and indirect CP-violating amplitudes interfere, leading to the term C_{int}^l . The latest theoretical analyses [110, 111] point towards a constructive interference, corresponding to the plus sign in (78). The correction C_S^l encodes additional contributions due to scalar operators. Both $C_{\gamma\gamma}^l$ and C_S^l are helicity suppressed and thus have in general a negligible effect on the $K_L \rightarrow \pi^0 e^+ e^-$ branching ratio.

The coefficients $Y_{A,V,S}$ take the form

$$\begin{aligned} Y_A &= y_A + \frac{s_w^2 c_w^2 m_Z^2}{2\pi\alpha^2 \lambda_t^{(ds)}} \left(C_{l1}^{\text{RS}} - C_{l2}^{\text{RS}} - \tilde{C}_{l1}^{\text{RS}} + \tilde{C}_{l2}^{\text{RS}} \right), \\ Y_V &= y_V - \frac{s_w^2 c_w^2 m_Z^2}{2\pi\alpha^2 \lambda_t^{(ds)}} \left(C_{l1}^{\text{RS}} + C_{l2}^{\text{RS}} + \tilde{C}_{l1}^{\text{RS}} + \tilde{C}_{l2}^{\text{RS}} \right), \\ Y_S &= \frac{s_w^4 c_w^4 m_Z^4}{\alpha^2 m_l m_s} \left(C_{l3}^{\text{RS}} + \tilde{C}_{l3}^{\text{RS}} \right), \end{aligned} \quad (80)$$

where $y_V = 0.73 \pm 0.04$ represents the SM contribution to the Wilson coefficient of the semileptonic vector operator [107], and C_{l1-3}^{RS} and $\tilde{C}_{l1-3}^{\text{RS}}$ involve the 12 entries of the appropriate mixing matrices. The coefficients C_{l1-3}^{RS} and $\tilde{C}_{l1-3}^{\text{RS}}$ entering Y_V are understood to be evaluated at a low-energy scale $\mu \approx 1 \text{ GeV}$. In our numerical analysis we use leading-order RG running to determine these coefficients from the initial conditions of $C_{3-6,l1-3}^{\text{RS}}$ and $\tilde{C}_{3-6,l1-3}^{\text{RS}}$ given in (44) and (69). The effect of the new-physics contributions is mainly felt in Y_A , as the corresponding contributions in Y_V cancel each other to a large extent and Y_S is highly suppressed. In consequence, RG effects influence the obtained results only in a minor way.

The SM predictions for the branching ratios of $K_L \rightarrow \pi^0 l^+ l^-$ are

$$\begin{aligned} \mathcal{B}(K_L \rightarrow \pi^0 e^+ e^-)_{\text{SM}} &= \{3.5 \pm 0.9, 1.6 \pm 0.6\} \cdot 10^{-11}, \\ \mathcal{B}(K_L \rightarrow \pi^0 \mu^+ \mu^-)_{\text{SM}} &= \{1.4 \pm 0.3, 0.9 \pm 0.2\} \cdot 10^{-11}, \end{aligned} \quad (81)$$

for constructive (destructive) interference. Better measurements of the $K_S \rightarrow \pi^0 l^+ l^-$ decay rate would allow to improve the quoted errors, which are currently dominated by the uncertainty due to the chiral-perturbation-theory parameter $|a_S|$.

The integrated forward-backward CP asymmetry for $K_L \rightarrow \pi^0 \mu^+ \mu^-$ is given by [103]

$$A_{\text{FB}}(K_L \rightarrow \pi^0 \mu^+ \mu^-) = \frac{(1.3 \pm 0.1) \text{Im} Y_V \mp 0.057 |a_S| \text{Re} Y_S \pm (1.7 \pm 0.2) |a_S|}{\mathcal{B}(K_L \rightarrow \pi^0 \mu^+ \mu^-)} \cdot 10^{-12}, \quad (82)$$

and the corresponding SM predictions read

$$A_{\text{FB}}(K_L \rightarrow \pi^0 \mu^+ \mu^-)_{\text{SM}} = \{21 \pm 4, -12 \pm 4\} \% \quad (83)$$

in the case of constructive (destructive) interference. Despite the fact that the predictions of the decays $K_L \rightarrow \pi^0 l^+ l^-$ are not fully under theoretical control, the latter transitions

represent promising channels to study new physics. In particular, the different impact of helicity-suppressed contributions to the muon and electron modes makes the comparison of $K_L \rightarrow \pi^0 \mu^+ \mu^-$ and $K_L \rightarrow \pi^0 e^+ e^-$ a powerful tool for analyzing the chiral properties of non-standard flavor interactions.

4.3.5 Important Formulas for $B \rightarrow X_q \nu \bar{\nu}$, $B_q \rightarrow \mu^+ \mu^-$, and $B \rightarrow X_s l^+ l^-$

In the following we assemble the formulas that we will employ in the numerical analysis of rare semileptonic and purely leptonic B decays. We thereby focus on the theoretically cleanest observables arising from the quark-level transitions $b \rightarrow q \nu \bar{\nu}$ and $b \rightarrow ql^+ l^-$.

Summing over the three neutrino flavors and neglecting effects proportional to small quark masses, the branching ratio of $B \rightarrow X_q \nu \bar{\nu}$ can be written as

$$\mathcal{B}(B \rightarrow X_q \nu \bar{\nu}) = \mathcal{B}(B \rightarrow X_c l \bar{\nu})_{\text{exp}} \frac{3\alpha^2}{4\pi^2 s_w^4 C} \frac{|\lambda_t^{(qb)}|^2}{\lambda_c^{(bb)}} (|X_L|^2 + |X_R|^2), \quad (84)$$

where $\mathcal{B}(B \rightarrow X_c l \bar{\nu})_{\text{exp}} = 0.1064 \pm 0.0011$ denotes the experimental value of the semileptonic branching ratio [94], and the appropriate value of the electromagnetic coupling is $\alpha(m_Z) = 1/127.9$. In order to minimize the theoretical uncertainties, we have normalized the $B \rightarrow X_q \nu \bar{\nu}$ decay rate to the charmless semileptonic rate $\Gamma(B \rightarrow X_u l \bar{\nu})$ following [112]. Like in the case of the $B \rightarrow X_s \gamma$ decay [113], this modification is offset by the phase-space ratio C defined by

$$C = \frac{\lambda_u^{(bb)}}{\lambda_c^{(bb)}} \frac{\Gamma(B \rightarrow X_c l \bar{\nu})}{\Gamma(B \rightarrow X_u l \bar{\nu})}. \quad (85)$$

In our numerical analyses we employ $C = 0.546_{-0.033}^{+0.023}$, which has recently been extracted from a global fit to the moments of the inclusive $B \rightarrow X_c l \bar{\nu}$ and $B \rightarrow X_s \gamma$ decay distributions [114].

The coefficients $X_{L,R}$ take the form

$$X_L = X_t + \frac{s_w^4 c_w^2 m_Z^2}{\alpha^2 \lambda_t^{(qb)}} C_\nu^{\text{RS}}, \quad X_R = \frac{s_w^4 c_w^2 m_Z^2}{\alpha^2 \lambda_t^{(qb)}} \tilde{C}_\nu^{\text{RS}}, \quad (86)$$

and the coefficients C_ν^{RS} and $\tilde{C}_\nu^{\text{RS}}$ contain the 13 or 23 elements of the relevant mixing matrices.

In the SM one finds for the branching ratios of the $B \rightarrow X_q \nu \bar{\nu}$ decay modes

$$\begin{aligned} \mathcal{B}(B \rightarrow X_d \nu \bar{\nu})_{\text{SM}} &= (1.6 \pm 0.1) \cdot 10^{-6}, \\ \mathcal{B}(B \rightarrow X_s \nu \bar{\nu})_{\text{SM}} &= (3.5 \pm 0.2) \cdot 10^{-5}, \end{aligned} \quad (87)$$

where the error on $\mathcal{B}(B \rightarrow X_d \nu \bar{\nu})$ is in equal shares due to the uncertainty on C and the CKM elements, while the uncertainty of $\mathcal{B}(B \rightarrow X_s \nu \bar{\nu})$ arises almost solely from the one entering the semileptonic phase-space ratio. In view of the small theoretical errors, measurements of $B \rightarrow X_d \nu \bar{\nu}$ would constitute unique probes of the flavor sector of the underlying theory. Besides the inclusive $b \rightarrow q \nu \bar{\nu}$ transitions, also the $B \rightarrow K^{(*)} \nu \bar{\nu}$ channels provide opportunities to search for new physics. Since the pattern of deviations observed in these exclusive modes

follows the one in $B \rightarrow X_s \nu \bar{\nu}$ decays, our discussion of non-standard effects in $B \rightarrow X_q \nu \bar{\nu}$ essentially also applies to the modes $B \rightarrow K^{(*)} \nu \bar{\nu}$.

The branching ratios for the $B_q \rightarrow \mu^+ \mu^-$ decays can be expressed as

$$\begin{aligned} \mathcal{B}(B_q \rightarrow \mu^+ \mu^-) &= \frac{G_F^2 \alpha^2 m_{B_q}^3 f_{B_q}^2 \tau_{B_q}}{64\pi^3 s_w^4} |\lambda_t^{(qb)}|^2 \sqrt{1 - \frac{4m_\mu^2}{m_{B_q}^2}} \\ &\times \left(\frac{4m_\mu^2}{m_{B_q}^2} |C_A - C'_A|^2 + m_{B_q}^2 \left[1 - \frac{4m_\mu^2}{m_{B_q}^2} \right] \left| \frac{m_b C_S - m_q C'_S}{m_b + m_q} \right|^2 \right), \end{aligned} \quad (88)$$

where m_{B_q} , f_{B_q} , and τ_{B_q} are the mass, decay constant, and lifetime of the B_q meson. The electromagnetic coupling α entering the branching ratios should be evaluated at m_Z .

The expressions for the coefficients $C_{A,S}$ and $C'_{A,S}$ read

$$\begin{aligned} C_A &= c_A - \frac{s_w^4 c_w^2 m_Z^2}{\alpha^2 \lambda_t^{(qb)}} \left(C_{l1}^{\text{RS}} - C_{l2}^{\text{RS}} \right), & C'_A &= \frac{s_w^4 c_w^2 m_Z^2}{\alpha^2 \lambda_t^{(qb)}} \left(\tilde{C}_{l1}^{\text{RS}} - \tilde{C}_{l2}^{\text{RS}} \right), \\ C_S &= \frac{2s_w^4 c_w^2 m_Z^2}{\alpha^2 m_b \lambda_t^{(qb)}} C_{l3}^{\text{RS}}, & C'_S &= \frac{2s_w^4 c_w^2 m_Z^2}{\alpha^2 m_q \lambda_t^{(qb)}} \tilde{C}_{l3}^{\text{RS}}, \end{aligned} \quad (89)$$

where $c_A = 0.96 \pm 0.02$ denotes the SM contribution to the Wilson coefficient of the axial-vector current [97, 98], and the coefficients C_{l1-3}^{RS} and $\tilde{C}_{l1-3}^{\text{RS}}$ contain the 13 or 23 elements of the mixing matrices in the case of $B_d \rightarrow \mu^+ \mu^-$ and $B_s \rightarrow \mu^+ \mu^-$, respectively. While C_A and C'_A are scale independent, the coefficients C_S and C'_S have a non-trivial RG evolution. Since the scalar interactions arising from tree-level Higgs-boson exchange are numerically insignificant, the running of C_S and C'_S can however be set to zero without influencing the results for the $B_q \rightarrow \mu^+ \mu^-$ branching fractions in an essential way.

The SM branching ratios of the $B_q \rightarrow \mu^+ \mu^-$ decay channels evaluate to

$$\begin{aligned} \mathcal{B}(B_d \rightarrow \mu^+ \mu^-)_{\text{SM}} &= (1.2 \pm 0.1) \cdot 10^{-10}, \\ \mathcal{B}(B_s \rightarrow \mu^+ \mu^-)_{\text{SM}} &= (3.8 \pm 0.4) \cdot 10^{-9}. \end{aligned} \quad (90)$$

These predictions are obtained by normalizing the decay rates to the well-measured meson mass differences $(\Delta m_q)_{\text{exp}}$. This eliminates the dependence on CKM parameters and the bulk of the hadronic uncertainties by trading the decay constants for less uncertain hadronic parameters [115]. The dominant source of error is nevertheless still provided by the hadronic input. Leptonic B -meson decays belong to the channels that can be studied by three out of the four major CERN Large Hadron Collider (LHC) experiments, namely ATLAS, CMS, and LHCb. These experiments will probe the branching fraction of $B_s \rightarrow \mu^+ \mu^-$ down to its SM value and might reveal a signal of new physics well ahead of the direct searches.

Normalizing the $B \rightarrow X_s l^+ l^-$ decay width to $\Gamma(B \rightarrow X_u l \bar{l})$ and neglecting effects proportional to the strange-quark mass, the branching ratio of the rare semileptonic decay integrated over the range $s \in [s_0, s_1]$ of the rescaled invariant dilepton mass $s \equiv q^2/m_{b,\text{pole}}^2 \in [0, 1]$ can be

written as

$$\mathcal{B}(B \rightarrow X_s l^+ l^-)^{s \in [s_0, s_1]} = \frac{\mathcal{B}(B \rightarrow X_c e \bar{\nu})_{\text{exp}}}{C} \frac{\lambda_u^{(bb)}}{\lambda_c^{(bb)}} \int_{s_0}^{s_1} ds \frac{1}{\Gamma(B \rightarrow X_u e \bar{\nu})} \frac{d\Gamma(B \rightarrow X_s l^+ l^-)}{ds}, \quad (91)$$

where

$$\begin{aligned} \frac{d\Gamma(B \rightarrow X_s l^+ l^-)}{ds} &= \frac{G_F^2 m_{b,\text{pole}}^5 |\lambda_t^{(sb)}|^2}{48\pi^3} \left(\frac{\alpha}{4\pi}\right)^2 (1-s)^2 \left[\left(4 + \frac{8}{s}\right) |C_{7,\text{BR}}^{\gamma\text{eff}}(s)|^2 \right. \\ &+ (1+2s) \left(|C_{9,\text{BR}}^{l\text{eff}}(s)|^2 + |C_{10,\text{BR}}^{l\text{eff}}(s)|^2 + |\tilde{C}_{9,\text{BR}}^{l\text{eff}}(s)|^2 + |\tilde{C}_{10,\text{BR}}^{l\text{eff}}(s)|^2 \right) \\ &\left. + 12 \text{Re} \left(C_{7,\text{BR}}^{\gamma\text{eff}}(s) C_{9,\text{BR}}^{l\text{eff}}(s)^* \right) + \frac{d\Gamma^{\text{brems}}(B \rightarrow X_s l^+ l^-)}{ds} \right]. \end{aligned} \quad (92)$$

Here α is taken to be renormalized at the scale m_b , and $C_{7,\text{BR}}^{\gamma\text{eff}}(s)$, $C_{9,10,\text{BR}}^{l\text{eff}}(s)$, and $\tilde{C}_{9,10,\text{BR}}^{l\text{eff}}(s)$ denote the low-energy Wilson coefficients of the electromagnetic dipole, vector, and axial-vector semileptonic operators and their counterparts obtained by exchanging left- with right-handed quark fields. The effective Wilson coefficients $C_{9,10,\text{BR}}^{l\text{eff}}(s)$ include all known real and virtual QCD and electroweak SM corrections [116, 117, 118, 119, 120, 121, 122], while the last term encodes the finite bremsstrahlung corrections calculated in [123]. At leading order the coefficients $C_{7,\text{BR}}^{\gamma\text{eff}}(s)$ and $C_{9,10,\text{BR}}^{l\text{eff}}(s)$ are identical to C_7^γ and $C_{9,10}^l$. Beyond leading order the definitions of the effective Wilson coefficients are affected by the presence of both the QCD and the electroweak penguin operators Q_{3-6} and Q_{7-10} as well as their chirality-flipped analogs. In our analyses of the $b \rightarrow sl^+l^-$ observables we include all new-physics corrections to $C_{9,\text{BR}}^{l\text{eff}}(s)$ and $\tilde{C}_{9,\text{BR}}^{l\text{eff}}(s)$ stemming from the one-loop matrix elements of the operators Q_{3-10} and \tilde{Q}_{3-10} . However, the inclusion of these effects has only a minor impact on the results.

At the matching scale $\mu_{\text{KK}} = \mathcal{O}(M_{\text{KK}})$ the new contributions to the Wilson coefficients $C_{9,10}^l$ and $\tilde{C}_{9,10}^l$ arising in the RS scenario are

$$\begin{aligned} C_9^{l\text{RS}} &= \frac{\alpha_s s_w^2 c_w^2 m_Z^2}{4\pi\alpha^2 \lambda_t^{(sb)}} \left(C_{l1}^{\text{RS}} + C_{l2}^{\text{RS}} \right), & C_{10}^{l\text{RS}} &= -\frac{\alpha_s \tilde{s}_w^2 c_w^2 m_Z^2}{4\pi\alpha^2 \lambda_t^{(sb)}} \left(C_{l1}^{\text{RS}} - C_{l2}^{\text{RS}} \right), \\ \tilde{C}_9^{l\text{RS}} &= \frac{\alpha_s s_w^2 c_w^2 m_Z^2}{4\pi\alpha^2 \lambda_t^{(sb)}} \left(\tilde{C}_{l1}^{\text{RS}} + \tilde{C}_{l2}^{\text{RS}} \right), & \tilde{C}_{10}^{l\text{RS}} &= \frac{\alpha_s s_w^2 c_w^2 m_Z^2}{4\pi\alpha^2 \lambda_t^{(sb)}} \left(\tilde{C}_{l1}^{\text{RS}} - \tilde{C}_{l2}^{\text{RS}} \right), \end{aligned} \quad (93)$$

where the coefficients C_{l1-3}^{RS} and $\tilde{C}_{l1-3}^{\text{RS}}$ depend on the 23 entries of the appropriate mixing matrices. Notice that C_7^γ does not receive corrections at tree level. The Wilson coefficients C_9^l and \tilde{C}_9^l depend of the renormalization scale, while C_{10}^l and \tilde{C}_{10}^l are scale independent. In our analysis we include the running of C_9^l and \tilde{C}_9^l at leading order in the strong coupling constant. Although RG effects change the values of C_9^l and \tilde{C}_9^l drastically, the inclusion of the running has only a slight impact on the $b \rightarrow sl^+l^-$ observables, because the contributions due to the semileptonic vector operators are generically much smaller than the corresponding axial-vector corrections.

In order to allow for an understanding of the importance of the different new-physics contributions to $B \rightarrow X_s l^+ l^-$ in the RS model, we derive an approximate formula for the branching ratio integrated over the low- q^2 region with $q^2 \in [1, 6] \text{ GeV}^2$. Neglecting new-physics effects arising from the one-loop matrix elements of Q_{3-10} and \tilde{Q}_{3-10} , we find in terms of the Wilson coefficients evaluated at the low-energy scale $\mu = m_b$ the expression

$$\mathcal{B}(B \rightarrow X_s l^+ l^-)^{q^2 \in [1, 6] \text{ GeV}^2} = 1.68 \left[1 + 0.17 \text{Re} C_9^{l \text{RS}} - 0.29 \text{Re} C_{10}^{l \text{RS}} + 0.03 \left(|C_9^{l \text{RS}}|^2 + |C_{10}^{l \text{RS}}|^2 + |\tilde{C}_9^{l \text{RS}}|^2 + |\tilde{C}_{10}^{l \text{RS}}|^2 \right) \right] \cdot 10^{-6}. \quad (94)$$

The corresponding SM prediction amounts to

$$\mathcal{B}(B \rightarrow X_s l^+ l^-)_{\text{SM}}^{q^2 \in [1, 6] \text{ GeV}^2} = (1.7 \pm 0.2) \cdot 10^{-6}, \quad (95)$$

when individual uncertainties are added in quadrature. At present the dominant source of error is associated to non-perturbative effects related to the cut on the invariant hadronic mass M_{X_s} [124, 125, 126] and to unknown enhanced non-local power corrections of $\mathcal{O}(\alpha_s \Lambda_{\text{QCD}}/m_b)$ [127]. We assume that in combination these non-perturbative effects introduce an uncertainty of 5%. The sensitivity of the SM prediction on the Wilson coefficients $C_{9,10}^l$ and $\tilde{C}_{9,10}^l$ in the high- q^2 region, $q^2 > 14 \text{ GeV}^2$, is essentially the same as the one for low q^2 , while at high q^2 theory uncertainties are considerably larger than in the low- q^2 range. We therefore restrict our attention to the low- q^2 region as far as $B \rightarrow X_s l^+ l^-$ is concerned. We emphasize, however, that all of our findings also apply in a similar fashion to the high- q^2 range.

We also consider the so-called normalized $B \rightarrow X_s l^+ l^-$ forward-backward asymmetry defined as

$$\bar{A}_{\text{FB}}(B \rightarrow X_s l^+ l^-) = \left(\frac{d\Gamma(B \rightarrow X_s l^+ l^-)}{ds} \right)^{-1} \int_{-1}^1 dz \text{sgn}(z) \frac{d^2\Gamma(B \rightarrow X_s l^+ l^-)}{ds dz}, \quad (96)$$

where for a vanishing strange-quark mass one has

$$\int_{-1}^1 dz \text{sgn}(z) \frac{d^2\Gamma(B \rightarrow X_s l^+ l^-)}{ds dz} = \frac{G_F^2 m_{b,\text{pole}}^5 |\lambda_t^{(sb)}|^2}{48\pi^3} \left(\frac{\alpha}{4\pi} \right)^2 (1-s)^2 \times \left[-3s \text{Re} \left(C_{9,\text{FB}}^{l \text{eff}}(s) C_{10,\text{FB}}^{l \text{eff}}(s)^* - \tilde{C}_{9,\text{FB}}^{l \text{eff}}(s) \tilde{C}_{10,\text{FB}}^{l \text{eff}}(s)^* \right) - 6 \text{Re} \left(C_{7,\text{FB}}^{\gamma \text{eff}}(s) C_{10,\text{FB}}^{l \text{eff}}(s)^* \right) + A_{\text{FB}}^{\text{brems}}(B \rightarrow X_s l^+ l^-) \right]. \quad (97)$$

The variable $z \equiv \cos \theta$ denotes the cosine of the angle between the directions of the momenta of the decaying B meson and the positively-charged lepton measured in the dilepton center-of-mass frame. We include all known effects [116, 118, 119, 120, 121, 122, 128, 129, 130]

associated with $C_{9,\text{FB}}^{l\text{eff}}(s)$, $\tilde{C}_{9,\text{FB}}^{l\text{eff}}(s)$, and $A_{\text{FB}}^{\text{brems}}(B \rightarrow X_s l^+ l^-)$ in our numerical analysis. The matching corrections to the original Wilson coefficients $C_{9,10}^l$ and $\tilde{C}_{9,10}^l$ have been given in (93).

The position of the zero of the forward-backward asymmetry, q_0^2 , is known to be especially sensitive to non-standard contributions, because in the SM it can be predicted without significant perturbative and hadronic uncertainties. Assuming that q_0^2 does not differ much from its SM prediction, and suppressing subleading non-standard effects associated to the one-loop matrix elements of the operators Q_{3-10} and \tilde{Q}_{3-10} , we obtain the approximate relation

$$q_0^2 = 3.56 \left[\frac{1 - 0.09 \text{Re} C_9^{l\text{RS}} - 0.22 \text{Re} C_{10}^{l\text{RS}} + 0.02 \text{Re} \left(C_9^{l\text{RS}} C_{10}^{l\text{RS}*} - \tilde{C}_9^{l\text{RS}} \tilde{C}_{10}^{l\text{RS}*} \right)}{1 + 0.16 \text{Re} C_9^{l\text{RS}} - 0.22 \text{Re} C_{10}^{l\text{RS}} - 0.03 \text{Re} \left(C_9^{l\text{RS}} C_{10}^{l\text{RS}*} - \tilde{C}_9^{l\text{RS}} \tilde{C}_{10}^{l\text{RS}*} \right)} \right] \text{GeV}^2, \quad (98)$$

where the Wilson coefficients are understood to be evaluated at the scale m_b . The SM prediction for the latter quantity reads

$$q_{0,\text{SM}}^2 = (3.6 \pm 0.3) \text{GeV}^2, \quad (99)$$

when individual uncertainties are added in quadrature. The bulk of the quoted error stems from non-perturbative effects related to the M_{X_s} cut [124, 125, 126] and unknown $\mathcal{O}(\alpha_s \Lambda_{\text{QCD}}/m_b)$ power corrections [127]. We assume again that these non-perturbative effects combined lead to an error of 5%. Precision measurements of the decay distributions of $B \rightarrow X_s l^+ l^-$, possible at a super flavor factory, will allow to probe the nature of the weak interactions encoded in those Wilson coefficients of the semileptonic operators which are not accessible to $B \rightarrow X_s \gamma$.

4.3.6 Important Formulas for $B \rightarrow K^* l^+ l^-$

We focus on the decay $B \rightarrow K^* l^+ l^-$ as one of the phenomenologically most relevant $b \rightarrow s l^+ l^-$ transition and discuss the normalized forward-backward asymmetry $\bar{A}_{\text{FB}}(B \rightarrow K^* l^+ l^-)$ and the longitudinal K^* polarization $F_L(B \rightarrow K^* l^+ l^-)$, which are already accessible experimentally. It is straightforward to extend the discussion to other decay channels [131], angular distributions [132, 133, 134, 135], and CP asymmetries [135, 136].

In the kinematic region where the dilepton invariant mass is sufficiently above the real photon pole and below the charm threshold, $q^2 \in [1, 6] \text{GeV}^2$, the relevant transversity amplitudes can be written within QCD factorization as [136, 137, 138]

$$\begin{aligned} A_{\perp}^{L,R} &= \frac{\sqrt{2} N (m_B^2 - q^2)}{m_B} \left\{ \left[(C_9^l + \tilde{C}_9^l) \mp (C_{10}^l + \tilde{C}_{10}^l) \right] \xi_{\perp} + \frac{2m_b m_B}{q^2} (\mathcal{T}_{\perp} + \tilde{\mathcal{T}}_{\perp}) \right\}, \\ A_{\parallel}^{L,R} &= -\frac{\sqrt{2} N (m_B^2 - q^2)}{m_B} \left\{ \left[(C_9^l - \tilde{C}_9^l) \mp (C_{10}^l - \tilde{C}_{10}^l) \right] \xi_{\perp} + \frac{2m_b m_B}{q^2} (\mathcal{T}_{\perp} - \tilde{\mathcal{T}}_{\perp}) \right\}, \quad (100) \\ A_0^{L,R} &= -\frac{N (m_B^2 - q^2)^2}{2m_B m_{K^*} \sqrt{q^2}} \left\{ \left[(C_9^l - \tilde{C}_9^l) \mp (C_{10}^l - \tilde{C}_{10}^l) \right] \xi_{\parallel} - \frac{2m_b}{m_B} (\mathcal{T}_{\parallel} - \tilde{\mathcal{T}}_{\parallel}) \right\}, \end{aligned}$$

with

$$N \equiv \left[\frac{G_F^2 \alpha^2}{3027 \pi^5 m_B^3} |\lambda_t^{(sb)}|^2 q^2 \sqrt{q^4 + m_B^4 + m_{K^*}^4 - 2(q^2 m_B^2 + q^2 m_{K^*}^2 + m_B^2 m_{K^*}^2)} \right]^{1/2}. \quad (101)$$

Kinematical terms suppressed by $m_{K^*}^2/m_B^2$ have been neglected here and the mass of the charged leptons has been set to zero. The form factors $\xi_{\perp,\parallel}$ are discussed in Appendix B. The functions $\mathcal{T}_{\perp,\parallel}$ include besides the usual one-loop matrix elements of the four-quark operators Q_{3-6} also the two-loop matrix elements of the current-current operators $Q_{1,2}$ and hard spectator-scattering effects, which give sizable contributions to the imaginary parts. Explicit expressions for $\mathcal{T}_{\perp,\parallel}$ can be found in [137, 138]. The functions $\tilde{\mathcal{T}}_{\perp,\parallel}$ are defined in analogy to $\mathcal{T}_{\perp,\parallel}$, and include the one-loop matrix elements of the chirality-flipped operators \tilde{Q}_{3-6} . The electromagnetic coupling constant and the Wilson coefficients entering (100) and (101) are evaluated at the scale m_b .

In terms of the transversity amplitudes, the dilepton spectrum is given by

$$\frac{d\Gamma(B \rightarrow K^* l^+ l^-)}{dq^2} = |A_{\perp}|^2 + |A_{\parallel}|^2 + |A_0|^2, \quad (102)$$

where $A_i A_j^* \equiv A_i^L A_j^{L*} + A_i^R A_j^{R*}$ for $i, j = \perp, \parallel, 0$. Expressed through $A_i^{L,R}$ and $d\Gamma/dq^2$, the normalized forward-backward asymmetry and the longitudinal K^* polarization of $B \rightarrow K^* l^+ l^-$ take the simple form

$$\begin{aligned} \bar{A}_{\text{FB}}(B \rightarrow K^* l^+ l^-) &= \frac{3}{2} \left(\frac{d\Gamma(B \rightarrow K^* l^+ l^-)}{dq^2} \right)^{-1} \text{Re} \left(A_{\perp}^R A_{\parallel}^{R*} - A_{\perp}^L A_{\parallel}^{L*} \right), \\ F_{\text{L}}(B \rightarrow K^* l^+ l^-) &= \left(\frac{d\Gamma(B \rightarrow K^* l^+ l^-)}{dq^2} \right)^{-1} |A_0|^2. \end{aligned} \quad (103)$$

In order to elucidate the importance of the different new-physics contributions to the exclusive $b \rightarrow s l^+ l^-$ observables in the RS model, we present approximate formulas for the forward-backward asymmetry and the longitudinal K^* polarization integrated over $q^2 \in [1, 6] \text{ GeV}^2$. Ignoring small effects due to new-physics contributions stemming from the one-loop matrix elements of Q_{3-10} and \tilde{Q}_{3-10} , and neglecting terms suppressed by $m_{K^*}^2/m_B^2$, we obtain for the

quantities appearing in (103) the approximations⁷

$$\begin{aligned}
\int_{1 \text{ GeV}^2}^{6 \text{ GeV}^2} dq^2 \frac{d\Gamma(B \rightarrow K^* l^+ l^-)}{dq^2} &= 1.59 \left[1 + 0.16 \text{Re} C_9^{l\text{RS}} - 0.28 \text{Re} C_{10}^{l\text{RS}} - 0.01 \text{Im} C_9^{l\text{RS}} \right. \\
&\quad - 0.17 \text{Re} \tilde{C}_9^{l\text{RS}} + 0.20 \text{Re} \tilde{C}_{10}^{l\text{RS}} - 0.05 \text{Re} \left(C_9^{l\text{RS}} \tilde{C}_9^{l\text{RS}*} + C_{10}^{l\text{RS}} \tilde{C}_{10}^{l\text{RS}*} \right) \\
&\quad \left. + 0.03 \left(|C_9^{l\text{RS}}|^2 + |C_{10}^{l\text{RS}}|^2 + |\tilde{C}_9^{l\text{RS}}|^2 + |\tilde{C}_{10}^{l\text{RS}}|^2 \right) \right] \cdot 10^{-7} \text{ps}^{-1}, \\
\int_{1 \text{ GeV}^2}^{6 \text{ GeV}^2} dq^2 \frac{3}{2} \text{Re} \left(A_{\perp}^R A_{\parallel}^{R*} - A_{\perp}^L A_{\parallel}^{L*} \right) &= -0.08 \left[1 - 1.38 \text{Re} C_9^{l\text{RS}} - 0.23 \text{Re} C_{10}^{l\text{RS}} \right. \\
&\quad \left. - 0.15 \text{Im} C_{10}^{l\text{RS}} + 0.32 \text{Re} \left(C_9^{l\text{RS}} C_{10}^{l\text{RS}*} - \tilde{C}_9^{l\text{RS}} \tilde{C}_{10}^{l\text{RS}*} \right) \right] \cdot 10^{-7} \text{ps}^{-1}, \\
\int_{1 \text{ GeV}^2}^{6 \text{ GeV}^2} dq^2 |A_0|^2 &= 1.17 \left[1 + 0.23 \text{Re} \left(C_9^{l\text{RS}} - \tilde{C}_9^{l\text{RS}} \right) - 0.27 \text{Re} \left(C_{10}^{l\text{RS}} - \tilde{C}_{10}^{l\text{RS}} \right) \right. \\
&\quad - 0.06 \text{Re} \left(C_9^{l\text{RS}} \tilde{C}_9^{l\text{RS}*} + C_{10}^{l\text{RS}} \tilde{C}_{10}^{l\text{RS}*} \right) \\
&\quad \left. + 0.03 \left(|C_9^{l\text{RS}}|^2 + |C_{10}^{l\text{RS}}|^2 + |\tilde{C}_9^{l\text{RS}}|^2 + |\tilde{C}_{10}^{l\text{RS}}|^2 \right) \right] \cdot 10^{-7} \text{ps}^{-1},
\end{aligned} \tag{104}$$

where $C_{9,10}^{l\text{RS}}$ and $\tilde{C}_{9,10}^{l\text{RS}}$ denote the low-energy Wilson coefficients. The corresponding initial conditions are given in (93).

The SM predictions for the normalized forward-backward asymmetry and the longitudinal K^* polarization read

$$\begin{aligned}
\bar{A}_{\text{FB}}(B \rightarrow K^* l^+ l^-)_{\text{SM}}^{q^2 \in [1,6] \text{ GeV}^2} &= (-0.05 \pm 0.03), \\
F_{\text{L}}(B \rightarrow K^* l^+ l^-)_{\text{SM}}^{q^2 \in [1,6] \text{ GeV}^2} &= 0.74 \pm 0.12.
\end{aligned} \tag{105}$$

They are plagued by sizable uncertainties due to the form factors $\xi_{\perp, \parallel}$ and unknown power corrections of $\mathcal{O}(\Lambda_{\text{QCD}}/m_b)$. Our estimates include a 10% error due to the latter terms. The given numbers can already be compared with existing measurements performed at BaBar [139, 140] and Belle [141, 142]. The large increase of statistics expected at the LHCb experiment will allow for precision measurements of these observables. Full angular analyses in $B \rightarrow Kl^+l^-$ [131] and $B \rightarrow K^*l^+l^-$ decays [134, 135] as well as experimental studies of CP-violating observables [135, 136] also seem promising, and offer a unique window on physics at and above the electroweak scale.

⁷Terms with coefficients smaller than 0.01 have been discarded here. The same applies to (107).

In the kinematic range above the charm resonances, $q^2 > 14 \text{ GeV}^2$, the relevant transversity amplitudes can be calculated in a rigorous way by performing an expansion in Λ_{QCD}/m_b and m_c^2/m_b^2 . Following [143] one finds the expressions

$$\begin{aligned}
A_{\perp}^{L,R} &= -\sqrt{2}N(m_B^2 - q^2) \left\{ \left[\left(C_{9,A}^{l\text{eff}}(q^2) + \tilde{C}_{9,A}^{l\text{eff}}(q^2) \right) \mp \left(C_{10}^l + \tilde{C}_{10}^l \right) \right] g(q^2) \right. \\
&\quad \left. - \frac{2m_b}{q^2} g_+(q^2) C_{7,A}^{\gamma\text{eff}}(q^2) \right\}, \\
A_{\parallel}^{L,R} &= -\sqrt{2}N \left\{ \left[\left(C_{9,A}^{l\text{eff}}(q^2) - \tilde{C}_{9,A}^{l\text{eff}}(q^2) \right) \mp \left(C_{10}^l - \tilde{C}_{10}^l \right) \right] f(q^2) \right. \\
&\quad \left. + \frac{2m_b}{q^2} \left[(m_B^2 - m_{K^*}^2) g_+(q^2) + q^2 g_-(q^2) \right] C_{7,A}^{\gamma\text{eff}}(q^2) \right\}, \\
A_0^{L,R} &= -\frac{N(m_B^2 - q^2)}{2m_{K^*}\sqrt{q^2}} \left\{ \left[\left(C_{9,A}^{l\text{eff}}(q^2) - \tilde{C}_{9,A}^{l\text{eff}}(q^2) \right) \mp \left(C_{10}^l - \tilde{C}_{10}^l \right) \right] \left[f(q^2) + (m_B^2 - q^2) a_+(q^2) \right] \right. \\
&\quad \left. + \frac{2m_b}{m_B^2} \left[(q^2 - m_{K^*}^2) g_+(q^2) + q^2 (g_-(q^2) + (m_B^2 - q^2) h(q^2)) \right] C_{7,A}^{\gamma\text{eff}}(q^2) \right\},
\end{aligned} \tag{106}$$

with the form factors $f(q^2)$, $g(q^2)$, $a_+(q^2)$, $g_{\pm}(q^2)$, and $h(q^2)$ given in Appendix B. The explicit expressions for the effective Wilson coefficients $C_{9,A}^{l\text{eff}}(q^2)$ and $C_{7,A}^{\gamma\text{eff}}(q^2)$ can be found in [143]. The coefficient $\tilde{C}_{9,A}^{l\text{eff}}(q^2)$ is defined in analogy to $C_{9,A}^{l\text{eff}}(q^2)$ with the one-loop matrix elements Q_{3-6} replaced by those of \tilde{Q}_{3-6} . All Wilson coefficients are evaluated at the scale m_b .

Omitting again small new-physics contributions from one-loop matrix elements of Q_{3-10} and \tilde{Q}_{3-10} , we obtain for the relevant quantities integrated from above the charm resonances to the endpoint of the spectrum, $q^2 \in [14 \text{ GeV}^2, (m_B - m_{K^*})^2] = [14, 19.2] \text{ GeV}^2$, the approximate expressions

$$\begin{aligned}
\int_{14 \text{ GeV}^2}^{19.2 \text{ GeV}^2} dq^2 \frac{d\Gamma(B \rightarrow K^* l^+ l^-)}{dq^2} &= 1.86 \left[1 + 0.24 \text{Re} C_9^{l\text{RS}} - 0.28 \text{Re} C_{10}^{l\text{RS}} \right. \\
&\quad - 0.16 \text{Re} \tilde{C}_9^{l\text{RS}} + 0.19 \text{Re} \tilde{C}_{10}^{l\text{RS}} + 0.02 \text{Im} C_9^{l\text{RS}} - 0.01 \text{Im} \tilde{C}_9^{l\text{RS}} \\
&\quad - 0.04 \text{Re} \left(C_9^{l\text{RS}} \tilde{C}_9^{l\text{RS}*} + C_{10}^{l\text{RS}} \tilde{C}_{10}^{l\text{RS}*} \right) \\
&\quad \left. + 0.03 \left(|C_9^{l\text{RS}}|^2 + |C_{10}^{l\text{RS}}|^2 + |\tilde{C}_9^{l\text{RS}}|^2 + |\tilde{C}_{10}^{l\text{RS}}|^2 \right) \right] \cdot 10^{-7} \text{ ps}^{-1},
\end{aligned}$$

$$\int_{14 \text{ GeV}^2}^{19.2 \text{ GeV}^2} dq^2 \frac{3}{2} \text{Re} \left(A_{\perp}^R A_{\parallel}^{R*} - A_{\perp}^L A_{\parallel}^{L*} \right) = 0.75 \left[1 + 0.30 \text{Re} C_9^{l\text{RS}} - 0.24 \text{Re} C_{10}^{l\text{RS}} \right]$$

$$\begin{aligned}
& - 0.02 \operatorname{Im} C_{10}^{l\text{RS}} - 0.07 \operatorname{Re} \left(C_9^{l\text{RS}} C_{10}^{l\text{RS}*} - \tilde{C}_9^{l\text{RS}} \tilde{C}_{10}^{l\text{RS}*} \right) \Big] \cdot 10^{-7} \text{ ps}^{-1}, \\
\int_{14 \text{ GeV}^2}^{19.2 \text{ GeV}^2} dq^2 |A_0|^2 &= 0.76 \left[1 + 0.24 \operatorname{Re} \left(C_9^{l\text{RS}} - \tilde{C}_9^{l\text{RS}} \right) - 0.27 \operatorname{Re} \left(C_{10}^{l\text{RS}} - \tilde{C}_{10}^{l\text{RS}} \right) \right. \\
&+ 0.02 \operatorname{Im} \left(C_9^{l\text{RS}} - \tilde{C}_9^{l\text{RS}} \right) - 0.07 \operatorname{Re} \left(C_9^{l\text{RS}} \tilde{C}_9^{l\text{RS}*} + C_{10}^{l\text{RS}} \tilde{C}_{10}^{l\text{RS}*} \right) \\
&\left. + 0.03 \left(|C_9^{l\text{RS}}|^2 + |C_{10}^{l\text{RS}}|^2 + |\tilde{C}_9^{l\text{RS}}|^2 + |\tilde{C}_{10}^{l\text{RS}}|^2 \right) \right] \cdot 10^{-7} \text{ ps}^{-1}.
\end{aligned} \tag{107}$$

In the high- q^2 region the SM predictions are given by

$$\begin{aligned}
\bar{A}_{\text{FB}}(B \rightarrow K^* l^+ l^-)_{\text{SM}}^{q^2 \in [14, 19.2] \text{ GeV}^2} &= 0.40 \pm 0.11, \\
F_{\text{L}}(B \rightarrow K^* l^+ l^-)_{\text{SM}}^{q^2 \in [14, 19.2] \text{ GeV}^2} &= 0.36 \pm 0.07.
\end{aligned} \tag{108}$$

Like in the low- q^2 region, the quoted uncertainties arise mainly from the form factors and unknown power corrections. The additional non-perturbative error due to $\mathcal{O}(\Lambda_{\text{QCD}}/m_b)$ terms is estimated to be about 10% and included in the total uncertainties. The different sensitivity to short-distance dynamics in the low- and high- q^2 ranges makes combinations of measurements of $\bar{A}_{\text{FB}}(B \rightarrow K^* l^+ l^-)$ and $F_{\text{L}}(B \rightarrow K^* l^+ l^-)$ in different kinematic regions powerful probes of new physics.

4.3.7 Important Formulas for $B \rightarrow \tau \nu_\tau$

Among the purely leptonic and semileptonic decays of kaons and B mesons induced by the charged-current interactions, we focus on the $B \rightarrow \tau \nu_\tau$ decay, which in the SM provides a direct measurement of the product of the CKM matrix element $|V_{ub}|$ and the B -meson decay constant. The plethora of available $K \rightarrow (\pi) l \nu$ data [144] will be used in Section 5.3 to set bounds on the violation of the unitarity of the first row of the generalized CKM matrix. Another interesting test in the field of semileptonic kaon decays consists in the comparison of the value of $|V_{us}|$ determined in the helicity-suppressed $K \rightarrow l \nu$ decays with the one extracted from the helicity-allowed $K \rightarrow \pi l \nu$ modes [144]. While the presence of non-vanishing right-handed currents can lead to different extractions of $|V_{us}|$, the possible shifts in the $W u_{RS} s_R$ coupling predicted in the RS framework are, due to the strong chiral suppression, too small to lead to any observable effect.

In the RS model, the branching ratio of the $B \rightarrow \tau \nu_\tau$ decay can be written in terms of the coefficients (71) as

$$\mathcal{B}(B \rightarrow \tau \nu_\tau) = \frac{\tau_B f_B^2 m_B m_\tau^2}{16\pi} \left(1 - \frac{m_\tau^2}{m_B^2} \right)^2 \left| C_l^{\text{RS}} - \tilde{C}_l^{\text{RS}} \right|^2. \tag{109}$$

The dependence on the lepton mass arises from helicity conservation, which suppresses the muon and electron channels.

From the global fit of the unitarity triangle, we obtain the following SM prediction

$$\mathcal{B}(B \rightarrow \tau\nu_\tau)_{\text{SM}} = (0.90 \pm 0.19) \cdot 10^{-4}. \quad (110)$$

The major part of the total error stems from the uncertainty due to the B -meson decay constant $f_B \equiv f_{B_d} = (0.200 \pm 0.020) \text{ GeV}$ [46]. Notice that the indirect fit prediction (110) is 2.1σ below the current world average $\mathcal{B}(B \rightarrow \tau\nu_\tau)_{\text{exp}} = (1.73 \pm 0.35) \cdot 10^{-4}$ [145, 146, 147, 148]. While at the moment systematic errors in the lattice determinations of f_B in conjunction with limited experimental statistics do not allow to draw a definite conclusion about the presence of new physics in $B \rightarrow \tau\nu_\tau$, we will investigate whether the RS model can in principle reproduce the observed deviation.

5 Numerical Analysis

This part of our article is devoted to a thorough numerical analysis of new-physics effects in the quark flavor sector. We begin our discussion with a concise description of the algorithm used to scan the parameter space of the RS model. We then introduce four benchmark scenarios, three of them specifically devised to suppress potentially dangerous contributions to processes such as $Z^0 \rightarrow b\bar{b}$ and $K-\bar{K}$ mixing. We will investigate in detail to which extent the different scenarios allow us to relax the strong constraints arising from electroweak precision tests and quark flavor physics. Next we analyze the potential size of new-physics effects in the charged-current sector, paying special attention to the non-unitarity of the CKM matrix and the extraction of the elements $|V_{ub}|$, $|V_{cb}|$, and $|V_{tb}|$. Then follows a comprehensive study of $\Delta F = 2$ and $\Delta F = 1$ flavor-changing transitions. We find that rare decays of K and B_s mesons are particularly interesting in the minimal RS framework, as their branching ratios can be enhanced considerably with respect to the SM even after taking into account the constraints imposed by $Z^0 \rightarrow b\bar{b}$ and ϵ_K . We emphasize that whereas many observables within the K , $B_{d,s}$, and D systems are strongly correlated in the RS model, there are in general no correlations between observables belonging to different sectors. While at first sight the observed correlations appear to be very promising to distinguishing the RS scenario from other extensions of the SM, we will show that they indeed arise in a wide class of models of new physics and hence do not constitute unmistakable signals of warped extra dimensions. In each case we will discuss the origin of the observed pattern. Comments on how our results would change in a RS model with custodial protection round off our phenomenological survey.

5.1 Parameter Scan

In a first step we determine sets of Yukawa matrices $\mathbf{Y}_{u,d}$ that allow one to reproduce the observed values of the Wolfenstein parameters $\bar{\rho}$ and $\bar{\eta}$. Since the latter two quantities are to leading order in hierarchies independent of the zero-mode profiles $F(c_{A_i})$ [10], it turns out to be computationally expensive to find suitable pairs of Yukawa matrices $\mathbf{Y}_{u,d}$ by a simple random sampling. To generate proper sets we proceed in the following way. We

randomly pick one element of the Yukawa matrices keeping its phase ϕ and modulus y arbitrary. Using uniform initial distribution the remaining elements are then generated in the ranges $\arg((Y_{u,d})_{ij}) \in [0, 2\pi[$ and $|(Y_{u,d})_{ij}| \in [0, Y_{\max}]$, where the upper limit Y_{\max} varies between the different benchmark scenarios. Next we calculate the Wolfenstein parameters $\bar{\rho}$ and $\bar{\eta}$ by means of (I:102) and minimize the function

$$\chi^2(x) = \sum_n \left(\frac{x_{\text{exp}}(n) - x_{\text{theo}}(n)}{\sigma_{\text{exp}}(n)} \right)^2, \quad x = \{\bar{\rho}, \bar{\eta}\}, \quad (111)$$

with respect to ϕ and y , requiring $y \leq Y_{\max}$. Here $x_{\text{exp}}(n)$ and $x_{\text{theo}}(n)$ denote the experimental and theoretical value of the n^{th} observable and $\sigma_{\text{exp}}(n)$ is the standard deviation of the corresponding measurement.

After the elements of the Yukawa matrices $\mathbf{Y}_{u,d}$ have been fixed, we choose a random value for the bulk mass parameter $c_{u_3} \in]-1/2, c_{u_3}^{\max}]$ with $c_{u_3}^{\max} = 2$ or $5/2$ depending on the scenario, and calculate the whole set of observables $x = \{m_u, m_d, m_s, m_c, m_b, m_t, A, \lambda, \bar{\rho}, \bar{\eta}\}$ in terms of the zero-mode profiles of the remaining c_{A_i} using the leading-order Froggatt-Nielsen relations (I:96) and (I:102).⁸ The values of the zero-mode profiles $F(c_{A_i})$ are then determined from the best fit to the $\chi^2(x)$ function supplemented by the constraints $F(c_{A_i}) \leq F(c_{u_3}^{\max})$. Points with $\chi^2(x)/\text{dof} > 11.5/10$, corresponding to 68% CL, are rejected, while for points that pass the test, we recompute $\chi^2(x)$ using exact formulas for the quark masses and Wolfenstein parameters and remove all points that show a deviation of more than 3σ in at least one observable.

In order to assure that our algorithm populates the whole parameter space without introducing spurious correlations, we have inspected the final distributions of parameters. While the magnitudes and phases of the elements of the Yukawa matrices are all nearly flatly distributed, the shapes of the distributions of the quark masses and Wolfenstein parameters are almost Gaussian with a width of at most twice the corresponding experimental uncertainty. We consider this as a strong indication that we achieve full coverage of the parameter space in an unbiased way. These features are basic prerequisites guaranteeing that correlations between different observables have indeed a physical origin and are not artifacts of an imperfect Monte Carlo sampling.

5.2 Benchmark Scenarios

In order to assess the robustness of predictions, it is important to investigate how sensitively they depend on the values of the most relevant parameters of the model. We therefore study four different benchmark scenarios that differ by the allowed maximal magnitude of the Yukawa couplings, the structure of the bulk masses matrices, and the value of the logarithm of the

⁸The choice of c_{u_3} as a prior is motivated by the fact that this bulk mass parameter is special in the sense that it determines the degree of compositeness of the top quark. While the lower limit of the allowed range of c_{u_3} is motivated by the fact that the right-handed top quark should be localized near the IR brane, the upper limit is chosen in a somewhat *ad hoc* way. Allowing for $c_{u_3}^{\max} \gg 1$ would however take away an attractive feature of the RS model, namely that it explains the quark hierarchies in terms of fundamental parameters of $\mathcal{O}(1)$.

warp factor. Three out of the four benchmark scenarios are designed specifically to suppress harmful contributions to electroweak precision and quark flavor observables and therefore present particular cases of viable models of warped extra dimensions with improved prospects for discovery at the LHC. Our benchmark scenarios are defined as follows:

- Scenario 1 (S1): “standard”

The magnitudes of the entries $|(Y_{u,d})_{ij}|$ of the Yukawa matrices have to be bounded from above in order for the Yukawa couplings to be perturbative. In our first scenario, we employ $Y_{\max} = 3$, which coincides with the upper limit estimated by means of naive dimensional analysis [18]. This is the standard choice for Y_{\max} employed in several articles on flavor effects in warped extra-dimension models [11, 18, 19, 21, 30, 31, 36]. No further restrictions on the bulk mass parameters are imposed and the logarithm of the warp factor is set to $L = \ln(10^{16}) \approx 37$, as needed to explain the hierarchy between the Planck and the electroweak scales.

- Scenario 2 (S2): “large”

This scenario differs from the first one by the choice of Y_{\max} . Since it is *a priori* not clear if the theory should be weakly coupled in the Yukawa or in any other sector, and up to what cutoff scale weak coupling should hold, the bound $Y_{\max} = 3$ might be regarded as being too restrictive. In fact, in order to avoid fine-tuning in the Higgs sector the UV cutoff has to be very close to the KK scale, and requiring weak coupling up to M_{KK} allows for Yukawa couplings that are larger by a factor of 4 than the latter limit [10]. In our second benchmark scenario we entertain this possibility and consequently allow for $Y_{\max} = 12$. This choice has the attractive property that it helps to reduce some particularly dangerous flavor-changing couplings in ϵ_K [18].

- Scenario 3 (S3): “aligned”

In this scenario we consider only the subclass of models characterized by common bulk masses c_{d_i} in the sector of right-handed down-type quarks. This is a viable solution, since by virtue of the moderate hierarchy, the mass splittings in the down-type quark sector can be naturally accommodated by $\mathcal{O}(1)$ variations of the Yukawa couplings. The equality of bulk mass parameters can be achieved by imposing an $U(3)$ flavor symmetry, under which the fields that give rise to the right-handed down-type quark zero modes transform as triplets and all other fields transform as singlets [30]. Besides the natural suppression of vast corrections to ϵ_K [30], this scenario has the appealing feature that it leads to a unique pattern of deviations in the $K \rightarrow \pi\nu\bar{\nu}$ sector.

- Scenario 4 (S4): “little”

From a purely phenomenological point of view, it is possible to lower the UV cutoff from the Planck scale to a value only few orders of magnitude above the TeV scale, even though in this case a true solution to the hierarchy problem is postponed to higher energy. Since many amplitudes in the RS model are enhanced by L , it is worthwhile to address the question to what extent certain experimental constraints can be avoided by such a choice [149]. This will be done in our last scenario, where we consider a “volume-truncated”

	S1	S2	S3	S4
c_{Q_1}	-0.63 ± 0.03	-0.67 ± 0.03	-0.66 ± 0.02	-1.34 ± 0.16
c_{Q_2}	-0.57 ± 0.05	-0.61 ± 0.03	-0.59 ± 0.03	-1.04 ± 0.18
c_{Q_3}	-0.34 ± 0.32	-0.52 ± 0.09	-0.24 ± 0.43	-0.49 ± 0.34
c_{u_1}	-0.68 ± 0.04	-0.68 ± 0.04	-0.65 ± 0.03	-1.58 ± 0.18
c_{u_2}	-0.51 ± 0.12	-0.51 ± 0.12	-0.50 ± 0.12	-0.79 ± 0.26
c_{u_3}	$] - 1/2, 2]$	$] - 1/2, 2]$	$] - 1/2, 2]$	$] - 1/2, 5/2]$
c_{d_1}	-0.65 ± 0.03	-0.66 ± 0.03	-0.60 ± 0.02	-1.44 ± 0.17
c_{d_2}	-0.62 ± 0.03	-0.62 ± 0.03	-0.60 ± 0.02	-1.28 ± 0.17
c_{d_3}	-0.58 ± 0.03	-0.58 ± 0.03	-0.60 ± 0.02	-1.05 ± 0.13

Table 1: Central values and statistical uncertainties of the bulk mass parameters in the different benchmark scenarios. The shown errors correspond to 1σ ranges when fitting the distributions to a Gaussian function. See text for details.

variant of our first scenario characterized by $L = \ln(10^3) \approx 7$. Unfortunately, in this “little” RS scenario [149] no improvement concerning ϵ_K can be achieved compared to the standard benchmark scenario [36].

The statistical approach outlined in the last section provides us with distributions of bulk mass parameters rather than with their precise values. The obtained results are different in the individual benchmark scenarios, and in order to make our article self-contained, we summarize the central values and statistical uncertainties of the parameters c_{A_i} for the four cases in Table 1. All distributions are nearly Gaussian, apart from those of c_{Q_3} , which feature a small tail to higher values, and those of c_{u_3} , which are chosen as flat priors in the range $] - 1/2, 2]$ for the scenarios S1 to S3, while we allow for $] - 1/2, 5/2]$ in the case of scenario S4. Notice that while the central values of the bulk mass parameters in the benchmark scenarios S1 to S3 are very similar, the splitting between the individual c_{A_i} parameters is on average much bigger in scenario S4 due to the smaller “volume factor” L . We have verified that the precise form of the distributions is essentially independent of the details of the algorithm used to scan the parameter space.

As it turns out, the majority of flavor observables is largely insensitive to the choice of the benchmark scenario. For all these observables we will only present plots showing the results for a parameter scan in our standard scenario S1 and describe possible differences occurring in the remaining benchmark scenarios in words.

5.3 Quark Mixing Matrices

In this section we study non-standard effects in the flavor-mixing matrices appearing in the charged-current sector, focusing on the generalized CKM matrix. In all cases we adjust the

phases of the SM quark fields according to the standard CKM phase convention [47], which is defined by the requirements that the matrix elements V_{ud} , V_{us} , V_{cb} , V_{tb} are real, and that

$$\text{Im } V_{cs} = \frac{V_{us}V_{cb}}{V_{ud}^2 + V_{us}^2} \text{Im } V_{ub}. \quad (112)$$

These five conditions fix the phase differences between the six quark fields uniquely.

The physically most meaningful definition of the CKM matrix is based on the effective four-fermion interactions induced by the exchange of the entire tower of W^\pm bosons and their KK excitations. Unlike the CKM matrix in the SM, the left-handed quark mixing matrix \mathcal{V}_L appearing in (13) is not a unitary matrix [9, 10, 34, 150]. Following our previous work [10], we consider as two measures of this effect the deviation from unity of the sum of the squares of the matrix elements in the first row and the lack of closure of the unitarity triangle [151]. To quantify the deviations in these two observables, we define

$$\Delta_1^{\text{non}} \equiv 1 - (|V_{ud}|^2 + |V_{us}|^2 + |V_{ub}|^2), \quad \Delta_2^{\text{non}} \equiv 1 + \frac{V_{ud}V_{ub}^*}{V_{cd}V_{cb}^*} + \frac{V_{td}V_{tb}^*}{V_{cd}V_{cb}^*}, \quad (113)$$

with

$$V_{ij} \equiv \left[1 + \frac{m_W^2}{2M_{\text{KK}}^2} \left(1 - \frac{1}{2L} \right) \right]^{-1} (\mathcal{V}_L)_{ij}, \quad i, j = 1, 2, 3. \quad (114)$$

The prefactor in the last relation arises because an extraction of a CKM element generally involves normalization of the semileptonic amplitude relative to the Fermi constant G_F . The fact that in the RS model the value of G_F determined from muon decay differs from the one in the SM by the finite correction (I:141) will play an important role in what follows. Tests of the unitarity of the CKM matrix involving the first column or second row and column suffer from larger experimental uncertainties [47] and therefore cannot compete with the constraints imposed by (113) at present.

The predictions for Δ_1^{non} and Δ_2^{non} obtained in our standard parameter scenario are shown in Figure 2, where they are compared with the current experimental situation. The regions of 68% and 95% probability following from a combined analysis of $K \rightarrow (\pi)l\nu$ branching ratios and a global fit to the CKM matrix are indicated by the shaded bands and the egg-shaped regions. The corresponding central values and 68% CL ranges read

$$(\Delta_1^{\text{non}})_{\text{exp}} = 0.00022 \pm 0.00065, \quad (\Delta_2^{\text{non}})_{\text{exp}} = (0.001 \pm 0.024) + (0.001 \pm 0.015) i. \quad (115)$$

The quoted total uncertainty of $(\Delta_1^{\text{non}})_{\text{exp}}$ has been obtained by combining the individual errors 0.00051 and 0.00041 associated to $|V_{ud}|$ and $|V_{us}|$ [144] in quadrature. The prediction for $(\Delta_2^{\text{non}})_{\text{exp}}$ has been derived using a customized version of the CKMfitter package [52]. The input parameters entering our global CKM analysis are collected in Appendix B.

The distribution of scatter points in the left plot of Figure 2 illustrates that unitarity violations in the first row of the generalized CKM matrix are typically too small to be observable with present data. The smallness of the corrections to Δ_1^{non} has two sources. First, flavor-dependent effects arising from the t -dependent terms in (14) are highly suppressed by products of the zero-mode profiles $F(c_{Q_i})$ and as a result are negligibly small. Second, the t -independent contributions to (14) cancel almost exactly against the multiplicative factor in (114) arising

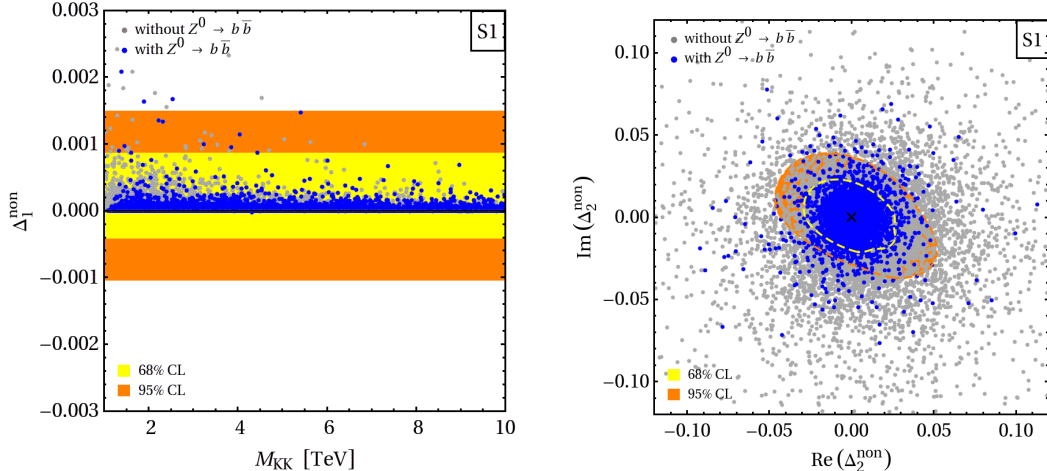


Figure 2: Predictions for Δ_1^{non} and Δ_2^{non} in the benchmark scenario S1. The blue (light gray) points are consistent (inconsistent) with the measured $Z^0 \rightarrow b\bar{b}$ couplings at the 99% CL. The solid black line (left plot) and the black cross (right plot) indicate the SM expectations. For comparison the regions of 68% (yellow) and 95% (orange) probability following from a combined analysis of $K \rightarrow (\pi)l\nu$ branching ratios (left) and a global CKM fit (right) are also displayed. See text for details.

from the normalization of the semileptonic rates to G_F . Notice that flavor-independent corrections also cancel in any ratio of purely leptonic rates involving light quarks. In consequence, the RS predictions for $|V_{us}/V_{ud}|$ obtained from the ratio $\Gamma(K \rightarrow \mu\nu)/\Gamma(\pi \rightarrow \mu\nu)$ turn out to be basically indistinguishable from the SM expectation.

A detection of a unitarity violation in the charged-current interactions by means of Δ_2^{non} offers much better prospects. This is illustrated in the right plot of Figure 2. We see that the lack of closure of the unitarity triangle predicted in the RS model, while typically at the same level as the uncertainty in (115), can also exceed it. The actual value of Δ_2^{non} is determined by a complicated interplay of the contributions arising almost entirely from the CKM elements V_{ub}, V_{cb}, V_{td} , and V_{tb} . The observable Δ_2^{non} therefore depends very sensitively on the exact localization of the $SU(2)_L$ quark doublet (t_L, b_L) . In view of the typical size of the corrections to Δ_2^{non} , an improvement of the determination of the unitarity triangle, expected from the LHC and later from a super flavor factory, might allow to detect the non-unitarity of the generalized CKM matrix induced in the RS framework.

We now turn our attention to the direct extraction of the CKM elements $|V_{ub}|$, $|V_{cb}|$, and $|V_{tb}|$. The value of $|V_{ub}/V_{cb}|$ can be determined from the relative ratio of charmless over charmed semileptonic B decays. It also enters the expression for the quantity

$$R_u \equiv \left| \frac{V_{ud}V_{ub}^*}{V_{cd}V_{cb}^*} \right| = \left(1 - \frac{\lambda^2}{2} \right) \frac{1}{\lambda} \left| \frac{V_{ub}}{V_{cb}} \right|, \quad (116)$$

which measures the length of the side of the rescaled unitarity triangle opposite to the angle β . Notice that in order to arrive at the final expression we have used that the ratio V_{ud}/V_{cd}

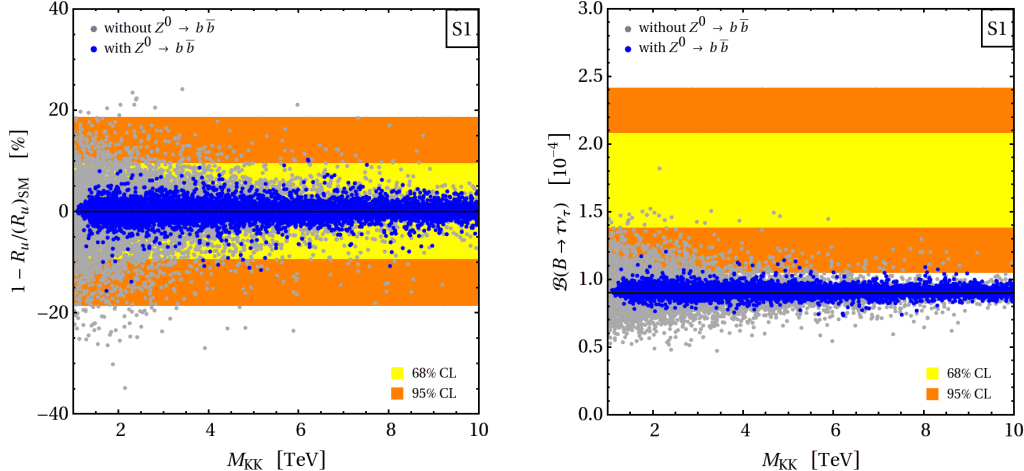


Figure 3: Relative shift in R_u and the branching ratio for $B \rightarrow \tau\nu_\tau$ as a function of M_{KK} in the S1 parameter scenario. The blue (light gray) points are consistent (inconsistent) with the measured $Z^0 \rightarrow b\bar{b}$ couplings at the 99% CL. The solid black lines indicate the SM predictions. The regions of 68% (yellow) and 95% (orange) probability following from a combination of semileptonic B decay data (left) and the BaBar and Belle measurements of the $B \rightarrow \tau\nu_\tau$ branching ratio (right) are also displayed. See text for details.

in the RS model is to an excellent approximation given by its SM value.

A combination of the present experimental information coming from inclusive and exclusive measurements of semileptonic B decays gives [47]

$$(R_u)_{\text{exp}} = 0.42 \pm 0.04. \quad (117)$$

The quoted total uncertainty should be compared with the relative corrections to R_u predicted in the RS framework. The results of a parameter scan in the standard scenario are displayed on the left in Figure 3. It is evident from the plot that the relative corrections in the ratio $|V_{ub}/V_{cb}|$ are typically smaller than the current combined experimental and theoretical accuracy of about 10%. Similar statements apply to the direct extraction of the elements $|V_{ub}|$ and $|V_{cb}|$ from semileptonic and purely leptonic B decays. In the case of $|V_{ub}|$ this is illustrated by the right plot in Figure 3, which shows the standard benchmark scenario predictions for the $B \rightarrow \tau\nu_\tau$ branching ratio. We see that in the RS framework it is not possible to explain the 2.1σ deviation between the value (110), following from a global fit to the unitarity triangle, and the current experimental world average indicated by the shaded bands. The typical relative corrections in $|V_{cb}|$ do not exceed the 7% (8%) level for scatter points that satisfy (violate) the $Z^0 \rightarrow b\bar{b}$ constraint, and the observed pattern of deviations follows the one seen in R_u and the branching ratio of $B \rightarrow \tau\nu_\tau$.

A direct determination of $|V_{tb}|$ without assuming unitarity is possible from measurements of the single top-quark production cross section. The measured cross sections $\sigma(p\bar{p} \rightarrow tb + X, tqb + X) = (2.3_{-0.5}^{+0.6})$ pb [152] and $\sigma(p\bar{p} \rightarrow tb + X, tqb + X) = (3.94 \pm 0.88)$ pb [153] translate

into the limits $|V_{tb}| > 0.78$ and $|V_{tb}| > 0.71$ at 95% CL by CDF and DØ, respectively. We find that in the RS model the prediction for $|V_{tb}|$ is strictly below the corresponding value in the SM. The relative corrections are however safely within the current experimental limit, as they do not surpass the level of 1% (15%) for parameter points that satisfy (violate) the constraint imposed by the precision measurement of the $Z^0 \rightarrow b\bar{b}$ couplings. The value of $|V_{tb}|$ will be further constrained as soon as the LHC will start to take data. Simulation studies by ATLAS [154] and CMS [155] suggest that the cross section of the most promising single-top-production channel, namely $pp \rightarrow tqb + X$, is measurable with a total error of 10%, which implies that $|V_{tb}|$ can be determined with 5% accuracy. At this level of precision one becomes sensitive to non-standard effects affecting the $Wt_L b_L$ coupling in the RS framework.

For the sake of completeness, we mention that the non-unitarity of the CKM matrix has been analyzed previously in [9, 34]. However, a thorough discussion of all relevant effects is missing in these articles. On the other hand, a detailed discussion of the breakdown of the unitarity of the quark mixing matrix in the framework of a RS model with custodial protection has been presented very recently in [150]. Unfortunately, in the latter paper the CKM matrix is defined via the $Wu_{iL}d_{jL}$ vertex and not the effective four-fermion interactions induced by the exchange of the entire tower of the W^\pm boson and its KK excitations. As explained in detail above, defining V_{ij} as part of the charged-current coupling is unphysical, since in practice it is impossible to determine the CKM elements without reference to G_F . The exact meaning of the results obtained in [150] thus remains cloudy, preventing us from a straightforward comparison with our findings.

Before proceeding, we would like to add two further comments. First, in Figures 2 and 3 we have only shown predictions corresponding to our standard benchmark scenario. Plots for the remaining parameter scenarios have been omitted since they look essentially the same. Second, we note that the correlations between the $Wu_{iL}b_L$ and $Wt_L d_{iL}$ vertices and the $Z^0 b_L \bar{b}_L$ coupling are in general different in warped extra-dimension models with an extended electroweak sector, because the custodial symmetry cannot simultaneously protect all of these vertices [156]. We therefore expect that, depending on the exact realization of the model, the corrections to the $Wu_{iL}b_L$ and $Wt_L d_{iL}$ couplings could be less correlated with the ones appearing in the $Z^0 b_L \bar{b}_L$ vertex. To illustrate this possibility, we have shown in the plots of Figures 2 and 3 scatter points that fulfill (blue) and violate (light gray) the constraints following from the measurements of the $Z^0 \rightarrow b\bar{b}$ couplings. It is apparent that removing the stringent $Z^0 \rightarrow b\bar{b}$ constraint leads to much brighter experimental prospects for a detection of a unitarity violation of the generalized CKM matrix or deviations in the branching ratios of semileptonic and purely leptonic B decays. Detailed analyses of the effective charged-current interactions in extended RS models would however be required to make definite statements about how much these prospects would improve.

5.4 Neutral-Meson Mixing

The observation of neutral-meson mixing has played a central role in unraveling the flavor structure of the SM. While these glory days have passed, even today measurements of the magnitudes and phases of $\Delta F = 2$ amplitudes provide some of the most stringent constraints on models of physics beyond the SM. Due to enhancements in the RG evolution and in the

matrix elements, these constraints turn out to be particularly severe for scenarios that generate transitions between quarks of different chiralities. As a result, in such models the scale of new physics is typically pushed to values beyond the reach of direct searches at the LHC. The questions that we want to address in this section is how severe the constraints from $\Delta F = 2$ observables are in the RS framework, and if it is possible to ameliorate them so as to build viable models with a warped extra dimension that are accessible at the LHC.

5.4.1 Numerical Analysis of $K-\bar{K}$ Mixing

Let us begin this section by giving explicit results for the various neutral-meson mixing amplitudes in terms of the Wilson coefficients in (24). These formulas will enable us to understand which Wilson coefficient generically furnishes the dominant contribution to a given $\Delta F = 2$ observable. Making the dependence on the matching scale μ_{KK} explicit, we find the following approximate formula for the $K-\bar{K}$ mixing amplitude,

$$\langle K^0 | \mathcal{H}_{\text{eff,RS}}^{\Delta S=2} | \bar{K}^0 \rangle \propto C_1^{\text{RS}} + \tilde{C}_1^{\text{RS}} + 114.8 \left(1 + 0.14 \ln \left(\frac{\mu_{\text{KK}}}{3 \text{ TeV}} \right) \right) \left(C_4^{\text{RS}} + \frac{C_5^{\text{RS}}}{3.1} \right), \quad (118)$$

where the large scale-independent coefficient consists of a factor of about 15 arising from the chiral enhancement of the hadronic matrix elements [157, 158], and a factor of about 8 due to the RG evolution [42, 43, 44] from 3 TeV down to 2 GeV. Assuming that all Wilson coefficients are of similar size, this relation implies that C_4^{RS} gives the dominant contribution to both Δm_K and $|\Delta \epsilon_K|$ in the RS framework. In the case of $B_{d,s}-\bar{B}_{d,s}$ and $D-\bar{D}$ mixing the chiral enhancement of the matrix elements of the mixed-chirality operators is much less pronounced and amounts to at most a factor of 2. Taking further into account that for bottom and charm mesons the Wilson coefficients are only evolved down to 4.6 GeV and 2.8 GeV, respectively, the appropriate factors that replace the numerical coefficients 114.8 and 3.1 in the expression (118) read 7.4 and 2.7 (13.3 and 2.9) in the $B_{d,s}$ (D) sector. These moderate enhancement factors suggest that in the case of the $B_{d,s}-\bar{B}_{d,s}$ and $D-\bar{D}$ mixing amplitudes, the contribution from the sum of C_1^{RS} and \tilde{C}_1^{RS} can compete with the one arising from C_4^{RS} and C_5^{RS} . Our numerical analysis will confirm this model-independent conclusion.

We are now ready to analyze the impact of new-physics effects on $K-\bar{K}$ mixing in the RS framework. The predictions for $|\epsilon_K|$ in the four different benchmark scenarios introduced in Section 5.2 are displayed in Figure 4. All shown points reproduce the correct quark masses and CKM parameters within errors. Scatter points that are consistent with $Z^0 \rightarrow b\bar{b}$ are colored blue, while the subset of scatter points that in addition satisfies $|\epsilon_K| \in [1.2, 3.2] \cdot 10^{-3}$ is colored in orange. The latter constraint guarantees that the theoretical prediction for $|\epsilon_K|$ obtained by adding the SM and RS contributions is consistent with the measurement at 95% CL after combining theoretical and experimental errors. One can immediately see from all four panels that the values of $|\epsilon_K|$ are typically a factor of about 100 bigger than the SM prediction [11, 18, 21, 30, 36]. This is the generic case, for which the Wilson coefficient C_4^{RS} gives the by far largest contribution to $|\epsilon_K|$. The order-of-magnitude enhancement of $|\epsilon_K|$ is explained by the following observations. First, it turns out that even for low KK scales the magnitude of the RS contribution to Δm_K typically does not exceed the SM contribution by an unacceptably large amount (given the huge SM uncer-

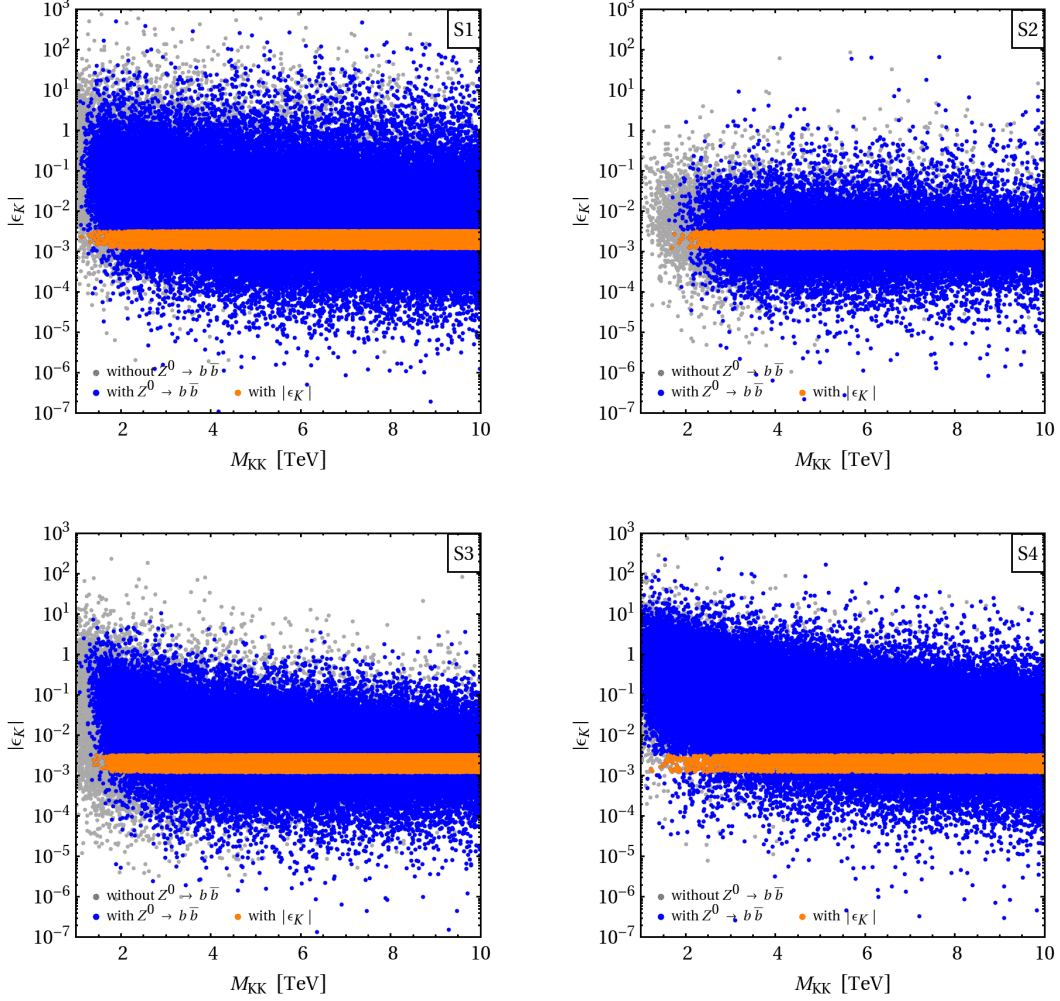


Figure 4: Predictions for $|\epsilon_K|$ as a function of M_{KK} in the different benchmark scenarios. The blue (light gray) points are consistent (inconsistent) with $Z^0 \rightarrow b\bar{b}$ at the 99% CL. The subset of points that is in agreement with both the $Z^0 b\bar{b}$ couplings and the experimental value of $|\epsilon_K|$ at 95% CL is colored orange. See text for details.

tainties). Second, the ratio of imaginary to real part of the $K-\bar{K}$ mixing amplitude is strongly suppressed in the SM due to the smallness of $\text{Im}(V_{ts}^* V_{td})$. Numerically, one finds $(\text{Im} M_{12}^{K*}/\text{Re} M_{12}^{K*})_{\text{SM}} \approx -2A^4 \lambda^{10} (1 - \bar{\rho}) \bar{\eta} \eta_{tt} S_0(m_t^2/m_W^2)/(\lambda^2 \eta_{cc} m_c^2/m_W^2) \approx -1/150$, where $S_0(m_t^2/m_W^2) \approx 2.35$ originates from the one-loop box diagrams containing a top quark, while $\eta_{tt} \approx 0.57$ [159] and $\eta_{cc} \approx 1.50$ [160] summarize higher-order QCD corrections in the top- and charm-quark sectors. Under the natural assumption that the phase in $(M_{12}^{K*})_{\text{RS}}$ is of $\mathcal{O}(1)$, it follows then that $|\epsilon_K|_{\text{RS}}/|\epsilon_K|_{\text{SM}} = |(\text{Im} M_{12}^{K*})_{\text{RS}}/(\text{Im} M_{12}^{K*})_{\text{SM}}| \sim |(\text{Re} M_{12}^{K*})_{\text{RS}}/(\text{Im} M_{12}^{K*})_{\text{SM}}| \sim |(\text{Re} M_{12}^{K*})_{\text{SM}}/(\text{Im} M_{12}^{K*})_{\text{SM}}| \sim 100$. Large deviations of $|\epsilon_K|_{\text{RS}}$ from this generic value require a tuning of parameters, for example an adjustment of the phase of the associated combination of Yukawa couplings so that $(\text{Im} M_{12}^{K*})_{\text{RS}}/(\text{Im} M_{12}^{K*})_{\text{SM}}$ becomes of $\mathcal{O}(1)$.

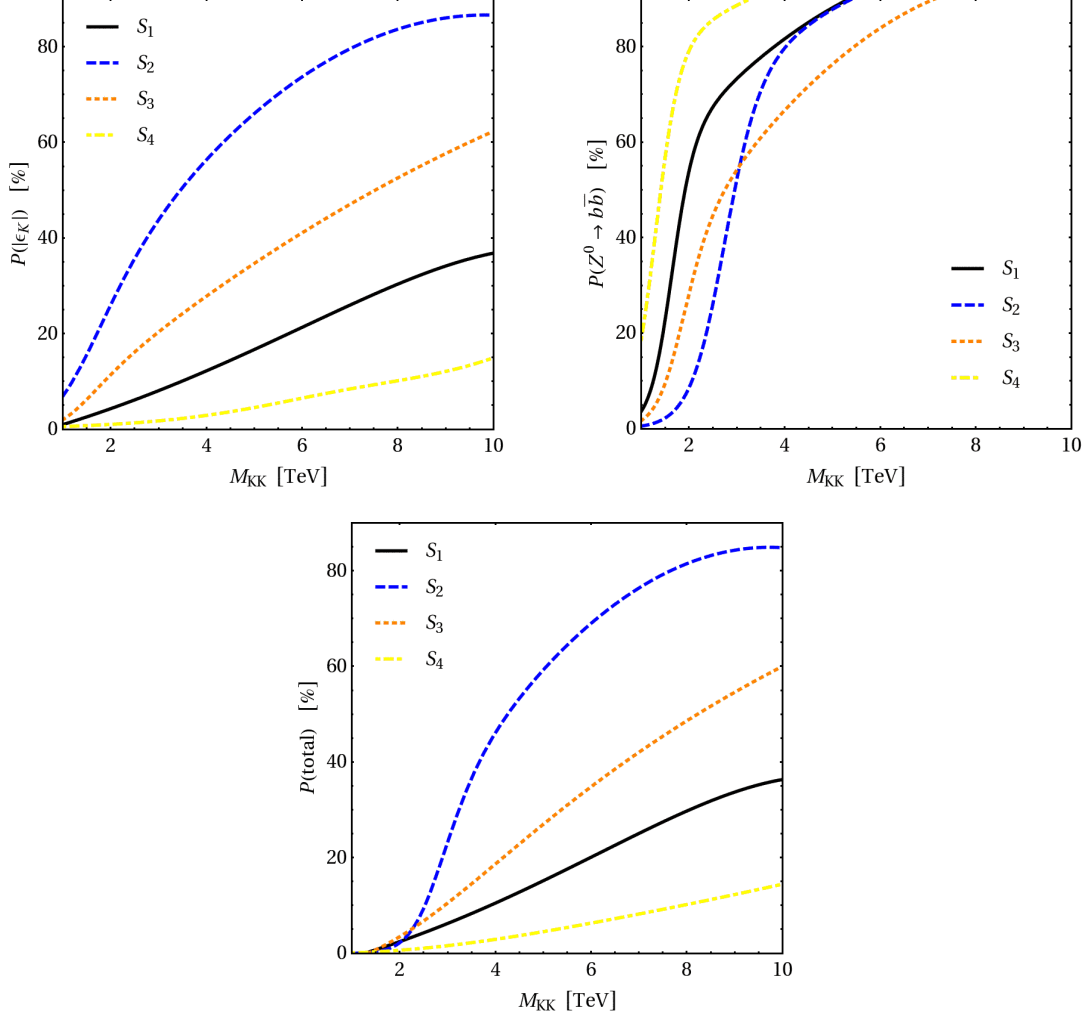


Figure 5: Percentage of scatter points as a function of M_{KK} that are consistent with the experimental values of $|\epsilon_K|$ (upper left), $Z^0 \rightarrow b\bar{b}$ (upper right), and both constraints (lower panel). The shown lines correspond to our four different parameter scenarios. See text for details.

In order to achieve an acceptable amount of CP violation in the kaon sector, the contribution arising from C_4^{RS} needs to be suppressed. The most obvious way to reduce the magnitude of C_4^{RS} consists in increasing the overall size of the elements of the down-type Yukawa matrix, since $C_4^{\text{RS}} \sim (L/M_{KK}^2) (4\pi\alpha_s/Y_d^2) (2m_s m_d/v^2)$ as first noted in [18]. Here Y_d represents a combination of elements of the down-type Yukawa matrix. How effective this suppression is can be assessed by comparing the total number of orange points in the upper left and right plot of Figure 4. We observe that compared to our default scenario S_1 , in the benchmark scenario S_2 the fraction of points that satisfy the experimental constraint from $|\epsilon_K|$ is enhanced from 20% to 74%. To further quantify the improvement, we calculate the fraction $P(|\epsilon_K|)$ of points fulfilling the $|\epsilon_K|$ constraint by dividing the range $M_{KK} \in [1, 10]$ TeV into bins of 100 GeV and

fitting the binned data using an appropriate function. In the case at hand, we find that the combination of a Fermi function and a second-order polynomial is perfectly suited to reproduce the observed decoupling behavior.⁹ The corresponding result is indicated by the blue dashed curve in the upper left plot in Figure 5. We see that even for $M_{\text{KK}} = 1$ TeV roughly 7% of the points satisfy the $|\epsilon_K|$ constraint, which constitutes a noticeable improvement relative to the case of the standard scenario S1, in which this fraction is less than 1%. This improvement however comes with a price. This is illustrated by the blue dashed curve in the upper right plot in Figure 5, which shows the fraction $P(Z^0 \rightarrow b\bar{b})$ of points that lead to an agreement with the measured $Z^0 b\bar{b}$ couplings as a function of M_{KK} . For $P(Z^0 \rightarrow b\bar{b}) > 25\%$ we find $M_{\text{KK}} > 1.6$ TeV in the standard scenario S1, while $M_{\text{KK}} > 2.5$ TeV in scenario S2, which allows for larger Yukawa couplings. This feature is readily understood from the scaling $(g_L^b)_{\text{RS}} \sim -(F^2(c_{b_L})/M_{\text{KK}}^2) (Lm_Z^2 + Y_d^2 v^2)$ [10] of the RS corrections to the $Z^0 b_L \bar{b}_L$ vertex. The individual terms arise here from the deviation of the Z^0 -boson profile from a constant and the mixing of zero and KK fermion modes. For larger Yukawa couplings, effects due to the mixing of fermion zero-modes with their KK excitations get enhanced, and as a consequence the $Z^0 \rightarrow b\bar{b}$ constraint tends to become more stringent. Yet since the $|\epsilon_K|$ constraint is generically more difficult to satisfy than the one originating from $Z^0 \rightarrow b\bar{b}$, the overall picture still improves when one allows for larger Yukawa couplings. The improvement can be read off from the blue dashed curve in the lower plot of Figure 5. In order for the fraction $P(\text{total})$ of the points that fulfill both constraints to reach 10%, one has to require $M_{\text{KK}} > 3.9$ TeV in scenario S1, whereas the weaker limit $M_{\text{KK}} > 2.6$ TeV applies in the case of benchmark scenario S2.

A second possibility to protect $|\epsilon_K|$ from excessive corrections is to arrange for common bulk mass parameters $c_d \equiv c_{d_i}$ in the sector of the right-handed down-type quarks [30]. This subclass of models is considered in our benchmark scenario S3. In the case of “alignment” of down-type quark bulk mass parameters, certain mixing matrices differ from the ones present in the RS model with “hierarchical” c_{d_i} parameters. The phenomenologically most important change occurs in the case of $(\tilde{\Delta}_D)_{mn} \otimes (\tilde{\Delta}_d)_{mn}$, which becomes quasi-diagonal. To derive an expression for the off-diagonal elements one has to expand the flavor matrices defined in (9) up to $\mathcal{O}(v^2/M_{\text{KK}}^2)$. Employing (I:70), we find that the relation (19) receives the correction

$$\begin{aligned} (\tilde{\delta}_D)_{mn} \otimes (\tilde{\delta}_d)_{mn} = \frac{m_{d_m} m_{d_n}}{M_{\text{KK}}^2} & \left[(U_d^\dagger)_{mi} (U_d)_{in} (\tilde{\delta}_D)_{ij} (U_d^\dagger)_{mj} (U_d)_{jn} \right. \\ & \left. + (W_d^\dagger)_{mi} (W_d)_{in} (\tilde{\delta}_d)_{ij} (W_d^\dagger)_{mj} (W_d)_{jn} \right] \end{aligned} \quad (119)$$

from the terms in (9) involving both even $\mathbf{C}_m^{(A)}(\phi)$ and odd $\mathbf{S}_m^{(A)}(\phi)$ fermion profiles. Here a summation over the indices i, j is understood. Neglecting terms suppressed by $F^2(c_{Q_i})$ and $F^2(c_{Q_i})F^2(c_{Q_j})$, the elements of $(\tilde{\delta}_D)_{ij}$ take the form

$$(\tilde{\delta}_D)_{ij} = \frac{2(3 + c_{Q_i} - c_{Q_j})}{(3 + 2c_{Q_i})(3 - 2c_{Q_j})(2 + c_{Q_i} - c_{Q_j})} \frac{F^2(c_{Q_i})}{F^2(c_{Q_j})}. \quad (120)$$

⁹It is not possible to attach a rigorous statistical meaning to the calculated fractions $P(|\epsilon_K|)$, $P(Z^0 \rightarrow b\bar{b})$, and $P(\text{total})$, since they depend on the way in which the results are binned and the fit is performed. The same statement applies to the fraction $P(\epsilon'_K/\epsilon_K)$ introduced below.

An analogous expression holds in the case of $(\tilde{\delta}_d)_{ij}$ with c_{Q_i} replaced by c_{d_i} . Since all bulk mass parameters are close to $-1/2$ it is also a good approximation to replace the rational function of c_{Q_i} and c_{Q_j} in (120) by the numerical factor $3/8$.

Using the scaling relations (I:96) and (7), it is straightforward to deduce from (19) and (119) that to leading order in hierarchies one has

$$(\tilde{\Delta}_D)_{mn} \otimes (\tilde{\Delta}_d)_{mn} \sim \begin{cases} F(c_{Q_m})F(c_{Q_n})F(c_{d_m})F(c_{d_n}), & \text{“hierarchical”}, \\ F(c_{Q_m})F(c_{Q_n})F^2(c_d) \left(\delta_{mn} + \frac{Y_d^2 v^2}{2M_{\text{KK}}^2} \right), & \text{“aligned”}. \end{cases} \quad (121)$$

For clarity we have not shown higher-order terms in v/M_{KK} in the flavor-diagonal contribution. Notice that the $\mathcal{O}(v^2/M_{\text{KK}}^2)$ correction arising in the “aligned” case is solely due to the first term in (119) involving left-handed rotations \mathbf{U}_d . Compared to the latter correction, the contribution from the second term in (119) is further suppressed, since the universality of $(\tilde{\delta}_d)_{ij} \sim 1$ in combination with the unitarity of the \mathbf{W}_d matrices renders it negligibly small.

The relation (121) implies that there is a suppression of the Wilson coefficient C_4^{RS} in the “aligned” relative to the “hierarchical” case. We find the following scaling

$$\frac{(C_4^{\text{RS}})^{\text{“aligned”}}}{(C_4^{\text{RS}})^{\text{“hierarchical”}}} \sim \frac{Y_d^2 v^2}{2M_{\text{KK}}^2} \frac{F(c_{d_1})}{F(c_{d_2})} \sim \frac{Y_d^2 v^2}{2M_{\text{KK}}^2} \frac{m_d}{m_s} \frac{1}{\lambda} \approx 8 \cdot 10^{-3}, \quad (122)$$

where in the first step we used that $F(c_d) \approx F(c_{d_2})$, in the second employed the scaling relation (I:107), and finally set $M_{\text{KK}} = 3 \text{ TeV}$ and $Y_d = 3$ to obtain the numerical estimate. Our results (121) and (122) agree with the findings in [30] derived by means of the mass-insertion approximation. The equivalence of our exact approach and the mass-insertion approximation follows from the “IR dominance” of the overlap integrals (9) and the boundary conditions in (I:63), which connect the odd $\mathbf{S}_n^{(A)}(\pi^-)$ with the even $\mathbf{C}_n^{(A)}(\pi)$ fermion profiles. While the suppression factor of $\mathcal{O}(100)$ appearing in (122) looks very promising in itself, only a rigorous numerical analysis including all contributions can tell us to which extent RS realizations with “alignment” allow one to relax the stringent constraint from $|\epsilon_K|$.

The results of such an analysis are depicted in the lower left and upper left panels of Figures 4 and 5. It is apparent that, relative to the standard scenario S1, in scenario S3 corresponding to the “aligned” case it is easier to obtain a consistent description of the experimental data on $|\epsilon_K|$. Numerically, we find that 37% of the total number of points satisfy the latter constraint and that $P(|\epsilon_K|) > 10\%$ for $M_{\text{KK}} > 1.9 \text{ TeV}$. We have also studied the effect of a slight “misalignment” of the bulk mass parameters c_d , which effectively simulates the presence of flavor non-universal brane kinetic terms. In agreement with [30], we find that the obtained results depend very sensitively on the exact amount of non-universality and that already small deviations from $c_{d_1} = c_{d_2} = c_{d_3}$ can easily spoil the $\mathcal{O}(v^2/M_{\text{KK}}^2)$ suppression in (122). One also observes from the orange dotted line in Figure 5 that the $Z^0 b\bar{b}$ constraint turns out to be more stringent in the “aligned” RS framework. This feature is easy to explain. In RS realizations with “alignment”, the singlet b_R lives further away from the IR brane compared to the original “hierarchical” case. Typically one has $c_{b_R} = c_d \approx -0.60$ instead of $c_{b_R} \approx -0.58$. In order to obtain the correct value of the bottom-quark mass, the doublet (t_L, b_L) thus needs

to be localized more closely to the IR brane. This is not a favorable option, since placing (t_L, b_L) too close to the IR brane generates an unacceptably large correction to the $Z^0 b_L \bar{b}_L$ coupling. Quantitatively, we find that demanding $P(Z^0 \rightarrow b\bar{b}) > 25\%$ sets the lower limit $M_{\text{KK}} > 2.0 \text{ TeV}$. Notice that in warped extra-dimension models with custodial protection of the $Z^0 b_L \bar{b}_L$ vertex this problem is not present, because the corrections to the $Z^0 \rightarrow b\bar{b}$ couplings are small and largely independent of the bulk mass parameters. Nevertheless, as demonstrated by the orange dotted curve in the lower plot of Figure 5, universal bulk mass parameters c_d nevertheless help to lower the bound on the KK scale following from a combination of constraints. Numerically, we obtain for $P(\text{total}) > 10\%$ the bound $M_{\text{KK}} > 3.0 \text{ TeV}$, which constitutes an improvement relative to the “hierarchical” case.

The presence of the “volume factor” L in (24) suggests that a third cure for the “flavor problem” in the $\Delta S = 2$ sector is to reduce the UV cutoff sufficiently below the Planck scale. Indeed, the alleviation of the $|\epsilon_K|$ constraint has been mentioned as one of the attractive features of “little” RS scenarios [149]. However, a careful analysis reveals that the naive conjecture of a reduction of terms proportional to L is flawed in the case of $|\epsilon_K|$ [36]. This feature is illustrated by the lower right and upper left plots Figures 4 and 5. We see that in scenario S4 featuring $L = \ln(10^3) \approx 7$ instead of $L = \ln(10^{16}) \approx 37$, the percentage of points that are in agreement with the measured value of $|\epsilon_K|$ amounts to only 6% and that, in particular, $P(|\epsilon_K|) \approx 1\%$ for $M_{\text{KK}} = 1 \text{ TeV}$. The origin of the enhancement of flavor-changing $\Delta S = 2$ effects is the phenomenon of “UV dominance”, which arises whenever the bulk mass parameters determining the strange-quark mass satisfy the critical condition $c_{Q_2} + c_{d_2} < -2$ [36]. The relevant overlap integrals (9) are then dominated by the region near the UV brane, thereby partially evading the RS-GIM mechanism. New physics contributions to $|\epsilon_K|$ are then exponentially enhanced with respect to the standard scenario S1 with $L = \ln(10^{16}) \approx 37$. While in “little” RS scenarios thus no improvement concerning $|\epsilon_K|$ can be achieved, unless the UV cutoff is raised above several 10^3 TeV , this class of models still helps to relax the constraint arising from $Z^0 \rightarrow b\bar{b}$. This can be seen from the yellow dashed-dotted curve in the upper right panel of Figure 5, which reaches $P(Z^0 \rightarrow b\bar{b}) > 25\%$ once $M_{\text{KK}} > 1.1 \text{ TeV}$ is satisfied. On the other hand, it is clearly visible from the yellow dashed-dotted curve in the lower plot of Figure 5 that if one requires the constraints from both $|\epsilon_K|$ and $Z^0 \rightarrow b\bar{b}$ to hold, then the bounds on M_{KK} are even stronger in scenario S4 than in the default scenario S1. Demanding as usual $P(\text{total}) > 10\%$ translates in the case of the “little” RS model into the rather severe limit $M_{\text{KK}} > 8.0 \text{ TeV}$. Further details on RS variants with “volume-truncated” background can be found in [36].

It should have become clear from the above discussion and explanations that obtaining a natural solution to the “flavor problem” in the $\Delta S = 2$ sector, with KK gauge-boson masses in the reach of the LHC, is difficult in the framework of warped extra dimensions [11, 18, 21, 30, 36]. Our detailed numerical analysis of anarchic RS realizations shows that requiring only a moderate amount of fine-tuning, $P(|\epsilon_K|) = 10\%$, implies that the mass of the first-level KK gluon mode has to fulfill

$$M_{g^{(1)}} \approx 2.45 M_{\text{KK}} \gtrsim 10 \text{ TeV} . \quad (123)$$

However, consistency with $|\epsilon_K|$ can be achieved for masses of the first KK excitation in the ballpark of 3 TeV by either allowing for larger Yukawa couplings, or by “alignment” in the

right-handed down-type quark sector. Both solutions have their shortcomings. In the first case the constraint from $B \rightarrow X_s \gamma$ typically becomes more stringent [21], while in the second scenario the natural flavor suppression (122) in $|\epsilon_K|$ can be impaired by the presence of flavor non-universal brane kinetic terms [30], making this setup radiatively unstable.

5.4.2 Numerical Analysis of $B_{d,s}-\bar{B}_{d,s}$ Mixing

In the following we will study the impact of new-physics effects on the $B_{d,s}-\bar{B}_{d,s}$ mixing amplitudes, taking into account the stringent constraints on the parameter space imposed by $|\epsilon_K|$. Since the new CP-odd phases appearing in the $s \rightarrow d$ and $b \rightarrow d, s$ transitions are highly uncorrelated, we will see that large departures in both $S_{\psi\phi}$ and A_{SL}^s from their SM values are possible, which are consistent with all remaining constraints in the $\Delta F = 2$ sector.

We start our survey in the B_d system. In Figure 6 we display the predictions for ϕ_{B_d} versus C_{B_d} as well as $\Delta\Gamma_d/\Gamma_d$ and $A_{\text{SL}}^d/(A_{\text{SL}}^d)_{\text{SM}}$ versus $S_{\psi K_S}$ obtained in scenario S1. Our findings are however largely independent of the choice of the benchmark scenario. In all three panels the shown blue points reproduce the correct quark masses and mixings within errors and satisfy the constraints from both $|\epsilon_K|$ and $Z^0 \rightarrow b\bar{b}$. The SM prediction is indicated by a black cross, and the yellow (orange) colored contour corresponds to the experimentally preferred 68% (95%) CL region. Turning our attention to the predictions in the $C_{B_d}-\phi_{B_d}$ plane, we observe that while shifts of more than ± 0.3 and $\pm 10^\circ$ are possible in C_{B_d} and ϕ_{B_d} , the corrections are on average small and thus no cause of concern. Notice that there is a slight tension [41, 48, 55, 161] of 2.1σ between the SM expectation, $(\phi_{B_d})_{\text{SM}} = 0^\circ$, and the value $\phi_{B_d} = (-5.8 \pm 2.8)^\circ$ extracted from our global fit. The coefficient $C_{B_d} = 0.89 \pm 0.17$, on the other hand, shows good agreement with the SM value $(C_{B_d})_{\text{SM}} = 1$. In our analysis the bulk of the discrepancy in ϕ_{B_d} is due to the correlation between the observable $\mathcal{B}(B \rightarrow \tau\nu_\tau)$ and the angle β [162]. Obviously, the disagreement is not large enough to exclude the possibility of a statistical origin of the tension, but it is interesting to note that the RS model can naturally accommodate a small phase ϕ_{B_d} of the order of a few degrees with both signs. In the case of the observables $\Delta\Gamma_d/\Gamma_d$, $A_{\text{SL}}^d/(A_{\text{SL}}^d)_{\text{SM}}$, and $S_{\psi K_S}$, we find that the RS predictions are in general compatible with the current direct experimental determinations, which read $(\Delta\Gamma_d/\Gamma_d)_{\text{exp}} = 0.009 \pm 0.037$, $(A_{\text{SL}}^d)_{\text{exp}} = -0.0047 \pm 0.0046$, and $S_{\psi K_S} = 0.672 \pm 0.023$ [94]. Notice that the values $\Delta\Gamma_d/\Gamma_d = 0.0049 \pm 0.0010$ and $A_{\text{SL}}^d = -0.0018 \pm 0.0007$ following from our global analysis are much more precise than the corresponding direct extractions, and that the slight disagreement in ϕ_{B_d} translates into a tension in $A_{\text{SL}}^d/(A_{\text{SL}}^d)_{\text{SM}}$. We conclude that the RS-GIM mechanism makes warped extra-dimension models naturally consistent with the available data on Δm_d , while it does not exclude the presence of a new-physics contribution to the mixing phase ϕ_{B_d} of the right size to be directly tested with improved measurements of $\Delta\Gamma_d/\Gamma_d$, A_{SL}^d , and $S_{\psi K_S}$. Similar conclusions have been drawn in [11].

We now move onto the B_s system. Our results for ϕ_{B_s} versus C_{B_s} , as well as $\Delta\Gamma_s/\Gamma_s$ and $A_{\text{SL}}^s/(A_{\text{SL}}^s)_{\text{SM}}$ versus $S_{\psi\phi}$ obtained in the parameter scenario S1 are shown in Figure 7. In this case we only include points in the plots that satisfy the constraints from $|\epsilon_K|$, $Z^0 \rightarrow b\bar{b}$, and $B_d-\bar{B}_d$ mixing. The SM predictions are indicated by black crosses, while the yellow (orange) colored contours resemble the experimentally favored regions at 68% (95%) CL. Focusing first on the predictions in the $C_{B_s}-\phi_{B_s}$ plane, we see that shifts of up to ± 0.4 in C_{B_s} and

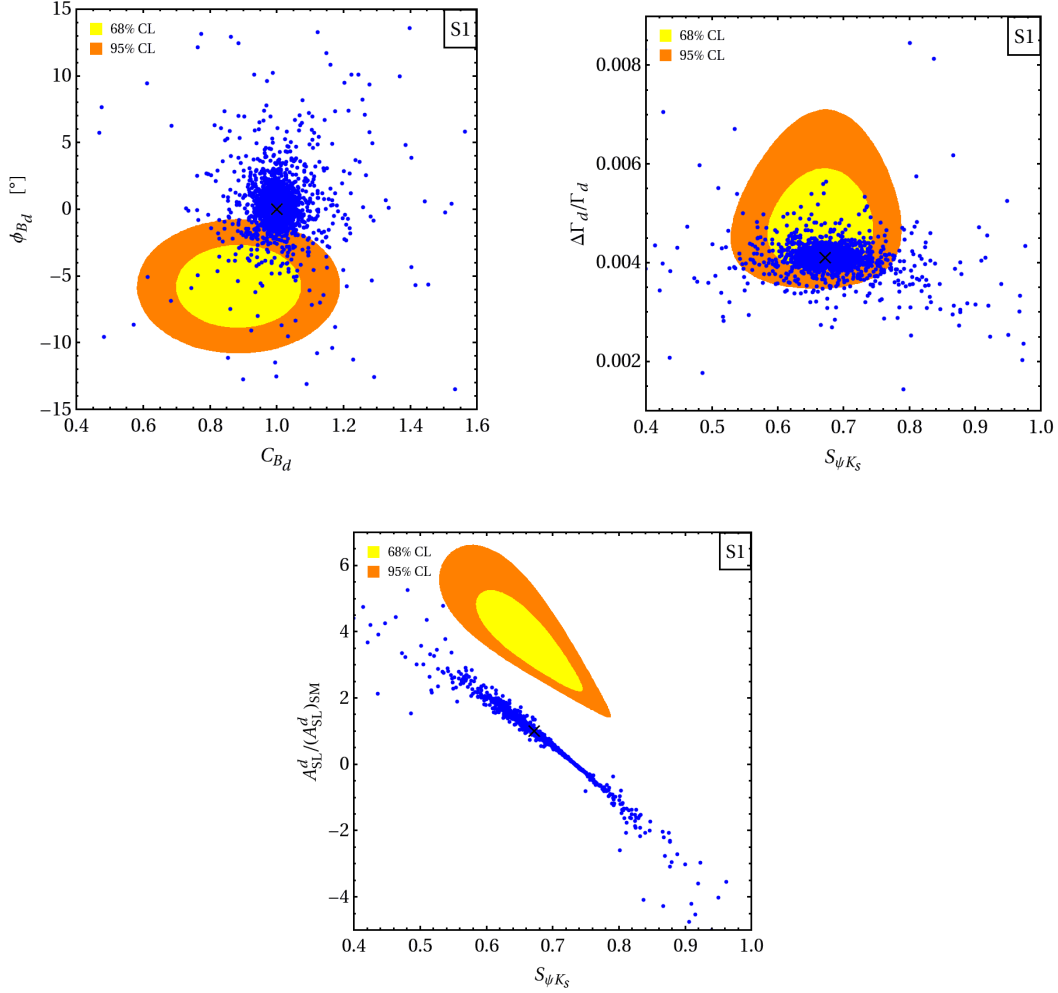


Figure 6: Predictions for ϕ_{B_d} versus C_{B_d} (upper left), as well as $\Delta\Gamma_d/\Gamma_d$ (upper right) and $A_{\text{SL}}^d/(A_{\text{SL}}^d)_{\text{SM}}$ (lower panel) versus $S_{\psi K_S}$. The blue points reproduce the measured values of $|\epsilon_K|$ and the $Z^0 b\bar{b}$ couplings at the 95% and 99% CL, respectively. The black crosses indicate the SM predictions and the yellow (orange) contours the experimentally favored regions of 68% (95%) probability. See text for details.

large corrections in ϕ_{B_s} are possible in the RS model. For comparison, we show the results of a model-independent analysis of new-physics contributions to $B_s-\bar{B}_s$ mixing employing the parametrization (30). We obtain two solutions for ϕ_{B_s} , reflecting the twofold ambiguity inherent in the measurement of time-dependent tagged angular analysis of $B_s \rightarrow \psi\phi$ decays, *i.e.*, $\varphi_s \leftrightarrow 90^\circ - \varphi_s$ and $\Delta\Gamma_s \leftrightarrow -\Delta\Gamma_s$. The numerical results of the two solutions are $\phi_{B_s} = (-19.0 \pm 10.8)^\circ$ and $\phi_{B_s} = (-69.9 \pm 10.1)^\circ$, which implies a deviation of $\varphi_s = |\beta_s| - \phi_{B_s}$ of more than 2.5σ from its SM value $(\varphi_s)_{\text{SM}} \approx 1^\circ$. For the magnitude of the $B_s-\bar{B}_s$ mixing amplitude we find $C_{B_s} = 0.93 \pm 0.19$, in agreement with the SM expectation. Our global fit is based on the combined CDF and DØ measurement of Δm_s [163, 164] and the two-dimensional

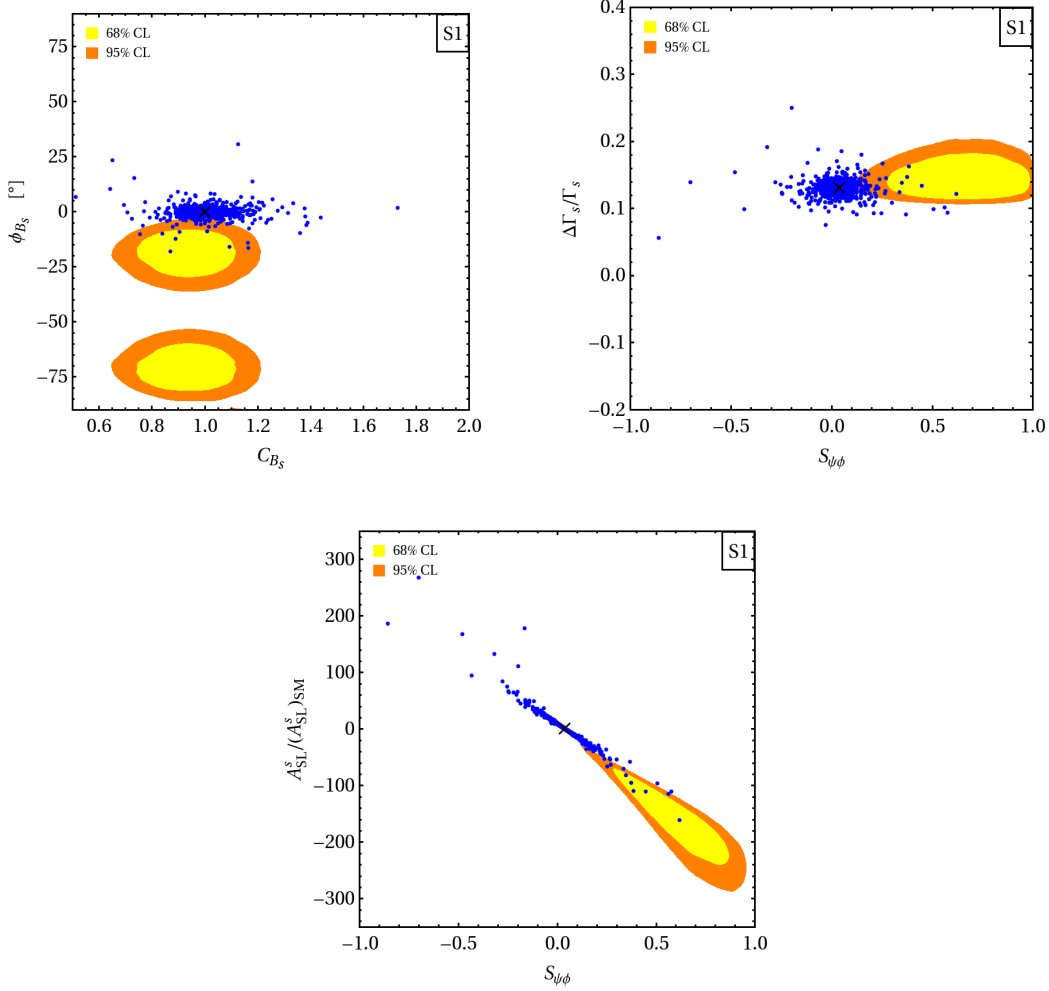


Figure 7: Predictions for ϕ_{B_s} versus C_{B_s} (upper left), as well as $\Delta\Gamma_s/\Gamma_s$ (upper right) and $A_{\text{SL}}^s/(A_{\text{SL}}^s)_{\text{SM}}$ (lower panel) versus $S_{\psi\phi}$. The blue points reproduce the measured values of $|\epsilon_K|$, the $Z^0 b\bar{b}$ couplings, and $B_d-\bar{B}_d$ mixing at the 95%, 99%, and 95% CL. The black crosses indicate the SM predictions and the yellow (orange) contours the experimentally preferred regions of 68% (95%) probability. See text for details.

CL for ϕ_{B_s} and $\Delta\Gamma_s$ obtained from the flavor-tagged analysis of mixing-induced CP violation in $B_s \rightarrow \psi\phi$ [165, 166]. Concerning the remaining observables in the B_s system, we observe that compared to the SM value $(S_{\psi\phi})_{\text{SM}} \approx 0.04$ the large range $[-0.5, 0.5]$ of $S_{\psi\phi}$ is attainable in the RS framework, and that also the semileptonic CP asymmetry A_{SL}^s can be enhanced by more than two orders of magnitude relative to its SM value $(A_{\text{SL}}^s)_{\text{SM}} \approx 2 \cdot 10^{-5}$. In particular, the values $S_{\psi\phi} = 0.63 \pm 0.35$ and $A_{\text{SL}}^s = -0.0032 \pm 0.0020$ favored by the existing data can be obtained. On the other hand, the predicted corrections in $\Delta\Gamma_s/\Gamma_s$ are typically small and compatible with both the experimentally favored range $\Delta\Gamma_s/\Gamma_s = 0.15 \pm 0.03$ and the SM expectation $(\Delta\Gamma_s/\Gamma_s)_{\text{SM}} \approx 0.13$.

The plots in Figures 6 and 7 display strong correlations between the various observables. In order to better understand the pattern of deviations we express $\Delta\Gamma_{d,s}/\Gamma_{d,s}$ and $A_{\text{SL}}^{d,s}/(A_{\text{SL}}^{d,s})_{\text{SM}}$ through $S_{\psi K_S}$ and $S_{\psi\phi}$, respectively. For the B_d system, one finds (keeping terms to first order in the deviation of $S_{\psi K_S}$ from its SM value $\sin 2\beta$)

$$\begin{aligned}\frac{\Delta\Gamma_d}{\Gamma_d} &\approx -\left(\frac{\Delta m_d}{\Gamma_d}\right)_{\text{exp}} \left[\text{Re}(\Gamma_{12}^d/M_{12}^d)_{\text{SM}} + \frac{\text{Im}(\Gamma_{12}^d/M_{12}^d)_{\text{SM}}}{\cos 2\beta} (\sin 2\beta - S_{\psi K_S}) \right] C_{B_d}^{-1} \\ &= (0.004 - 0.0005 S_{\psi K_S}) C_{B_d}^{-1}, \\ \frac{A_{\text{SL}}^d}{(A_{\text{SL}}^d)_{\text{SM}}} &\approx \left[1 + \frac{\text{Re}(\Gamma_{12}^d/M_{12}^d)_{\text{SM}}}{\text{Im}(\Gamma_{12}^d/M_{12}^d)_{\text{SM}}} \frac{1}{\cos 2\beta} (\sin 2\beta + S_{\psi K_S}) \right] C_{B_d}^{-1} \\ &= (11.7 - 15.3 S_{\psi K_S}) C_{B_d}^{-1},\end{aligned}\tag{124}$$

where in the last step we have inserted the central values of the SM predictions quoted in (35).

In the case of the B_s system the corresponding expressions simplify, since $\sin 2|\beta_s| \approx 0$ and $\cos 2|\beta_s| \approx 1$. Keeping terms to first order in $S_{\psi\phi}$ but neglecting small corrections due to $|\beta_s| \neq 0$, one obtains

$$\begin{aligned}\frac{\Delta\Gamma_s}{\Gamma_s} &\approx -\left(\frac{\Delta m_s}{\Gamma_s}\right)_{\text{exp}} \left[\text{Re}(\Gamma_{12}^s/M_{12}^s)_{\text{SM}} + \text{Im}(\Gamma_{12}^s/M_{12}^s)_{\text{SM}} S_{\psi\phi} \right] C_{B_s}^{-1} \\ &= (0.131 - 0.0006 S_{\psi\phi}) C_{B_s}^{-1}, \\ \frac{A_{\text{SL}}^s}{(A_{\text{SL}}^s)_{\text{SM}}} &\approx \frac{\text{Re}(\Gamma_{12}^s/M_{12}^s)_{\text{SM}}}{\text{Im}(\Gamma_{12}^s/M_{12}^s)_{\text{SM}}} S_{\psi\phi} C_{B_s}^{-1} \\ &= -238.1 S_{\psi\phi} C_{B_s}^{-1},\end{aligned}\tag{125}$$

where the final numerical values correspond to the SM predictions given in (35). The strong correlation between A_{SL}^s and $S_{\psi\phi}$ has been first pointed out in [167]. That this correlation also exists in the RS scenario has been emphasized in [11]. Given the model-independent character [54] of the linear relation between $A_{\text{SL}}^s/(A_{\text{SL}}^s)_{\text{SM}}$ and $S_{\psi\phi}$, which can only be violated if there is sizable direct CP-violation due to new physics in the decay, the observation of a correlation that follows the pattern in (125) is however not a ‘‘smoking gun’’ signal unique to the RS model. The same statement applies to the remaining correlations following from the relations (124) and (125).

We close this section by adding some comments concerning the model dependence of the obtained results. As already mentioned earlier, in RS scenarios with custodial $SU(2)$ symmetry electroweak corrections to $B_{d,s}-\bar{B}_{d,s}$ mixing can compete with the corrections due to KK gluon exchange. In rough accordance with [11], we find that purely electroweak effects in C_1^{RS} , \tilde{C}_1^{RS} , and C_5^{RS} are relative to (24) modified by factors of about 2.5, 94.6, and -10.9 . We remark that in the custodial model a cancellation between the strong and electroweak part in C_5^{RS} occurs since the individual contributions have approximately equal size but opposite signs. The ratios

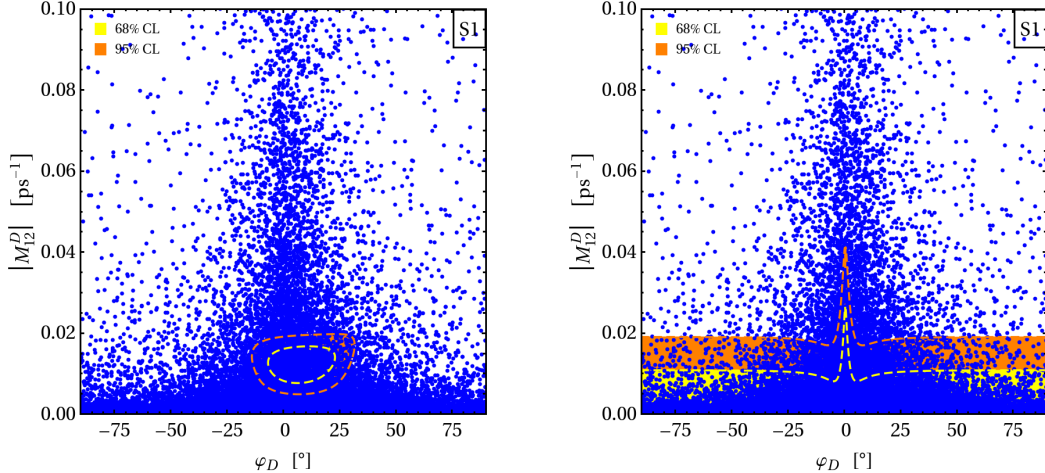


Figure 8: Predictions for $|M_{12}^D|_{\text{RS}}$ versus φ_D compared to the experimentally allowed 68% (95%) CL regions shown in yellow (orange), assuming $(M_{12}^D)_{\text{SM}} = 0$ (left) and allowing for $(M_{12}^D)_{\text{SM}} \in [-0.02, 0.02] \text{ ps}^{-1}$ (right). The blue scatter points reproduce the measured values of $|\epsilon_K|$, the $Z^0 \rightarrow b\bar{b}$ couplings, and $B_d-\bar{B}_d$ mixing at 95%, 99%, and 95% CL. See text for details.

of the full RS contributions in the custodial relative to the original model are thus 1.3, 1.9, and -0.3 . Compared to Figures 6 and 7, these changes, in combination with the relaxation of the $Z^0 \rightarrow b\bar{b}$ constraint due to custodial protection [156], allow for somewhat larger effects in the $B_{d,s}-\bar{B}_{d,s}$ mixing observables. The pattern of departures from the SM expectations, however, remains unchanged. We leave a detailed analysis of neutral-meson mixing in the RS model with custodial symmetry $SU(2)_L \times SU(2)_R \times P_{LR}$ for future work.

5.4.3 Numerical Analysis of $D-\bar{D}$ Mixing

Short-distance contributions from new physics can also affect the dispersive part of the $D-\bar{D}$ mixing amplitude M_{12}^D in a significant way. Similarly to the case of the K_L-K_S mass difference, the calculation of $|M_{12}^D|$ is plagued by long-distance contributions [168]. In order to grasp the impact of non-perturbative effects on the obtained results we proceed in the following way. We write the full amplitude M_{12}^D as the sum of the RS amplitude $(M_{12}^D)_{\text{RS}} = |M_{12}^D|_{\text{RS}} e^{-2i\varphi_D}$ and the real SM amplitude, $(M_{12}^D)_{\text{SM}}$, containing both short- and long-distance contributions. We then consider two diametrically opposed cases. In the first case, the SM contribution to $(M_{12}^D)_{\text{SM}}$ is set to zero, and the constraint on $|M_{12}^D|$ and the phase φ_D is directly applied to the RS contribution. In the second case, we take $(M_{12}^D)_{\text{SM}}$ to be flatly distributed in the range $[-0.02, 0.02] \text{ ps}^{-1}$, so that the SM contribution alone can saturate the experimental bound. We will see that even with the latter conservative treatment of the theoretical uncertainties entering the SM prediction, the available experimental data on $D-\bar{D}$ mixing have a non-trivial impact on the allowed model parameters in the RS framework.

In Figure 8 we show the predictions of the RS model in the $\varphi_D-|M_{12}^D|_{\text{RS}}$ plane obtained

from a general scan in the benchmark scenario S1. The blue points satisfy the constraints from $|\epsilon_K|$, $Z^0 \rightarrow b\bar{b}$, and $B_d-\bar{B}_d$ mixing. For comparison, the 68% (95%) CL regions favored by the data are underlaid in yellow (orange). They have been obtained from a simultaneous fit to the data from BaBar [56], Belle [57, 58], and CDF [59], employing the two different treatments of theoretical uncertainties described above. Our fit is based on the experimental inputs $x_D = 0.0098_{-0.0026}^{+0.0024}$, $y_D = 0.0083 \pm 0.0016$, $(x_D^2 + y_D^2)/2 \leq (1.3 \pm 2.7) \cdot 10^{-4}$, $|q/p|_D = 0.87_{-0.15}^{+0.17}$, and $\tau_D = (0.4101 \pm 0.0015)$ ps, as well as the corresponding correlation matrix [94, 169]. These numbers imply for the dispersive and absorptive parts of the off-diagonal mixing elements $(M_{12}^D)_{\text{exp}} \approx \pm 0.012 \text{ ps}^{-1}$ and $(\Gamma_{12}^D)_{\text{exp}} \approx \pm 0.020 \text{ ps}^{-1}$. The distribution of scatter points shows that large corrections to both the magnitude and phase of the $D-\bar{D}$ mixing amplitude can occur in the RS framework. In particular, the entire range of CP-violating phases $\varphi_D \in [-90^\circ, 90^\circ]$ can be populated. From the inspection of the two panels it is evident that the power of the $D-\bar{D}$ constraint depends in a crucial way on the treatment of the large theoretical uncertainties plaguing the calculation of $(M_{12}^D)_{\text{SM}}$. If the constraint on $|M_{12}^D|$ and the phase φ_D is applied to the RS contribution alone, neglecting the SM contribution, then the impact of the $D-\bar{D}$ constraint is quite stringent. On the other hand, it turns out to be much weaker, though non-negligible, if one allows the SM contribution alone to saturate the experimental bounds. This feature implies that a breakthrough in the theoretical control over the quantity $(M_{12}^D)_{\text{SM}}$ is required to resolve whether the observed size of ΔM_D is completely due to SM dynamics or contains a sizable or maybe even leading contribution due to new physics.

Our above findings suggest that KK gluon exchange in the RS model can potentially lead to sizable CP asymmetries in various D -meson decay channels. The Cabibbo-favored channel with the best trade-off between theoretical simplicity and experimental accessibility is $D \rightarrow \phi K_S$ [61]. In Figure 9 we show the correlation between $S_{\psi K_S}^D$ and A_{SL}^D for a parameter scan in the benchmark scenario S1. The shown points are consistent with the constraints arising from $|\epsilon_K|$, $Z^0 \rightarrow b\bar{b}$, and $B_d-\bar{B}_d$ mixing. The black crosses indicate the SM prediction. In the left panel we have set $(M_{12}^D)_{\text{SM}} = 0$, while in the right panel $(M_{12}^D)_{\text{SM}}$ is allowed to vary freely in the range $[-0.02, 0.02] \text{ ps}^{-1}$. In both panels, blue (red) points indicate solutions with $\Gamma_{12}^D = +0.020 \text{ ps}^{-1}$ ($\Gamma_{12}^D = -0.020 \text{ ps}^{-1}$) that are in agreement with the measured values of x_D , y_D , and $|q/p|_D$. The shown light gray points are not consistent with these constraints. While *a priori* RS dynamics could generate values for $S_{\phi K_S}^D$ that exceed ± 0.05 , the experimental constraint on $|q/p|_D$ and consequently on A_{SL}^D implies an allowed range of at most $S_{\phi K_S}^D \in [-0.02, 0.01]$ due to the strong correlation between the two CP asymmetries. We observe that for realistic values of A_{SL}^D there is a strict linear correlation between these two CP asymmetries, with the slope determined by the prefactor $y_D/(x_D^2 + y_D^2) \approx 50$ entering (41). Any violation of this correlation would signal the presence of direct CP violation in the decay $D \rightarrow \phi K_S$. Like in the case of $B_{d,s}-\bar{B}_{d,s}$ mixing, an observation of the correlation between A_{SL}^D and $S_{\phi K_S}^D$ will however not tell us whether it is due to KK exchange or some other kind of new physics. For example, it seems difficult to disentangle the corrections predicted in the RS framework from those arising in the littlest-Higgs model with T -parity studied in [61]. CP violation due to RS dynamics can also be searched for in the non-leptonic channels $D \rightarrow K_S K^+ K^-$, $K^+ K^-$, $\pi^+ \pi^-$, and $K^+ \pi^-$. A comprehensive study of these transitions is beyond the scope of this article.

Let us again comment on the model dependence of our results for $D-\bar{D}$ mixing. Similar to

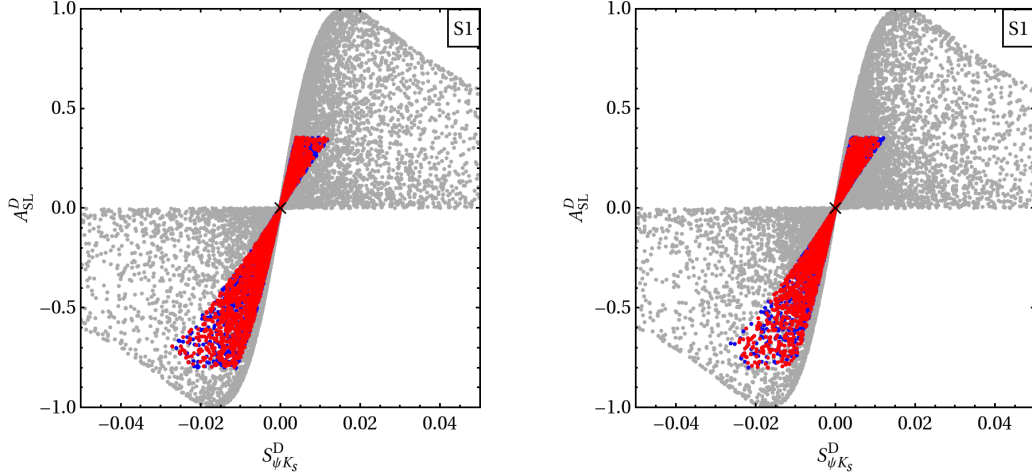


Figure 9: Predictions for $S_{\psi K_S}^D$ versus A_{SL}^D assuming $(M_{12}^D)_{SM} = 0$ (left) and allowing for $(M_{12}^D)_{SM} \in [-0.02, 0.02] \text{ ps}^{-1}$ (right). All the shown scatter points reproduce the measured values of $|\epsilon_K|$, the $Z^0 \rightarrow b\bar{b}$ couplings, and $B_d - \bar{B}_d$ mixing at 95%, 99%, and 95% CL. Blue (red) points are obtained for $\Gamma_{12}^D = +0.020 \text{ ps}^{-1}$ ($\Gamma_{12}^D = -0.020 \text{ ps}^{-1}$). They satisfy the constraints arising from the $D - \bar{D}$ mixing measurements at 95% CL, while the light gray points do not. See text for details.

$B_{d,s} - \bar{B}_{d,s}$ oscillations, also in this case electroweak corrections can compete with the corrections due to KK gluon exchange in models with $SU(2)_L \times SU(2)_R \times P_{LR}$ gauge symmetry in the bulk. Numerically, we find that purely electroweak effects in C_1^{RS} , \tilde{C}_1^{RS} , and C_5^{RS} are relative to (24) modified by factors of about 3.4, 2.5, and -0.9 . While this feature allows for somewhat larger effects, the pattern of deviations from the SM expectations remains unchanged. In this context, we also point out that the custodial protection mechanism *simultaneously* suppresses corrections to the $Z^0 d_{iL} \bar{d}_{jL}$ as well as the $Z^0 u_{iR} \bar{u}_{jR}$ couplings if the quark sector is implemented as in [11, 19, 170, 171]. The same conclusion has been drawn independently in [150]. This feature implies, in particular, that the chirality of the $Z^0 tc$ interactions in this specific RS variant is predicted not to be right-handed [17] but left-handed. Of course, other choices of the quantum numbers of the right-handed up-type quarks are possible, so that the RS framework does not lead to a firm prediction of the chirality of the $Z^0 tc$ interactions.

5.5 Rare Leptonic Decays of Kaons and B Mesons

This section is devoted to detailed studies of non-standard effects in rare decay modes of kaons and B mesons arising from the tree-level exchange of neutral gauge bosons, their KK excitations, and the Higgs boson. In the former case, the special role of the $K \rightarrow \pi \nu \bar{\nu}$ and $K_L \rightarrow \pi^0 l^+ l^-$ modes is emphasized, which due to their theoretical cleanliness and their enhanced sensitivity to non-standard flavor and CP violation are unique tools to discover or, if no deviation is found, to set severe constraints on the parameter space of RS models. In the latter case, we begin our discussion with $B_q \rightarrow \mu^+ \mu^-$ and $B \rightarrow X_q \nu \bar{\nu}$ and stress the power

of these decay modes in probing the short-distance physics related to Z^0 -penguin diagrams. We conclude our explorations in the B -meson sector by studying the numerical impact of the exchange of the Z^0 boson and its KK modes on $B \rightarrow X_s l^+ l^-$ and $B \rightarrow K^* l^+ l^-$. In this context we investigate whether the predictions for the decay distributions lie within the experimentally allowed bounds. A discussion on how the obtained results depend on the choice of the bulk gauge group and the implementation of the fermionic sector complement our phenomenological survey.

5.5.1 Numerical Analysis of $K \rightarrow \pi \nu \bar{\nu}$, $K_L \rightarrow \pi^0 l^+ l^-$, and $K_L \rightarrow \mu^+ \mu^-$

We begin our investigations by studying the rare decays $K_L \rightarrow \pi^0 \nu \bar{\nu}$ and $K^+ \rightarrow \pi^+ \nu \bar{\nu}$, which offer the cleanest window into the sector of $s \rightarrow d$ transitions. In Figure 10 we display the predictions for the branching ratio of the neutral mode versus that of the charged one. The blue points correspond to parameter values that reproduce the correct quark masses and mixings and satisfy the constraints from $|\epsilon_K|$, $Z^0 \rightarrow b\bar{b}$, and $B_d - \bar{B}_d$ mixing. For comparison, the central value and the 68% CL range of the experimental world average $\mathcal{B}(K^+ \rightarrow \pi^+ \nu \bar{\nu}(\gamma))_{\text{exp}} = (1.73_{-1.05}^{+1.15}) \cdot 10^{-10}$ based on seven events [172] is indicated by the vertical dashed black line and the yellow band. The experimental 90% CL upper limit $\mathcal{B}(K_L \rightarrow \pi^0 \nu \bar{\nu})_{\text{exp}} < 2.6 \cdot 10^{-8}$ [173] is not displayed in the figure. The central values of the SM predictions (74) are indicated by the black cross. As can be seen from the left panel showing the results of a parameter scan in the benchmark scenario S1, the branching fractions of both $K \rightarrow \pi \nu \bar{\nu}$ channels can be significantly enhanced compared to the SM prediction. In particular, it is even possible to saturate the model-independent Grossman-Nir (GN) bound [174]

$$\mathcal{B}(K_L \rightarrow \pi^0 \nu \bar{\nu}) \leq \frac{\kappa_L}{\kappa_+(1 + \Delta_{\text{EM}})} \mathcal{B}(K^+ \rightarrow \pi^+ \nu \bar{\nu}(\gamma)) \approx 4.3 \mathcal{B}(K^+ \rightarrow \pi^+ \nu \bar{\nu}(\gamma)), \quad (126)$$

which represents an enhancement of $\mathcal{B}(K_L \rightarrow \pi^0 \nu \bar{\nu})$ by almost a factor of 50 over the SM expectation for values of $\mathcal{B}(K^+ \rightarrow \pi^+ \nu \bar{\nu}(\gamma))$ at the upper end of the experimentally favored range. The inequality (126) is indicated by the straight dotted black line in the figure, and the inaccessible area is colored light gray. Because the weak phase entering the $s \rightarrow d \nu \bar{\nu}$ transition can take essentially any value in the standard scenario S1, the predictions for the charged and neutral mode are highly uncorrelated, so that, similar to what is observed in the case of the general minimal supersymmetric SM (MSSM) [175], every point in the $\mathcal{B}(K^+ \rightarrow \pi^+ \nu \bar{\nu}(\gamma)) - \mathcal{B}(K_L \rightarrow \pi^0 \nu \bar{\nu})$ plane that satisfies the GN bound can be attained. Interestingly, due to the slow decoupling of the RS corrections, enhancements of the rate of the neutral mode by almost an order of magnitude are possible even for $M_{\text{KK}} = 10 \text{ TeV}$. This feature, illustrated in the upper panel of Figure 10, implies that measurements of $K_L \rightarrow \pi^0 \nu \bar{\nu}$ can in principle probe scales far above those accessible to direct searches at the LHC. As we will show in Section 5.6.1, the possible enhancements in the $K \rightarrow \pi \nu \bar{\nu}$ system are reduced noticeably if one takes into account the constraint following from ϵ'_K / ϵ_K , because large shifts in the neutrino modes typically appear together with an unacceptable amount of direct CP violation in $K \rightarrow \pi \pi$.

While the pattern of deviations found in the benchmark scenarios S2 and S4 follows that observed in the standard case S1, a strikingly different picture emerges in the scenario S3, which features common bulk mass parameters c_{d_i} . This is illustrated in the lower right panel

of Figure 10. To understand the observed pattern, we first recall that in the benchmark scenario S3 right-handed currents entering $|\epsilon_K|$ in form of the Wilson coefficients \tilde{C}_1^{RS} , C_4^{RS} , and C_5^{RS} as well as $K \rightarrow \pi\nu\bar{\nu}$ in form of $\tilde{C}_\nu^{\text{RS}}$ are parametrically suppressed by factors of v^2/M_{KK}^2 and thus numerically subleading compared to the left-handed corrections C_1^{RS} and C_ν^{RS} , which to leading order in L are proportional to $(\Delta_D)_{12} \otimes (\Delta_D)_{12}$ and $(\Delta_D)_{12}$. Furthermore, the fact that the left-handed contribution $(\Delta_D)_{12} \otimes (\Delta_D)_{12}$ factorizes as $(\Delta_D)_{12} \otimes (\Delta_D)_{12} \approx ((\Delta_D)_{12})^2 = |(\Delta_D)_{12}|^2 e^{2i\varphi_{12}}$ implies that $|\epsilon_K|$ as well as $K \rightarrow \pi\nu\bar{\nu}$ are governed by the same weak phase φ_{12} . The requirement $|\epsilon_K|_{\text{RS}} \propto \text{Im}((\Delta_D)_{12} \otimes (\Delta_D)_{12}) \approx 0$ then forces φ_{12} in the standard CKM phase convention (112) to satisfy $\varphi_{12} \approx n\pi/2$ with $n = 0, 1, 2, 3$. One can show in a model-independent fashion that in such a situation only two branches of solutions in the $\mathcal{B}(K^+ \rightarrow \pi^+\nu\bar{\nu}(\gamma))$ - $\mathcal{B}(K_L \rightarrow \pi^0\nu\bar{\nu})$ plane are allowed [176]. The first branch features $\mathcal{B}(K_L \rightarrow \pi^0\nu\bar{\nu}) \approx \mathcal{B}(K_L \rightarrow \pi^0\nu\bar{\nu})_{\text{SM}}$, while the second one runs through the SM point (74) with a slope approximately equal to the one of the GN bound (126).

In order to understand why the second branch of solutions is absent in the case at hand requires further analysis. To leading order in hierarchies, the 12 elements of the charged-current matrix \mathbf{V}_L and the mixing matrix Δ_D take in the case of ‘‘alignment’’ the form¹⁰

$$(V_L)_{12} = \left[\frac{(\mathbf{M}_d \mathbf{M}_d^\dagger)_{21}}{(\mathbf{M}_d \mathbf{M}_d^\dagger)_{11}} - \frac{(M_u)_{21}}{(M_u)_{11}} \right] \frac{F(c_{Q_1})}{F(c_{Q_2})},$$

$$(\Delta_D)_{12} = -\frac{1}{2} \left[\frac{(\mathbf{M}_d \mathbf{M}_d^\dagger)_{21}}{(\mathbf{M}_d \mathbf{M}_d^\dagger)_{11}} + \frac{(\mathbf{Y}_d \mathbf{Y}_d^\dagger)_{23}^*}{(\mathbf{Y}_d \mathbf{Y}_d^\dagger)_{33}} \frac{(\mathbf{M}_d \mathbf{M}_d^\dagger)_{31}}{(\mathbf{M}_d \mathbf{M}_d^\dagger)_{11}} \right] F(c_{Q_1}) F(c_{Q_2}).$$
(127)

Here \mathbf{M}_d denotes the minors of \mathbf{Y}_d , *i.e.*, the element $(\mathbf{M}_d)_{ij}$ gives the determinant of the matrix obtained by deleting the i^{th} row and the j^{th} column of \mathbf{Y}_d . The same definitions apply in the case of $(M_u)_{ij}$.

It is clear that sizable corrections in $K \rightarrow \pi\nu\bar{\nu}$ correspond to large values of $|(\Delta_D)_{12}|$. Looking at (127) we see that $|(\Delta_D)_{12}|$ grows with decreasing $(\mathbf{Y}_d \mathbf{Y}_d^\dagger)_{33}$ and/or decreasing $(\mathbf{M}_d \mathbf{M}_d^\dagger)_{11}$. The first option requires however a tuning of parameters, because $(\mathbf{Y}_d \mathbf{Y}_d^\dagger)_{33} = \sum_i |(Y_d)_{3i}|^2$, which tells us that in an anarchic setup the latter object has a natural size of $\mathcal{O}(Y_{\text{max}}^2)$. Barring accidental cancellations, we are thus left with the second option. Yet in the limit $(\mathbf{M}_d \mathbf{M}_d^\dagger)_{11} \rightarrow 0$, the expressions (127) are approximated by

$$(V_L)_{12} \approx \frac{(\mathbf{M}_d \mathbf{M}_d^\dagger)_{21}}{(\mathbf{M}_d \mathbf{M}_d^\dagger)_{11}} \frac{F(c_{Q_1})}{F(c_{Q_2})},$$

$$(\Delta_D)_{12} \approx -\frac{1}{2} \left[1 + \frac{(\mathbf{Y}_d \mathbf{Y}_d^\dagger)_{22}}{(\mathbf{Y}_d \mathbf{Y}_d^\dagger)_{33}} \right] \frac{(\mathbf{M}_d \mathbf{M}_d^\dagger)_{21}}{(\mathbf{M}_d \mathbf{M}_d^\dagger)_{11}} F(c_{Q_1}) F(c_{Q_2}),$$
(128)

¹⁰It turns out that the Froggatt-Nielsen analysis performed in [10] is still applicable in the ‘‘aligned’’ case once the expressions for down-quark masses m_d, m_s, m_b and the rotations matrices \mathbf{U}_d and \mathbf{W}_d have been adjusted appropriately [177]. In particular, it is relatively easy to show that the relations (127) simply follow from the ZMA results (I:A.1) and (I:A.2) by applying the replacements $\mathbf{Y}_d \rightarrow \mathbf{Y}_d \mathbf{Y}_d^\dagger$ and $\mathbf{M}_d \rightarrow \mathbf{M}_d \mathbf{M}_d^\dagger$.

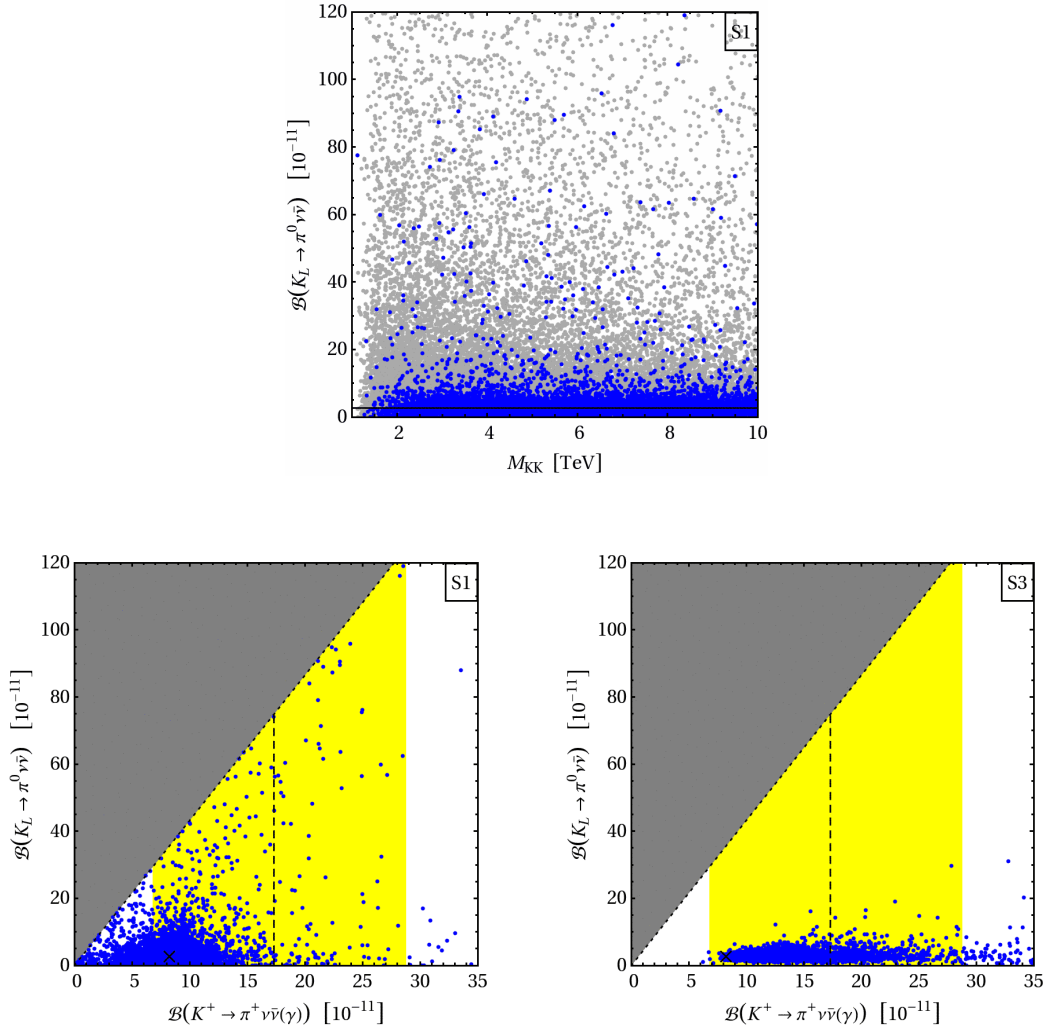


Figure 10: Predictions for $\mathcal{B}(K_L \rightarrow \pi^0 \nu \bar{\nu})$ as a function of M_{KK} (upper panel). The solid line represents the SM prediction. The lower left (right) panel shows the results for $\mathcal{B}(K^+ \rightarrow \pi^+ \nu \bar{\nu}(\gamma))$ versus $\mathcal{B}(K_L \rightarrow \pi^0 \nu \bar{\nu})$ in the benchmark scenario S1 (S3). In both panels the black cross indicates the SM point, the straight dotted black line and the light gray shaded area shows the GN bound, and the vertical dashed black line and the yellow band display the experimental central value and 68% CL range for $\mathcal{B}(K^+ \rightarrow \pi^+ \nu \bar{\nu}(\gamma))$. The gray scatter points in the upper panel reproduce the measured values of the $Z^0 \rightarrow b\bar{b}$ couplings at 99% CL, while the blue points additionally reproduce the measured values of $|\epsilon_K|$ and $B_d - \bar{B}_d$ mixing parameters at 95% CL. See text for details.

so that in the standard CKM phase convention (112), *i.e.*, after rotating away the phase of $(V_L)_{12}$, one ends up with

$$(\Delta_D)_{12} e^{-i \arg((V_L)_{12})} \approx -\frac{1}{2} \left[1 + \frac{(\mathbf{Y}_d \mathbf{Y}_d^\dagger)_{22}}{(\mathbf{Y}_d \mathbf{Y}_d^\dagger)_{33}} \right] \frac{|(\mathbf{M}_d \mathbf{M}_d^\dagger)_{21}|}{(\mathbf{M}_d \mathbf{M}_d^\dagger)_{11}} F(c_{Q_1}) F(c_{Q_2}) < 0. \quad (129)$$

Using (45) and (67), we find that this inequality implies that $\text{Re}(X_{\text{RS}}) < 0$ and $\text{Im}(X_{\text{RS}}) \approx 0$ for the quantity X_{RS} defined in (73). Recalling that in the SM one has $\text{Re}(X_{\text{SM}}) \approx -1.2$ and $\text{Im}(X_{\text{SM}}) \approx 0.3$, we then deduce from (72) that in the limit (128) the “aligned” scenario predicts constructive interference in the branching ratio of $K^+ \rightarrow \pi^+ \nu \bar{\nu}$, while the $K_L \rightarrow \pi^0 \nu \bar{\nu}$ rate is expected to approximately take its SM value. Invoking the $|\epsilon_K|$ constraint further drives the solutions toward (129), as it singles out solutions with $\varphi_{12} \approx \pi$, so that $\text{Re}(X_{\text{RS}}) < 0$ and $\text{Im}(X_{\text{RS}}) \approx 0$ turn out to hold in the “aligned” case even when $|(\Delta_D)_{12}|$ is small. We conclude that in the benchmark scenario S3 the allowed points in the $\mathcal{B}(K^+ \rightarrow \pi^+ \nu \bar{\nu}(\gamma))$ – $\mathcal{B}(K_L \rightarrow \pi^0 \nu \bar{\nu})$ plane should show the striking feature that they all lie on a horizontal line to the right of the SM point (74). This feature is clearly exhibited in the right panel of Figure 10.

The above discussion highlights that the $K \rightarrow \pi \nu \bar{\nu}$ decays offer a unique tool to study the fermion geography in the down-type quark sector of models with warped extra dimensions, since they provide, in combination with $|\epsilon_K|$, a powerful way to test the universality of new-physics contributions in $\Delta S = 1$ and $\Delta S = 2$ transitions. Precision measurements of the $K_L \rightarrow \pi^0 \nu \bar{\nu}$ and $K^+ \rightarrow \pi^+ \nu \bar{\nu}$ branching fractions feasible at high-intensity proton-beam facilities such as NA62, J-PARC, and Project X should therefore be primary goals of the future flavor-physics program and pursued with great vigor.

While theoretically not as clean as $K \rightarrow \pi \nu \bar{\nu}$, the $K_L \rightarrow \pi^0 l^+ l^-$ channels offer the unique opportunity to look for and to constraint additional $\Delta S = 1$ effective operators that are not accessible to the neutrino modes. In Figure 11 we show various predictions for $K_L \rightarrow \pi^0 l^+ l^-$ and their correlation with the $K_L \rightarrow \pi^0 \nu \bar{\nu}$ mode. All plots correspond to our default scenario S1. The predictions in the remaining benchmark scenarios are essentially indistinguishable from the ones displayed. The shown blue points reproduce the correct quark masses and mixings and satisfy the constraints from $|\epsilon_K|$, $Z^0 \rightarrow b \bar{b}$, and $B_d - \bar{B}_d$ mixing. The central values of the SM predictions (74), (81), and (83) are indicated by black crosses. In the case of the $K_L \rightarrow \pi^0 l^+ l^-$ observables we have assumed constructive interference between the direct and indirect CP-violating amplitudes. We observe that enhancements of the branching ratio of both $K_L \rightarrow \pi^0 l^+ l^-$ modes by a factor of about 5 are possible without violating any constraints. On the other hand, the RS predictions for $A_{\text{FB}}(K_L \rightarrow \pi^0 \mu^+ \mu^-)$ can be smaller than the SM value by almost a factor of 10. Notice that enhancements/suppressions in $\mathcal{B}(K_L \rightarrow \pi^0 \mu^+ \mu^-)$ and $A_{\text{FB}}(K_L \rightarrow \pi^0 l^+ l^-)$ are anti-correlated, since the branching ratio enters (82) in the denominator. The pattern of the correlations seen in the upper left panel of Figure 11 arises because the coefficient of the semileptonic vector operator, Y_V , is suppressed with respect to the coefficient of the axial-vector operator, Y_A , by a factor of about $(1 - 4s_w^2) \approx 0.08$, and scalar interactions play essentially no role. This factor stems from the coupling of the Z^0 boson and its KK excitations to the charged lepton pair. The ratio Y_V/Y_A determines the angle between the two possible branches of $\mathcal{B}(K_L \rightarrow \pi^0 \mu^+ \mu^-)$ as a function of $\mathcal{B}(K_L \rightarrow \pi^0 e^+ e^-)$. Since Y_V/Y_A is generically small in the RS model, the two branches are hardly visible in the latter

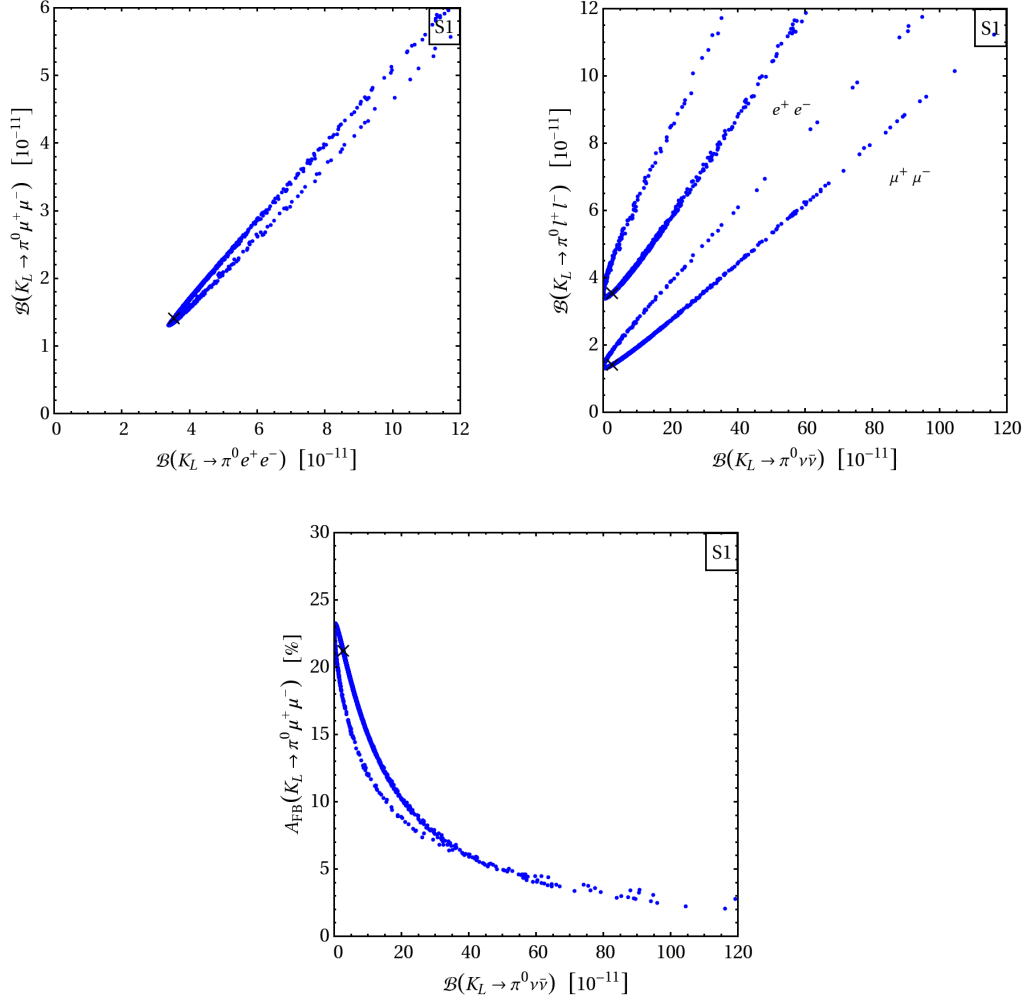


Figure 11: Prediction for $\mathcal{B}(K_L \rightarrow \pi^0 e^+ e^-)$ versus $\mathcal{B}(K_L \rightarrow \pi^0 \mu^+ \mu^-)$ (upper left), $\mathcal{B}(K_L \rightarrow \pi^0 \nu \bar{\nu})$ versus $\mathcal{B}(K_L \rightarrow \pi^0 l^+ l^-)$ (upper right), and $\mathcal{B}(K_L \rightarrow \pi^0 \nu \bar{\nu})$ versus $A_{\text{FB}}(K_L \rightarrow \pi^0 \mu^+ \mu^-)$ (lower panel). The black crosses indicate the SM points while the blue scatter points reproduce the measured values of $|\epsilon_K|$, the $Z^0 b \bar{b}$ couplings, and $B_d - \bar{B}_d$ mixing at 95%, 99%, and 95% CL. See text for details.

figure. The correlations observed in the upper right and lower panel of Figure 11 have a similar origin. In this case they are a result of the interplay of the coupling of the Z^0 boson and its KK excitations to a pair of charged and neutral leptons. While the former is mostly axial-vector like, the latter is purely left-handed. The observed correlations between $K_L \rightarrow \pi^0 \nu \bar{\nu}$ and $K_L \rightarrow \pi^0 l^+ l^-$ should therefore be considered a generic feature of models where the couplings of heavy neutral gauge bosons to leptons are SM-like, rather than a specific characteristic of the RS framework.

Interesting complementary information can be obtained from the $K_L \rightarrow \mu^+ \mu^-$ decay mode, which has been measured precisely. The predictions for $\mathcal{B}(K_L \rightarrow \mu^+ \mu^-)$ as a function of

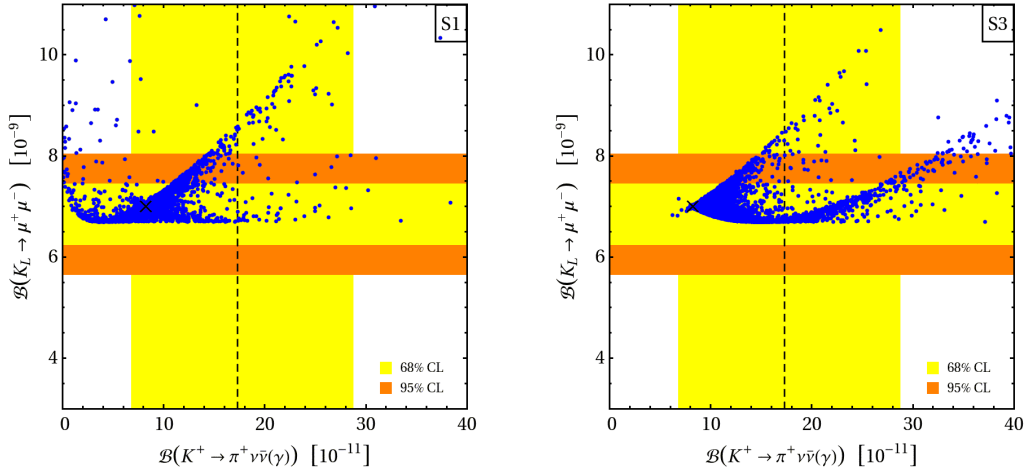


Figure 12: Prediction for $\mathcal{B}(K^+ \rightarrow \pi^+ \nu \bar{\nu}(\gamma))$ versus $\mathcal{B}(K_L \rightarrow \mu^+ \mu^-)$ in scenario S1 (left) and S3 (right). The black crosses indicate the SM point, while the blue scatter points reproduce the measured values of $|\epsilon_K|$, the $Z^0 \rightarrow b\bar{b}$ couplings, and $B_d - \bar{B}_d$ mixing at 95%, 99%, and 95% CL. For comparison, the experimental central value (vertical dashed line) and 68% CL range for $\mathcal{B}(K^+ \rightarrow \pi^+ \nu \bar{\nu}(\gamma))$ (yellow vertical band) as well as the 68% (yellow horizontal band) and 95% (orange horizontal band) CL regions for $\mathcal{B}(K_L \rightarrow \mu^+ \mu^-)$ including both experimental and theoretical errors are shown. See text for details.

$\mathcal{B}(K^+ \rightarrow \pi^+ \nu \bar{\nu}(\gamma))$ in the parameter scenarios S1 and S3 are displayed in the left and right panels of Figure 12, respectively. The blue scatter points again reproduce the correct quark masses and the CKM elements and satisfy the constraints from $|\epsilon_K|$, $Z^0 \rightarrow b\bar{b}$, and $B_d - \bar{B}_d$ mixing. The central values of the SM predictions (74) and (77) are indicated by black crosses. In obtaining the figures we have assumed that the two-photon amplitude in $K_L \rightarrow \mu^+ \mu^-$ has positive sign. The 68% (95%) CL regions are underlaid in yellow (orange). In the case of the $K_L \rightarrow \mu^+ \mu^-$ branching ratio the error band includes the theory error, which in fact by far dominates over the experimental uncertainty. We observe that the branching ratio of $K_L \rightarrow \mu^+ \mu^-$ can reach values up to 10^{-8} , which represents an enhancement of more than 40% relative to both the SM prediction and the measured value, $\mathcal{B}(K_L \rightarrow \mu^+ \mu^-)_{\text{exp}} = (6.84 \pm 0.11) \cdot 10^{-9}$ [47]. A positive linear correlation between $K^+ \rightarrow \pi^+ \nu \bar{\nu}$ and $K_L \rightarrow \mu^+ \mu^-$ is also visible in the panels. This correlation originates from the fact that $K^+ \rightarrow \pi^+ \nu \bar{\nu}$ measures the vector, while $K_L \rightarrow \mu^+ \mu^-$ measures the axial-vector component of the $Z^0 d\bar{s}$ vertex. Since the SM flavor-changing Z^0 penguin is purely left-handed and the RS contribution is dominated in our case by the very same component, the SM and new-physics contributions enter both decay modes with the same sign. Notice that the correlation is more pronounced in scenario S3 than in S1, because the right-handed contributions to the $Z^0 d\bar{s}$ vertex are further suppressed in the former benchmark scenario. In a RS variant with custodial protection, the correlation between $K^+ \rightarrow \pi^+ \nu \bar{\nu}$ and $K_L \rightarrow \mu^+ \mu^-$ has been found to be an inverse one [19]. Precision measurements of $K^+ \rightarrow \pi^+ \nu \bar{\nu}$ accompanied by major theoretical progress in the prediction of

$K_L \rightarrow \mu^+ \mu^-$ thus would allow one to identify the chiral structure of the $Z^0 d \bar{s}$ vertex and in this way to select between different models of non-standard interactions.

We close this section with a critical comparison of our results with the findings of [19], which analyses the rare decays $K \rightarrow \pi \nu \bar{\nu}$, $K_L \rightarrow \pi^0 l^+ l^-$, and $K_L \rightarrow \mu^+ \mu^-$ in the context of a warped extra-dimension scenario with custodial protection of the $Z^0 d_{iL} \bar{d}_{jL}$ vertices. Our discussion will shed some light on the model dependence of the obtained results and applies in a similar fashion to the rare B -meson decays examined below. We start with a comparison of the left- and right-handed couplings of the Z^0 boson to down-type quarks. Focusing on the corrections arising from the non-trivial overlap integrals of gauge-boson and fermion profiles and employing the implementation of the quark sector as described in [11, 19, 170, 171], we find that the ratios of the flavor-changing corrections to the Z^0 -boson couplings in the two models under consideration are given by

$$\begin{aligned} \frac{(g_L^d)^{\text{custodial}}}{(g_L^d)^{\text{original}}} &= -\frac{(1/2 - s_w^2/3) (\Delta'_D)_{ij}}{(1/2 - s_w^2/3) (L (\Delta_D)_{ij} - (\Delta'_D)_{ij})} \approx -\frac{1}{L}, \\ \frac{(g_R^d)^{\text{custodial}}}{(g_R^d)^{\text{original}}} &= -\frac{c_w^2 L (\Delta_d)_{ij} - s_w^2/3 (\Delta'_d)_{ij}}{s_w^2/3 (L (\Delta_d)_{ij} - (\Delta'_d)_{ij})} \approx -\frac{3c_w^2}{s_w^2}, \end{aligned} \tag{130}$$

where in the last step we have used that $(\Delta_{D,d})_{ij} \approx (\Delta'_{D,d})_{ij}$ and neglected subleading terms in $L \approx 37$. The $\Delta_{D,d}^{(i)}$ matrices are defined in (I:122). From the first relation it is obvious that only the leading term in L appearing in the left-handed couplings is protected by the combination of the custodial and the left-right exchange symmetry, while no such protection is active for the subleading terms. This implies that the corrections to the $Z^0 d_{iL} \bar{d}_{jL}$ vertices arising from the gauge sector are *parametrically* suppressed by a factor of L in the $SU(2)_L \times SU(2)_R \times P_{LR}$ model relative to the original RS model, rather than by a purely numerical factor of about 100 as claimed in [11, 19]. On the other hand, we find that the $Z^0 d_{iR} \bar{d}_{jR}$ vertices in the model with custodial protection are enhanced in magnitude by a factor of about 10 relative to the original RS formulation, which is in accordance with [11, 19]. We will present a more detailed discussion of the implementation of the custodial protection mechanism, treating the effects of a brane-localized Higgs in the $SU(2)_L \times SU(2)_R \times P_{LR}$ model exactly, in a forthcoming publication [37].

From (130) we observe that $(g_R^d)^{\text{custodial}}/(g_L^d)^{\text{original}} \approx -c_w^2/(1/2 - s_w^2/3) (\Delta_d)_{ij}/(\Delta_D)_{ij} \approx -2 (\Delta_d)_{ij}/(\Delta_D)_{ij}$. The scaling relations (I:128) then imply that $|(g_R^d)^{\text{custodial}}/(g_L^d)^{\text{original}}| \sim (F(c_{d_i})F(c_{d_j}))/ (F(c_{Q_i})F(c_{Q_j}))$ up to a factor of $\mathcal{O}(1)$, which tells us that in order to have effects in rare kaon decays of similar magnitude in the custodially protected and the original RS model requires $F(c_{d_1})F(c_{d_2}) \approx F(c_{Q_1})F(c_{Q_2})$. Notice that to arrive at these relations, we used the fact that the bulk masses do not depend on whether one considers the custodially protected or the original RS model, since the c_{A_i} parameters are determined by the quark masses and mixings. Yet the locations of the zero-modes are not unique solutions [9], a feature that manifests itself in the invariance under a set of reparametrization transformations [10]. In particular, a simultaneous rescaling of the fermion profiles for $SU(2)_L$ doublet and singlet fields by opposite factors, while leaving the 5D Yukawa couplings invariant, allows one to redistribute effects between the left- and right-handed sectors. This freedom in combination with the scaling

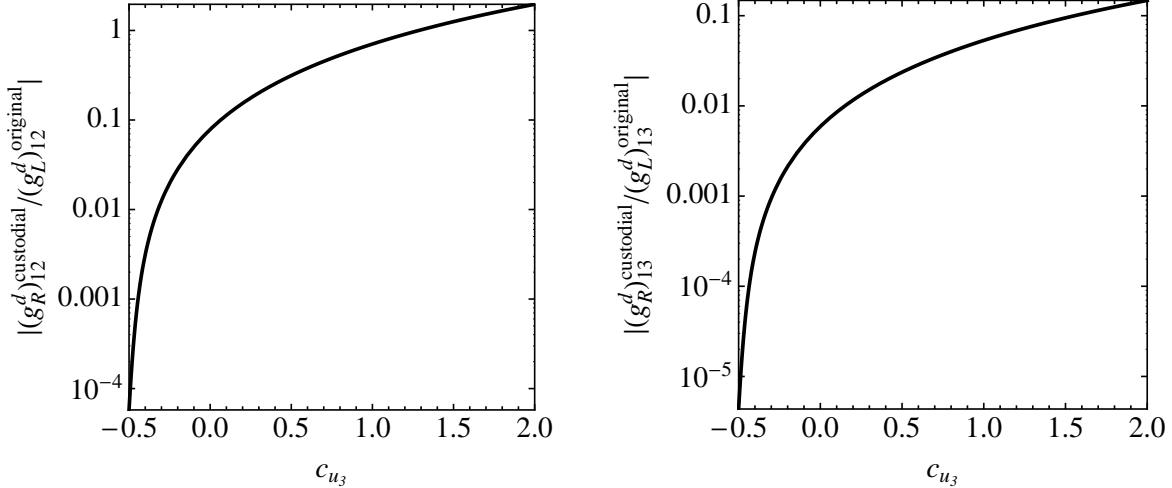


Figure 13: Predictions for $|(g_R^d)_{ij}^{\text{custodial}}/(g_L^d)_{ij}^{\text{original}}|$ as a function of the bulk mass parameter c_{u_3} for the cases $ij = 12$ (left) and 13 (right). The shown curves correspond to the choice $Y_u = Y_d = 1$. See text for details.

relations (I:128) can be used to express $(F(c_{d_1})F(c_{d_2}))/F(c_{Q_1})F(c_{Q_2})$ through the quark masses, Wolfenstein parameters, and $F(c_{u_3})$. To leading power in hierarchies we find

$$\left| \frac{(g_R^d)_{12}^{\text{custodial}}}{(g_L^d)_{12}^{\text{original}}} \right| \sim \frac{m_d m_s Y_u^4 v^2}{2A^4 \lambda^{10} m_t^4 Y_d^2} [F(c_{u_3})]^4 = 0.08 \frac{Y_u^4}{Y_d^2} [F(c_{u_3})]^4, \quad (131)$$

which implies that the ratio of right- to left-handed $Z^0 d\bar{s}$ couplings can be enhanced by localizing the right-handed top quark closer to the IR brane. Analogous formulas hold in the case of the $Z^0 \rightarrow b\bar{d}(b\bar{s})$ transitions with $(m_d m_s)/(A^4 \lambda^{10})$ replaced by $(m_d m_b)/(A^2 \lambda^6)$ ($(m_s m_b)/(A^2 \lambda^4)$). The corresponding numerical factors replacing 0.08 in (131) are 0.006 and 0.005, respectively.

The above considerations make it clear that the degree of compositeness of the top quark plays a crucial role in the context of FCNC interactions as it determines the relative size of left- to right-handed couplings. To make the latter statement more quantitative we plot in Figure 13 the ratio $|(g_R^d)_{ij}^{\text{custodial}}/(g_L^d)_{ij}^{\text{original}}|$ as a function of c_{u_3} for the cases $ij = 12$ and 13 . The case $ij = 23$ is not shown explicitly, since it basically resembles the one of $ij = 13$. The displayed curves have been obtained by assuming for simplicity that the various elements of the up- and down-type Yukawa matrices are all equal to 1. The strong dependence of the results on c_{u_3} , arising from the factor $[F(c_{u_3})]^4 \approx (1 + 2c_{u_3})^2$ in (131), is clearly visible in both panels. We furthermore see that requiring $|(g_R^d)_{12}^{\text{custodial}}/(g_L^d)_{12}^{\text{original}}| \gtrsim 1$ translates into the limit $c_{u_3} \gtrsim 1$ on the bulk mass parameter of the right-handed top quark. In the case of the $Z^0 \rightarrow b\bar{d}(b\bar{s})$ transitions the corresponding limit is $c_{u_3} \gtrsim 6$. We conclude that in order to obtain $Z^0 d_{iR} \bar{d}_{jR}$ couplings in the custodially protected model comparable in magnitude to the $Z^0 d_{iL} \bar{d}_{jL}$ couplings in the original RS framework requires, barring a conspiracy of undetermined $\mathcal{O}(1)$ factors, parametrically large values of c_{u_3} . Such a choice seems however

unnatural, since $c_{u_3} > 1$ implies that the corresponding bulk mass exceeds the curvature scale, in which case the right-handed top quark should be treated as a brane-localized and not a bulk fermion. The finding of [19] that $\mathcal{O}(1)$ enhancements in $K \rightarrow \pi\nu\bar{\nu}$, $K_L \rightarrow \pi^0 l^+ l^-$, and $K_L \rightarrow \mu^+ \mu^-$ due to right-handed interactions are possible in the RS model with custodial protection has thus to be taken with a grain of salt, because these solutions typically feature bulk mass parameters c_{u_3} that lie quite significantly above $-1/2$. In this context it is also important to realize that in the limit from the right $c_{u_3} \rightarrow -1/2^+$, which is sufficient to generate the large mass of the top quark, the ratio $|(g_R^d)_{12}^{\text{custodial}}/(g_L^d)_{12}^{\text{original}}|$ scales as $1/L^2$ and consequently $|(g_R^d)_{12}^{\text{custodial}}/(g_L^d)_{12}^{\text{custodial}}|$ becomes proportional to $1/L$. This means that in this case the right-handed couplings are not L -enhanced but rather L -suppressed relative to the custodially protected left-handed couplings, and that the branching fractions of $K \rightarrow \pi\nu\bar{\nu}$, $K_L \rightarrow \pi^0 l^+ l^-$, and $K_L \rightarrow \mu^+ \mu^-$ are predicted to be SM-like. A detailed analysis of rare kaon decays in the $SU(2)_L \times SU(2)_R \times P_{LR}$ model will be presented elsewhere.

5.5.2 Numerical Analysis of $B_q \rightarrow \mu^+ \mu^-$ and $B \rightarrow X_q \nu \bar{\nu}$

In this section we perform numerical studies of the impact of virtual KK exchange on the predictions of $B_q \rightarrow \mu^+ \mu^-$ and $B \rightarrow X_q \nu \bar{\nu}$, where $q = d, s$. We begin with the purely semileptonic modes. The predictions for $\mathcal{B}(B_s \rightarrow \mu^+ \mu^-)$ as a function of $\mathcal{B}(B_d \rightarrow \mu^+ \mu^-)$ obtained from a parameter scan in the scenario S1 are displayed in the upper left panel of Figure 14. This plot is also representative for the results obtained in the other benchmark scenarios. The blue points are in agreement with the observed quark masses and CKM elements and satisfy the constraints from $|\epsilon_K|$, $Z^0 \rightarrow b\bar{b}$, and $B_d - \bar{B}_d$ mixing. The central values of the SM predictions (90) are indicated by the black cross. The distribution of points indicates that large uncorrelated enhancements by a factor of 10 are possible in both the B_d and B_s decay modes without violating existing constraints. We also see that large deviations from the relation $\mathcal{B}(B_s \rightarrow \mu^+ \mu^-) = (f_{B_s}^2 m_{B_s} \tau_{B_s} |V_{ts}|^2)/(f_{B_d}^2 m_{B_d} \tau_{B_d} |V_{td}|^2) \mathcal{B}(B_d \rightarrow \mu^+ \mu^-) \approx 32.8 \mathcal{B}(B_d \rightarrow \mu^+ \mu^-)$ [115], which is valid in models with constrained MFV (CMFV) [26], can naturally appear in the RS model. This feature is indicated by the orange dotted line. Notice that the 95% CL upper limit $\mathcal{B}(B_s \rightarrow \mu^+ \mu^-)_{\text{exp}} < 5.3 \cdot 10^{-8}$ based on 5 fb^{-1} of data at DØ [178], which is a factor of 14 above the SM expectation,¹¹ almost starts to constrain the parameter space of the RS model. The experimentally disfavored region is indicated by the red band in the left panel of Figure 14. Both CDF and DØ should reach limits in the ballpark of $2 \cdot 10^{-8}$ for 8 fb^{-1} of data. For comparison we have also included in the plot the minimum of $\mathcal{B}(B_s \rightarrow \mu^+ \mu^-)$ allowing for a signal discovery with 5σ significance with 2 fb^{-1} of integrated luminosity, which is expected to be $6 \cdot 10^{-9}$ at LHCb [181]. This sensitivity is indicated by the dashed red line in the panel. A discovery at the SM level requires about 6 fb^{-1} (100 fb^{-1}) of data at LHCb (ATLAS or CMS) and will require several years of LHC running [181, 182, 183]. The existing limit in the case of $B_d \rightarrow \mu^+ \mu^-$ is much weaker, $\mathcal{B}(B_d \rightarrow \mu^+ \mu^-)_{\text{exp}} < 1.8 \cdot 10^{-8}$ at 95% CL [179]. It is therefore not shown in the plot. While it should be possible to improve the latter bound at LHCb by an order of magnitude with 10 fb^{-1} , an observation/discovery of $B_d \rightarrow \mu^+ \mu^-$ at the SM level is even challenging for a super flavor factory.

¹¹An unofficial average of the CDF [179] and DØ data yields an upper bound of $4.5 \cdot 10^{-8}$ at 95% CL [180].

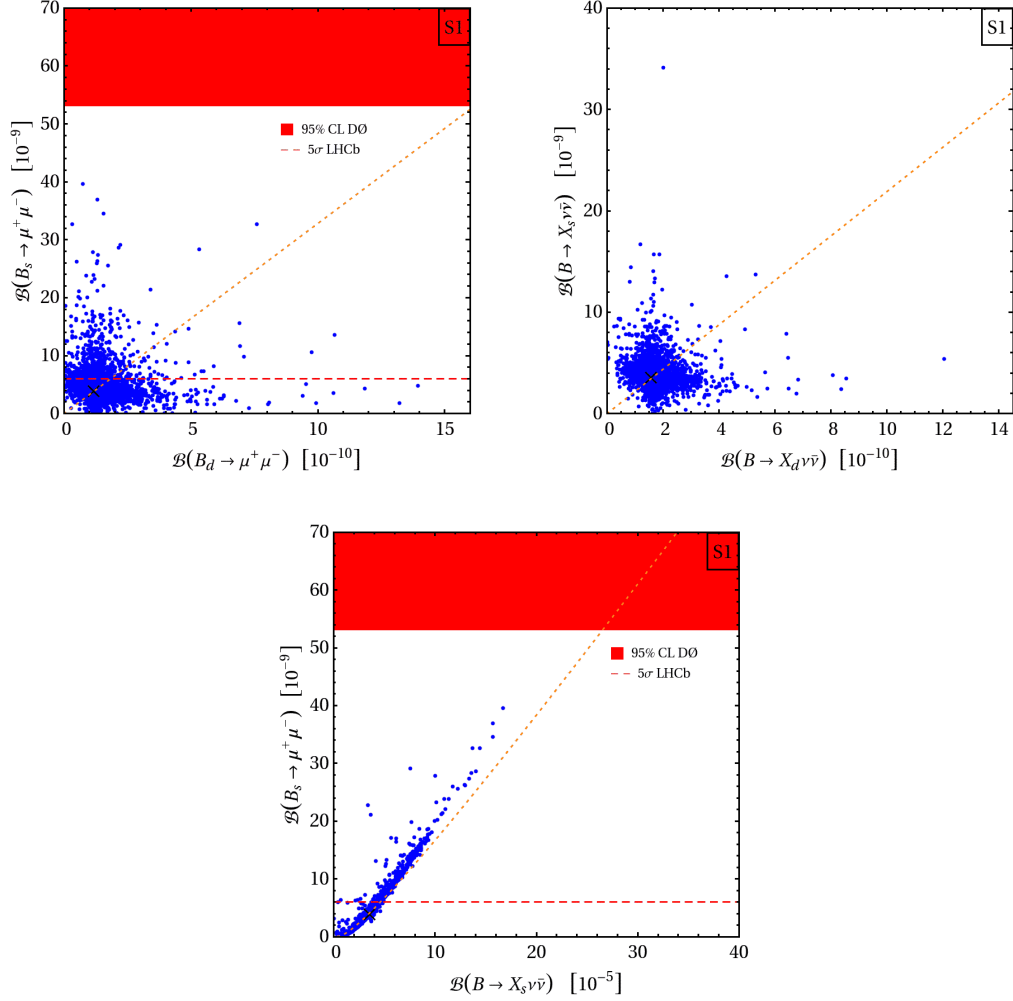


Figure 14: Prediction for $\mathcal{B}(B_d \rightarrow \mu^+ \mu^-)$ versus $\mathcal{B}(B_s \rightarrow \mu^+ \mu^-)$ (upper left), $\mathcal{B}(B \rightarrow X_d \nu \bar{\nu})$ versus $\mathcal{B}(B \rightarrow X_s \nu \bar{\nu})$ (upper right), and $\mathcal{B}(B \rightarrow X_s \nu \bar{\nu})$ versus $\mathcal{B}(B_s \rightarrow \mu^+ \mu^-)$ (lower panel). All panels show results obtained in benchmark scenario S1. The black crosses indicate the SM point, while the blue scatter points reproduce the measured values of $|\epsilon_K|$, the $Z^0 b \bar{b}$ couplings, and $B_d - \bar{B}_d$ mixing at 95%, 99%, and 95% CL. In the upper left panel the current 95% CL upper limit on $\mathcal{B}(B_s \rightarrow \mu^+ \mu^-)$ from DØ and the minimum branching fraction allowing for a 5σ discovery at LHCb are indicated by the red band and dashed line, respectively. The orange dotted lines in the upper panels represent the CMFV correlation between the two purely leptonic/semileptonic modes, while the orange dotted curve in the lower panel indicates the model-independent prediction obtained under the assumption that only left-handed operators contribute to the branching fractions. See text for details.

We now move onto the rare semileptonic modes. The predictions for $\mathcal{B}(B \rightarrow X_d \nu \bar{\nu})$ versus $\mathcal{B}(B \rightarrow X_s \nu \bar{\nu})$ corresponding to the benchmark scenario S1 are shown in the upper right

panel of Figure 14. Similar results are obtained in the remaining scenarios. Like in the case of $B_q \rightarrow \mu^+\mu^-$, we see that enhancements of an order of magnitude are allowed in both $B \rightarrow X_q\nu\bar{\nu}$ decay modes and that the deviations do not follow the linear relation $\mathcal{B}(B \rightarrow X_s\nu\bar{\nu}) = |V_{ts}|^2/|V_{td}|^2 \mathcal{B}(B \rightarrow X_d\nu\bar{\nu}) \approx 21.9 \mathcal{B}(B \rightarrow X_d\nu\bar{\nu})$ predicted in CMFV scenarios. The latter correlation is indicated by the orange dotted line in the panel. While theoretically the cleanest and thus the most attractive mode, the existing bound on the branching ratio of the inclusive $b \rightarrow s\nu\bar{\nu}$ transition is very weak, $\mathcal{B}(B \rightarrow X_s\nu\bar{\nu})_{\text{exp}} < 6.4 \cdot 10^{-4}$ at 90% CL [184]. Stronger bounds exist in the case of the exclusive modes, $\mathcal{B}(B \rightarrow K\nu\bar{\nu}) < 1.4 \cdot 10^{-5}$ [185] and $\mathcal{B}(B \rightarrow K^*\nu\bar{\nu}) < 8.0 \cdot 10^{-5}$ [186] both at 90% CL. While fully inclusive measurements will be notoriously difficult to perform even with the highest available luminosity at a super flavor factory, an observation of $B \rightarrow K^*\nu\bar{\nu}$ is expected to be possible with 50 ab^{-1} of integrated luminosity at such a machine [187]. Since the pattern of deviations observed in the exclusive transitions follows the one in $B \rightarrow X_s\nu\bar{\nu}$, our discussion of non-standard effects in $B \rightarrow X_s\nu\bar{\nu}$ essentially also apply to the modes $B \rightarrow K^{(*)}\nu\bar{\nu}$.

In the lower panel of Figure 14, we finally show the correlation between $\mathcal{B}(B \rightarrow X_s\nu\bar{\nu})$ and $\mathcal{B}(B_s \rightarrow \mu^+\mu^-)$. The plot clearly shows that for large values of the branching ratios there is a linear relation between the rates of $B \rightarrow X_s\nu\bar{\nu}$ and $B_s \rightarrow \mu^+\mu^-$. This pattern arises since both modes receive in effect only corrections from tree-level exchange of the Z^0 boson and its KK excitations. Scalar contributions to $B_s \rightarrow \mu^+\mu^-$ are highly suppressed, and corrections due to KK photons do not contribute to the purely leptonic rate since they couple vectorial. Given that in the RS model without custodial protection the contribution from right-handed operators are suppressed with respect to the left-handed ones, it is easy to show that the branching ratios in question satisfy approximately

$$\mathcal{B}(B_s \rightarrow \mu^+\mu^-) \approx \left(1.1 - 3.3 \left[\frac{\mathcal{B}(B \rightarrow X_s\nu\bar{\nu})}{10^{-5}} \right]^{1/2} + 2.6 \frac{\mathcal{B}(B \rightarrow X_s\nu\bar{\nu})}{10^{-5}} \right) \cdot 10^{-9}. \quad (132)$$

This relation is indicated by the orange dotted curve in the lower panel of Figure 14. Deviation from the behavior (132) measure the strength of the $Z^0 b_R \bar{s}_R$ relative to the $Z^0 b_L \bar{s}_L$ coupling. Notice that while $\mathcal{B}(B \rightarrow X_s\nu\bar{\nu})$ depends quadratically on the $Z^0 b_R \bar{s}_R$ coupling, $\mathcal{B}(B_s \rightarrow \mu^+\mu^-)$ contains also linear terms, so that small right-handed contributions will have a bigger impact in the purely leptonic than in the semileptonic mode. Furthermore, in the $B \rightarrow X_s\nu\bar{\nu}$ decay non-zero right-handed couplings necessarily enhance the branching fraction, whereas in the $B_s \rightarrow \mu^+\mu^-$ mode both constructive and destructive interference is possible. From (69), (88), and (89) one can convince oneself that in the minimal RS model right-handed operators typically add to the $B_s \rightarrow \mu^+\mu^-$ rate, which implies that the slope of the correlation between $\mathcal{B}(B \rightarrow X_s\nu\bar{\nu})$ and $\mathcal{B}(B_s \rightarrow \mu^+\mu^-)$ should be steeper than the one predicted in (132). This is indeed what is observed in the plot. Notice that in the case where right-handed new-physics contributions dominate over left-handed ones, $B \rightarrow X_s\nu\bar{\nu}$ and $B_s \rightarrow \mu^+\mu^-$ are again correlated. In the absence of additional contributions to the $Z^0 b_L \bar{s}_L$ vertex, the predictions in the $\mathcal{B}(B \rightarrow X_s\nu\bar{\nu})$ - $\mathcal{B}(B_s \rightarrow \mu^+\mu^-)$ plane form a parabola-like curve that is tilted to the right. Depending on whether the right-handed contributions interfere constructively or destructively in $B_s \rightarrow \mu^+\mu^-$, the predictions fall on the upper or lower branch of the curve.

5.5.3 Numerical Analysis of $B \rightarrow X_s l^+ l^-$ and $B \rightarrow K^* l^+ l^-$

Our explorations in the sector of semileptonic B -meson decays are rounded off by a study of the numerical impact of the exchange of the Z^0 boson and its KK excitations on the decays $B \rightarrow X_s l^+ l^-$ and $B \rightarrow K^* l^+ l^-$. Before we present our findings, let us stress again that effects of electromagnetic dipole operators entering the effective Hamiltonian for $b \rightarrow s l^+ l^-$ first at the one-loop level are not included in our analysis. The possibility that such loop-suppressed effects could have a non-negligible impact on the obtained results for the various $b \rightarrow s l^+ l^-$ observables should be kept in mind. We leave a detailed analysis of this issue for future work.

The predictions for the inclusive $B \rightarrow X_s l^+ l^-$ channel are shown in Figure 15. All panels show results for the benchmark scenario S1 that reproduce the correct hierarchies in the quark sector. Scatter points that fulfill (violate) the constraints arising from the measurements of the $Z^0 \rightarrow b\bar{b}$ couplings are colored blue (light gray). In the upper left panel we display $\mathcal{B}(B \rightarrow X_s l^+ l^-)^{q^2 \in [1,6] \text{ GeV}^2}$ as a function of M_{KK} . The central value of the SM expectation (95) is indicated by the black line, while the yellow (orange) band represents the 68% (95%) CL interval of the experimental world average $\mathcal{B}(B \rightarrow X_s l^+ l^-)_{\text{exp}}^{q^2 \in [1,6] \text{ GeV}^2} = (1.63 \pm 0.53) \cdot 10^{-6}$ [188, 189]. It is evident from the figure that, although enhancements of a factor of 2 are possible, the vast majority of points that satisfy the $Z^0 \rightarrow b\bar{b}$ constraints lead to values of the inclusive branching ratio that lie within the experimentally allowed range. This feature is expected [112] in models in which the modification of the flavor structure is closely connected to the third generation. We also add that in warped setups with custodial protection of the $Z^0 b_L \bar{b}_L$ vertex the correlation between $Z^0 \rightarrow b\bar{b}$ and $b \rightarrow s l^+ l^-$ is in general different compared to the case discussed here. However, at the end of Section 5.5.1 we have shown that $|(g_R^d)_{ij}^{\text{custodial}} / (g_L^d)_{ij}^{\text{original}}| \ll 1$ for the case $ij = 23$ unless the bulk mass parameter c_{u_3} describing the localization of the right-handed top quark is much bigger than 1. We thus expect the effects in $b \rightarrow s l^+ l^-$ due to exchange of the Z^0 boson and its KK modes to be even smaller in the custodially protected RS model for natural choices of c_{u_3} . A detailed study of this question is postponed to a forthcoming publication.

An observable that is theoretically even cleaner than the $B \rightarrow X_s l^+ l^-$ branching ratio, is the zero of the forward-backward asymmetry, q_0^2 . The results for q_0^2 as a function of the new-physics scale M_{KK} are given in the upper right plot of Figure 15. The solid black line and the yellow (orange) band indicate the central value and the 68% (95%) CL interval of the theory prediction (99). Like in the case of the branching ratio, we see that points that satisfy the $Z^0 \rightarrow b\bar{b}$ constraint usually lead to deviations in q_0^2 that do not exceed the level of 20%. The moderate size of the corrections will make it difficult, but certainly not impossible at a super flavor factory, to distinguish the RS model from the SM on the basis of a measurement of q_0^2 . In the lower panel of Figure 15 we finally present the correlation between $\mathcal{B}(B \rightarrow X_s l^+ l^-)^{q^2 \in [1,6] \text{ GeV}^2}$ and $\mathcal{B}(B_s \rightarrow \mu^+ \mu^-)$. We observe that without the $Z^0 \rightarrow b\bar{b}$ constraint the predictions form a tilted parabola-shaped area, which is transformed into a boomerang-shaped area by the $Z^0 \rightarrow b\bar{b}$ constraint, which eliminates in particular points leading to a simultaneous enhancement of both branching fractions. Enhancements in the purely leptonic mode thus occur more frequently for values of $\mathcal{B}(B \rightarrow X_s l^+ l^-)^{q^2 \in [1,6] \text{ GeV}^2}$ below the SM expectation (95). This feature is easily understood. Both decay modes receive the dominant contribution from the new-physics contributions $C_{10}^{l\text{RS}}$ and C_A^{RS} to the axial-vector couplings $C_{10}^l \approx -4.4 + C_{10}^{l\text{RS}}$

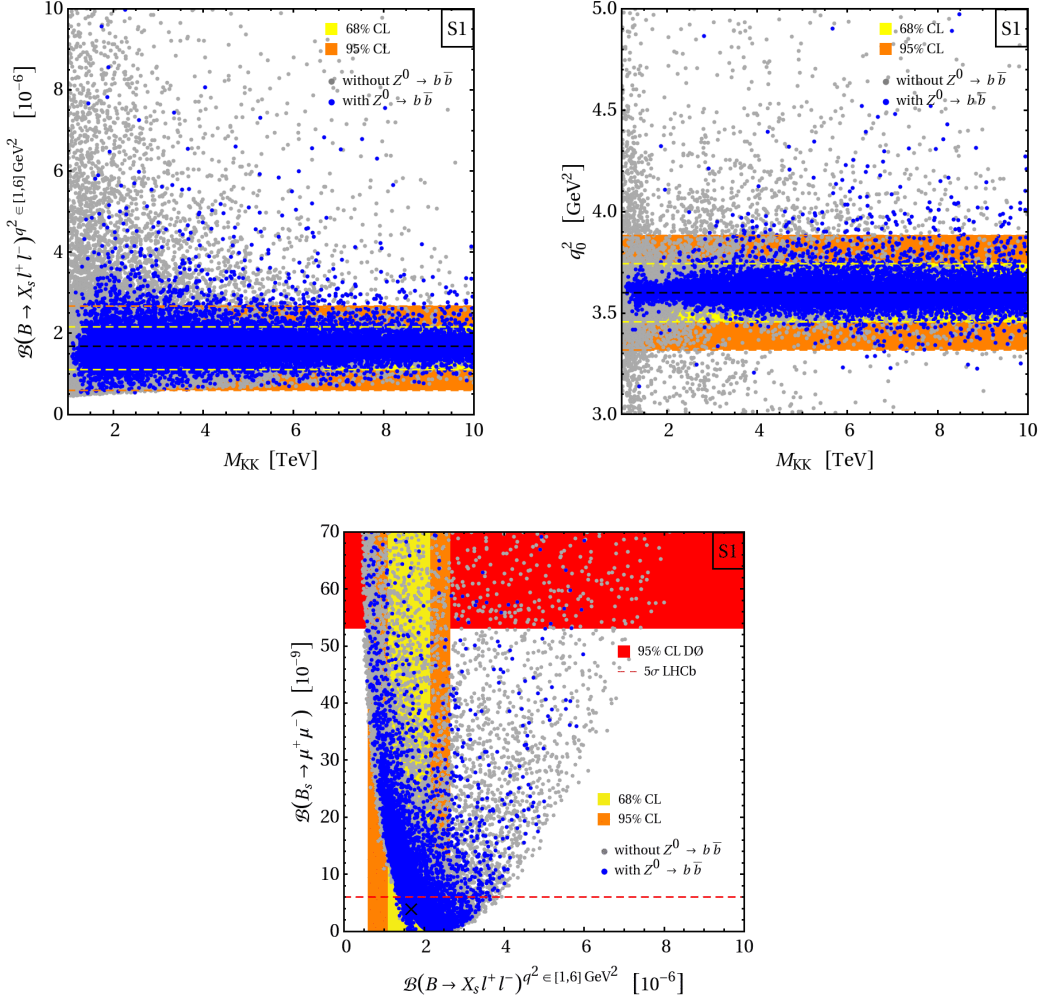


Figure 15: Prediction for $\mathcal{B}(B \rightarrow X_s l^+ l^-)$ and q_0^2 versus M_{KK} (upper panels) and $\mathcal{B}(B \rightarrow X_s \nu \bar{\nu})$ versus $\mathcal{B}(B_s \rightarrow \mu^+ \mu^-)$ (lower panel). The shown results correspond to benchmark scenario S1. The blue (light gray) points are consistent (inconsistent) with the measured $Z^0 \rightarrow b \bar{b}$ couplings at the 99% CL. The solid black lines and the black cross indicate the SM expectation. For comparison the regions of 68% (yellow) and 95% (orange) CL are also displayed. In the lower panel the 95% CL exclusion of $\mathcal{B}(B_s \rightarrow \mu^+ \mu^-)$ and the minimum of the branching fraction allowing for a discovery with 5σ at LHCb are indicated by the red band and dashed line. See text for details.

and $C_A \approx 0.96 + C_A^{\text{RS}}$. Since the coefficients C_{10}^{RS} and C_A^{RS} are aligned in flavor space and the SM contribution has opposite sign, constructive interference in $B \rightarrow X_s l^+ l^-$ typically implies destructive interference in $B_s \rightarrow \mu^+ \mu^-$ and *vice versa*.

We now leave behind the sector of inclusive $b \rightarrow s l^+ l^-$ decay distributions and continue our survey in the area of exclusive decays. We emphasize that our study will be exploratory and will focus on $B \rightarrow K^* l^+ l^-$ observables that can already be accessed at BaBar [139, 140]

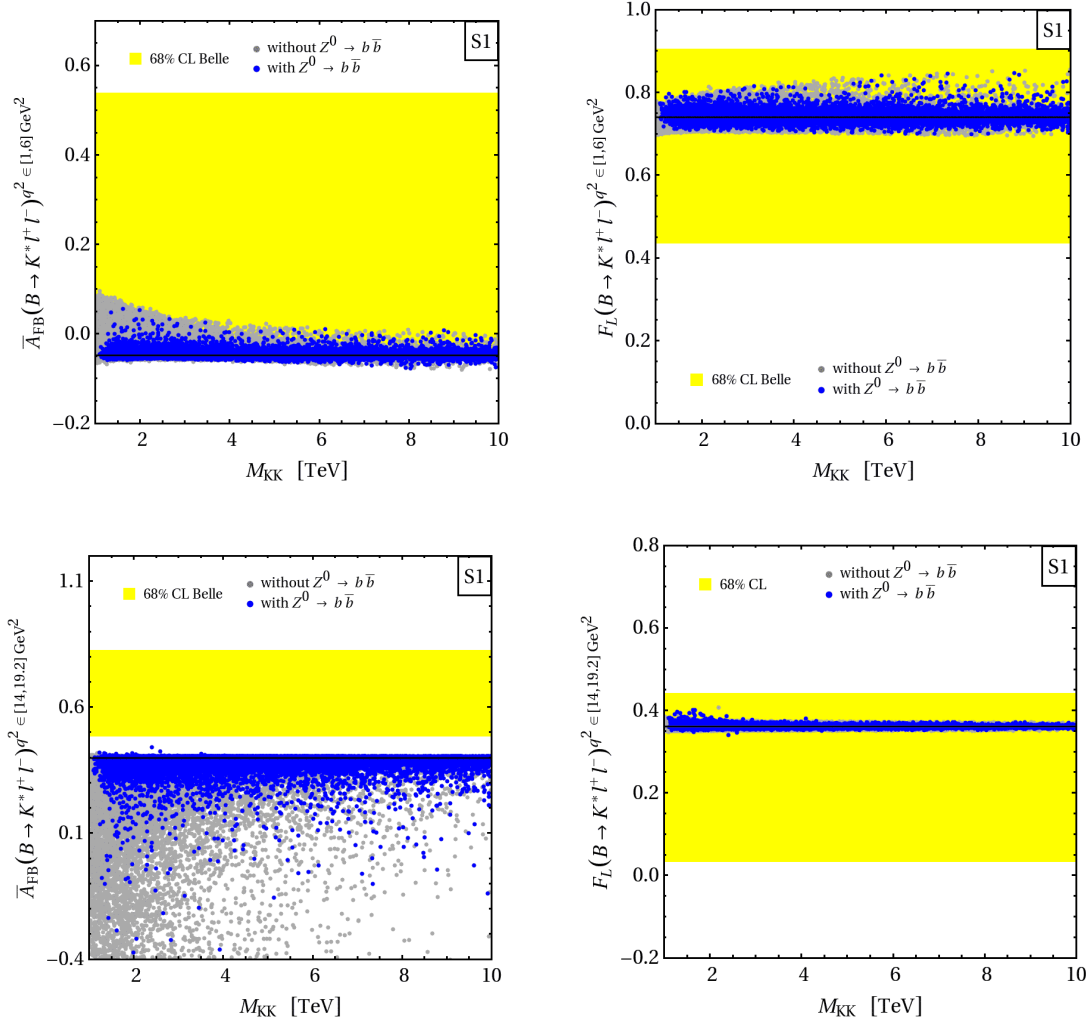


Figure 16: Predictions for $\bar{A}_{\text{FB}}(B \rightarrow K^* l^+ l^-)_{q^2 \in [q_1^2, q_2^2]}$ and $F_L(B \rightarrow K^* l^+ l^-)_{q^2 \in [q_1^2, q_2^2]}$ as a function of M_{KK} with $[q_1^2, q_2^2] = [1, 6] \text{ GeV}^2$ ($[q_1^2, q_2^2] = [14, 19.2] \text{ GeV}^2$) shown in the upper (lower) row. All displayed results have been obtained in benchmark scenario S1. The blue (light gray) scatter points are consistent (inconsistent) with the measured $Z^0 \rightarrow b\bar{b}$ couplings at the 99% CL. The solid black lines indicate the central values of the SM expectations. For comparison the regions of 68% (yellow) CL favored by experiment are also displayed. See text for details.

and Belle [141, 142]. An extension of the discussion to other decay channels [131], angular distributions [132, 133, 134, 135], and CP asymmetries [135, 136] is straightforward, but reserved for the future. The panels in Figure 16 show the results for the normalized forward-backward asymmetry $\bar{A}_{\text{FB}}(B \rightarrow K^* l^+ l^-)$ and the longitudinal K^* polarization $F_L(B \rightarrow K^* l^+ l^-)$ integrated over the low- and high- q^2 regions for points reproducing the measured hierarchies in the quark sector. Scatter points that fulfill (violate) the constraints arising from the measure-

ments of the $Z^0 \rightarrow b\bar{b}$ couplings are colored blue (light gray). The central values of the SM expectations are indicated by the solid black lines. In the upper left panel the measurement $\bar{A}_{\text{FB}}(B \rightarrow K^*l^+l^-)_{\text{exp}}^{q^2 \in [1,6] \text{ GeV}^2} = 0.26_{-0.30}^{+0.27} \text{stat} \pm 0.07_{\text{syst}}$ [142] is underlaid in form of a yellow band. The quoted Belle result agrees well with the latest BaBar measurement [140]. It has slightly smaller errors but includes events with dilepton invariant masses down to 0.1 GeV^2 , which is theoretically problematic due to the presence of very light $q\bar{q}$ resonances. Compared to the experimental central value, which is shifted toward the positive side from the SM expectation (105), the new-physics corrections in the normalized forward-backward asymmetry are quite small but positive. We see that only values in the range $[-6\%, 5\%]$ ($[-6\%, 10\%]$) can be achieved after (before) imposing the $Z^0 \rightarrow b\bar{b}$ constraint. The upper right panel of Figure 16 demonstrates that the size of the possible corrections in $F_L(B \rightarrow K^*l^+l^-)_{\text{exp}}^{q^2 \in [1,6] \text{ GeV}^2}$ due to the exchange of the Z^0 -boson and its KK modes is also limited. Values of the integrated longitudinal K^* polarization in the range of $[0.70, 0.81]$, corresponding to relative shifts of $[-5\%, 9\%]$ compared to the SM prediction (105), can be realized. The related experimental result $F_L(B \rightarrow K^*l^+l^-)_{\text{exp}}^{q^2 \in [1,6] \text{ GeV}^2} = 0.67 \pm 0.23_{\text{stat}} \pm 0.05_{\text{syst}}$ [142] is indicated by the yellow band. The central value of the most recent BaBar result [140] is smaller by almost a factor of 2 but agrees with the cited number from Belle within errors. The smallness of the observed deviations is a result of the weak dependence of the observables on the numerically dominant semileptonic Wilson coefficient $C_{10}^{l\text{RS}}$. Since the sensitivity of $\bar{A}_{\text{FB}}(B \rightarrow K^*l^+l^-)$ and $F_L(B \rightarrow K^*l^+l^-)$ to the electromagnetic dipole coefficients $C_{7,\text{RS}}^\gamma$ and $\tilde{C}_{7,\text{RS}}^\gamma$ is much more pronounced, larger effects might occur if loop-suppressed corrections are included in the analysis. To determine the exact impact of effects due to Q_7^γ and \tilde{Q}_7^γ , however, would require a dedicated study.

The panels in the lower row of Figure 16 show the high- q^2 predictions for the observables in question. In the case of the normalized forward-backward asymmetry we find that the RS tree-level corrections tend to reduce the SM value (108) and allow for values in the range $[-39\%, 41\%]$ if one does require the $Z^0 \rightarrow b\bar{b}$ constraint to be fulfilled. The yellow shaded band in the same panel represents a naive combination of the Belle measurements $\bar{A}_{\text{FB}}(B \rightarrow K^*l^+l^-)_{\text{exp}}^{q^2 \in [14,18,16] \text{ GeV}^2} = 0.70_{-0.22}^{+0.16} \text{stat} \pm 0.07_{\text{syst}}$ and $\bar{A}_{\text{FB}}(B \rightarrow K^*l^+l^-)_{\text{exp}}^{q^2 > 16 \text{ GeV}^2} = 0.66_{-0.16}^{+0.11} \text{stat} \pm 0.04_{\text{syst}}$ [142], which are compatible with the BaBar result in the high- q^2 bin [140] but have better precision. Concerning the observed high values of $\bar{A}_{\text{FB}}(B \rightarrow K^*l^+l^-)$, we would like to point out that arbitrary complex left-handed coefficients $C_{9,10}^l$ can enhance the forward-backward asymmetry only by a couple of percent relative to the SM value. Larger values of $\bar{A}_{\text{FB}}(B \rightarrow K^*l^+l^-)$ up to about 55% are possible if one allows for arbitrary complex right-handed coefficients $\tilde{C}_{9,10}^l$. To achieve values in the ballpark of 70% requires the inclusion of the electromagnetic dipole coefficients C_7^γ and \tilde{C}_7^γ . In particular, C_7^γ needs to be complex and almost anti-parallel to the SM contribution. In the lower right panel of Figure 16 we finally show the predictions for $F_L(B \rightarrow K^*l^+l^-)_{\text{exp}}^{q^2 \in [14,19.2] \text{ GeV}^2}$. For comparison, the naive average of the BaBar result $F_L(B \rightarrow K^*l^+l^-)_{\text{exp}}^{q^2 > 10.24 \text{ GeV}^2} = 0.71_{-0.22}^{+0.20} \text{stat} \pm 0.04_{\text{syst}}$ [140] and the Belle measurements $F_L(B \rightarrow K^*l^+l^-)_{\text{exp}}^{q^2 \in [14,18,16] \text{ GeV}^2} = -0.15_{-0.23}^{+0.27} \text{stat} \pm 0.07_{\text{syst}}$ and $F_L(B \rightarrow K^*l^+l^-)_{\text{exp}}^{q^2 > 16 \text{ GeV}^2} = 0.12_{-0.13}^{+0.15} \text{stat} \pm 0.02_{\text{syst}}$ [142] is indicated by the yellow band. We see that the predictions for the longitudinal K^* polarization are all essentially SM-like. This feature is easy to understand if one realizes that as a consequence of (106) the dependence

on the dominant axial-vector coefficient $C_{10}^{l\text{RS}}$ almost drops out in the ratio (103) determining $F_L(B \rightarrow K^*l^+l^-)$. We mention that values of $F_L(B \rightarrow K^*l^+l^-)$ integrated over the high- q^2 region significantly below the SM expectation (108) would hint towards the presence of right-handed currents.

It has been argued in [139, 140, 141, 142] that the available experimental data shows a slight preference for new-physics scenarios where the sign of C_7^γ is opposite with respect to the SM expectation $\text{sgn}(C_{7,\text{SM}}^\gamma) = -1$. While much larger data sets are certainly needed to draw a definite conclusion, it is important to emphasize that models with $\text{sgn}(C_7^\gamma) = +1$ and only small non-standard contributions to the semileptonic coefficients $C_{9,10}^l$ are disfavored at the 3σ level by the combination of the $\mathcal{B}(B \rightarrow X_s\gamma)$ and $\mathcal{B}(B \rightarrow X_sl^+l^-)$ measurements [190]. Hypothetical new-physics scenarios with flipped-sign C_7^γ only are thus at variance with the available data on the inclusive $b \rightarrow s\gamma, l^+l^-$ transitions. This observation elucidates the fact that to bound the values of the various Wilson coefficients one should exploit all available experimental information in the $b \rightarrow s\gamma$ and $b \rightarrow sl^+l^-$ sector, combining both inclusive and exclusive channels.

5.6 Rare Non-Leptonic Decays of Kaons and B Mesons

We finally turn our attention to the vast array of non-leptonic kaon and B -meson decays, focusing on a few of the most interesting observables. We start out with a detailed numerical analysis of the CP-violating ratio ϵ'_K/ϵ_K and investigate its correlation with the rare $K \rightarrow \pi\nu\bar{\nu}$ and $K_L \rightarrow \pi^0l^+l^-$ decays. Subsequently, we will consider the RS contributions to a variety of exclusive B -meson decays into final states containing two pseudoscalar mesons or a pseudoscalar and a vector meson. One important question that we will address in this context is whether possible discrepancies in the $b \rightarrow s$ sector, as suggested by experiment, can be explained in the context of warped extra-dimension models.

5.6.1 Numerical Analysis of ϵ'_K/ϵ_K

Within the SM the smallness of direct CP violation in $K \rightarrow \pi\pi$ is the result of a destructive interference between the positive contribution due to QCD penguins and the negative contribution arising from electroweak penguin diagrams. In new-physics models in which the $\Delta I = 1/2$ and $\Delta I = 3/2$ contributions to $s \rightarrow dq\bar{q}$ processes are affected in a different way, this partial cancellation is usually much less pronounced or even absent. A qualitative understanding of the situation in the minimal RS model can be obtained from the approximate relation

$$\left(\frac{\epsilon'_K}{\epsilon_K}\right)_{\text{RS}} \propto 1 + [-0.1, 0.1]B_6^{(1/2)} - 12B_8^{(3/2)}, \quad (133)$$

which has been obtained from the second expression in (47) by inserting typical values of the Wilson coefficients C_{3-10}^{RS} and $\tilde{C}_{3-10}^{\text{RS}}$. The smallness (largeness) of the coefficient multiplying the hadronic parameter $B_6^{(1/2)}$ ($B_8^{(3/2)}$) is easily explained by the structure of ϵ'_K/ϵ_K within the SM. While both the QCD and electroweak penguin contributions are strongly enhanced by RG effects, the former correction results mainly from the mixing of Q_6 with $Q_{1,2}$ and is

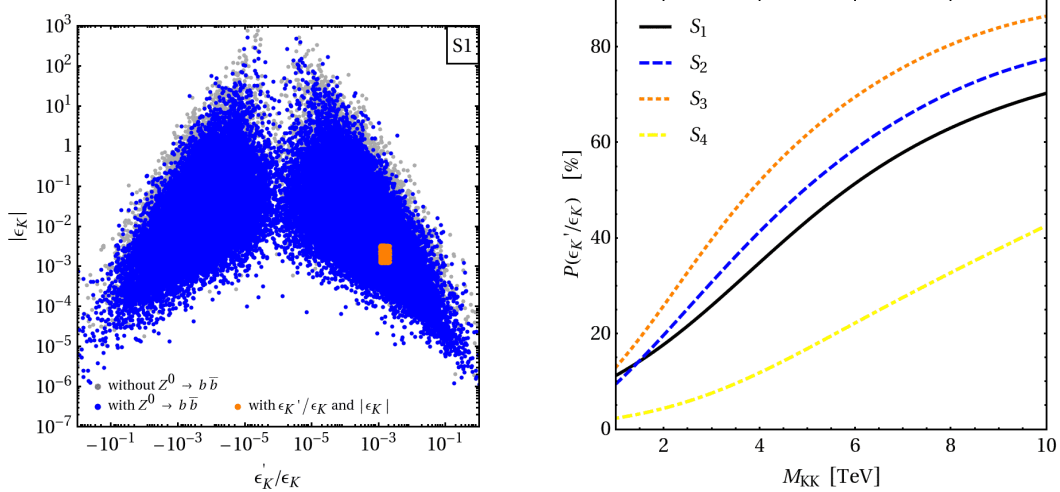


Figure 17: Left panel: Correlation between ϵ'_K/ϵ_K and $|\epsilon_K|$ in the benchmark scenario S1. The blue (light gray) points are consistent (inconsistent) with $Z^0 \rightarrow b\bar{b}$ at the 99% CL. The points that are in agreement with the experimental values of both ϵ'_K/ϵ_K and $|\epsilon_K|$ at 95% CL are marked in orange. Right panel: Percentage of scatter points as a function of M_{KK} that are consistent with ϵ'_K/ϵ_K . The shown lines correspond to our four different parameter scenarios. See text for details.

thus essentially unaffected by new physics. On the other hand, mixing with the current-current operators plays only a very minor role in the case of the electroweak penguins, so that any new-physics contribution to the initial conditions in this sector directly feeds through into ϵ'_K/ϵ_K . This implies that electroweak penguin operators give the dominant correction to direct CP violation in the kaon sector. Our numerical analysis confirms this model-independent conclusion. Notice that the sign of $(\epsilon'_K/\epsilon_K)_{RS}$ in (133) is not fixed, so that the prediction for the total ratio ϵ'_K/ϵ_K can be positive or negative. An enhancement (depletion) of ϵ'_K/ϵ_K occurs if the imaginary part of the enhanced electroweak penguin contribution has opposite (identical) sign with respect to the SM Z^0 -penguin amplitude.

It is also important to bear in mind that the observables ϵ'_K/ϵ_K and $|\epsilon_K|$ are not independent from each other if the experimental constraint on $|\epsilon_K|$ is ignored and ϵ'_K/ϵ_K is calculated fully in theory. Since the central value of the theory prediction (52) is below the world average for ϵ'_K/ϵ_K , models are disfavored in which there are new positive contributions to $|\epsilon_K|$ and negative contributions to ϵ'_K . The correlation between ϵ'_K/ϵ_K and $|\epsilon_K|$ in the benchmark scenario S1 is shown in the left panel of Figure 17. All shown points reproduce the correct quark masses and mixings. Scatter points that are consistent with $Z^0 \rightarrow b\bar{b}$ are colored blue, while those points that lie inside the 95% CL ranges $\epsilon'_K/\epsilon_K \in [11.3, 21.7] \cdot 10^{-4}$ and $|\epsilon_K| \in [1.2, 3.2] \cdot 10^{-3}$ are marked in orange. The plot has been obtained by setting the non-perturbative parameters $R_{6,8}$ entering (47) equal to 1. It is evident from the distribution of points that solutions featuring unacceptably large values of $|\epsilon_K|$ are typically also in conflict with ϵ'_K/ϵ_K , since they predict too low values for the latter observable. For points in line with $|\epsilon_K|$, it is however still possible to obtain values for ϵ'_K/ϵ_K in the range $[-1, 1] \cdot 10^{-1}$. The wide spread of viable results suggests

that the data on ϵ'_K/ϵ_K impose non-trivial constraints on the allowed model parameters even if the $|\epsilon_K|$ constraint is satisfied.

The right plot in Figure 17 illustrates how severe the ϵ'_K/ϵ_K constraint is in each of the four benchmark scenarios. In our numerical analysis a point is considered compatible with ϵ'_K/ϵ_K , if it is possible to bring the theoretical prediction into agreement with the measured value at the 95% CL by varying the hadronic parameters and light quark masses in the ranges given in (50) and (50), requiring in addition $B_6^{(1/2)} > B_8^{(3/2)}$. Although calculations of the hadronic matrix elements $\langle(\pi\pi)_0|Q_6|K\rangle$ and $\langle(\pi\pi)_2|Q_8|K\rangle$ that are free from systematic uncertainties do not exist at present, we believe that this is a very conservative treatment of theoretical errors. The shown $P(\epsilon'_K/\epsilon_K)$ curves correspond again to the best fits to the data after binning in M_{KK} with a bin size of 100 GeV and using the functional form of a Fermi function times a quadratic polynomial. We find that 46%, 61%, 61%, and 21% of the total number of generated points are consistent with ϵ'_K/ϵ_K in the scenario S1, S2, S3, and S4, respectively. One can make sense out this percentages if one recalls the pattern of enhancements and depletions of $\Delta F = 2$ and $\Delta F = 1$ contributions in the different benchmark scenarios. Compared to the default scenario S1, corrections to $|\epsilon_K|$ are typically less pronounced in S2 and S3, because these scenarios are specifically designed to suppress $|\epsilon_K|$ by either allowing for larger Yukawa couplings or by eliminating flavor mixing that arises from the non-universality of the right-handed down-type quark profiles. On the other hand the corrections to $s \rightarrow dZ^0$ entering ϵ'_K/ϵ_K are only indirectly affected. They tend to be smaller as well, since the parameter scenarios S2 and S3 show a preference for a stronger localization of the first two SM-like doublets towards the UV to account for the correct values of the quark mass. In the benchmark scenario S4 the situation is reversed. Numerically, we find that demanding $P(\epsilon'_K/\epsilon_K) > 25\%$ sets lower limits of $M_{KK} > 2.9, 2.5, 2.0,$ and 6.6 TeV in the scenario S1, S2, S3, and S4. In terms of the mass of the first KK mode this means 7.1, 4.9, 6.1, and 16.2 TeV. These numbers imply that with our conservative treatment of errors the ϵ'_K/ϵ_K constraint is typically weaker than the constraint from $|\epsilon_K|$ but stronger than the one arising from $Z^0 \rightarrow b\bar{b}$.

We also mention that potentially large corrections to ϵ'_K/ϵ_K can arise from the presence of the chromomagnetic dipole operator Q_8^g and its chirality-flipped partner \tilde{Q}_8^g . In the context of scenarios with hierarchical fermion profiles, this issue has been analyzed in a model-independent fashion in [40]. Interestingly, the contributions to ϵ'_K/ϵ_K from C_8^g and \tilde{C}_8^g and to ϵ_K from C_4^{RS} depend in an opposite way on the Yukawa couplings. This makes it difficult to decouple flavor-violating effects using these parameters and will lead to a “tension” between tree- and loop-level effects, similar to what happens in the case of $B \rightarrow X_s \gamma$ and ϵ_K [21]. A study of this anti-correlation including the first KK level of the quarks and the zero-mode of the Higgs field has been very recently presented in [25]. There it has been pointed out that the constraint stemming from the chromomagnetic dipole-operator contributions to ϵ'_K/ϵ_K yields a lower bound of at least 5.5 TeV on the mass of the first KK excitation. Notice that the correlation between ϵ'_K/ϵ_K and $|\epsilon_K|$ has not been studied in [25], since ϵ'_K/ϵ_K has been normalized to the experimental value $|\epsilon_K|_{\text{exp}}$ and not to $|\epsilon_K|$.¹² A more realistic evaluation of the chromomagnetic dipole contribution to ϵ'_K/ϵ_K including the correlation between ϵ'_K/ϵ_K

¹²If we normalize ϵ'_K/ϵ_K to the experimental rather than the theoretical value of $|\epsilon_K|$, we find that requiring $P(\epsilon'_K/\epsilon_K) = 25\%$ sets the limits 4.6, 6.5, 3.2, and 3.0 TeV on the mass of the first KK excitation in scenario S1, S2, S3, and S4. Notice that in this case the bound is solely due to the electroweak penguin contribution.

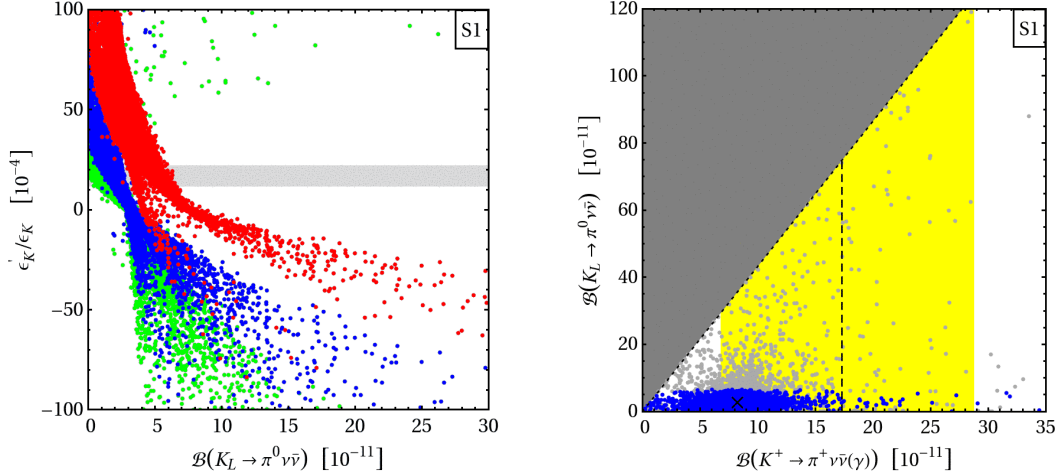


Figure 18: Left panel: Correlation between the $K_L \rightarrow \pi^0 \nu \bar{\nu}$ branching fraction and ϵ'_K/ϵ_K in benchmark scenario S1. All points reproduce the quark hierarchies and the measured values of $|\epsilon_K|$, $Z^0 \rightarrow b\bar{b}$, and $B_d-\bar{B}_d$ mixing at 95%, 99%, and 95% CL. The blue points correspond to the central value for ϵ'_K/ϵ_K obtained for $R_{6,8} = 1$, while the red (green) points illustrate the maximal (minimal) achievable values of ϵ'_K/ϵ_K for the same set of points obtained by varying the hadronic parameters. For comparison the experimental 95% CL (light gray) is also displayed. Right panel: Impact of ϵ'_K/ϵ_K on the predictions in the $\mathcal{B}(K^+ \rightarrow \pi^+ \nu \bar{\nu}(\gamma))-\mathcal{B}(K_L \rightarrow \pi^0 \nu \bar{\nu})$ plane in parameter scenario S1. The blue (light gray) scatter points are consistent (inconsistent) with the measured value of ϵ'_K/ϵ_K . See text for details.

and $|\epsilon_K|$ would be worthwhile, but is beyond the scope of this work.

The marked sensitivity of ϵ'_K/ϵ_K to modifications of the electroweak penguin sector leads to stringent correlations between ϵ'_K/ϵ_K and the $s \rightarrow d\nu\bar{\nu}$, $s \rightarrow dl^+l^-$ observables. This feature is illustrated in Figure 18, where the left panel shows the predictions for ϵ'_K/ϵ_K as a function of the branching fraction of $K_L \rightarrow \pi^0 \nu \bar{\nu}$ in scenario S1. All scatter points reproduce the hierarchies in the quark sector as well as the measured values of $|\epsilon_K|$, $Z^0 \rightarrow b\bar{b}$, and $B_d-\bar{B}_d$ mixing. The blue points correspond to the values for ϵ'_K/ϵ_K for fixed $R_{6,8} = 1$, while the red (green) points are obtained by scanning the hadronic parameters over the ranges (50) and (51), requiring in addition $B_6^{(1/2)} > B_8^{(3/2)}$, and determining the maximal (minimal) values of ϵ'_K/ϵ_K . The light gray band represents the experimental 95% CL. We observe that in our default scenario S1 enhancements (suppressions) of $\mathcal{B}(K_L \rightarrow \pi^0 \nu \bar{\nu})$ tend to be accompanied by suppressions (enhancements) of ϵ'_K/ϵ_K . The large enhancements of $\mathcal{B}(K_L \rightarrow \pi^0 \nu \bar{\nu})$ found earlier in Section 5.5.1 are hence disfavored by the measured amount of direct CP violation in $K \rightarrow \pi\pi$. This is explicitly demonstrated for our default scenario S1 in the right panel of Figure 18, which shows the predictions for $\mathcal{B}(K^+ \rightarrow \pi^+ \nu \bar{\nu}(\gamma))$ versus $\mathcal{B}(K_L \rightarrow \pi^0 \nu \bar{\nu})$ before (gray points) and after (blue points) imposing the ϵ'_K/ϵ_K constraint. We see that even with a conservative treatment of errors, *i.e.*, scanning over hadronic parameters, ϵ'_K/ϵ_K has a non-negligible impact on the possible new-physics effects in rare K decays within the RS model.

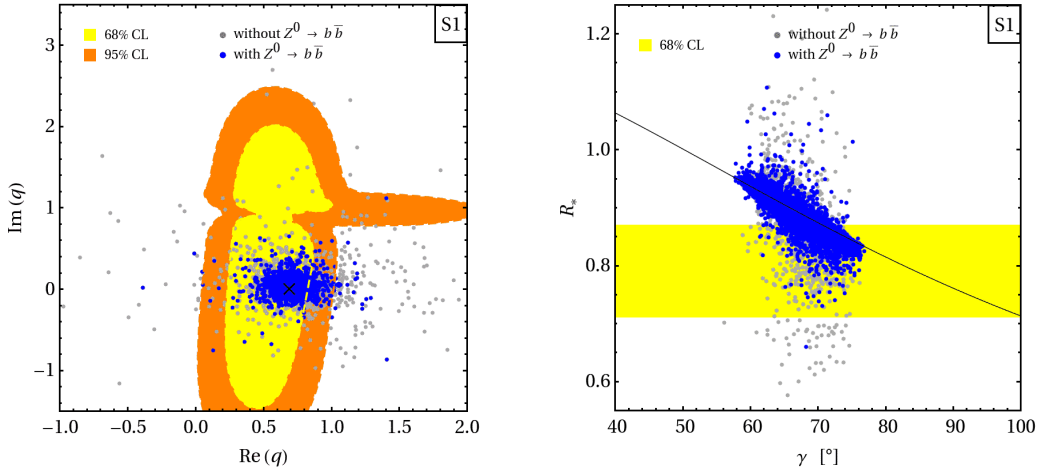


Figure 19: Left panel: Predictions in the $\text{Re}(q)$ – $\text{Im}(q)$ plane. The black cross indicates the SM expectation. For comparison the regions of 68% (yellow) and 95% CL (orange) following from a fit to the current $B \rightarrow K\pi, \pi\pi$ data are also displayed. Right panel: Predictions for R_* as a function of γ . The black line indicates the SM prediction while the yellow band corresponds to the experimental 68% CL. The blue (light gray) points shown in both panels are consistent (inconsistent) with the measured $Z^0 \rightarrow b\bar{b}$ couplings at the 99% CL. See text for details.

Notice that values of $B_8^{(3/2)}$ near the upper end of the range shown in (50) are particularly problematic in this respect, since they amplify the electroweak penguin contributions to ϵ'_K/ϵ_K . As enhancements of the branching fractions $K_L \rightarrow \pi^0\nu\bar{\nu}$ and $K_L \rightarrow \pi^0l^+l^-$ are strongly correlated with each other, similar statements apply to the rare kaon decay modes with charged leptons in the final state. The same strong anti-correlation between $\mathcal{B}(K_L \rightarrow \pi^0\nu\bar{\nu})$ and ϵ'_K/ϵ_K is also present in the parameter scenarios S2 and S4. It arises because both observables receive the dominant correction from the imaginary part of the left-handed $s \rightarrow dZ^0$ amplitude, which relative to the SM contribution enters linearly and with opposite sign in ϵ'_K/ϵ_K , whereas it appears quadratically and with the same sign in $\mathcal{B}(K_L \rightarrow \pi^0\nu\bar{\nu})$. Interestingly, in new-physics models in which the $s \rightarrow d$ transitions are dominated by right-handed operators the correlation between ϵ'_K/ϵ_K and $\mathcal{B}(K_L \rightarrow \pi^0\nu\bar{\nu})$ is predicted to be a negative one too. This model-independent conclusion follows from the fact that in both $K_L \rightarrow \pi^0\nu\bar{\nu}$ and ϵ'_K/ϵ_K the left- and right-handed Z^0 -boson contribution interfere destructively, see (48) and (67). Studies of the correlation between $\mathcal{B}(K_L \rightarrow \pi^0\nu\bar{\nu})$ and ϵ'_K/ϵ_K therefore will not allow to test the chiral nature of the electroweak penguin operators in the $s \rightarrow d$ sector. The correlation between $\mathcal{B}(K^+ \rightarrow \pi^+\nu\bar{\nu})$ and ϵ'_K/ϵ_K is weaker compared to the one present in the neutral sector. As a result, larger departures from the SM expectation in the charged mode are possible even after enforcing the ϵ'_K/ϵ_K constraint.

5.6.2 Numerical Analysis of Non-Leptonic B Decays

We conclude our comprehensive phenomenological survey with a numerical analysis of the most interesting observables in the vast field of exclusive hadronic B -meson decays. As the considered observables turn out to be largely independent of the specific choice for the parameter scenario, we will in the following only show results corresponding to our default benchmark scenario S1. Moreover only scatter points that reproduce the mass and mixing hierarchies in the quark sector and the constraints arising from $|\epsilon_K|$ and B_d - \bar{B}_d mixing will be included in the plots. To illustrate the impact of the $Z^0 \rightarrow b\bar{b}$ constraint, we discriminate between points that are consistent (inconsistent) with the constraint by coloring them in blue (light gray).

In the left panel of Figure 19 we display our predictions in the electroweak penguin parameter q given in (54). The SM expectation is indicated by a black cross, while the yellow (orange) colored contours show the regions of 68% (95%) CL obtained in [191] from a χ^2 fit to the $B \rightarrow K\pi$ and $B \rightarrow \pi\pi$ data. The latter data has a strong impact in the fit, yielding two almost degenerate minima with $|q|_{\text{exp}} = 0.8_{-0.3}^{+0.2}$, $\phi_{\text{exp}} = (45_{-28}^{+18})^\circ$ and $|q|_{\text{exp}} = 1.3 \pm 0.4$, $\phi_{\text{exp}} = (63_{-9}^{+10})^\circ$ [191]. We see that while most of the scatter points fall into the range $|q|_{\text{SM}} = 0.69 \pm 0.18$, $\phi_{\text{SM}} = (0.2 \pm 2.1)^\circ$ some solutions differ visibly from the SM expectation both in magnitude and/or phase. These points all feature an enhanced electroweak penguin sector. Notice that larger deviations would be possible if the stringent constraint arising from $Z^0 \rightarrow b\bar{b}$ would be relaxed. Even in such a case, however, corrections that would accommodate the second minimum in the χ^2 fit¹³ are disfavored by the existing $b \rightarrow sl^+l^-$ data. This is a model-independent conclusion that holds in all new-physics models where the couplings between neutral gauge bosons and leptons are not suppressed relative to the couplings to light quarks (like it happens to be the case in RS models), and where electromagnetic dipole operators do not receive sizable corrections that (partially) cancel the effects from the semileptonic operators. Removing the ϵ_K constraint, on the other hand, does not change the obtained results qualitatively, since the new-physics contributions to the $s \rightarrow d$ and $b \rightarrow s$ sector are highly uncorrelated in all RS models with flavor anarchy.

In the right and left panel of Figure 19 and 20 we present the predictions for R_* and R_{00} as a function of the angle γ of the unitarity triangle. The black lines represent the central values of the SM expectations, and the yellow bands are the experimentally preferred ranges at 68% probability. Like in the case of q , we observe that the RS contributions to the ratios R_* and R_{00} typically do not exceed the uncertainties of the measurements, which are similar in size to the theoretical errors. We remark that an enhancement (suppression) of R_* and R_{00} relative to the SM corresponds to destructive (constructive) interference between the new-physics and the SM electroweak penguin contribution. It is also interesting to note that the RS contribution to R_* (R_{00}) is a factor of 7 (11) more sensitive to the real than the imaginary part of C_9 . The weak dependence of R_{00} on γ in combination with the fact that $R_{00} < 1$ is a practically model-independent SM prediction (which can be understood in terms of a negative interference between QCD and electroweak penguins) implies that improved measurements of the latter ratio could turn out to be valuable in probing the nature of the electroweak penguin sector of warped extra-dimension models.

¹³Such corrections typically feature negative values of $\text{Im} K_9$ of a few 10^{-4} and positive values of $\text{Re} K_9$ that are smaller by an order of magnitude.

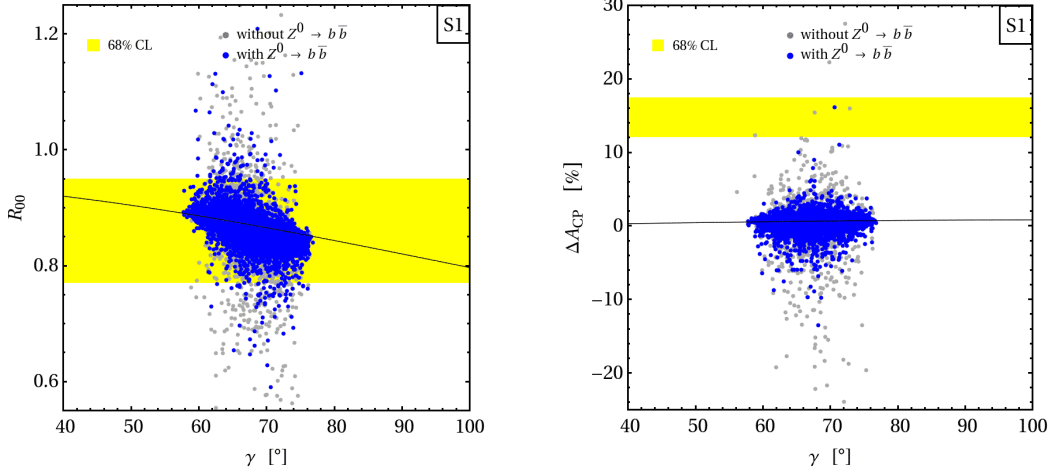


Figure 20: Predictions for R_{00} and ΔA_{CP} as a function of γ . The black lines display the central value of the SM expectation while the yellow bands illustrate the corresponding experimental 68% CL. The shown blue (light gray) scatter points reproduce the values of the $Z^0 b\bar{b}$ couplings at 99% CL. See text for details.

We now turn our attention to the so-called $\bar{B} \rightarrow \pi \bar{K}$ puzzle. Our predictions for ΔA_{CP} are shown in the right panel of Figure 20. The black line represents the central value of the SM theory prediction as a function of γ . For comparison we also show the 68% CL range of ΔA_{CP} favored by the updated BaBar and Belle measurements of the CP asymmetries in $\bar{B}^0 \rightarrow \pi^+ K^-$ and $B^- \rightarrow \pi^0 K^-$ decays (yellow band). Obviously the RS corrections in ΔA_{CP} are typically at the level of a few percent only, *i.e.*, too small to explain the 3.5σ discrepancy between experiment and SM expectation. We remark that in order to achieve agreement in ΔA_{CP} within 1σ of the combined experimental and theoretical error, the coefficient K_9 should satisfy¹⁴

$$(0.5 + 45 \text{Re} K_9) \cdot 10^{-3} \lesssim \text{Im} K_9 \lesssim (0.9 - 75 \text{Re} K_9) \cdot 10^{-3}. \quad (134)$$

This formula has been obtained by setting $C_7^{\text{RS}} = -s_w^2/c_w^2 C_9^{\text{RS}} \approx -1/3 C_9^{\text{RS}}$ and neglecting the matching corrections to the QCD penguins, C_{3-6} , as well as the chirality-flipped operators, \tilde{C}_{3-10} (which are all good approximations in the considered setup). The relatively weak dependence on $\text{Re} K_9$ implies that ΔA_{CP} essentially measures the imaginary part of K_9 , which has to be positive in order to enhance ΔA_{CP} . Assuming now that K_9 has the correct phase to fulfill (134), the relations (17), (44), and (48) can be used to derive the rough bound

$$M_{\text{KK}} \lesssim \sqrt{5 L F(c_{Q_2}) F(c_{Q_3})} \text{ TeV} \approx 1.7 \text{ TeV} \quad (135)$$

on the KK mass scale. Here only the L -enhanced corrections in (44) have been included, and the quoted numerical result corresponds to the central values for $c_{Q_{2,3}}$ in our default benchmark

¹⁴The given inequality is only a crude approximation that should allow one to gain an understanding of how low the KK mass scale would have to be in order to reach values for ΔA_{CP} in the ballpark of 15%.

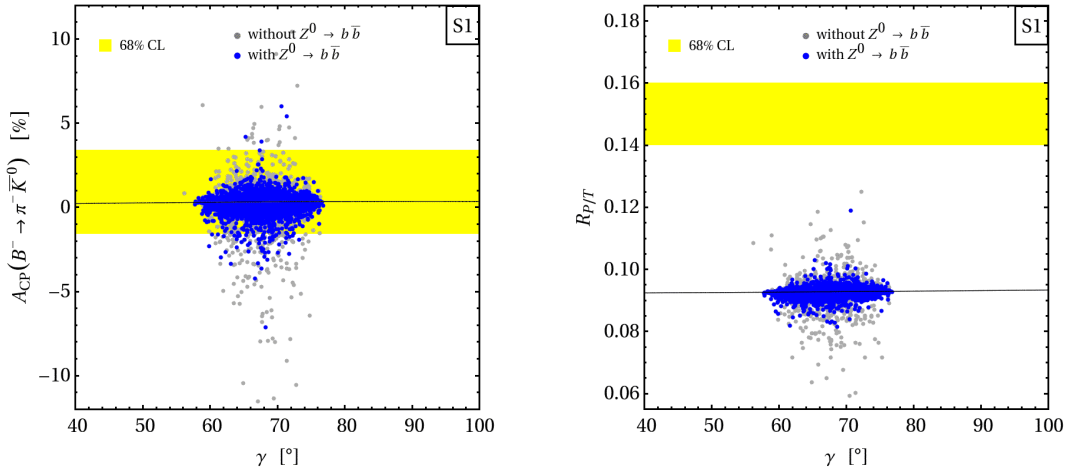


Figure 21: Predictions for $A_{\text{CP}}(B^- \rightarrow \pi^- \bar{K}^0)$ and $R_{P/T}$ as a function of γ . The black lines and yellow bands represent the central value of the SM expectation and the corresponding experimental 68% CL, respectively. Blue (light gray) points are consistent (inconsistent) with $Z^0 \rightarrow b\bar{b}$ at 99% CL. See text for details.

scenario S1 as given in Table 1. Recalling that the $Z^0 \rightarrow b\bar{b}$ constraint typically forces the KK scale to lie above 2 TeV in the original RS model, it is clear that there is a generic tension between large effects in ΔA_{CP} due to a modified electroweak penguin sector and the precision measurements involving bottom quarks at the Z^0 -pole. We also emphasize that in RS variants with custodial protection of the $Z^0 d_{iL} \bar{d}_{jL}$ couplings the effects in ΔA_{CP} are even smaller than in the minimal RS scenario, because the right-handed quark profile functions are naturally more UV-localized than their left-handed counterparts. A resolution of the $\bar{B} \rightarrow \pi \bar{K}$ puzzle therefore seems to be difficult in the RS framework in general.

Our predictions for $A_{\text{CP}}(B^- \rightarrow \pi^- \bar{K}^0)$ and $R_{P/T}$ are shown in the left and right panels of Figure 21. The black lines and yellow bands depict the central values of the SM prediction and the experimental 68% CL ranges. While in the case of $A_{\text{CP}}(B^- \rightarrow \pi^- \bar{K}^0)$ we see that it is possible to saturate the experimental limits, corresponding to shifts in the CP asymmetry of a couple of percent, the typical deviations in the penguin-to-tree ratio $R_{P/T}$ are much smaller than the difference between the central value of the theory prediction and the experimental determination. Although the discrepancy between $(R_{P/T})_{\text{exp}}$ and $(R_{P/T})_{\text{SM}}$ is in view of the sizable SM error not significant, it is still interesting to ask how an electroweak penguin sector that would improve the agreement between experiment and theory may look like. Neglecting again subleading contributions to $R_{P/T}$ from QCD penguins and operators with opposite chirality, and setting $C_7^{\text{RS}} = -s_w^2/c_w^2 C_9^{\text{RS}}$, it is easy to show that points that lead to the same value for $R_{P/T}$ lie on circles in the $\text{Re}K_9 - \text{Im}K_9$ plane. For example, to bring $R_{P/T}$ within 1σ of the experimental central value, the following condition has to be fulfilled

$$5.0 \cdot 10^{-6} \lesssim (\text{Re}K_9 + 0.0014)^2 + (\text{Im}K_9 - 0.0030)^2 \lesssim 6.1 \cdot 10^{-6}. \quad (136)$$

This inequality implies that, like in the case of ΔA_{CP} , an enhancement of $R_{P/T}$ relative to its

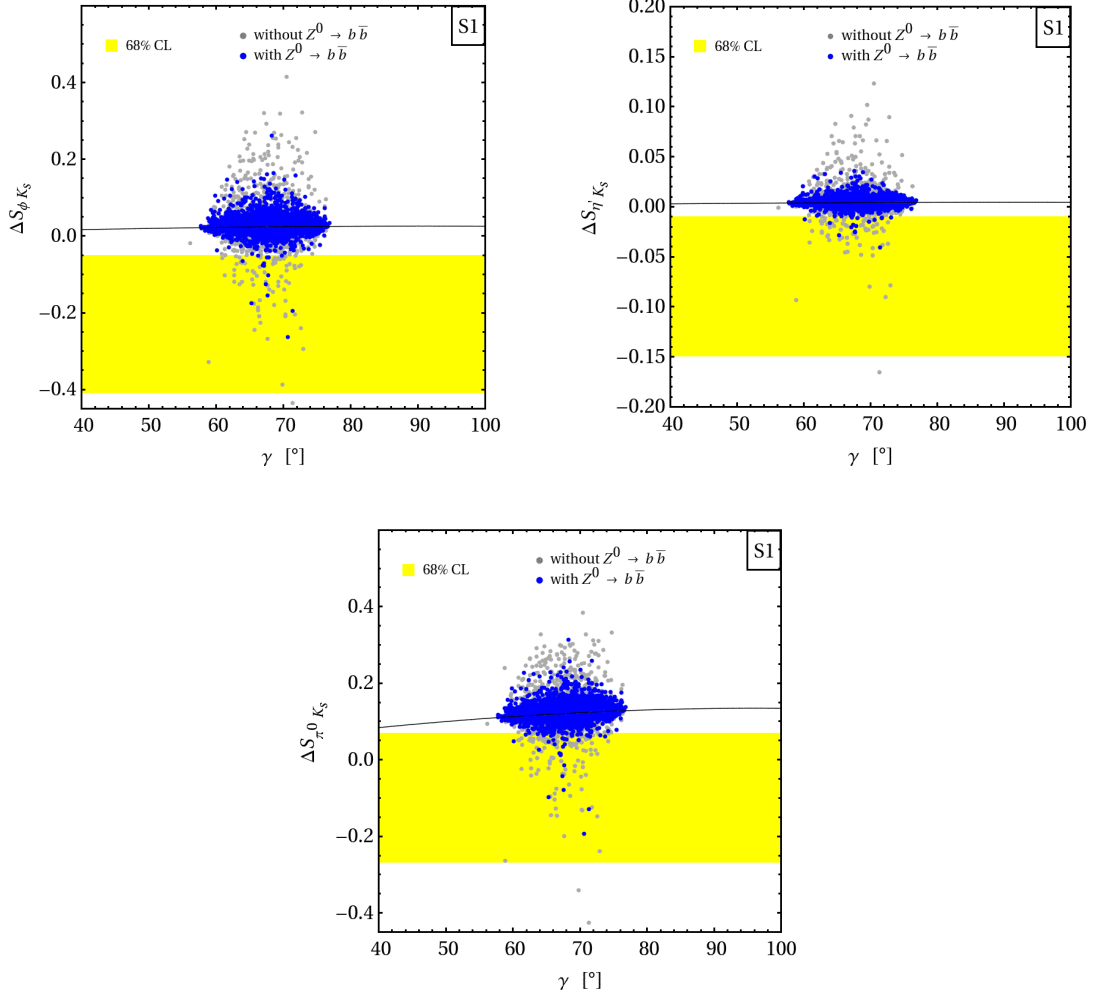


Figure 22: Predictions for $\Delta S_{\phi K_S}$, $\Delta S_{\eta' K_S}$, and $\Delta S_{\pi^0 K_S}$ as a function of γ . The black lines and yellow bands correspond to the central values expected in the SM and the associated experimental 68% CL regions. Scatter points colored blue (light gray) satisfy (fail to satisfy) the $Z^0 \rightarrow b\bar{b}$ constraint at 99% CL. See text for details.

SM value requires the imaginary part of K_9 to be positive and of order $7 \cdot 10^{-4}$. Such values of $\text{Im}K_9$ again call for $M_{KK} \lesssim 2$ TeV, at variance with the parameter region preferred by the $Z^0 b\bar{b}$ couplings.

In Figure 22, we finally show the predictions for the shifts $\Delta S_{\phi K_S}$, $\Delta S_{\eta' K_S}$, and $\Delta S_{\pi^0 K_S}$ as a function of γ . The central values of the SM predictions (black lines) and the experimental 68% CL ranges (yellow bands) are displayed for comparison. It is evident that in all three cases it is possible to improve the agreement between theory and experiment. The maximal deviations in $\Delta S_{\phi K_S}$ and $\Delta S_{\pi^0 K_S}$ ($\Delta S_{\eta' K_S}$) are at the level of ± 0.2 (± 0.02), corresponding to corrections in K_{7-10} of order 10^{-4} . In order to explain this pattern, we first note that $\Delta S_{\phi K_S}$, $\Delta S_{\eta' K_S}$, and $\Delta S_{\pi^0 K_S}$ depend only very weakly on the real parts of the electroweak penguin

coefficients K_{7-10} . Setting again $C_7^{\text{RS}} = -s_w^2/c_w^2 C_9^{\text{RS}}$ and ignoring all corrections from QCD penguin and chirality-flipped operators, we find that the dependence of $\Delta S_{\phi K_S}$ and $\Delta S_{\pi^0 K_S}$ on $\text{Im}K_9$ is more pronounced by a factor of roughly 10 than the one of $\Delta S_{\eta' K_S}$. Furthermore, positive values of $\text{Im}K_9$ lead to negative shifts $\Delta S_{\phi K_S}$ and $\Delta S_{\pi^0 K_S}$ and *vice versa*, while in the case of $\Delta S_{\eta' K_S}$ the correlation is a positive one. A simultaneous improvement in all three observables is therefore in general not possible in the RS framework.

6 Conclusions and Outlook

We have presented a detailed and comprehensive study of flavor-violating effects in the original RS scenario, which features an $SU(2)_L \times U(1)_Y$ bulk gauge symmetry and a minimal, brane-localized Higgs sector. The complete analytic expressions up to $\mathcal{O}(v^2/M_{\text{KK}}^2)$ for all relevant effective four-fermion interactions induced by the exchange of gauge or Higgs bosons have been derived. In contrast to previous studies of quark flavor physics in RS models, the given expressions encode the summation over the entire KK tower and not only one (or a few) KK excitations. Employing the methods and results presented in the first part of this sequel, it would be easy to include higher-order contributions in v^2/M_{KK}^2 in closed form as well.

Next we have applied these general findings to weak decay processes, focusing on observables in the quark sector. We first have obtained the complete tree-level expressions for the relevant effective $\Delta F = 2$ Hamiltonians, giving rise to the mixing of neutral K , $B_{d,s}$, and D mesons with their antiparticles. Next followed a derivation of the effective $\Delta F = 1$ Hamiltonians describing the $b \rightarrow sq\bar{q}$, $s \rightarrow d\nu\bar{\nu}$, $b \rightarrow sl^+l^-$, and $b \rightarrow ul\bar{\nu}$ transitions arising from the tree-level exchange of KK gluons and photons, the Z^0 and W^\pm bosons and their KK excitations, as well as the Higgs boson. We then collected the formulas needed for the phenomenological analysis of neutral-meson mixing, as well as rare non-leptonic and leptonic decays of kaons and B mesons. Besides quantities that have already received much attention in the literature, such as $K-\bar{K}$ and $B-\bar{B}$ mixing, the discussed observables include many that were not often considered before, ranging from $D-\bar{D}$ mixing to the (semi-)leptonic processes $B \rightarrow \tau\nu_\tau$, $B \rightarrow \mu^+\mu^-$, $B \rightarrow X_s(K^*)l^+l^-$ to ϵ'_K/ϵ_K and non-leptonic decays such as $\bar{B} \rightarrow \pi\bar{K}$. Throughout our discussion we tried to be as general as possible, so that the given formulas can be applied to any SM extension with flavor-violating contributions to both left- and right-handed dimension-six operators.

After this preparatory work, we have presented dedicated numerical analyses of the various flavor observables. In order to investigate how sensitively the predictions depend on the most relevant parameters of the minimal RS model, we have studied four different parameter scenarios in detail. Besides the default scenario (S1, “standard”), we investigated the consequences of larger Yukawa couplings (S2, “large”), of common right-handed down-type bulk masses (S3, “aligned”), and the impact of a reduction of the “volume” of the extra dimension (S4, “little”). The latter three benchmark scenarios are designed specifically to suppress harmful contributions to electroweak precision and quark flavor observables, and we have quantified the improvement that can be achieved in the $Z^0 \rightarrow b\bar{b}$ and ϵ_K observables in each case. While the average amount of tuning required in order to satisfy the stringent constraints from the bottom-quark Z^0 -pole observables and indirect CP violation in the kaon sector depend on the

particular scenario, we found that most other flavor observables are largely insensitive to such a choice.

We began our phenomenological survey in the charged-current sector, emphasizing that the exchange of the entire KK tower of the W^\pm bosons generically induces unitarity violations in the columns and rows of the quark-mixing matrices. While the non-standard effects in the elements of the generalized CKM matrix involving only light quarks are small after correct normalization to the Fermi constant G_F , the corrections in the heavy-quark sector can be of the order of a few percent. This leads to a non-closure of the unitary triangle. While this effect is severely constrained by the $Z^0 \rightarrow b\bar{b}$ precision observables in the minimal RS scenario, it can still be at the level of the current experimental uncertainties. We have furthermore pointed out that the prospects for a detection of a unitarity violation of the left-handed quark-mixing matrix or deviations in the branching ratios of semileptonic and purely leptonic B decays are better in RS realizations with extended bulk gauge symmetry, because the custodial symmetry cannot simultaneously protect the $Z^0 b_L \bar{b}_L$ and the $W u_{iL} d_{jL}$ vertices.

A first key observation gleaned from the analyses of $\Delta F = 2$ observables is that the four-quark operators induced by KK gluon exchange give the by far dominant (leading) contributions to the effective Hamiltonians describing $K-\bar{K}$ ($B_{d,s}-\bar{B}_{d,s}$ and $D-\bar{D}$) mixing. This implies that mixing phenomena mainly probe the extra-dimensional aspects of the strong interactions, but are to first approximation insensitive to the precise embedding of the electroweak gauge symmetry in the higher-dimensional geometry. A second important finding is that, in spite of the RS-GIM mechanism, a residual “little CP problem” in the $\Delta F = 2$ sector is found in all considered benchmark scenarios in the form of excessive contributions to ϵ_K arising from dimension-six operators involving quarks of different chiralities. Our detailed numerical analysis showed that fulfilling the latter constraint with only a moderate amount of tuning implies that the mass of the first-level KK gluon mode has to lie above 10 TeV in the parameter scenario S1, and even higher in scenario S4. An acceptable amount of indirect CP violation in the kaon sector can be achieved for masses of the first KK excitation below 5 TeV by allowing for larger down-type Yukawa couplings (S2), or by “alignment” in the right-handed down-type quark sector (S3). Yet both solutions have their limitations. In the first case loop contributions to dipole operators are parametrically enhanced, making it impossible to fully decouple flavor-violating effects, while the second scenario has potential problems with loop-induced misalignment and additional flavor violation from brane kinetic terms. Since the new CP-odd phases appearing in the $s \rightarrow d$, $b \rightarrow s$, and $c \rightarrow u$ transitions are highly uncorrelated, we found that even after enforcing the ϵ_K constraint it is possible to obtain CP-violating effects in $B_s-\bar{B}_s$ and $D-\bar{D}$ mixing that exceed by far the SM expectations. While both A_{SL}^s and $S_{\psi\phi}$ as well as A_{SL}^D and $S_{\psi K_s}^D$ turn out to be strongly correlated, we have stressed that the same linear correlations arise in a wide class of scenarios of new physics, so that they cannot be regarded as unmistakable signals of warped extra-dimension models.

Subsequently we have argued that, in contrast to the $\Delta F = 2$ sector, the predictions for $\Delta F = 1$ observables depend strongly on the exact realization of both the gauge and fermionic sectors, because they receive the dominant contributions from tree-level exchange of the Z^0 boson and its KK excitations. While these effects are enhanced by the logarithm of the warp factor L in models with $SU(2)_L \times U(1)_Y$ gauge symmetry, they are absent in the $Z^0 d_{iL} \bar{d}_{jL}$ couplings if the bulk gauge group is extended to $SU(2)_L \times SU(2)_R \times U(1)_X \times P_{LR}$ and an

appropriate embedding of the left-handed down-type quarks is chosen. If the right-handed down-type quarks are embedded into triplet representations, which is necessary to arrive at $U(1)_X$ invariant Yukawa couplings, then the $Z^0 d_{iR} \bar{d}_{jR}$ couplings are enhanced by one order of magnitude relative to the minimal RS model. Despite this enhancement, we found that right-handed currents in the $b \rightarrow d, s$ sector remain small in the custodial RS model, since the involved right-handed quark profiles are naturally more UV-localized than their left-handed counterparts. Larger effects are possible in the $s \rightarrow d$ sector, but this would require the bulk mass parameter of the right-handed top quark to be larger than about 1, which is rather far away from the critical value $-1/2$ required for IR localization. We concluded that, while the pattern of new-physics effects in processes such as $B_{d,s} \rightarrow \mu^+ \mu^-$, $B \rightarrow X_{d,s} \nu \bar{\nu}$, $K_L \rightarrow \mu^+ \mu^-$, $K \rightarrow \pi \nu \bar{\nu}$, and $K_L \rightarrow \pi^0 l^+ l^-$ is model dependent, order-of-magnitude enhancements of the branching fractions of rare B - and K -meson decays seem only possible in the minimal RS scenario, after satisfying the $Z^0 \rightarrow b \bar{b}$ constraint by tuning.

We have also extended earlier studies of $\Delta F = 1$ quark processes by examining observables which have not (or only partly) been considered in the literature. Our work covers $B \rightarrow \tau \nu_\tau$, $B \rightarrow X_s(K^*) l^+ l^-$, ϵ'_K/ϵ_K , and $\bar{B} \rightarrow \pi \bar{K}$ as well as other observables in the field of exclusive hadronic B -meson decays. The key question that we have addressed in the context of the decays $B \rightarrow \tau \nu_\tau$ and $\bar{B} \rightarrow \pi \bar{K}$ is whether possible discrepancies, as suggested by experiment, may be explained in scenarios with warped extra dimensions. We found that it is not possible to explain the tension in $B \rightarrow \tau \nu_\tau$, since the corrections to the $b \rightarrow ul\bar{\nu}$ transition that are consistent with $Z^0 \rightarrow b \bar{b}$ do not exceed the level of 1%. The new-physics effects in ΔA_{CP} usually also turn out to be too small to resolve the $\bar{B} \rightarrow \pi \bar{K}$ puzzle. From general considerations we have deduced that a notable improvement of the overall consistency between experiment and theory in exclusive hadronic B -meson decays would call for masses of the first KK excitations below 5 TeV, which in the minimal RS framework is problematic in view of the stringent $Z^0 \rightarrow b \bar{b}$ constraint. In the case of the CP-violating parameter ϵ'_K/ϵ_K , we have pointed out that the marked sensitivity of this ratio to the electroweak penguin sector leads to a strong correlation between ϵ'_K/ϵ_K and the $s \rightarrow d \nu \bar{\nu}$ and $s \rightarrow dl^+ l^-$ observables. We have explicitly shown that even if hadronic uncertainties are treated conservatively, the ϵ'_K/ϵ_K constraint has a non-negligible impact on possible new-physics effects in rare K decays. In particular, large enhancements in $K_L \rightarrow \pi^0 \nu \bar{\nu}$ decay have been shown to be disfavored by the measured amount of direct CP violation in $K \rightarrow \pi \pi$. As enhancements of the branching fractions for $K_L \rightarrow \pi^0 \nu \bar{\nu}$ and $K_L \rightarrow \pi^0 l^+ l^-$ are strongly correlated with each other, similar statements apply to the rare kaon decay modes with charged leptons in the final state. The correlation between $K^+ \rightarrow \pi^+ \nu \bar{\nu}$ and ϵ'_K/ϵ_K is weaker, and consequently departures from the SM expectation in the charged mode are possible even after enforcing the ϵ'_K/ϵ_K constraint.

The present work, which is a sequel to [10] and [36], concludes our detailed and rather comprehensive survey of quark flavor physics in the minimal RS model. We hope that it will provide a useful reference for many experimental analyses searching for new-physics signals at present and future flavor factories such as LHCb and a super flavor factory. Extensions of the minimal model with an enlarged electroweak gauge group in the bulk, and with a more complicated matter sector, will be explored in a future publication.

Acknowledgments

We are grateful to L. Gründer for collaboration at early stages of this work. It is also a pleasure to thank A. Azatov, C. Bobeth, J. Brod, F. Goertz, M. Gorbahn, S. Jäger, A. Lenz, T. Pfoh, M. Toharia, G. Zanderighi, L. Zhu, and J. Zupan for useful discussions and helpful correspondence. The research of SC is supported by the DFG cluster of excellence “Origin and Structure of the Universe”.

A RG Evolution of Penguin Coefficients

In this appendix we present analytic and numerical formulas relating the weak-scale Wilson coefficients $C_{3-10}(m_W)$ of the QCD and electroweak penguins with their initial conditions $C_{3-10}(M_{\text{KK}})$ evaluated at $M_{\text{KK}} \gg m_t$. If not stated otherwise, the results are obtained at leading-logarithmic order in QCD and take into account that in the RS model one has $C_4(M_{\text{KK}}) = -3C_5(M_{\text{KK}}) = C_6(M_{\text{KK}})$ and $C_8(M_{\text{KK}}) = C_{10}(M_{\text{KK}}) = 0$ at tree level. Analog formulas for $\tilde{C}_{3-10}(m_W)$ are not explicitly shown. Since QCD is chirality-blind they can simply be obtained by the replacing the original Wilson coefficients by the chirality-flipped coefficients in the expressions presented below.

For new-physics scales $M_{\text{KK}} \in [1, 10]$ TeV, we find to excellent approximation

$$\begin{aligned}
C_3(m_W) &= (0.416 \eta^2 - 0.962 \eta + 1.570) C_3(M_{\text{KK}}) - (0.002 \eta^2 - 0.242 \eta + 0.263) C_6(M_{\text{KK}}), \\
C_4(m_W) &= - (0.505 \eta^2 - 1.465 \eta + 1.017) C_3(M_{\text{KK}}) - (0.416 \eta^2 - 1.190 \eta - 0.189) C_6(M_{\text{KK}}), \\
C_5(m_W) &= - (0.034 \eta^2 - 0.036 \eta - 0.001) C_3(M_{\text{KK}}) + (0.192 \eta^2 - 0.592 \eta + 0.090) C_6(M_{\text{KK}}), \\
C_6(m_W) &= (0.002 \eta^2 + 0.093 \eta - 0.102) C_3(M_{\text{KK}}) + (1.376 \eta^2 - 3.005 \eta + 2.703) C_6(M_{\text{KK}}), \\
C_7(m_W) &= 0.987 \eta^{0.143} C_7(M_{\text{KK}}), \\
C_8(m_W) &= (0.371 \eta^{-1.143} - 0.329 \eta^{0.143}) C_7(M_{\text{KK}}), \\
C_9(m_W) &= (0.528 \eta^{-0.571} + 0.487 \eta^{0.286}) C_9(M_{\text{KK}}), \\
C_{10}(m_W) &= (-0.528 \eta^{-0.571} + 0.487 \eta^{0.286}) C_9(M_{\text{KK}}),
\end{aligned} \tag{A1}$$

where $\eta \equiv \alpha_s(M_{\text{KK}})/\alpha_s(m_t)$ is the relevant ratio of strong coupling constants. The numerically suppressed contributions $C_{7,9}(M_{\text{KK}})$ entering the QCD penguin coefficients $C_{3-6}(m_W)$ through mixing have been suppressed here for simplicity.

Inserting $\eta \approx 0.73$, which corresponds to $M_{\text{KK}} = 3$ TeV, into the above expressions and restoring the dependence on the coefficient $C_9(3 \text{ TeV})$ in the QCD penguins, we obtain numerically

$$\begin{aligned}
C_3(m_W) &= 1.09 C_3(3 \text{ TeV}) - 0.09 C_6(3 \text{ TeV}) - 0.01 C_9(3 \text{ TeV}), \\
C_4(m_W) &= -0.22 C_3(3 \text{ TeV}) + 0.84 C_6(3 \text{ TeV}) + 0.02 C_9(3 \text{ TeV}),
\end{aligned}$$

$$\begin{aligned}
C_5(m_W) &= 0.01 C_3(3 \text{ TeV}) - 0.24 C_6(3 \text{ TeV}) - 0.01 C_9(3 \text{ TeV}), \\
C_6(m_W) &= -0.03 C_3(3 \text{ TeV}) + 1.26 C_6(3 \text{ TeV}) + 0.03 C_9(3 \text{ TeV}), \\
C_7(m_W) &= 0.94 C_7(3 \text{ TeV}), \\
C_8(m_W) &= 0.21 C_7(3 \text{ TeV}), \\
C_9(m_W) &= 1.08 C_9(3 \text{ TeV}), \\
C_{10}(m_W) &= -0.18 C_9(3 \text{ TeV}).
\end{aligned} \tag{A2}$$

Contributions proportional to $C_7(3 \text{ TeV})$ in $C_{3-6}(m_W)$ receive coefficients smaller than 0.01 and have been discarded.

We also present numerical formulas for the Wilson coefficients $C_{3-10}(m_b)$ and $C_{3-10}(m_c)$ evaluated at the bottom- and charm-quark mass scale, respectively. Performing the evolution below m_W at next-to-leading logarithmic accuracy in QCD and QED [64, 65, 66, 67, 68], we arrive at

$$\begin{aligned}
C_3(m_b) &= 1.25 C_3(3 \text{ TeV}) - 0.17 C_6(3 \text{ TeV}) + 0.01 C_7(3 \text{ TeV}) - 0.03 C_9(3 \text{ TeV}), \\
C_4(m_b) &= -0.53 C_3(3 \text{ TeV}) + 0.62 C_6(3 \text{ TeV}) - 0.01 C_7(3 \text{ TeV}) + 0.06 C_9(3 \text{ TeV}), \\
C_5(m_b) &= 0.03 C_3(3 \text{ TeV}) - 0.06 C_6(3 \text{ TeV}) - 0.01 C_9(3 \text{ TeV}), \\
C_6(m_b) &= -0.08 C_3(3 \text{ TeV}) + 1.97 C_6(3 \text{ TeV}) - 0.01 C_7(3 \text{ TeV}) + 0.09 C_9(3 \text{ TeV}), \\
C_7(m_b) &= 0.88 C_7(3 \text{ TeV}) - 0.01 C_9(3 \text{ TeV}), \\
C_8(m_b) &= -0.01 C_6(3 \text{ TeV}) + 0.78 C_7(3 \text{ TeV}), \\
C_9(m_b) &= -0.01 C_7(3 \text{ TeV}) + 1.24 C_9(3 \text{ TeV}), \\
C_{10}(m_b) &= -0.48 C_9(3 \text{ TeV}),
\end{aligned} \tag{A3}$$

and

$$\begin{aligned}
C_3(m_c) &= 1.43 C_3(3 \text{ TeV}) - 0.17 C_6(3 \text{ TeV}) + 0.02 C_7(3 \text{ TeV}) - 0.07 C_9(3 \text{ TeV}), \\
C_4(m_c) &= -0.81 C_3(3 \text{ TeV}) + 0.41 C_6(3 \text{ TeV}) - 0.03 C_7(3 \text{ TeV}) + 0.12 C_9(3 \text{ TeV}), \\
C_5(m_c) &= 0.05 C_3(3 \text{ TeV}) + 0.19 C_6(3 \text{ TeV}) - 0.01 C_7(3 \text{ TeV}), \\
C_6(m_c) &= -0.12 C_3(3 \text{ TeV}) + 3.19 C_6(3 \text{ TeV}) - 0.06 C_7(3 \text{ TeV}) + 0.20 C_9(3 \text{ TeV}), \\
C_7(m_c) &= 0.90 C_7(3 \text{ TeV}) - 0.01 C_9(3 \text{ TeV}), \\
C_8(m_c) &= -0.03 C_6(3 \text{ TeV}) + 1.72 C_7(3 \text{ TeV}) - 0.01 C_9(3 \text{ TeV}), \\
C_9(m_c) &= 0.01 C_3(3 \text{ TeV}) - 0.02 C_7(3 \text{ TeV}) + 1.43 C_9(3 \text{ TeV}), \\
C_{10}(m_c) &= 0.01 C_6(3 \text{ TeV}) - 0.76 C_9(3 \text{ TeV}).
\end{aligned} \tag{A4}$$

The above relations imply that neglecting the running between M_{KK} and m_W would lead to results for $C_{6,8,10}(m_b)$ that are smaller than the correct ones by about 25% to 60%. In the

Parameter	Value \pm Error	Reference
G_F	$1.16637 \cdot 10^{-5} \text{ GeV}^{-2}$	[47]
s_w^2	0.2312	[192]
m_W	80.398 GeV	[192]
m_Z	91.1875 GeV	[192]
m_h	150 GeV	
$\alpha(m_Z)$	1/127.9	[192]
$\alpha_s(m_Z)$	0.118 ± 0.003	[47]
m_t	$(144 \pm 5) \text{ GeV}$	[70]
m_b	$(2.3 \pm 0.1) \text{ GeV}$	[47]
m_c	$(560 \pm 40) \text{ MeV}$	[47]
m_s	$(50 \pm 15) \text{ MeV}$	[47]
m_d	$(3.0 \pm 2.0) \text{ MeV}$	[47]
m_u	$(1.5 \pm 1.0) \text{ MeV}$	[47]
λ	0.2265 ± 0.0008	[52]
A	0.807 ± 0.018	[52]
$\bar{\rho}$	$0.147^{+0.029}_{-0.017}$	[52]
$\bar{\eta}$	0.343 ± 0.016	[52]

Table B1: Parameters used in the SM predictions and the generation of RS parameter points. The quoted values of the quark masses correspond to $\overline{\text{MS}}$ masses evaluated at a scale of 1 TeV.

case of $C_{6,8,10}(m_c)$ the associated reductions range between 30% and 45%. For the remaining Wilson coefficients the effects are less pronounced. We conclude that the inclusion of the RG evolution between the KK scale and the weak scale is important in order to obtain accurate results.

B Input Parameters

Here we collect the values of the experimental and theoretical parameters used in our numerical analysis. They are thematically ordered in Tables B1 to B7. In the case of the exclusive hadronic B -meson decay observables, parameters related to $\eta^{(\prime)}$ mesons, such as their decay constants, form factors, and the η - η' mixing angles in the quark-flavor basis have not been spelled out. They can be found in [83, 84].

Our predictions for the $B \rightarrow K^* l^+ l^-$ observables depend on the $B \rightarrow K^*$ matrix elements, which can be parametrized in terms of seven q^2 -dependent QCD form factors V , $A_{0,1,2}$, and

Parameter	Value \pm Error	Reference
m_K	497.6 MeV	[47]
f_K	156.1 MeV	[47]
B_1^{sd}	0.54 ± 0.05	[46]
B_2^{sd}	0.7 ± 0.2	[46]
B_3^{sd}	1.0 ± 0.4	[46]
B_4^{sd}	0.9 ± 0.2	[46]
B_5^{sd}	0.6 ± 0.1	[46]
$(m_s + m_d)$	(135 ± 18) MeV	[46]
ϕ_ϵ	$(43.51 \pm 0.05)^\circ$	[47]
κ_ϵ	0.92 ± 0.02	[48]
$(\Delta m_K)_{\text{exp}}$	$3.4833 \cdot 10^{-15}$ GeV	[47]
$m_t(m_t)$	(163.8 ± 1.3) GeV	[70]
$m_c(m_c)$	$(1.27^{+0.07}_{-0.11})$ GeV	[47]
η_{tt}	0.57 ± 0.01	[159]
η_{cc}	1.50 ± 0.37	[160]
η_{ct}	0.47 ± 0.05	[193, 194]

Table B2: Parameters used in the $K-\bar{K}$ mixing observables. The given values for the B_i^{sd} parameters and the sum $(m_s + m_d)$ correspond to the RI-MOM scheme taken at the scale 2 GeV.

$T_{1,2,3}$ as

$$\begin{aligned}
\langle K^*(p_B - q) | \bar{s} \gamma_\mu (1 - \gamma_5) b | B(p_B) \rangle &= -2 \epsilon_{\mu\nu\alpha\beta} \epsilon^{*\nu} p_B^\alpha q^\beta \frac{V}{m_B + m_{K^*}} - i \epsilon_\mu^* (m_B + m_{K^*}) A_1 \\
&+ i (2p_B - q)_\mu (\epsilon^* \cdot q) \frac{A_2}{m_B + m_{K^*}} + i q_\mu (\epsilon^* \cdot q) \frac{2m_{K^*}}{q^2} [A_3 - A_0],
\end{aligned} \tag{B1}$$

$$\begin{aligned}
\langle K^*(p_B - q) | \bar{s} \sigma_{\mu\nu} q^\nu (1 + \gamma_5) b | B(p_B) \rangle &= -2i \epsilon_{\mu\nu\alpha\beta} \epsilon^{*\nu} p_B^\alpha q^\beta T_1 \\
&+ [\epsilon_\mu^* (m_B^2 - m_{K^*}^2) - (\epsilon^* \cdot q)(2p_B - q)_\mu] T_2 + (\epsilon^* \cdot q) \left[q_\mu - \frac{q^2}{m_B^2 - m_{K^*}^2} (2p_B - q)_\mu \right] T_3,
\end{aligned}$$

where

$$A_3 \equiv \frac{m_B + m_{K^*}}{2m_{K^*}} A_1 - \frac{m_B - m_{K^*}}{2m_{K^*}} A_2. \tag{B2}$$

Here $\epsilon^{*\mu}$ denotes the polarization vector of the K^* and p_B^μ the four momentum of the B meson.

In the large recoil limit, the QCD form factors obey symmetry relations and can be expressed at leading order in the $1/E$ expansion in terms of two universal form factors $\xi_{\perp,||}$

Parameter	Value \pm Error	Reference
m_{B_d}	5.2795 GeV	[47]
f_{B_d}	(200 ± 20) MeV	[46]
B_1^{bd}	0.81 ± 0.08	[46]
B_2^{bd}	0.84 ± 0.10	[46]
B_3^{bd}	0.89 ± 0.13	[46]
B_4^{bd}	1.14 ± 0.13	[46]
B_5^{bd}	1.72 ± 0.19	[46]
$(m_b + m_d)$	(4.22 ± 0.08) GeV	[46]
η_B	0.55 ± 0.01	[159]
$\sin 2\beta$	0.672 ± 0.023	[94]
$(\Delta m_d / \Gamma_d)_{\text{exp}}$	0.78 ± 0.01	[94]
$\text{Re}(\Gamma_{12}^d / M_{12}^d)$	$(-5.26_{-1.28}^{+1.15}) \cdot 10^{-3}$	[55]
$\text{Im}(\Gamma_{12}^d / M_{12}^d)$	$(-4.8_{-1.2}^{+1.0}) \cdot 10^{-4}$	[55]
m_{B_s}	5.3661 GeV	[47]
f_{B_s}	(245 ± 25) MeV	[46]
B_1^{bs}	0.80 ± 0.08	[46]
B_2^{bs}	0.85 ± 0.10	[46]
B_3^{bs}	0.90 ± 0.13	[46]
B_4^{bs}	1.15 ± 0.13	[46]
B_5^{bs}	1.74 ± 0.19	[46]
$(m_b + m_s)$	(4.30 ± 0.08) GeV	[46]
$\sin 2\beta_s$	$(-0.0368_{-0.0017}^{+0.0018})$	[52]
$(\Delta m_s / \Gamma_s)_{\text{exp}}$	26.3 ± 0.6	[94]
$\text{Re}(\Gamma_{12}^s / M_{12}^s)$	$(-4.97 \pm 0.94) \cdot 10^{-3}$	[55]
$\text{Im}(\Gamma_{12}^s / M_{12}^s)$	$(2.06 \pm 0.57) \cdot 10^{-5}$	[55]

Table B3: Parameters used in the $B_{d,s}-\bar{B}_{d,s}$ mixing observables. The given values for the B_i^{bd} and B_i^{bs} parameters and the sums $(m_b + m_{d,s})$ are $\overline{\text{MS}}$ quantities normalized at the scale 4.2 GeV.

[196]. Symmetry-breaking corrections at order α_s have been calculated using QCD factorization [197] and are included in our numerical analysis. Within the QCD factorization approach, we employ a factorization scheme where the universal form factors $\xi_{\perp,\parallel}$ are related to V and $A_{1,2}$ via [138]

$$\xi_{\perp} = \frac{m_B}{m_B + m_{K^*}} V, \quad \xi_{\parallel} = \frac{m_B + m_{K^*}}{2E} A_1 - \frac{m_B - m_{K^*}}{m_B} A_2. \quad (\text{B3})$$

Parameter	Value \pm Error	Reference
m_D	1.8645 MeV	[47]
f_D	(212 ± 14) MeV	[46]
B_1^{cu}	0.85 ± 0.09	[46]
B_2^{cu}	0.82 ± 0.09	[46]
B_3^{cu}	1.07 ± 0.12	[46]
B_4^{cu}	1.10 ± 0.11	[46]
B_5^{cu}	1.37 ± 0.14	[46]
$(m_c + m_u)$	(1.17 ± 0.12) GeV	[47, 195]
x_D	$0.0098^{+0.0024}_{-0.0026}$	[94, 169]
y_D	0.0083 ± 0.0016	[94, 169]
$(x_D^2 + y_D^2)/2$	$\leq (1.3 \pm 2.7) \cdot 10^{-4}$	[94, 169]
$ q/p _D$	$0.87^{+0.17}_{-0.15}$	[94, 169]
τ_D	(0.4101 ± 0.0015) ps	[94]

Table B4: Parameters used in the $D-\bar{D}$ mixing observables. The quoted values for the B_i^{cu} parameters and the sum of masses ($m_c + m_u$) is obtained in the RI-MOM scheme at the scale 2.8 GeV.

Here E denotes the energy of the emitted K^* in the B -meson rest frame.

In order to describe the q^2 -dependence of the universal form factors $\xi_{\perp,\parallel}$, we follow the light-cone sum rule calculation [198], which utilizes the parametrizations

$$\begin{aligned}
V(q^2) &= \frac{r_1}{1 - q^2/m_R^2} + \frac{r_2}{1 - q^2/m_{\text{fit}}^2}, \\
A_1(q^2) &= \frac{r_2}{1 - q^2/m_{\text{fit}}^2}, \\
A_2(q^2) &= \frac{r_1}{1 - q^2/m_{\text{fit}}^2} + \frac{r_2}{(1 - q^2/m_{\text{fit}}^2)^2}.
\end{aligned} \tag{B4}$$

In Table B7 we collect the values of the fit parameters $r_{1,2}$, m_R^2 , and m_{fit}^2 for V and $A_{1,2}$ derived in [198]. The central values and errors of the Gegenbauer moments $a_{1,K^*}^{\perp,\parallel}$ and $a_{2,K^*}^{\perp,\parallel}$ are also taken from the latter reference. The relative uncertainty of the form factors V , A_1 , and A_2 at zero-momentum transfer amounts to 11%, 12%, and 14%, adding individual sources of uncertainty in quadrature. In our numerical analysis we use the total relative uncertainty at maximal recoil to estimate the form-factor uncertainties for $q^2 > 0$. The quoted errors translate into uncertainties of 11% and 14% for ξ_{\perp} and ξ_{\parallel} , respectively.

The q^2 -dependent form factors f , g , a_+ , g_{\pm} , and h relevant for $B \rightarrow K^* l^+ l^-$ decay in the

Parameter	Value \pm Error	Reference
$B_6^{(1/2)}$	[0.8, 2.0]	[71]
$B_8^{(3/2)}$	[0.8, 1.2]	[71]
$m_s(m_c)$	(115 ± 20) MeV	[47]
$m_d(m_c)$	(6 ± 2) MeV	[47]
$ V_{cb} $	0.041 ± 0.002	[84]
$ V_{ub}/V_{cb} $	0.08 ± 0.02	[84]
γ	$(70 \pm 20)^\circ$	[84]
τ_{B_u}	1.67 ps	[84]
τ_{B_d}	1.54 ps	[84]
f_π/f_K	0.82	[84]
f_ϕ	221 MeV	[84]
f_ϕ^\perp	(175 ± 25) MeV	[84]
$F_0^{B \rightarrow \pi}(0)$	0.25 ± 0.05	[84]
$F_0^{B \rightarrow K}(0)$	0.31 ± 0.05	[84]
m_s	(80 ± 20) MeV	[84]
λ_B	(200 ± 150) MeV	[84]
α_2^π	0.3 ± 0.3	[84]
$\alpha_1^{\bar{K}}$	0.2 ± 0.2	[84]
$\alpha_2^{\bar{K}}$	0.1 ± 0.3	[84]
$\alpha_2^\phi, \alpha_{2,\perp}^\phi$	0 ± 0.3	[84]
ρ_A	1	[84]
φ_A^{PP}	-55°	[84]
φ_A^{PV}	-20°	[84]

Table B5: Parameters used to predict the ratio ϵ'_K/ϵ_K and the various non-leptonic B -meson decays. All scale-dependent quantities refer to 2 GeV unless indicated otherwise. See text for details.

Parameter	Value \pm Error	Reference
κ_L	$(2.353 \pm 0.014) \cdot 10^{-10}$	[96]
κ_+	$(0.5455 \pm 0.0026) \cdot 10^{-10}$	[96]
Δ_{EM}	-0.003	[96]
X_t	1.464 ± 0.041	[97, 98]
$P_{c,u}$	0.43 ± 0.04	[99, 100, 101, 102]
y_c	(-0.20 ± 0.03)	[104]
$y_{\gamma\gamma}$	0.4 ± 0.5	[105]
y_A	(-0.68 ± 0.03)	[107]
$ a_S $	1.20 ± 0.20	[108, 109]
y_V	0.73 ± 0.04	[107]
$\mathcal{B}(B \rightarrow X_c l \bar{\nu})_{\text{exp}}$	0.1064 ± 0.0011	[94]
C	$0.546^{+0.023}_{-0.033}$	[114]
τ_{B_d}	$(1.525 \pm 0.009) \text{ ps}$	[94]
τ_{B_s}	$(1.472^{+0.024}_{-0.026}) \text{ ps}$	[94]
c_A	0.96 ± 0.02	[97, 98]
m_μ	105.66 MeV	[47]
m_τ	1.777 GeV	[47]

Table B6: Parameters entering the predictions for the rare K - and B -meson decays.

	r_1	r_2	$m_R^2 [\text{GeV}^2]$	$m_{\text{fit}}^2 [\text{GeV}^2]$
V	0.923	-0.511	28.30	49.40
A_1	-	0.290	-	40.38
A_2	-0.084	0.342	-	52.00
T_1	0.823	-0.491	28.30	46.31
T_2	-	0.333	-	41.41
\tilde{T}_3	-0.036	0.368	-	48.10

Table B7: Parameters describing the q^2 -dependence of the form factors V , $A_{1,2}$, $T_{1,2}$, and \tilde{T}_3 . All results are taken from [198]. See text for details.

low-recoil limit depend on V , $A_{1,2}$, and $T_{1,2,3}$ via [143]

$$\begin{aligned}
 f &= (m_B + m_{K^*}) A_1, & g &= -\frac{V}{m_B + m_{K^*}}, & a_+ &= -\frac{A_2}{m_B + m_{K^*}}, \\
 g_+ &= T_1, & g_- &= \frac{m_B^2 - m_{K^*}^2}{q^2} (T_2 - T_1), & h &= \frac{T_1 - T_2}{q^2} - \frac{T_3}{m_B^2 - m_{K^*}^2},
 \end{aligned}
 \tag{B5}$$

with

$$T_3 \equiv \frac{m_B^2 - m_{K^*}^2}{q^2} (\tilde{T}_3 - T_2).
 \tag{B6}$$

The q^2 -dependence of the form factors $T_{1,2}$ and \tilde{T}_3 is modeled by [198]

$$\begin{aligned}
 T_1(q^2) &= \frac{r_1}{1 - q^2/m_R^2} + \frac{r_2}{1 - q^2/m_{\text{fit}}^2}, \\
 T_2(q^2) &= \frac{r_2}{1 - q^2/m_{\text{fit}}^2}, \\
 \tilde{T}_3(q^2) &= \frac{r_1}{1 - q^2/m_{\text{fit}}^2} + \frac{r_2}{(1 - q^2/m_{\text{fit}}^2)^2},
 \end{aligned}
 \tag{B7}$$

and the corresponding fit parameters $r_{1,2}$, m_R^2 , and m_{fit}^2 can be found in Table B7. The QCD form factors f , g , a_+ , g_{\pm} , and h all have an uncertainty at the level of 10%.

References

- [1] L. Randall and R. Sundrum, Phys. Rev. Lett. **83**, 3370 (1999) [arXiv:hep-ph/9905221].
- [2] H. Davoudiasl, J. L. Hewett and T. G. Rizzo, Phys. Lett. B **473**, 43 (2000) [arXiv:hep-ph/9911262].
- [3] A. Pomarol, Phys. Lett. B **486**, 153 (2000) [arXiv:hep-ph/9911294].
- [4] Y. Grossman and M. Neubert, Phys. Lett. B **474**, 361 (2000) [arXiv:hep-ph/9912408].
- [5] S. Chang, J. Hisano, H. Nakano, N. Okada and M. Yamaguchi, Phys. Rev. D **62**, 084025 (2000) [arXiv:hep-ph/9912498].
- [6] T. Gherghetta and A. Pomarol, Nucl. Phys. B **586**, 141 (2000) [arXiv:hep-ph/0003129].
- [7] N. Arkani-Hamed and M. Schmaltz, Phys. Rev. D **61**, 033005 (2000) [arXiv:hep-ph/9903417].
- [8] S. J. Huber and Q. Shafi, Phys. Lett. B **498**, 256 (2001) [arXiv:hep-ph/0010195].
- [9] S. J. Huber, Nucl. Phys. B **666**, 269 (2003) [arXiv:hep-ph/0303183].

- [10] S. Casagrande, F. Goertz, U. Haisch, M. Neubert and T. Pfoh, *JHEP* **0810**, 094 (2008) [arXiv:0807.4937 [hep-ph]].
- [11] M. Blanke, A. J. Buras, B. Duling, S. Gori and A. Weiler, *JHEP* **0903**, 001 (2009) [arXiv:0809.1073 [hep-ph]].
- [12] C. D. Froggatt and H. B. Nielsen, *Nucl. Phys. B* **147**, 277 (1979).
- [13] K. Agashe, G. Perez and A. Soni, *Phys. Rev. Lett.* **93**, 201804 (2004) [arXiv:hep-ph/0406101].
- [14] K. Agashe, G. Perez and A. Soni, *Phys. Rev. D* **71**, 016002 (2005) [arXiv:hep-ph/0408134].
- [15] G. Burdman, *Phys. Rev. D* **66**, 076003 (2002) [arXiv:hep-ph/0205329].
- [16] G. Burdman, *Phys. Lett. B* **590**, 86 (2004) [arXiv:hep-ph/0310144].
- [17] K. Agashe, G. Perez and A. Soni, *Phys. Rev. D* **75**, 015002 (2007) [arXiv:hep-ph/0606293].
- [18] C. Csaki, A. Falkowski and A. Weiler, *JHEP* **0809**, 008 (2008) [arXiv:0804.1954 [hep-ph]].
- [19] M. Blanke, A. J. Buras, B. Duling, K. Gemmler and S. Gori, *JHEP* **0903**, 108 (2009) [arXiv:0812.3803 [hep-ph]].
- [20] S. Chang, C. S. Kim and J. Song, *Phys. Rev. D* **77**, 075001 (2008) [arXiv:0712.0207 [hep-ph]].
- [21] K. Agashe, A. Azatov and L. Zhu, *Phys. Rev. D* **79**, 056006 (2009) [arXiv:0810.1016 [hep-ph]].
- [22] A. Azatov, M. Toharia and L. Zhu, *Phys. Rev. D* **80**, 035016 (2009) [arXiv:0906.1990 [hep-ph]].
- [23] A. Azatov, M. Toharia and L. Zhu, *Phys. Rev. D* **80**, 031701 (2009) [arXiv:0812.2489 [hep-ph]].
- [24] H. Davoudiasl and E. Ponton, *Phys. Lett. B* **680**, 247 (2009) [arXiv:0903.3410 [hep-ph]].
- [25] O. Gedalia, G. Isidori and G. Perez, *Phys. Lett. B* **682**, 200 (2009) [arXiv:0905.3264 [hep-ph]].
- [26] A. J. Buras, P. Gambino, M. Gorbahn, S. Jäger and L. Silvestrini, *Phys. Lett. B* **500**, 161 (2001) [arXiv:hep-ph/0007085].
- [27] G. D'Ambrosio, G. F. Giudice, G. Isidori and A. Strumia, *Nucl. Phys. B* **645**, 155 (2002) [arXiv:hep-ph/0207036].
- [28] G. Cacciapaglia, C. Csaki, J. Galloway, G. Marandella, J. Terning and A. Weiler, *JHEP* **0804**, 006 (2008) [arXiv:0709.1714 [hep-ph]].

- [29] A. L. Fitzpatrick, L. Randall and G. Perez, Phys. Rev. Lett. **100**, 171604 (2008) [arXiv:0710.1869 [hep-ph]].
- [30] J. Santiago, JHEP **0812**, 046 (2008) [arXiv:0806.1230 [hep-ph]].
- [31] C. Csaki, A. Falkowski and A. Weiler, Phys. Rev. D **80**, 016001 (2009) [arXiv:0806.3757 [hep-ph]].
- [32] C. Csaki and D. Curtin, Phys. Rev. D **80**, 015027 (2009) [arXiv:0904.2137 [hep-ph]].
- [33] C. Csaki, G. Perez, Z. Surujon and A. Weiler, arXiv:0907.0474 [hep-ph].
- [34] C. Cheung, A. L. Fitzpatrick and L. Randall, JHEP **0801**, 069 (2008) [arXiv:0711.4421 [hep-th]].
- [35] F. Goertz and T. Pfoh, JHEP **0810**, 035 (2008) [arXiv:0809.1378 [hep-ph]].
- [36] M. Bauer, S. Casagrande, L. Gr nder, U. Haisch and M. Neubert, Phys. Rev. D **79**, 076001 (2009) arXiv:0811.3678 [hep-ph].
- [37] S. Casagrande, F. Goertz, U. Haisch, M. Neubert and T. Pfoh, in preparation.
- [38] K. Agashe and R. Contino, Phys. Rev. D **80**, 075016 (2009) [arXiv:0906.1542 [hep-ph]].
- [39] K. Agashe, A. Delgado, M. J. May and R. Sundrum, JHEP **0308**, 050 (2003) [arXiv:hep-ph/0308036].
- [40] S. Davidson, G. Isidori and S. Uhlig, Phys. Lett. B **663**, 73 (2008) [arXiv:0711.3376 [hep-ph]].
- [41] M. Bona *et al.* [UT_{fit} Collaboration], JHEP **0803**, 049 (2008) [arXiv:0707.0636 [hep-ph]].
- [42] J. A. Bagger, K. T. Matchev and R. J. Zhang, Phys. Lett. B **412**, 77 (1997) [arXiv:hep-ph/9707225].
- [43] M. Ciuchini *et al.*, JHEP **9810**, 008 (1998) [arXiv:hep-ph/9808328].
- [44] A. J. Buras, M. Misiak and J. Urban, Nucl. Phys. B **586**, 397 (2000) [arXiv:hep-ph/0005183].
- [45] D. Becirevic *et al.*, Nucl. Phys. B **634**, 105 (2002) [arXiv:hep-ph/0112303].
- [46] V. Lubicz and C. Tarantino, Nuovo Cim. **123B**, 674 (2008) [arXiv:0807.4605 [hep-lat]].
- [47] C. Amsler *et al.* [Particle Data Group], Phys. Lett. B **667**, 1 (2008).
- [48] A. J. Buras and D. Guadagnoli, Phys. Rev. D **78**, 033005 (2008) [arXiv:0805.3887 [hep-ph]].
- [49] K. Anikeev *et al.*, arXiv:hep-ph/0201071.

- [50] E. A. Andriyash, G. G. Ovanesyan and M. I. Vysotsky, Phys. Lett. B **599**, 253 (2004) [arXiv:hep-ph/0310314].
- [51] E. A. Andriyash, G. G. Ovanesyan and M. I. Vysotsky, Phys. Atom. Nucl. **69**, 286 (2006) [arXiv:hep-ph/0502111].
- [52] J. Charles *et al.* [CKMfitter Group], Eur. Phys. J. C **41**, 1 (2005) [arXiv:hep-ph/0406184] and updated results available at: <http://ckmfitter.in2p3.fr/>
- [53] M. Bona *et al.* [UT_{fit} Collaboration], JHEP **0603**, 080 (2006) [arXiv:hep-ph/0509219].
- [54] M. Blanke, A. J. Buras, D. Guadagnoli and C. Tarantino, JHEP **0610**, 003 (2006) [arXiv:hep-ph/0604057].
- [55] A. Lenz and U. Nierste, JHEP **0706**, 072 (2007) [arXiv:hep-ph/0612167].
- [56] B. Aubert *et al.* [BaBar Collaboration], Phys. Rev. Lett. **98**, 211802 (2007) [arXiv:hep-ex/0703020].
- [57] M. Staric *et al.* [Belle Collaboration], Phys. Rev. Lett. **98**, 211803 (2007) [arXiv:hep-ex/0703036].
- [58] K. Abe *et al.* [Belle Collaboration], Phys. Rev. Lett. **99**, 131803 (2007) [arXiv:0704.1000 [hep-ex]].
- [59] T. Aaltonen *et al.* [CDF Collaboration], Phys. Rev. Lett. **100**, 121802 (2008) [arXiv:0712.1567 [hep-ex]].
- [60] Y. Grossman, Y. Nir and G. Perez, Phys. Rev. Lett. **103**, 071602 (2009) [arXiv:0904.0305 [hep-ph]].
- [61] I. I. Bigi, M. Blanke, A. J. Buras and S. Recksiegel, JHEP **0907**, 097 (2009) [arXiv:0904.1545 [hep-ph]].
- [62] A. J. Buras, M. Jamin and M. E. Lautenbacher, Nucl. Phys. B **408**, 209 (1993) [arXiv:hep-ph/9303284].
- [63] S. Bosch, A. J. Buras, M. Gorbahn, S. Jäger, M. Jamin, M. E. Lautenbacher and L. Silvestrini, Nucl. Phys. B **565**, 3 (2000) [arXiv:hep-ph/9904408].
- [64] A. J. Buras, M. Jamin, M. E. Lautenbacher and P. H. Weisz, Nucl. Phys. B **370**, 69 (1992) [Addendum-ibid. B **375**, 501 (1992)].
- [65] A. J. Buras, M. Jamin, M. E. Lautenbacher and P. H. Weisz, Nucl. Phys. B **400**, 37 (1993) [arXiv:hep-ph/9211304].
- [66] A. J. Buras, M. Jamin and M. E. Lautenbacher, Nucl. Phys. B **400**, 75 (1993) [arXiv:hep-ph/9211321].

- [67] M. Ciuchini, E. Franco, G. Martinelli and L. Reina, Phys. Lett. B **301**, 263 (1993) [arXiv:hep-ph/9212203].
- [68] M. Ciuchini, E. Franco, G. Martinelli and L. Reina, Nucl. Phys. B **415**, 403 (1994) [arXiv:hep-ph/9304257].
- [69] P. Gambino and U. Haisch, JHEP **0009**, 001 (2000) [arXiv:hep-ph/0007259].
- [70] The Tevatron Electroweak Working Group, arXiv:0803.1683 [hep-ex].
- [71] A. J. Buras and M. Jamin, JHEP **0401**, 048 (2004) [arXiv:hep-ph/0306217].
- [72] J. Bijnens and J. Prades, Nucl. Phys. Proc. Suppl. **96**, 354 (2001) [arXiv:hep-ph/0010008].
- [73] M. Knecht, S. Peris and E. de Rafael, Phys. Lett. B **508**, 117 (2001) [arXiv:hep-ph/0102017].
- [74] J. Bijnens, E. Gamiz and J. Prades, JHEP **0110**, 009 (2001) [arXiv:hep-ph/0108240].
- [75] T. Hambye, S. Peris and E. de Rafael, JHEP **0305**, 027 (2003) [arXiv:hep-ph/0305104].
- [76] T. Blum *et al.* [RBC Collaboration], Phys. Rev. D **68**, 114506 (2003) [arXiv:hep-lat/0110075].
- [77] P. Boucaud, V. Gimenez, C. J. D. Lin, V. Lubicz, G. Martinelli, M. Papinutto and C. T. Sachrajda, Nucl. Phys. B **721**, 175 (2005) [arXiv:hep-lat/0412029].
- [78] T. Bhattacharya *et al.*, Nucl. Phys. Proc. Suppl. **106**, 311 (2002) [arXiv:hep-lat/0111004].
- [79] T. Bhattacharya, G. T. Fleming, R. Gupta, G. Kilcup, W. Lee and S. R. Sharpe, Nucl. Phys. Proc. Suppl. **140**, 369 (2005) [arXiv:hep-lat/0409046].
- [80] M. Beneke, G. Buchalla, M. Neubert and C. T. Sachrajda, Phys. Rev. Lett. **83**, 1914 (1999) [arXiv:hep-ph/9905312].
- [81] M. Beneke, G. Buchalla, M. Neubert and C. T. Sachrajda, Nucl. Phys. B **591**, 313 (2000) [arXiv:hep-ph/0006124].
- [82] M. Beneke, G. Buchalla, M. Neubert and C. T. Sachrajda, Nucl. Phys. B **606**, 245 (2001) [arXiv:hep-ph/0104110].
- [83] M. Beneke and M. Neubert, Nucl. Phys. B **651**, 225 (2003) [arXiv:hep-ph/0210085].
- [84] M. Beneke and M. Neubert, Nucl. Phys. B **675**, 333 (2003) [arXiv:hep-ph/0308039].
- [85] Y. Y. Keum, H. n. Li and A. I. Sanda, Phys. Lett. B **504**, 6 (2001) [arXiv:hep-ph/0004004].
- [86] Y. Y. Keum, H. N. Li and A. I. Sanda, Phys. Rev. D **63**, 054008 (2001) [arXiv:hep-ph/0004173].

- [87] M. Gronau, O. F. Hernandez, D. London and J. L. Rosner, Phys. Rev. D **50**, 4529 (1994) [arXiv:hep-ph/9404283].
- [88] M. Gronau, O. F. Hernandez, D. London and J. L. Rosner, Phys. Rev. D **52**, 6374 (1995) [arXiv:hep-ph/9504327].
- [89] C. W. Bauer, D. Pirjol, I. Z. Rothstein and I. W. Stewart, Phys. Rev. D **70**, 054015 (2004) [arXiv:hep-ph/0401188].
- [90] C. W. Bauer, I. Z. Rothstein and I. W. Stewart, Phys. Rev. D **74**, 034010 (2006) [arXiv:hep-ph/0510241].
- [91] M. Beneke, G. Buchalla, M. Neubert and C. T. Sachrajda, Phys. Rev. D **72**, 098501 (2005) [arXiv:hep-ph/0411171].
- [92] M. Neubert and J. L. Rosner, Phys. Lett. B **441**, 403 (1998) [arXiv:hep-ph/9808493].
- [93] Y. Grossman, M. Neubert and A. L. Kagan, JHEP **9910**, 029 (1999) [arXiv:hep-ph/9909297].
- [94] E. Barberio *et al.* [Heavy Flavor Averaging Group], arXiv:0808.1297 [hep-ex] and updated results available at: <http://www.slac.stanford.edu/xorg/hfag>
- [95] M. Beneke, Phys. Lett. B **620**, 143 (2005) [arXiv:hep-ph/0505075].
- [96] F. Mescia and C. Smith, Phys. Rev. D **76**, 034017 (2007) [arXiv:0705.2025 [hep-ph]].
- [97] M. Misiak and J. Urban, Phys. Lett. B **451**, 161 (1999) [arXiv:hep-ph/9901278].
- [98] G. Buchalla and A. J. Buras, Nucl. Phys. B **548**, 309 (1999) [arXiv:hep-ph/9901288].
- [99] G. Isidori, F. Mescia and C. Smith, Nucl. Phys. B **718**, 319 (2005) [arXiv:hep-ph/0503107].
- [100] A. J. Buras, M. Gorbahn, U. Haisch and U. Nierste, Phys. Rev. Lett. **95**, 261805 (2005) [arXiv:hep-ph/0508165].
- [101] A. J. Buras, M. Gorbahn, U. Haisch and U. Nierste, JHEP **0611**, 002 (2006) [arXiv:hep-ph/0603079].
- [102] J. Brod and M. Gorbahn, Phys. Rev. D **78**, 034006 (2008) [arXiv:0805.4119 [hep-ph]].
- [103] F. Mescia, C. Smith and S. Trine, JHEP **0608**, 088 (2006) [arXiv:hep-ph/0606081].
- [104] M. Gorbahn and U. Haisch, Phys. Rev. Lett. **97**, 122002 (2006) [arXiv:hep-ph/0605203].
- [105] G. Isidori and R. Unterdorfer, JHEP **0401**, 009 (2004) [arXiv:hep-ph/0311084].
- [106] J. M. Gerard, C. Smith and S. Trine, Nucl. Phys. B **730**, 1 (2005) [arXiv:hep-ph/0508189].

- [107] A. J. Buras, M. E. Lautenbacher, M. Misiak and M. Münz, Nucl. Phys. B **423**, 349 (1994) [arXiv:hep-ph/9402347].
- [108] J. R. Batley *et al.* [NA48/1 Collaboration], Phys. Lett. B **576**, 43 (2003) [arXiv:hep-ex/0309075].
- [109] J. R. Batley *et al.* [NA48/1 Collaboration], Phys. Lett. B **599**, 197 (2004) [arXiv:hep-ex/0409011].
- [110] G. Buchalla, G. D'Ambrosio and G. Isidori, Nucl. Phys. B **672**, 387 (2003) [arXiv:hep-ph/0308008].
- [111] S. Friot, D. Greynat and E. De Rafael, Phys. Lett. B **595**, 301 (2004) [arXiv:hep-ph/0404136].
- [112] U. Haisch and A. Weiler, Phys. Rev. D **76**, 074027 (2007) [arXiv:0706.2054 [hep-ph]].
- [113] P. Gambino and M. Misiak, Nucl. Phys. B **611**, 338 (2001) [arXiv:hep-ph/0104034].
- [114] P. Gambino and P. Giordano, Phys. Lett. B **669**, 69 (2008) [arXiv:0805.0271 [hep-ph]].
- [115] A. J. Buras, Phys. Lett. B **566**, 115 (2003) [arXiv:hep-ph/0303060].
- [116] C. Bobeth, M. Misiak and J. Urban, Nucl. Phys. B **574**, 291 (2000) [arXiv:hep-ph/9910220].
- [117] H. H. Asatrian, H. M. Asatrian, C. Greub and M. Walker, Phys. Lett. B **507**, 162 (2001) [arXiv:hep-ph/0103087].
- [118] H. H. Asatryan, H. M. Asatrian, C. Greub and M. Walker, Phys. Rev. D **65**, 074004 (2002) [arXiv:hep-ph/0109140].
- [119] P. Gambino, M. Gorbahn and U. Haisch, Nucl. Phys. B **673**, 238 (2003) [arXiv:hep-ph/0306079].
- [120] C. Bobeth, P. Gambino, M. Gorbahn and U. Haisch, JHEP **0404**, 071 (2004) [arXiv:hep-ph/0312090].
- [121] M. Gorbahn and U. Haisch, Nucl. Phys. B **713**, 291 (2005) [arXiv:hep-ph/0411071].
- [122] T. Huber, E. Lunghi, M. Misiak and D. Wyler, Nucl. Phys. B **740**, 105 (2006) [arXiv:hep-ph/0512066].
- [123] H. H. Asatryan, H. M. Asatrian, C. Greub and M. Walker, Phys. Rev. D **66**, 034009 (2002) [arXiv:hep-ph/0204341].
- [124] K. S. M. Lee and I. W. Stewart, Phys. Rev. D **74**, 014005 (2006) [arXiv:hep-ph/0511334].
- [125] K. S. M. Lee, Z. Ligeti, I. W. Stewart and F. J. Tackmann, Phys. Rev. D **74**, 011501 (2006) [arXiv:hep-ph/0512191].

- [126] K. S. M. Lee and F. J. Tackmann, Phys. Rev. D **79**, 114021 (2009) [arXiv:0812.0001 [hep-ph]].
- [127] S. J. Lee, M. Neubert and G. Paz, Phys. Rev. D **75**, 114005 (2007) [arXiv:hep-ph/0609224].
- [128] A. Ghinculov, T. Hurth, G. Isidori and Y. P. Yao, Nucl. Phys. B **648**, 254 (2003) [arXiv:hep-ph/0208088].
- [129] H. M. Asatrian, K. Bieri, C. Greub and A. Hovhannisyan, Phys. Rev. D **66**, 094013 (2002) [arXiv:hep-ph/0209006].
- [130] H. M. Asatrian, H. H. Asatryan, A. Hovhannisyan and V. Poghosyan, Mod. Phys. Lett. A **19**, 603 (2004) [arXiv:hep-ph/0311187].
- [131] C. Bobeth, G. Hiller and G. Piranishvili, JHEP **0712**, 040 (2007) [arXiv:0709.4174 [hep-ph]].
- [132] F. Krüger and J. Matias, Phys. Rev. D **71**, 094009 (2005) [arXiv:hep-ph/0502060].
- [133] E. Lunghi and J. Matias, JHEP **0704**, 058 (2007) [arXiv:hep-ph/0612166].
- [134] U. Egede, T. Hurth, J. Matias, M. Ramon and W. Reece, JHEP **0811**, 032 (2008) [arXiv:0807.2589 [hep-ph]].
- [135] W. Altmannshofer, P. Ball, A. Bharucha, A. J. Buras, D. M. Straub and M. Wick, JHEP **0901**, 019 (2009) [arXiv:0811.1214 [hep-ph]].
- [136] C. Bobeth, G. Hiller and G. Piranishvili, JHEP **0807**, 106 (2008) [arXiv:0805.2525 [hep-ph]].
- [137] M. Beneke, T. Feldmann and D. Seidel, Nucl. Phys. B **612**, 25 (2001) [arXiv:hep-ph/0106067].
- [138] M. Beneke, T. Feldmann and D. Seidel, Eur. Phys. J. C **41**, 173 (2005) [arXiv:hep-ph/0412400].
- [139] B. Aubert *et al.* [BaBar Collaboration], Phys. Rev. D **73**, 092001 (2006) [arXiv:hep-ex/0604007].
- [140] B. Aubert *et al.* [BaBar Collaboration], Phys. Rev. D **79**, 031102 (2009) [arXiv:0804.4412 [hep-ex]].
- [141] A. Ishikawa *et al.* [Belle Collaboration], Phys. Rev. Lett. **96**, 251801 (2006) [arXiv:hep-ex/0603018].
- [142] J. T. Wei *et al.* [BELLE Collaboration], Phys. Rev. Lett. **103**, 171801 (2009) [arXiv:0904.0770 [hep-ex]].

- [143] B. Grinstein and D. Pirjol, Phys. Rev. D **70**, 114005 (2004) [arXiv:hep-ph/0404250].
- [144] M. Antonelli *et al.* [FlaviaNet Working Group on Kaon Decays], arXiv:0801.1817 [hep-ph] and updated results available at: <http://www.lnf.infn.it/wg/vus>
- [145] K. Ikado *et al.* [Belle Collaboration], Phys. Rev. Lett. **97**, 251802 (2006) [arXiv:hep-ex/0604018].
- [146] B. Aubert *et al.* [BaBar Collaboration], Phys. Rev. D **77**, 011107 (2008) [arXiv:0708.2260 [hep-ex]].
- [147] I. Adachi *et al.* [Belle Collaboration], arXiv:0809.3834 [hep-ex].
- [148] B. Aubert *et al.* [BaBar Collaboration], arXiv:0809.4027 [hep-ex].
- [149] H. Davoudiasl, G. Perez and A. Soni, Phys. Lett. B **665**, 67 (2008) [arXiv:0802.0203 [hep-ph]].
- [150] A. J. Buras, B. Duling and S. Gori, JHEP **0909**, 076 (2009) [arXiv:0905.2318 [hep-ph]].
- [151] J. D. Bjorken, Phys. Rev. D **39**, 1396 (1989).
- [152] T. Aaltonen *et al.* [CDF Collaboration], Phys. Rev. Lett. **103**, 092002 (2009) [arXiv:0903.0885 [hep-ex]].
- [153] V. M. Abazov *et al.* [D0 Collaboration], Phys. Rev. Lett. **103**, 092001 (2009) [arXiv:0903.0850 [hep-ex]].
- [154] ATLAS Collaboration, CERN-LHCC-99-15, ATLAS-TDR-15.
- [155] G. L. Bayatian *et al.* [CMS Collaboration], J. Phys. G **34**, 995 (2007).
- [156] K. Agashe, R. Contino, L. Da Rold and A. Pomarol, Phys. Lett. B **641**, 62 (2006) [arXiv:hep-ph/0605341].
- [157] G. Beall, M. Bander and A. Soni, Phys. Rev. Lett. **48**, 848 (1982).
- [158] F. Gabbiani, E. Gabrielli, A. Masiero and L. Silvestrini, Nucl. Phys. B **477**, 321 (1996) [arXiv:hep-ph/9604387].
- [159] A. J. Buras, M. Jamin and P. H. Weisz, Nucl. Phys. B **347**, 491 (1990).
- [160] S. Herrlich and U. Nierste, Nucl. Phys. B **419**, 292 (1994) [arXiv:hep-ph/9310311].
- [161] E. Lunghi and A. Soni, Phys. Lett. B **666**, 162 (2008) [arXiv:0803.4340 [hep-ph]].
- [162] O. Deschamps, arXiv:0810.3139 [hep-ph].
- [163] A. Abulencia *et al.* [CDF Collaboration], Phys. Rev. Lett. **97**, 242003 (2006) [arXiv:hep-ex/0609040].

- [164] DØ Collaboration, DØ note 5618-CONF v1.2, May 2, 2008.
- [165] T. Aaltonen *et al.* [CDF Collaboration], Phys. Rev. Lett. **100**, 161802 (2008) [arXiv:0712.2397 [hep-ex]].
- [166] V. M. Abazov *et al.* [DØ Collaboration], Phys. Rev. Lett. **101**, 241801 (2008) [arXiv:0802.2255 [hep-ex]].
- [167] Z. Ligeti, M. Papucci and G. Perez, Phys. Rev. Lett. **97**, 101801 (2006) [arXiv:hep-ph/0604112].
- [168] A. A. Petrov, Int. J. Mod. Phys. A **21**, 5686 (2006) [arXiv:hep-ph/0611361] and references therein.
- [169] A. J. Schwartz, arXiv:0911.1464 [hep-ex].
- [170] M. S. Carena, E. Ponton, J. Santiago and C. E. M. Wagner, Phys. Rev. D **76**, 035006 (2007) [arXiv:hep-ph/0701055].
- [171] A. D. Medina, N. R. Shah and C. E. M. Wagner, Phys. Rev. D **76**, 095010 (2007) [arXiv:0706.1281 [hep-ph]].
- [172] A. V. Artamonov *et al.* [E949 Collaboration], Phys. Rev. Lett. **101**, 191802 (2008) [arXiv:0808.2459 [hep-ex]].
- [173] J. K. Ahn *et al.* [E391a Collaboration], arXiv:0911.4789 [hep-ex].
- [174] Y. Grossman and Y. Nir, Phys. Lett. B **398**, 163 (1997) [arXiv:hep-ph/9701313].
- [175] A. J. Buras, T. Ewerth, S. Jäger and J. Rosiek, Nucl. Phys. B **714**, 103 (2005) [arXiv:hep-ph/0408142].
- [176] M. Blanke, arXiv:0904.2528 [hep-ph].
- [177] S. Casagrande, “Flavor Physics and Electroweak Precision Tests in Randall-Sundrum Models”, diploma thesis (unpublished), Johannes-Gutenberg Universität Mainz, Germany.
- [178] DØ Collaboration, DØ note 5906-CONF, March 12, 2009.
- [179] T. Aaltonen *et al.* [CDF Collaboration], Phys. Rev. Lett. **100**, 101802 (2008) [arXiv:0712.1708 [hep-ex]].
- [180] G. Punzi, “Flavour physics at the Tevatron”, talk given at the 2009 Europhysics Conference on High Energy Physics, Jagiellonian University Kraków, Poland, 16–22 July, 2009.
- [181] D. Martinez, LHCb note 2008-018, May 7, 2008.
- [182] G. Aad *et al.* [ATLAS Collaboration], arXiv:0901.0512 [hep-ex].

- [183] U. Langenegger, arXiv:hep-ex/0610039.
- [184] R. Barate *et al.* [ALEPH Collaboration], Eur. Phys. J. C **19**, 213 (2001) [arXiv:hep-ex/0010022].
- [185] K. F. Chen *et al.* [Belle Collaboration], Phys. Rev. Lett. **99**, 221802 (2007) [arXiv:0707.0138 [hep-ex]].
- [186] B. Aubert *et al.* [BaBar Collaboration], Phys. Rev. D **78**, 072007 (2008) [arXiv:0808.1338 [hep-ex]].
- [187] F. Renga, “Recoil Analysis and $B \rightarrow K^* \nu \bar{\nu}$ at SuperB”, talk given at SuperB Physics Workshop, Physics Department of the University of Warwick, 13–17 April, 2009.
- [188] B. Aubert *et al.* [BaBar Collaboration], Phys. Rev. Lett. **93**, 081802 (2004) [arXiv:hep-ex/0404006].
- [189] M. Iwasaki *et al.* [Belle Collaboration], Phys. Rev. D **72**, 092005 (2005) [arXiv:hep-ex/0503044].
- [190] P. Gambino, U. Haisch and M. Misiak, Phys. Rev. Lett. **94**, 061803 (2005) [arXiv:hep-ph/0410155].
- [191] R. Fleischer, S. Jäger, D. Pirjol and J. Zupan, Phys. Rev. D **78**, 111501 (2008) [arXiv:0806.2900 [hep-ph]].
- [192] S. Schael *et al.* [ALEPH Collaboration], Phys. Rept. **427**, 257 (2006) [arXiv:hep-ex/0509008] and updated results available at: <http://lepewwg.web.cern.ch/LEPEWWG/>
- [193] S. Herrlich and U. Nierste, Phys. Rev. D **52**, 6505 (1995) [arXiv:hep-ph/9507262].
- [194] S. Herrlich and U. Nierste, Nucl. Phys. B **476**, 27 (1996) [arXiv:hep-ph/9604330].
- [195] K. G. Chetyrkin and A. Retey, Nucl. Phys. B **583**, 3 (2000) [arXiv:hep-ph/9910332].
- [196] J. Charles, A. Le Yaouanc, L. Oliver, O. Pene and J. C. Raynal, Phys. Rev. D **60**, 014001 (1999) [arXiv:hep-ph/9812358].
- [197] M. Beneke and T. Feldmann, Nucl. Phys. B **592**, 3 (2001) [arXiv:hep-ph/0008255].
- [198] P. Ball and R. Zwicky, Phys. Rev. D **71** (2005) 014029 [arXiv:hep-ph/0412079].